

Ride Comfort and Active Suspension Systems towards Automated Driving – An Objective Target Value and a Method to investigate Actuator Requirements

Erik Stephan Enders

Vollständiger Abdruck der von der TUM School of Engineering and Design der Technischen
Universität München zur Erlangung eines
Doktors der Ingenieurwissenschaften (Dr.-Ing.)
genehmigten Dissertation.

Vorsitz: Prof. Dr.-Ing. Boris Lohmann

Prüfer der Dissertation:

1. Prof. Dr.-Ing. Markus Lienkamp
2. Assoc. Prof. Mathias R. Lidberg

Die Dissertation wurde am 30.05.2022 bei der Technischen Universität München eingereicht
und durch die TUM School of Engineering and Design am 05.10.2022 angenommen.

Eidesstattliche Erklärung

Ich, Erik Stephan Enders erkläre an Eides statt, dass ich die bei der promotionsführenden Einrichtung

TUM School of Engineering and Design

der TUM zur Promotionsprüfung vorgelegte Arbeit mit dem Titel:

Ride Comfort and Active Suspension Systems towards Automated Driving – An Objective Target Value and a Method to investigate Actuator Requirements

unter der Anleitung und Betreuung durch: **Prof. Dr.-Ing. Markus Lienkamp**

ohne sonstige Hilfe erstellt und bei der Abfassung nur die gemäß § 7 Abs. 6 und 7 angegebenen Hilfsmittel benutzt habe.

Ich habe keine Organisation eingeschaltet, die gegen Entgelt Betreuer*innen für die Anfertigung von Dissertationen sucht, oder die mir obliegenden Pflichten hinsichtlich der Prüfungsleistungen für mich ganz oder teilweise erledigt.

Ich habe die Dissertation in dieser oder ähnlicher Form in keinem anderen Prüfungsverfahren als Prüfungsleistung vorgelegt.

Teile der Dissertation wurden in _____ veröffentlicht.

Ich habe den angestrebten Doktorgrad noch nicht erworben und bin nicht in einem früheren Promotionsverfahren für den angestrebten Doktorgrad endgültig gescheitert.

Ich habe bereits am _____ bei der promotionsführenden Einrichtung _____ der Hochschule _____ unter Vorlage einer Dissertation mit dem Thema _____

die Zulassung zur Promotion beantragt mit dem Ergebnis:

Ich habe keine Kenntnis über ein strafrechtliches Ermittlungsverfahren in Bezug auf wissenschaftsbezogene Straftaten gegen mich oder eine rechtskräftige strafrechtliche Verurteilung mit Wissenschaftsbezug.

Die öffentlich zugängliche Promotionsordnung sowie die Richtlinien zur Sicherung guter wissenschaftlicher Praxis und für den Umgang mit wissenschaftlichem Fehlverhalten der TUM sind mir bekannt, insbesondere habe ich die Bedeutung von § 27 PromO (Nichtigkeit der Promotion) und § 28 PromO (Entzug des Doktorgrades) zur Kenntnis genommen. Ich bin mir der Konsequenzen einer falschen Eidesstattlichen Erklärung bewusst.

Mit der Aufnahme meiner personenbezogenen Daten in die Alumni-Datei bei der TUM bin ich

einverstanden, nicht einverstanden.

Ort, Datum, Unterschrift

Acknowledgment

The research documented in this thesis work was conducted during my time as research assistant at the Chair of Automotive Engineering at the Technical University of Munich. The research project was realized in cooperation with Bayerische Motorenwerke AG. The required funding and the majority of the needed equipment and materials was provided by Bayerische Motorenwerke AG.

First and foremost I want to thank Prof. Markus Lienkamp for providing me the option to pursue my doctoral degree at his institute. Markus, I have learned a lot during this time, technically and personally. I am truly grateful that you have given me this opportunity, although my CV has shown that I have not followed the typical path of a TUM doctoral candidate in my younger years. Next, I want to thank Prof. Mathias Lidberg for taking over the role as second examiner. Mathias, I look back on my time at Chalmers with great pleasure. Your vehicle dynamics course has been a crucial part of the educational foundation for my following development, in the end leading to this thesis work. My gratitude goes as well to Prof. Boris Lohmann for taking over the examination chairmanship.

My appreciation belongs to the people at BMW who co-initiated this research cooperation and supported me along the way, particularly Nathan Munzinger, Dr. Daniel Kilian, Dr. Serge Vos and Dr. Enrico Pellegrini. Furthermore, I am obliged to Georg Burkhard. Georg, you have not only been the perfect complement to me as a colleague, but you have also become one of my dear friends. I further want to thank all the other people within the vehicle dynamics development of BMW, with whom I have closely worked with, for their courtesy and support.

An integral part during my time at TUM have been my colleagues at the chair of automotive engineering, especially within the vehicle dynamics research group. I am honored to have worked alongside extremely talented and clever, yet humble and handsome people, such as Dr. Andreas Eisele, Dr. Matthias Förth, Dr. Thomas Zehelein, Dr. Stefan Büchner, Konstantin Riedel and Alexander Heilmeier. My sincere thanks go to Dr. Johannes Betz as research group leader for the support and guidance; to Dr. Andreas Schulze and Dr. Thomas Zehelein as research group leaders, considering me as a suitable candidate when I applied for the position as a research assistant.

Last but not least, thanks to all of my students. Independent of the topic and scope of your thesis work, I can assure you that I have learned together with every one of you. It would make me more than happy if you can say the same and wish you all the best for your future. I want to mention particularly Phillip Karle and Felix Fent, whom both followed into my footsteps at the Chair of Automotive Engineering. Knowing the both of you, I am sure you will succeed and leave a larger mark than myself.

Abstract

The progressive development towards automated and autonomous driving entails unknown challenges for vertical vehicle dynamics ride comfort development. This research determines a target value for ride comfort based on a vibration discomfort measure according to ISO 2631. A new simulation method using model predictive control is introduced, which allows to investigate effects of semi-active and active suspension actuator limitations on achievable ride comfort for a given scenario, defined by the road-surface profile, vehicle parameters, and driving speed. The results of an online survey support the theory of the increasing importance of ride comfort regarding automated driving. Suspension systems which are currently available cannot deliver ride comfort as demanded by customers during an automated drive on a low-quality road. A vibration discomfort value of $0.20 \pm 0.05 \text{ m s}^{-2}$ is identified as target value for ride comfort during automated driving, based on driving simulator studies. In an exemplary scenario, it could only be achieved with an active suspension system. The results indicate that active suspension system actuators should be able to supply a maximum force of 1 kN, and a maximum slew-rate of 40 kNs^{-1} , based on an investigation using an ideal model predictive control simulation model. Compared to state-of-the-art active suspension systems, future systems require lower maximum forces but higher maximum slew rates.

Zusammenfassung

Die fortschreitende Entwicklung hin zum automatisierten und autonomen Fahren birgt unbekannte Herausforderungen für die Entwicklung des vertikaldynamischen Fahrkomforts. In dieser Forschungsarbeit wird ein Zielwert für den Fahrkomfort erarbeitet, welcher durch die Messung des Schwingungs-diskomforts nach ISO 2631 definiert ist. Es wird eine neue, auf modellprädiktiver Regelung basierende Simulationsmethode eingeführt, die es ermöglicht, die Auswirkungen von semiaktiven und aktiven Federungsaktuatoren auf den erreichbaren Fahrkomfort für ein gegebenes Szenario zu untersuchen. Das Szenario wird durch das Straßenprofil, die Fahrzeugparameter und die Fahrgeschwindigkeit definiert. Die Ergebnisse einer Online-Umfrage stützen die Theorie hinsichtlich einer zunehmenden Bedeutung des Fahrkomforts unter dem Gesichtspunkt des automatisierten Fahrens. Heutige Fahrwerksysteme werden den Fahrkomfortansprüchen von Fahrzeuginsassen während einer automatisierten Fahrt bei schlechter Fahrbahn nicht gerecht. Als Zielwert für den erwünschten Fahrkomfort beim automatisierten Fahren wurde ein Diskomfort-Wert von $0.20 \pm 0.05 \text{ m s}^{-2}$ basierend auf Fahrstudien ermittelt. In einem beispielhaften Szenario konnte dieser Wert nur mit einem aktiven Fahrwerksystem erreicht werden. Die Ergebnisse zeigen, dass Aktoren aktiver Fahrwerke in der Lage sein sollten, eine maximale Stellkraft von 1 kN bei einer maximalen Stellrate von 40 kN s^{-1} zu liefern, basierend auf Simulationen mit einem idealen modellprädiktiven Regler. Im Vergleich zu heutigen aktiven Fahrwerksystemen benötigen zukünftige Systeme also weniger Maximalkraft, aber höhere maximale Stellraten.

Contents

List of Abbreviations	V
Formula Symbols	VII
1 Introduction	1
1.1 Motivation	1
1.2 Structure of the Thesis	2
2 State-of-the-Art	3
2.1 Fundamentals	3
2.1.1 Dynamic Systems	3
2.1.2 Vibration Analysis.....	4
2.1.3 Optimization	5
2.1.4 Statistics.....	5
2.2 Objectification of Ride Comfort	8
2.2.1 Comfort, Discomfort and Vibration Discomfort.....	8
2.2.2 Objectification Methods	10
2.3 Vertical Vehicle Dynamics	12
2.3.1 Suspension Systems	13
2.3.2 Vehicle Models	18
2.3.3 Control Systems.....	20
2.3.4 Road Models and Classification	23
3 Research Gap	25
3.1 Latest Research in the Field	25
3.2 Criticism	26
3.3 Aim and Limitations	27
3.4 Research Questions	27
4 Survey on Ride Comfort in Passenger Cars	29
4.1 Method	29
4.1.1 Questionnaire Design	29
4.1.2 Analysis.....	30

4.2 Results	30
4.2.1 General Information	30
4.2.2 Conventional versus Automated Driving	31
4.3 Discussion	34
5 Driving-Simulator Study I – Suspension Systems	35
5.1 Method	35
5.1.1 Driving Simulator	36
5.1.2 Study Design	38
5.1.3 Implementation	40
5.1.4 Execution	42
5.1.5 Analysis	43
5.1.6 Validation of the Driving Simulator	43
5.2 Results	45
5.2.1 Objective Assessment	45
5.2.2 Subjective Assessment	46
5.2.3 Motion-Sickness and Follow-up Interview	49
5.3 Discussion	50
6 Driving-Simulator Study II – A Target Value for Ride Comfort	51
6.1 Method	51
6.1.1 Study Design	51
6.1.2 Implementation	53
6.1.3 Execution	54
6.1.4 Analysis	54
6.2 Results	55
6.2.1 Objective Assessment	55
6.2.2 Motion Sickness and Follow-up Interview	57
6.3 Discussion	59
7 Derivation of Actuator Requirements	61
7.1 Method	61
7.1.1 Vehicle Model	62
7.1.2 Controller Synthesis	65
7.1.3 Boundary Conditions and Actuator Constraints	67
7.1.4 Test Scenario Definition	70
7.1.5 Implementation and Analysis Methods	73

7.2 Results	74
7.2.1 Model Validation	74
7.2.2 Preview Sensitivity	77
7.2.3 Influence of the Maximum Force and Slew-Rate	78
7.2.4 Power Limitation and Actuator Accuracy.....	79
7.2.5 Semi-Active Actuator performance	81
7.3 Discussion	84
8 Conclusion	85
9 Summary and Outlook	89
List of Figures	i
List of Tables	v
Bibliography	vii
Prior Publications: Journals; Scopus / Web of Science listed (peer-reviewed)	xxvii
Prior Publications: Conferences; Scopus / Web of Science listed (peer-reviewed)	xxix
Prior Publications: Conferences; not Scopus / Web of Science listed (not peer-reviewed)	xxxi
Prior Publications: Patent Applications	xxxiii
Supervised Student Thesis Works	xxxv
Appendix	xxxvii

List of Abbreviations

ABC	Active Body Control
ADMA	Automotive Dynamic Motion Analyzer
ARB	Anti-Roll Bar
BMW	Bayerische Motorenwerke
CAN	Controller Area Network
CID	Central Information Display
CoG	Center of Gravity
DFT	Discrete Fourier Transform
DiM	Driver in Motion
DoE	Design of Experiments
DoF	Degrees of Freedom
eABC	electric Active Body Control
EoM	Equations of Motion
FFT	Fast Fourier Transform
GHC	Ground-Hook Control
GPS	Global Positioning System
IMU	Inertial Measurement Unit
IRI	International Roughness Index
KPI	Key Performance Indicator
LMC	Lotus Modal Control
LQG	Linear-Quadratic Gaussian Regulator
LQR	Linear Quadratic Regulator
MBC	Magic Body Control
MPC	Model-Predictive Control
MR	Magneto-Rheological
MSI	Motion Sickness Indicator
OBD	On-Board Diagnostics
OEM	Original Equipment Manufacturer
PID	Proportional-Integral-Derivative
PSD	Power Spectral Density
RMS	Root Mean Square
SHC	Sky-Hook Control
SUV	Sports Utility Vehicle
TUM	Technical University of Munich
USB	Universal Serial Bus
VV	Variable-Valve

Formula Symbols

Formula Symbols	Unit	Description
α	-	significance level
$\alpha_{B,5\%}$	-	Bonferroni corrected 0.5 % significance level
\mathbf{A}	-	system matrix
$a_{w,iso}$	ms^{-2}	ISO 2631 weighted RMS acceleration
\mathbf{B}	-	input matrix
b_f	m	track-width front axle
b_r	m	track-width rear axle
\mathbf{C}	-	output matrix
c_{Bo}	Nm^{-1}	spring stiffness
\mathbf{c}_d	-	differential gain of a PID controller
\mathbf{c}_i	-	integral gain of a PID controller
\mathbf{c}_p	-	proportional gain of a PID controller
c_{St}	Nm^{-1}	anti-roll bar stiffness
c_{Wh}	Nm^{-1}	tire stiffness
\mathbf{D}	-	damping matrix
\mathbf{D}	-	feed-through matrix
d	-	Cohen's d
d_{Bo}	Ns m^{-1}	damping constant
d_{Wh}	Ns m^{-1}	tire damping
$e(t)$	-	control error
\mathbf{F}	-	feed-forward matrix of a state controller
F_{Ac}	N	actuator force
F_{dyn}	N	dynamic wheel load amplitude
$\mathcal{F}(f(x))$	-	Fourier transform of $f(x)$
F_{Wh}	N	normal force at the wheel

$G_d(n)$	-	reference displacement PSD of a road profile
$g_i(x)$	-	inequality constraints
$h_j(x)$	-	equality constraints
θ_{Bo}	rad	pitch angle
\mathbf{I}	-	identity matrix
$J(x)$	-	cost-function
$J_{Bo,x}$	kg m ²	roll inertia
$J_{Bo,y}$	kg m ²	pitch inertia
\mathbf{K}	-	stiffness matrix
λ	-	eigenvalue
l_{Cp}	m	tire contact patch length
l_f	m	distance CoG to front axle
l_p	m	road profile length
l_r	m	distance CoG to rear axle
\mathbf{M}	-	mass-matrix
m_{Bo}	kg	sprung mass
M_{St}	Nm	moment generated by the anti-roll bars
m_{Wh}	Ns m ⁻¹	unsprung mass
n_0	-	reference spacial frequency for a road profile
n / N	-	number of samples
n_h	-	number of hypotheses
p	-	probability
P_{Ac}	W	actuator power
Q	N	sum of external forces
q	-	generalized coordinates
R	J	dissipation energy
\mathbf{R}	-	feedback matrix of a state controller
R_i	-	sample rank
s_p	-	pooled standard deviation
s_{sus}	m	suspension travel
T	J	kinetic energy
t	-	t-test statistic
t	s	time

t_{Ac}	s	actuator time delay
t_c	s	control horizon time
t_{end}	s	simulation time
t_p	s	preview horizon time
t_s	s	sampling time
U	J	potential energy
U	-	Mann-Whitney-U test statistic
\mathbf{u}_{lim}	-	input constraints of a MPC
$\mathbf{u}(t)$	-	input vector
\mathbf{v}	-	eigenvector
$\mathbf{v}(t)$	-	disturbance vector
v_x	m	vehicle speed
φ_{Bo}	rad	roll angle
W	-	Wilcoxon test statistic
\mathbf{W}	-	weighting matrix of a MPC
w	-	waviness of a ISO road profile
w_{xx}	-	weighting factor for xx
$\mathbf{x}(t)$	-	state vector
x_{rms}	-	RMS value of the signal x
ψ	rad	yaw angle
\mathbf{y}_{lim}	-	output constraints of a MPC
\mathbf{y}_{set}	-	set-point for the controller
$\mathbf{y}(t)$	-	output vector
ω	-	angular frequency
Z	-	z-score
z_{Bo}	m	sprung mass position
z_{Ro}	m	road excitation position
z_{Wh}	m	un-sprung mass position

1 Introduction

Emission reduction, alternative propulsion systems, and automated driving are three main technical challenges for the automotive industry today. Automated driving is a much-debated topic. A survey with 1015 subjects of Bertelsmann in 2017 has shown that in average, people expect automated driving to be safe and ready to use by 2035, with two-thirds of the interviewees being skeptical towards automated driving [1, p. 3]. The most named use case for driving automation is freeway traveling (59%), with the most commonly expected activities being "looking at the environment" (73%) and "relaxing" (59%) [1, p. 6].

An online survey of Dornier Consulting with 110 participants has investigated the question of routine activities for single and group traveling. Individually the most expected activity is the use of media (internet, streaming, social media, etc.) with 81%, followed by working (67%) and reading (65%) [2, p. 16]. For driving in a group the most common answer was "having a conversation" (79%) [2, p. 16]. Another investigation showed that for short trips, activities like watching the surroundings and smartphone use are popular, while for longer trips, people prefer relaxing, sleeping, and working [3]. From a vehicle dynamics perspective, increasing levels of driving automation according to SAE J3016 [4] are likely to entail a focus shift from driving dynamics to ride comfort, because the aspects of self-driving vanish and the suspension system can be tuned with a focus on ride comfort.

1.1 Motivation

Current ride comfort development of Original Equipment Manufacturers (OEMs) is mainly based on subjective ratings of test-engineers, relative to previous and competitor models. The ratings are obtained from prototype vehicle testing. As will be shown in Chapter 3, ongoing research in vertical vehicle dynamics is focused on new methods, using simulation models and objective performance criteria, but no such methods exist for semi-active or active suspension systems. These methods are required to reduce physical testing time and development costs. Objective target values help to get unbiased, repeatable and reliable vehicle performance assessment. The objective value should correlate to the subjective judgment of customers. This correlation is particularly unknown for automated driving conditions.

The importance of ride comfort for automated driving should be determined in relation to other vehicle features. Current suspension systems should be tested in automated driving condition to re-evaluate their respective performance. An objective target value for ride comfort in automated driving conditions should be derived, which is required to enable objective development. A method to investigate vertical vehicle dynamics control system performance depending on actuator limitations is needed for requirement-based development of active suspensions. This research contributes to general ride comfort development regarding automated driving, and specifically to active suspension design.

1.2 Structure of the Thesis

This thesis work is structured according to Figure 1.1. The Introduction (Chapter 1) is followed by Chapter 2 State-of-the-Art, which summarizes the theoretical and technical basics required to understand this research. The research gap itself is outlined in Chapter 3, where the aim of this thesis and the research questions are derived from the current state of research. The main body of this thesis work consists of four parts (Chapter 4, Chapter 5, Chapter 6, and Chapter 7), each containing a Section for Method, Results, and Discussion. The thesis is closed by Chapter 8 Conclusion and Chapter 9 Summary and Outlook.

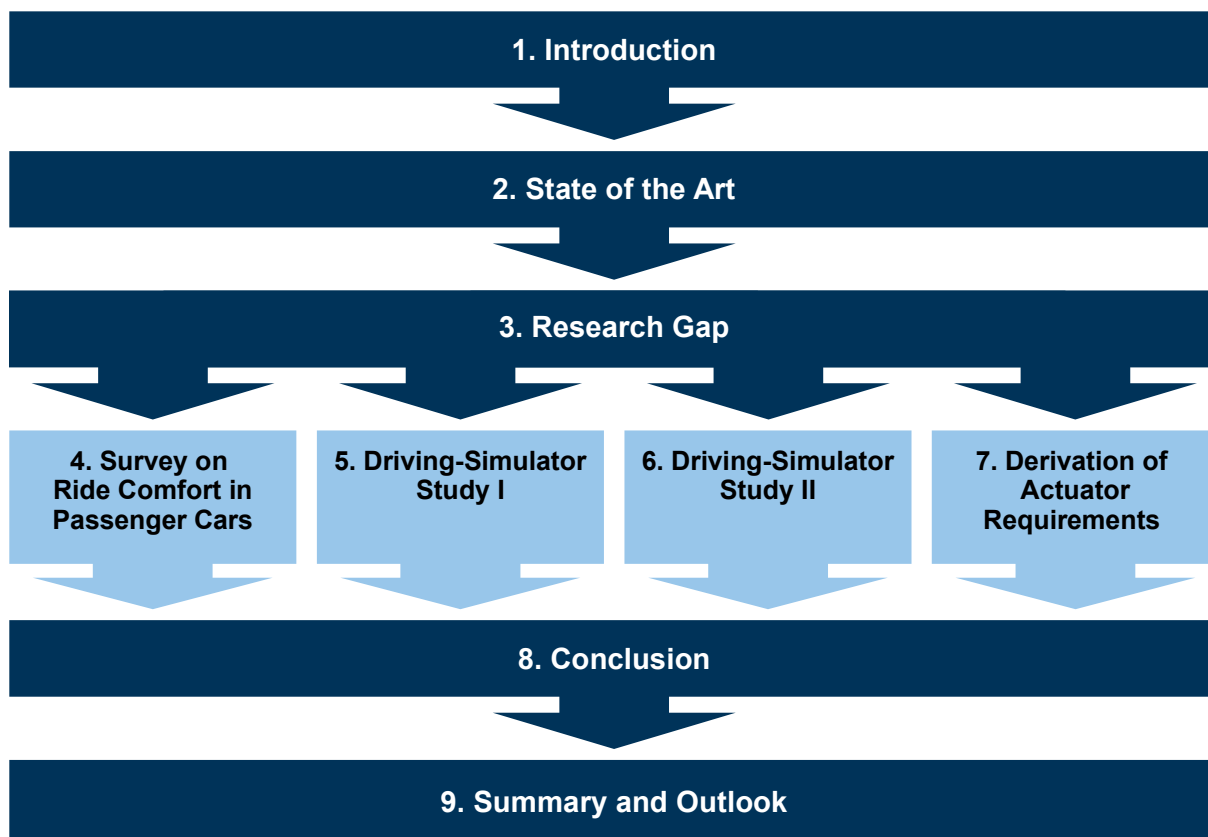


Figure 1.1: Overview of the thesis structure

2 State-of-the-Art

This section gives a summary of the State-of-the-Art. The required fundamentals in the theory of dynamic systems, vibration analysis methods, and statistics are recapitulated in Section 2.1. Section 2.2 explains the current state of research on comfort and discomfort, followed by a summary of already known methods for objectifying ride comfort. Section 2.3 contains all information on passive, semi-active, and active suspension systems, vehicle models, suspension control systems, and the classification of roads including their modeling for simulation purposes.

2.1 Fundamentals

A brief overview is given on the fundamentals required to follow the conducted research within this thesis work. It entails a summary of the basic principles of dynamic systems, vibration analysis, mathematical optimization, and statistics. These will be described in the following.

2.1.1 Dynamic Systems

Dynamic systems are mathematical descriptions of physical processes, which can be used to simulate and analyze them. Mechanical systems are characterized by their Equations of Motion (EoM). For vibration systems, these are often a system of linear second-order differential equations with constant coefficients, represented as mass, stiffness, and damping matrices, linearized for small oscillation around a reference condition. From the EoM a state-space representation of the system can be derived [5, pp. 28–31]. The state-space model is defined by its set of linear first-order differential equations with constant coefficients, defined as system matrix A , input matrix B , output matrix C , and feed-through matrix D , which are used to calculate the states x and outputs y :

$$\dot{x}(t) = Ax(t) + Bu(t) \quad (2.1a)$$

$$y(t) = Cx(t) + Du(t) \quad (2.1b)$$

Through modal-decomposition, eigenvalues and eigenvectors can be calculated [6]. The solution of the characteristic equation

$$\det(A - \lambda I) = 0, \quad (2.2)$$

gives the vector of eigenvalues λ , the eigenvectors v_i are obtained by solving

$$(A - \lambda_i I) v_i = 0 \quad (2.3)$$

for each eigenvalue λ_i .

The eigenvalues define the natural frequencies of a vibration system, and the eigenvectors describe the vibration mode. In control systems, the position of the closed-loop poles in the complex plane, which are defined by the eigenvalues of the closed loop system, can be used to analyze the stability of the control system, as well as for controller synthesis by pole placement. The open-loop system poles are shifted along the root-locus trajectory towards the closed-loop poles depending on the control law. For a continuous-time system, all real-parts of the closed-loop poles have to be negative to guarantee stability. For discrete-time systems, all closed-loop eigenvalues have to be located within the unit-circle in the z-plane. This can be used to tune a classic PID controller. When considering discrete-time signals, for example, in electronic vehicle control units, it is vital to consider the Nyquist-Shannon sampling theorem. The sampling frequency needs to be at least two times the reference frequency, to capture all relevant dynamics.

2.1.2 Vibration Analysis

The field of vibration analysis is broad and complex. In road vehicle development, there are different applications, from drivetrain development to general analysis of noise, vibration, and harshness. Within the scope of this research work, the emphasis is on low-frequency vibration, ranging from 0–20 Hz due to road irregularity, resulting in vibration which is perceived haptically and via the vestibular system. The analysis is performed based on acceleration measurements. In the time domain, characteristic values such as the maximum amplitude are used to specify the intensity. Road disturbances are stochastic phenomena superimposed by single events, such as pot-holes or bumps. For the analysis of vehicle vibration on stochastic disturbances, the Root Mean Square (RMS) value is suitable to describe the vibration level. For a discrete signal x_k , with n sampling points, its RMS value is defined as:

$$x_{\text{rms}} = \sqrt{\frac{1}{n} (x_1^2 + x_2^2 + \dots + x_n^2)} \quad (2.4)$$

Vibration signals can be described likewise in the frequency domain. Transfer functions are derived for dynamic models and then used to study their corresponding frequency response to input excitation [7, pp. 239–258]. For general signals, it is necessary to calculate their Fourier Transform. The standard Fourier Transform for an integrable function is

$$\mathcal{F}(f(t)) = \int_{-\infty}^{\infty} f(t)e^{-j\omega t} dt \quad (2.5)$$

For discrete-time signals, the Discrete Fourier Transform (DFT) has to be computed, defined for a signal x_k with N samples as

$$\mathcal{F}(x_k) = \sum_{n=0}^{N-1} x_n e^{-j2\pi \frac{1}{N} kn} \quad (2.6)$$

The DFT can be implemented and calculated as Fast Fourier Transform (FFT), a more computational effective version of a DFT. Another form of frequency analysis is the Welch method for Power Spectral Density (PSD) estimation. An FFT gives a signal's amplitude over the frequency, the PSD its power over frequency. An advantage of the PSD over the FFT is that its spectrum is independent of the signal length, making it more suitable to compare signals of different lengths. Further information is given in [8, pp. 150–203].

2.1.3 Optimization

Optimization is a discipline in mathematics to obtain the optimal solution to a problem, which may or may not be subject to constraints. The type of problem is characterized by a mathematical cost-function $J(x)$. This function can be linear, quadratic, non-linear, or of almost any other form. Constraints are formulated as equality $h(x)$ or inequality constraints $g(x)$, which means that the optimal solution needs to fulfill these statements to be valid. The general form of an optimization problem is given as:

$$\text{minimize } J(x) \tag{2.7a}$$

$$\text{subject to } g_i(x) \leq 0, \quad i = 1, \dots, m \tag{2.7b}$$

$$h_j(x) = 0, \quad j = 1, \dots, n \tag{2.7c}$$

Convex optimization is a subset of general optimization, denoted by minimizing convex functions, defined by a non-negative second-order derivative. Strictly convex functions only possess one minimum, regardless of whether they are in the two-, three-, or n-dimensional space. Convex optimization problems are well understood, and different formalisms are available to solve these problems. An overview of the application of various methods, including multi-objective and non-linear optimization for mechanical systems and vehicle engineering, can be found in [9].

2.1.4 Statistics

Statistics are an integral part of many disciplines in engineering. Starting in classic quality control for industrial production, ranging over to fatigue strength analysis in material sciences and ending up at modern data science and machine learning algorithms. In the field of behavioral sciences, statistics are one of the main cornerstones. This circumstance might be overlooked by engineers working on related topics, like human-machine interface development – or considering this thesis work – the field of ride comfort development.

The terms mean, median, mode, variance, standard error, quartile, and outlier are usually well known. On the other hand, statistical scales are less popular, yet they define permissible and non-permissible operations for the respective data. The most commonly known scale is the interval scale, which relates to the temperature scale in degrees Celsius. The intervals are equidistant, so a 2°C difference is the same between 10°C and 12°C degrees, as it is between –20°C and –22°C. If a zero reference is definable for the scale, as for the temperature scale in Kelvin, it is deductible that 200 K Kelvin is twice as warm as 100 K. Due to these characteristics, different operations can be applied on interval-scaled data sets, such as computation a mean value and an analysis of the variance. Physical measurements, like acceleration or angular rate measurements, can usually be treated as interval scaled data.

Ordinal scale rules apply if interval-scale data conditions are not fulfilled, but the data is qualitatively rank-able. Examples are school grades or subjective ratings. Operations on ordinal data sets are limited. Mode and median are permissible, while mean, variance, and standard deviation may not be computed. Even if mathematically feasible, because there are assigned numbers to the different ratings, like German school grades, it is non-permissible to compute these values from a statistical perspective.

It is always allowed to apply ordinal scale methods to interval scale data but rarely holds the opposite. Subjective ratings are classifiable as ordinal scaled data, independent of the type of rating scale. Statistical scales are described in detail with further examples by Cramer

and Kamps [10, pp. 5–7]. The Likert scale, used for subjective ratings within this research, is described by Coolican [11, p. 221].

Statistical significance is another term essential to understand, specifically when results of test person studies are analyzed and interpreted. Statistical significance is a mathematical measure to detect a difference between two data sets at a specified probability level. Usually, the level is 95 percent, which means there is only a five percent chance that one assumes the data sets to be different without actually being different. It is commonly known as type I error (false-positive). Suppose a null hypothesis is not rejectable at the desired confidence level. In that case, this is not evidence for the opposite of the null hypothesis. There is no proof that the data sets are the same.

A significant difference between two or more data sets does not imply practical relevance. Statistical significance is mainly dependent on the sample size and the variation in the data. If data-sets are sufficiently large, or their variations sufficiently small, results are mostly significant. If there is practical significance concerning the research question can only be determined and quantified by calculating effect sizes.

Several test methods and effect strength measures are applied within this thesis work. For statistical significance between two interval-scaled data sets, the independent two-sample t-test is used, defined as

$$t[d_f] = \frac{\bar{X}_1 - \bar{X}_2}{s_p \sqrt{2(n_1 + n_2)^{-1}}} \quad \text{with} \quad d_f = (n_1 + n_2) - 2, \quad (2.8)$$

where \bar{X}_1 and \bar{X}_2 are the sample mean values, s_p is the pooled standard deviation and n is the sample size. The t -value is not a function of d_f , which denotes the degrees of freedom. The degrees of freedom are reported for informational purposes as it hints towards the sample size and is relevant for underlying probability distributions. It is applied, if for each element in sample one, there is a corresponding element in sample two. The effect strength measure η^2 for a t-test is calculated as:

$$\eta^2 = \frac{t^2}{t^2 + d_f} \quad (2.9)$$

For ordinal scaled data sets and within-subject differences, the Wilcoxon signed-rank test is used. A rank is the ordinal value, which can be higher, lower or equal to another rank. The test is defined as

$$W = \sum_{i=1}^{N_r} [\text{sgn}(x_{2,i} - x_{1,i})R_i], \quad (2.10)$$

with the non zero data differences $(x_{2,i} - x_{1,i})$, the reduced sample size N_r and the corresponding ranks R_i . Zero-differences, which means that both ranks are the same, have no effect on the rank-sum, because it just adds zero. For two independent data sets corresponding to between-subject differences, the Mann-Whitney-U test statistic is calculated as

$$\min(U_i) \quad \text{with} \quad U_i = R_i - \frac{n_i(n_i + 1)}{2}, \quad i = \{1, 2\}. \quad (2.11)$$

U_1 and U_2 are the test statistics for sample one and sample two, calculated from the rank sums R_1 and R_2 and the sample sizes n_1 and n_2 . The smaller value of both is used to determine the significance level based on distribution tables, as it is done with the W value of the Wilcoxon test and the t value for the t -test. For large sample sizes, U and W are often assumed to be normally distributed based on the central limit theorem, equivalent to the finding that the importance of a normality assumption of a t -test decreases for an increasing sample size [12].

Based on the normality assumption for large enough data sets, the z -score is calculated for the Mann-Whitney- U test and the Wilcoxon test, based on the test statistic value T (either U or W), the mean value, and the variance:

$$z = \frac{T - \mu}{\sigma}. \quad (2.12)$$

The z -score can be used to calculate the effect size value η^2 analogue to the t -test as:

$$\eta^2 = \frac{z^2}{N_r}. \quad (2.13)$$

The η^2 value is further convertible to a common effect strength measure named Cohen's d [13]:

$$d = 2\sqrt{\eta^2(1 - \eta^2)^{-1}}. \quad (2.14)$$

Generally, Jacob Cohen defines it as the ratio of the difference in mean values to the pooled standard deviation:

$$d = \frac{\mu_1 - \mu_2}{s_p}. \quad (2.15)$$

Absolute values from 0.2 to 0.5 correspond to a small effect, 0.5 to 0.8 to a medium effect, and above 0.8 as large effect [14, pp. 20–27].

Additionally to independent two-sample tests, pairwise tests can be applied if there is a corresponding element in sample two, for each element in sample one. Corresponding implies that they are statistically dependent, for example because they are related to the same test subject. In an independent interval-scaled test, the sample means are tested for significant difference with regard to the variability in both samples. For an interval-scaled pairwise test, the mean value of the pairwise differences is tested to be significantly different from zero, with respect to the variability in pairwise-differences. Within this research, most tests are performed as independent two-sample tests, due to the study designs. Only the evaluation of a questionnaire is performed as pairwise test, because of the statistical dependency.

The "look-elsewhere" effect needs consideration when several hypotheses are evaluated within one investigation. The probability of a significant effect increases with the number of tested hypothesis' for the same effect. If the influence of a parameter is tested for more than two settings¹, Friedman or Kruskal-Wallis tests are performed. On the downside, this gives no information about the individual differences between the settings. Instead, pair-wise two-sample tests can be performed, using multiple null-hypothesis'.

To avoid the "look-elsewhere" effect, a Bonferroni correction can be applied to determine a corrected significance threshold. It is equivalent to or more conservative than the desired significance level.

¹For example something is tested at the settings "off", "50%", and "100%", instead just testing for "on" or "off"

The Bonferroni corrected five percent significance level $\alpha_{B,5\%}$ is obtained for the number of tested hypotheses n_h as:

$$\alpha_{B,5\%} = \frac{0.05}{n_h} \quad (2.16)$$

The application of the Bonferroni correction is conservative, which means that it can produce a type II error (false-negative). In this case a possibly false null hypothesis is not rejected (a significant effect tested as non-significant). Within the scope of this research, the correction was applied to minimize the chance of a type I error (false-positive), which would mean detecting a significant effect that is not.

Information on Design of Experiments (DoE), which was used as a basis to define test plans within this research, is given in [15]. This source contains further information on statistical methods for interval-scaled data sets. Test procedures for nominal and ordinal data can be found in [16, pp. 139–154].

2.2 Objectification of Ride Comfort

Objectification methods for lateral vehicle dynamics are well advanced, which can be seen by the works of Schimmel [17] and Pietsch [18]. In vertical dynamics, one must distinguish between development-centric and customer-centric objectification methods. Development-centric methods focus on phenomena like "body-comfort", "wheel-comfort", "engine-shake", "copying", and many more, which are described by Mitschke [19, pp. 530–531].

Customer-centric objectification methods focus on the vibration discomfort perceived by the occupant, independent of its source. In Subsection 2.2.1 the terms comfort, discomfort, and in particular vibration discomfort are described in detail. Subsection 2.2.2 summarizes existing methods for vertical vehicle dynamics objectification.

2.2.1 Comfort, Discomfort and Vibration Discomfort

The term ride comfort is used frequently in vertical vehicle dynamics development and is related to the isolation of the passenger from road-induced vibration. From a behavioral science perspective, this definition is imprecise, as can be seen when looking at comfort models for general sitting comfort.

Zhang et al. [20] describe the two entities comfort and discomfort as complementary and state the need to treat them separately. According to their findings, discomfort is related to biomechanical factors, whereas comfort is associated with relaxation and well-being, and reduced discomfort does not lead to comfort, but offers the possibility to perceive comfort [20, p. 388]. These findings were incorporated into an extended model for comfort perception by Looze et al. [21], which is displayed in Figure 2.1.

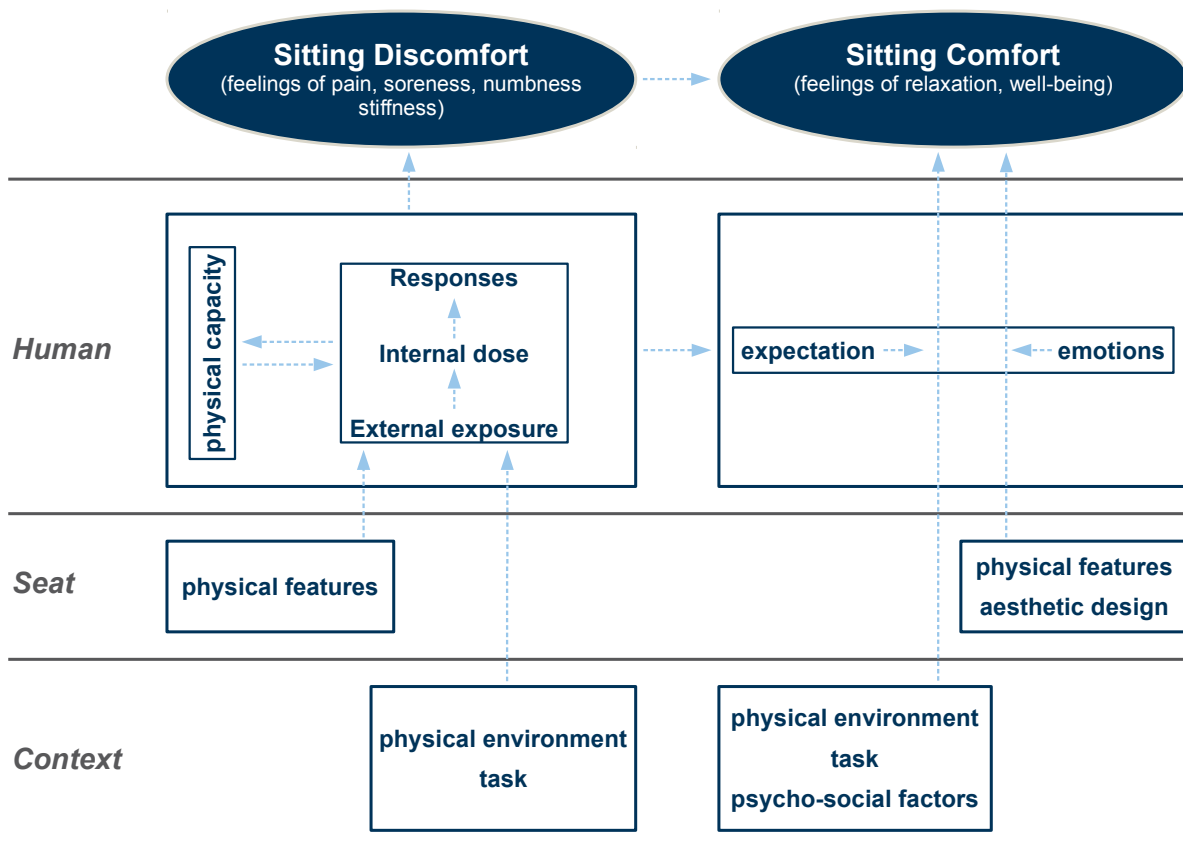


Figure 2.1: Sitting comfort model according to Looze et al. [21]

The model shows how different factors can influence comfort perception. On the left side, one can observe factors that directly influence the discomfort perception. The right side shows the comfort perception, which, as stated before, depends on the discomfort level. It is visible that soft factors like expectations and emotions, a task, or psycho-social factors do influence the comfort perception. This dependency is disregarded in current vehicle suspension ride comfort development. The latest research on sitting comfort perception has identified the need for an even more complex model [22]. The newest model for sitting comfort aims to give a framework for cognitive, postural, and physiological comfort perception [23].

Specific comfort models are not present for ride comfort in road vehicles. Discomfort is the relevant measure for vehicle development, because it is directly influenced via the technical vehicle design. Griffin [24] has summarized factors which result in separate shares to the overall discomfort in a vehicle, as can be seen in Figure 2.2. Generally, the Figure shows the shares of the total discomfort a person experiences. Individual persons will show varying sensibility for factors that contribute to the total discomfort. It is known as inter-subject variability. A persons sensibility may vary in different situations, known as intra-subject variability.

For vertical vehicle dynamics development, the vibration discomfort share is of interest. Within the scope of this research, the focus is on the vibration (factor) from stochastic road excitation. Longitudinal and lateral dynamics and single obstacles form individual research topics and are not considered.

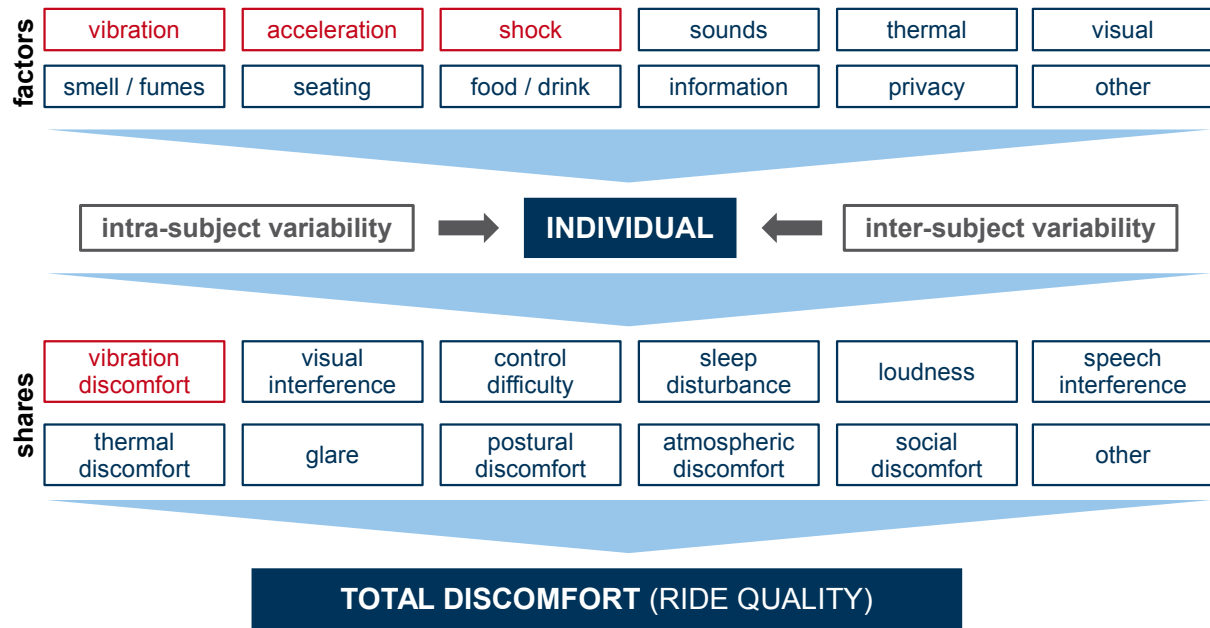


Figure 2.2: Different factors contributing to discomfort, modified in colors from Griffin [24, p. 44]. Red boxes are marked by the author to visualize factors related to vertical vehicle dynamics ride comfort within this thesis work

2.2.2 Objectification Methods

It is necessary to use numeric metrics to quantify the effects of vehicle components, such as the suspension system, on the perceived ride comfort. The human being senses vibration through the visual, vestibular, somatic, and auditory systems, where each system can sense vibration in more than one way [25, p. 15]. These stimuli are essential for the perceived vibration discomfort.

The goal of objectification methods for ride comfort is to provide an objective characteristic value, which corresponds to the subjective impression of a human being. Objective measures for vibration discomfort are calculated using acceleration and angular rate measurements. These measures can help to detect differences that are subjectively not noticeable and are independent of side effects like noise or static seating comfort [26].

Objectification methods for ride comfort are subdivided into customer-centric and development-centric methods, depicted in Figure 2.3. The development-centric methods are splittable into phenomenon-centric and vehicle-centric. The state of research for the three different types is summarized in the next section.

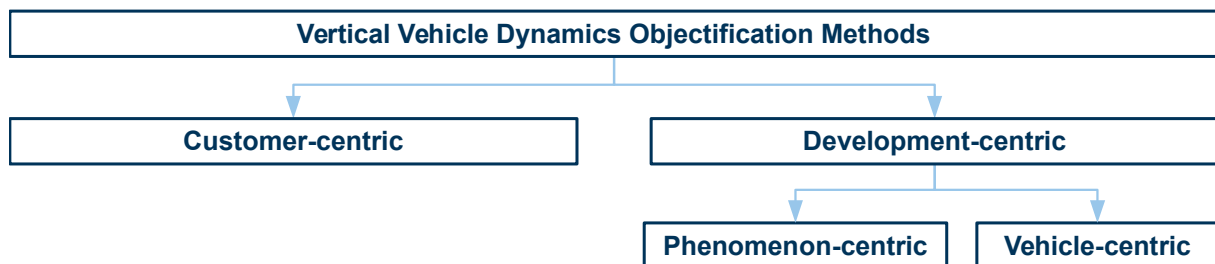


Figure 2.3: Categorization of objectification methods in vertical vehicle dynamics

Customer-centric Methods

Customer-centric objectification methods aim at quantifying the perceived vibration discomfort, independent of the vibration source. One of the first works regarding customer-centric objectification methods is from Simic [27] in the year 1970, who related the frequency-dependent sensitivity of a human being to vibration experienced while walking. Already in the year 1978 good correlation was found for RMS acceleration measurements to subjective ratings [28].

The frequency-dependent sensitivity in combination with RMS values is used in the standardized methods according to ISO 2631 [29], BS 6841 [30] and VDI 2057 [31]. These three methods are similar and follow the principle shown in Figure 2.4. Acceleration and angular rate signals are captured, modified by frequency-dependent filtering and directional dependent weighting, and then summarized as combined RMS discomfort value. The three methods slightly differ in their weighting functions and some additional discomfort values, in example for vibration with a high amount of transient phenomena or shocks [24].



Figure 2.4: Basic principle of standardized vibration assessment methods according to ISO 2631 [29], BS 6841 [30] and VDI 2057 [31]

An effective discomfort value of 0.5 m s^{-2} according to ISO 2631 [29] or VDI 2057 [31] is considered as threshold value for long-term activity. It is endurable without negative health effects, but barely reached in modern road vehicles [32, p. 491]. Negative health effects are observed for construction work and earth-moving machinery vehicle operation [33]. Extended methods, which aim to improve the standardized methods have been developed by Rericha [34], Klingner [35, 36], Hennecke [37], and Cucuz [38].

An independent investigation within the scope of a student-thesis work showed that the extended methods performed worse than the original methods, as they showed worse correlation to the subjective ratings than the standard methods subject-study [39]. Bitter [40, p. 141] likewise observed that the standardized methods are robust and give a good indication of discomfort, but the enhanced methods performed reasonably in his investigation.

Special methods regarding customer-centric objectification are based on neural networks [41] and random forests [42]. A problem with these methods is that they were not tested for generalization. Likewise, they were impossible to verify because the trained algorithms were unavailable. Another approach is the usage of perception dimensions with frequency weighted RMS values [43, 44]. In parallel to the research which is presented here, a new customer-centric objectification method is developed using body-based measurements [45, 46, 47].

Phenomenon-centric Methods

Phenomenon-centric objectification methods aim to characterize the vehicle vibration in terms of categories that are relevant to different vehicle assemblies, such as the suspension systems, bushings, the chassis, and the drive-train. Examples of these categories are "body- and wheel-vibration", "chassis tremble" or "engine shake". An extensive list of categories is described in full detail by Mitschke [19, pp. 530–531].

Kudritzki [48] introduced a ride-meter, which could display real-time scores on a computer regarding different categories during the test drive of a vehicle, which was based on RMS values calculated from different signals and filtering methods. A similar approach is applied by Jörissen [49], who uses spectral analysis of accelerometer and gyro signals. A mixture of time-domain (RMS values), and frequency-domain (PSD spectra) difference measures can be used to generate psychometric functions for difference detection [50, 51].

Another option is to define development-centric criteria specifically for single obstacles and short-wave excitation (harshness) performance [52, 53]. A method for long-duration discomfort assessment in vehicle seats does exist and is based on surface electromyography [54].

Vehicle-centric Methods

Vehicle-centric methods have a different approach compared to customer- and phenomenon-centric methods. These methods objectively describe the vehicle vibration behavior, for example to inspect changes between different vehicles or vehicle set-ups. Compared to development-centric methods, they do not aim to distinguish different phenomena specifically and do not quantify the perceived ride comfort itself like customer-centric methods. It is left to an engineer to interpret the results of a vehicle-centric objectification method. The vibration characteristic of a vehicle can be specified by using identified transfer functions [55, 56], modal decomposition [57] or co-variance analysis [58].

2.3 Vertical Vehicle Dynamics

The conflict of objectives between ride comfort and road holding characterizes vertical vehicle dynamics suspension development. Soft suspension systems, which offer good ride comfort, have poor performance in controlling dynamic wheel load variations. Stiffer suspensions with higher damping are good in road holding but result in an uncomfortable ride. Passive systems force a compromise between the two, depending on the type of vehicle. Semi-active and active suspensions help to resolve the target conflict but are restrained to specific characteristics of the dynamic system [59, 60]. They describe these constraints in transfer functions of the road excitation to the vertical body acceleration, suspension displacement, and dynamic wheel load variation [61, 62, 63].

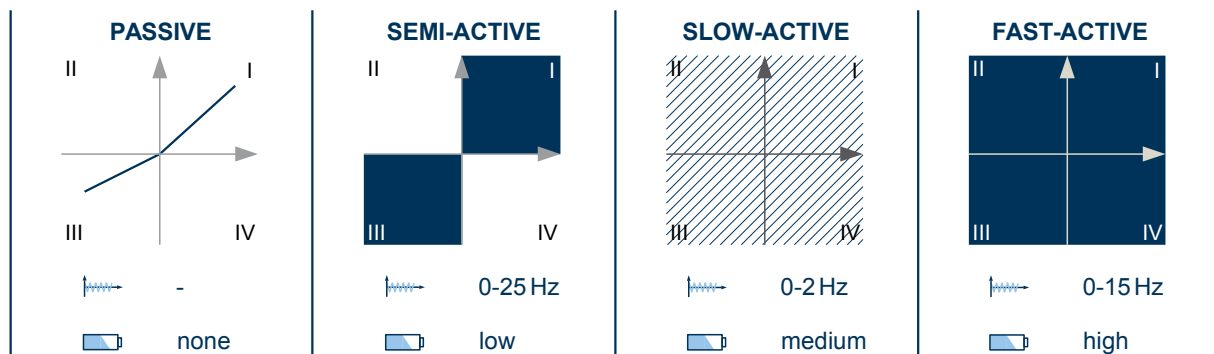


Figure 2.5: Classification of suspension systems as force (y-axis) over velocity (x-axis) pictograms, adapted from Kallenbach et al. [64], with added indicators for control bandwidth and actuator energy consumption

Suspension systems can be organized according to Figure 2.5, namely passive, semi-active, slow-active (including adaptive systems), and fast-active suspension systems. The pictograms show damper/actuator force (y-axis) over velocity (x-axis). Quadrants I and III are the passive quadrants, where a generated force is dissipative and adds damping to the system. Quadrants II and IV are non-dissipative, a generated force adds energy to the system.

- **Passive systems** have no actuators which consume energy, but cannot actively alter the dynamic vehicle behavior. They define the constant system dynamics for a vehicle.
- **Semi-active systems** have low energy requirements but can influence the suspension behavior in a broad frequency range. A drawback is their restriction to dissipative forces.
- **Slow-active systems** have medium actuator energy consumption and can supply non-dissipative forces. They are suited to counteract chassis movements from longitudinal and lateral acceleration and are often used to compensate for vehicle loading.
- **Fast active systems** can manipulate the system dynamics up to and above the wheel eigenfrequency with desired force within actuator limitations. They demand more energy than other systems and are more expensive due to the increased complexity.

A detailed description of the different systems is given in Subsection 2.3.1 Suspension Systems, followed by the introduction of vehicle models in Subsection 2.3.2 and vertical vehicle dynamics control systems in Subsection 2.3.3. Finally, road surface modeling and classification are presented in Subsection 2.3.4.

2.3.1 Suspension Systems

Springs, dampers, and Anti-Roll Bars (ARBs) determine the passive suspensions characteristics in conjunction with the body mass and the unsprung masses. Figure 2.6 shows the front and rear axle of a Bayerische Motorenwerke (BMW) 7-series (F01) indicating common installation points. The front axle is a double-wishbone, the rear axle an integral-link suspension. Springs and dampers are combined in struts, the ARBs are pivoted in the suspension sub-frames.

Most passive springs in modern road vehicles are coil springs made from steel, some exceptions being air-springs and steel or composite leaf springs. ARBs are in most cases made of steel and form a torsional spring. They connect both wheels of an axle, supported by bearings mounted to the chassis. Regular suspension springs carry the static weight of the vehicle and get compressed or extended in heave, pitch, roll, and single-wheel movement. The ARBs are only active in roll or single-wheel bump and then supply a parallel stiffness to the standard suspension springs.

The springs and ARBs in combination with the masses and tire stiffness define the un-dampened eigenfrequencies of the vehicle. A soft suspension with low eigenfrequencies is advantageous for ride comfort but requires a lot of suspension travel and is suboptimal for vehicle handling under longitudinal and lateral acceleration. For a stiff suspension with a high eigenfrequency, the opposite applies.

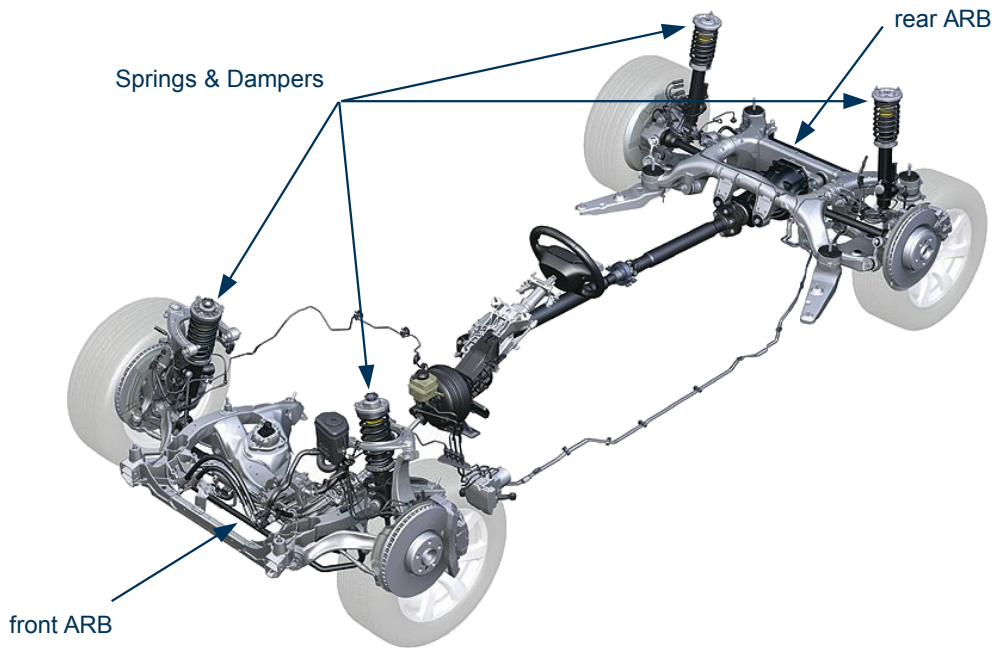


Figure 2.6: Front and rear suspension of a BMW 7-series (F01) [65, 66]

To avoid resonant vibration and control the vibration amplitude, damping is necessary. Suspension bearings and bushings add some damping due to friction, which is sub-optimal due to stick-slip effects. It should be as low as feasible. Viscous damping is added through suspension dampers to control the suspension dynamics favorably. Road vehicles suspension eigenfrequencies are in the range of 1–2 Hz, suspension damping is usually between 30–40% of critical damping. Wheel eigenfrequencies are generally found between 10–14 Hz.

Passive Suspension Elements

Figure 2.7 shows examples of passive spring, dampers and ARBs. Figure 2.7a shows a coil spring and two types of air springs. The dynamic system behavior of air-springs was extensively investigated by Boyraz [67, 68]. An example of an air suspension is given in [69]. Figure 2.7b shows a mono-tube, a twin-tube, and a twin-tube McPherson strut damper from left to right. Figure 2.7c shows an anti-roll bar (ARB).

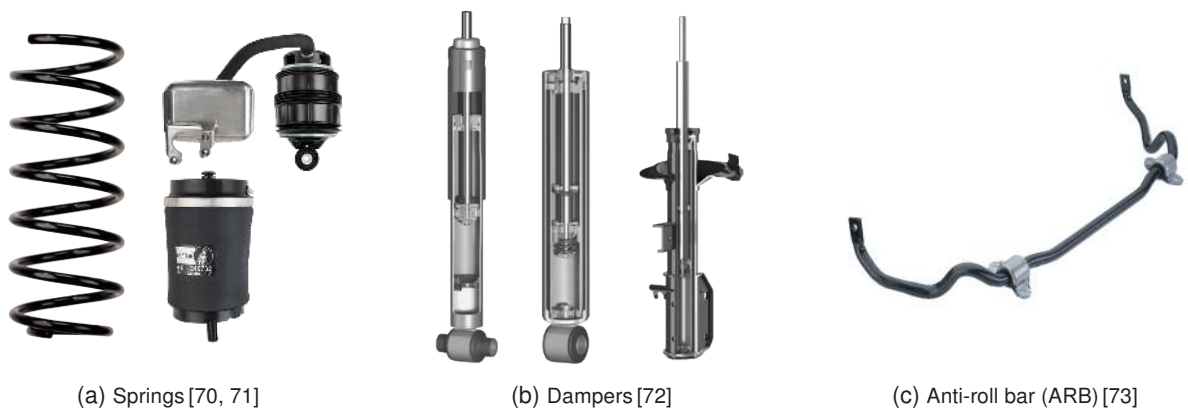


Figure 2.7: Passive suspension elements

Standard mono- and twin-tube dampers are commonly used at the rear axle, McPherson struts mainly at the front axle. The first hydraulic gas damper for planes was patented in 1934 [74]. It was an advancement of a shock-absorbing landing gear from 1933 [75]. Both systems were patented by the Cleveland Pneumatic Tool Company. Further information on dampers is supplied by Dixon [76] and Neal et al. [77].

A typical passive ARB is pictured in Figure 2.7c. It is a bend steel tube with attachment points at both ends. In its simplest form, an ARB has the shape of a "U". Due to the available installation space and required clearances, it might be altered with different bends. Technically, an ARB is a torsion spring. Its stiffness is determined by the relation of the lever lengths to diameter and wall thickness of the tube.

As stated in Section 1.1, the state-of-the-art design process in ride comfort is based on targets from previous experience [66, 78, 79, 80, 81]. For passive suspension systems, virtual methods can help with the basic suspension layout. Genetic algorithms or particle swarm optimization are options for parameter optimization of passive suspension systems [82, 83].

Multi-objective optimization methods can be applied to optimize the passive system for different road classes and traveling velocities [84]. The influence of damper characteristics on ride comfort can be evaluated with a semi-parametric damper model and a verified full vehicle model [85]. It is feasible to perform objective and subjective suspension tuning by using driving simulators [86].

Historic development of (Semi-)Active Suspension Systems

Citroen developed the first „active“ suspension system in France [87]. It was installed at the rear axle of the Traction Avant, and on both axles of the Citroen DS. Today, this system is classified as a slow-active or adaptive suspension system. It is composed of spheres filled with oil and air, combined with a pump, to allow self-leveling and adjustable ride height [88]. The spheres themselves are similar to an implementation in a landing gear from 1933 [75].

In 1974 Karnopp, Crosby and Harwood developed the idea of a semi-active suspension system in combination with the Sky-Hook Control (SHC) principle [89]. SHC is the most commonly used state-of-the-art control logic today and will be explained in Subsection 2.3.3 Control Systems.

The first semi-active suspension system for production cars came with the Toyota Soarer in 1983 [90]. The Lotus Formula One Team initiated fast-active suspension systems in cooperation with Cranfield University. Aerodynamicist Peter Wright and Professor David Williams invented a hydraulic system, initially in an attempt to prevent porpoising², later to regain lost downforce due to the ban of ground-effect side-skirts [91].

Wright and Williams derived the control system from fly-by-wire. It was successfully tested in a Lotus Esprit road car at the end of 1982, before being used in formula one in 1983 and 1987 [92]. The control algorithm, named Lotus Modal Control (LMC) was developed by Williams [93]. A more commonly known active suspension was developed by the Williams F1 Team, in collaboration with AP Racing [94]. It was introduced in 1987 and used until 1993, but was solely a slow-active system [91].

The first slow-active suspension for series production vehicles, named Magic Body Control (MBC), was introduced in 2001 by Daimler [95]. Its basic principle is a hydraulic adjustment of the suspension spring attachment points. The first fast-active system intended for series production vehicles was developed by Bose Corporation, which was presented to the public in 2004 and is

²porpoising: resonant pitch-oscillations due to aerodynamics on ground-effect race cars

depicted in Figure 2.8. It uses controlled bidirectional linear electric motors, torsion springs to carry the vehicle body, and mass-dampers integrated into the wheel carrier [96]. Due to cost and complexity, this system never made it into series production vehicles.



Figure 2.8: Bose active suspension [97]

Semi-Active Suspension Systems

Semi-active systems continually increased in market share in the 1990s and early 2000s. The most common semi-active systems are either Magneto-Rheological (MR) or Variable-Valve (VV) systems. MR dampers offer an increased working range in the force-velocity map [98, p. 138], but show a temperature dependency that leads to decreased performance at low temperatures and are more expensive compared to VV dampers [99, p.12]. Figure 2.9a shows an example of a VV damper named Continuous Damping Control by ZF. Figure 2.9b shows the Magnetic Ride system of Audi, which is a MR damper system.



(a) ZF Continuous Damping Control [100]



(b) Audi Magnetic-Ride [101]

Figure 2.9: Semi-active suspension systems

The shifting times between different damping curves are similar for both systems and lie around 0.015 s to 0.02 s [98, p. 141, 102, p. 24]. It translates to a maximum control frequency of about 60 Hz. This is five times higher than the usual unsprung-mass eigenfrequencies, and therefore fast enough to control the wheel dynamics. The maximum slew rate of these systems is around 125 kN s^{-1} [102, p. 24]. The modeling, design and control of MR dampers is described in [103, 16

104, 105]. Self-sensing MR damper are introduced by Hu [106]. Ahmadian [107] investigated improvements in ride comfort through semi-active suspension systems. Examples for the implementation of VV system are given in [108, 109, 110]. A recent summary on semi-active systems has been performed by Soliman [111].

Active Suspension Systems

The MBC system of Daimler is depicted in Figure 2.10 [112]. This system was combined with preview information through a camera system and later called Active Body Control (ABC). Other suspensions with similar foot-point adjustment systems are presented in [113, 114]. An advancement of the initial hydro-pneumatic system of Citroen is the Hydroactive CRONE suspension [115, 116].



Figure 2.10: Mercedes Benz Magic Body Control [117]

An alternative to foot-point adjustment are active-ARBs systems. Figure 2.11a shows the ZF Electromechanical Roll Control, and Figure 2.11b the Active Roll Stabilizer of Schaeffler. Both are 48 V electromechanical systems; the ZF system is described in detail by Sagewka et al. [118]. Previous systems were electro-hydraulic, like the Active Roll Control system of BMW [119].



(a) ZF Electromechanical Roll Control [120]

(b) Schaeffler Roll Stabilizer [121]

Figure 2.11: Slow-active suspension systems for roll control

A full-active suspension system used in series production cars is the electric Active Body Control (eABC) system of Daimler, depicted in Figure 2.12b [122]. It uses pressure reservoirs installed in the space of the ARB of the conventional suspension. The pressure is used to move the damper piston, which is equipped with semi-active damping valves. Another system intended for series production is the Audi AI suspension, shown in Figure 2.12a [123].

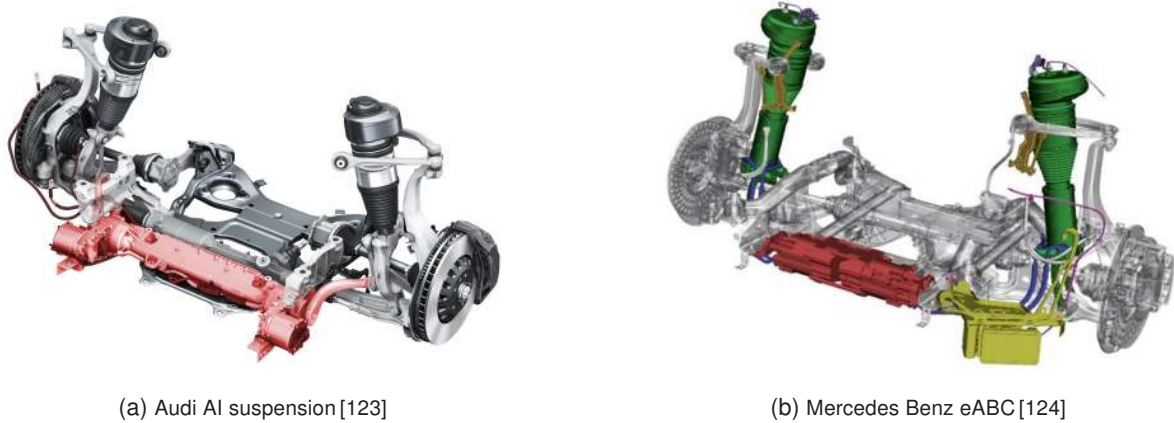


Figure 2.12: Fast-active suspension systems

There exist other systems, which are not yet planned or seen in production cars. An electro-magnetic active suspension is presented by Gysen et. al [125]. and a full-active air spring by Lenz et al. [126]. Other fast-active systems have been developed by Clearmotion [127], Tenneco [128] and ZF [129]. An overview of these systems, comprised of a summary of their performance parameters and technical comparison, has been performed by Mair [130].

A general overview on mechatronic systems for vertical vehicle dynamics and references to further reading is given by Heißing et. al [131]. Information on electromechanical actuators is supplied by Isermann [132, p. 451-461]. A test method for active suspension actuators, exemplary executed for active ARBs, was developed by Zilkens [133]. Based on actuator test data, map-based actuator modeling can be performed, and integrated into advanced vertical dynamics simulation models [134, 102, 135].

2.3.2 Vehicle Models

To describe the system dynamics of vehicles with respect to road excitation, mechanical models are needed which can be used in simulation or control systems. This section introduces the two most important models for vertical vehicle dynamics development, the quarter vehicle model and the five-mass vehicle model.

Quarter-Vehicle Model

A simple and efficient simulation model is the quarter-vehicle model, shown in Figure 2.13a. The left side shows a passive model. It represents the corner of a vehicle, where the upper two blocks correspond to the proportional sprung, and the un-sprung mass at the vehicle corner. The upper spring and damper belong to the suspension, the lower spring and damper represent the tire.

The model is characterized by the corresponding body mass at the vehicle corner m_{Bo} , the unsprung mass m_{Wh} , the suspension stiffness c_{Bo} , the tire stiffness c_{Wh} , the suspension damping d_{Bo} and an optional tire damping d_{Wh} . Based on a road excitation z_{Ro} , the resulting body z_{Bo} and wheel displacement z_{Wh} and their derivatives can be investigated with this model.

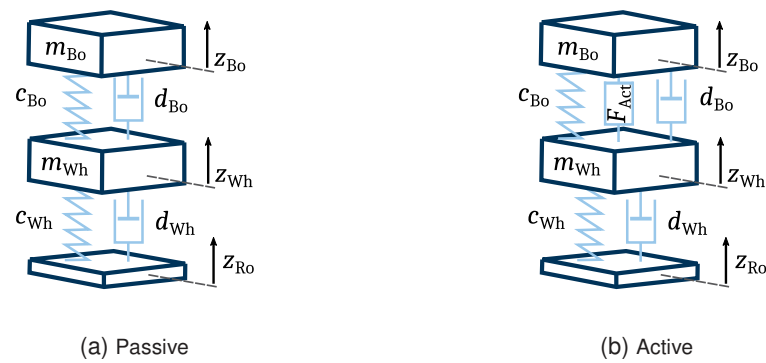


Figure 2.13: Quarter vehicle models, modified from Jazar [136, p. 856]

An extension of this model is depicted on the right of Figure 2.13b, which is extended by an actuator force F_{Act} . Both models can be used to analyze the objective conflict between ride comfort and road holding, perform parameter sensitivity analysis of different mass, stiffness, and damping parameters, or analyze different suspension control algorithms. Top-mount bushings can be incorporated into the quarter vehicle model [137].

Five-Mass Model

Analyzing the pitch and roll behavior of a two-track vehicle with two axles requires a five-mass model. This model is shown in Figure 2.14. The passive five-mass model possesses the same stiffness and damping parameters as the quarter vehicle model at each corner. The body mass is now the total sprung mass m_{Bo} , the body has roll inertia J_{xx} and pitch inertia J_{yy} . In contrast to the quarter vehicle model, which has two degrees of freedom, the five mass vehicle model has seven Degrees of Freedom (DoF). The model assumes the roll and pitch axis in the ground plane, and uses the small-angles assumption. It can be extended with actuator forces at each corner and passive or active ARBs on each axle.

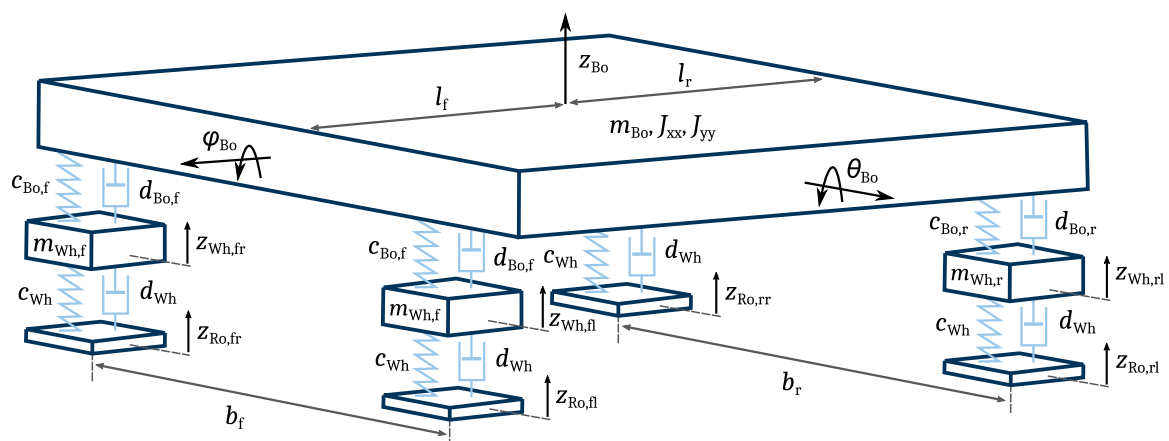


Figure 2.14: 5-mass model, similar to Jazar [136, p. 856]

Information on modeling for vehicle dynamics simulation is summarized in [138], and different vehicle suspension types are explained in [139]. A literature survey on vehicle dynamics model validation is given by Kutluay [140]. Halfmann [141, pp. 87–93] and Viehof [142] performed vertical dynamic model validation and analysis of different errors in vehicle models.

The tire to road contact modeling is a topic of ongoing research [143, 144, 145, pp. 231–286]. Especially the contact patch estimation and dynamics are of interest [146, 147]. Different modeling techniques were investigated as well [148]. The tire-road contact model has a strong influence on the dynamic wheel load variation but a marginal influence on ride comfort measures [149].

Within the scope of this thesis work, an extended version of the five-mass model is used for the investigation in Chapter 7. The EoM for the utilized model are derived in Subsection 7.1.1. Secondary stiffness and damping due to bushings is integrated into the main suspension stiffness and damping. This simplification is made to avoid large eigenfrequencies in the model, which in example occur when modeling the suspension top mount. Friction and stick-slip effects are assumed to be negligible, because within this research, all simulations are performed on medium to low quality roads.

2.3.3 Control Systems

Active and semi-active suspension control systems consist of an outer and an inner control loop. From a control systems perspective, this is called cascade control. The outer control loop calculates and demands control forces that need to be supplied by the actuators. The inner control loop, called the actuator control loop, uses the desired force as a reference value and regulates the actuator to supply the desired force [150]. In vertical vehicle dynamics, the outer control loop calculates the reference forces based on quantities that are related to the heave, pitch, and roll dynamics of the vehicle. These quantities are directly measured or estimated by using state-estimators [151].

PID-Control

One of the first control principles for vertical dynamics, the SHC principle by Dean Karnopp [89, 152, 153], is still one of the most commonly used controllers. Pure SHC is a proportional gain controller on the heave velocity of the vehicle body. It is a form of classic Proportional-Integral-Derivative (PID) controller, which is drawn as flow-diagram in Figure 2.15. Based on control errors $e(t)$, which are calculated from reference values y_{set} and the actual output values $y(t)$, control forces $u(t)$ are calculated based on gains (c_p , c_i , c_d), which are multiplied to the errors, the integrals of the errors and the derivatives of the errors respectively. The control forces $u(t)$ are used to manipulate the plant dynamics, which are subject to disturbances $v(t)$.

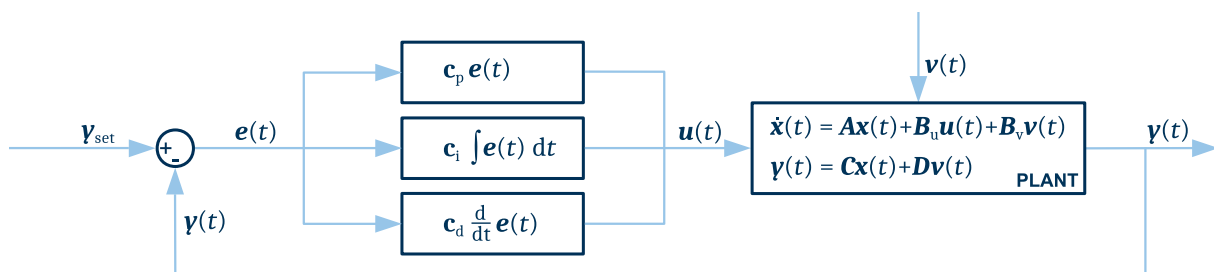


Figure 2.15: PID controller

The classic SHC principle of Karnopp [153] can be extended to modal SHC for heave, pitch and roll [154]. In any case, SHC uses set-points of zero for the inertial velocities³ and proportional gains (skyhook damping constants) to calculate the actuator forces. Pure SHC leads to large

³vertical velocity and roll/pitch rate with respect to the inertial reference frame

dynamic wheel load variations. The opposite of SHC is Ground-Hook Control (GHC), which was invented by Valasek [155]. He showed the possibility to combine SHC and GHC [156]. Another option is the combination of SHC with acceleration driven damping [157]. Latest advancements in terms of SHC are a new discrete two-state SHC logic, and the introduction of a triple-skyhook logic, which is a full PID controller [158, 159].

State-Feedback and Optimal Control

In contrast to SHC, LMC (Lotus Modal Control) was intended for active suspension systems, and its primary purpose was pitch and roll compensation while remaining compliant in heave and twist for attenuation of dynamic wheel load variation [92, 160]. The LMC logic is a form of state-feedback control, which is synthesized by pole-placement through the definition of desired stiffness and damping values in each eigenmode. Technical analysis of the physical system and the control logic has shown that the Lotus system is dynamically equivalent to an adaptive passive suspension, with the advantage of attitude control during handling maneuvers [161].

Figure 2.16 shows the basic principle of a state-feedback controller. A state-feedback controller can make use of a feed-forward share of the control force $u_{ff}(t)$, which is based on the time-dependent reference values $y_{set}(t)$ and the feed-forward matrix F . The second part of the control force, the feedback force $u_{fb}(t)$, is calculated based on the feedback matrix R and the states of the plant $x(t)$. In many real-world applications, some, or all of the system states are unknown, and therefore estimated using output signals $y(t)$.

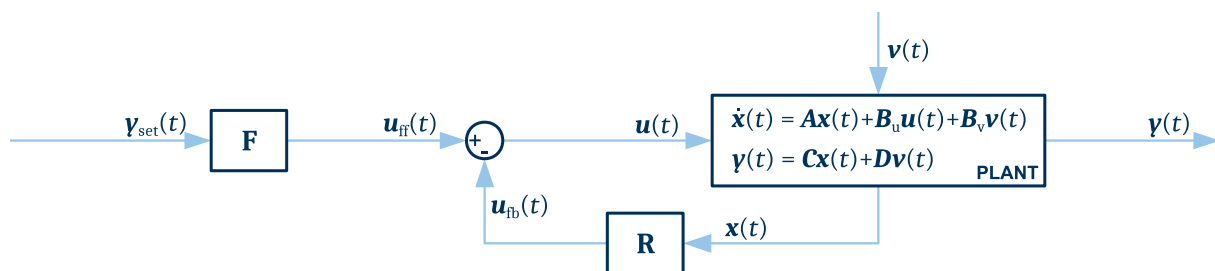


Figure 2.16: State-feedback controller

Examples of the application of the modal control principle have been given by Furihata [162], Braghin [163, 164] and Dogruer [165]. Synthesis of a state-feedback controller for vertical vehicle dynamics can be based on the classic pole-placement method through eigenvalue selection [166]. The theoretical combination of LMC and independent corner SHC has been shown by Williams [167]. LMC can be combined with modal SHC, demonstrated in simulation and real vehicle testing [168]. Similar to the modal control principle is decoupling control, which is applicable as well [169, 170].

Various optimal control applications are available [171]. Most commonly Linear Quadratic Regulator (LQR) and Linear-Quadratic Gaussian Regulator (LQG) control is used for vertical vehicle dynamics [172, 173, 174, 175]. H_∞ control is an alternative which can account for parameter uncertainties and results in a robust controller [176, 177]. Clipped optimal control can be applied with semi-active suspension systems [178].

Model Predictive Control

A special form of optimal control is Model-Predictive Control (MPC). LQR, LQG and H_∞ control are infinite-horizon optimal controllers, which means that feed-forward and feedback matrices

are synthesized based on pre-defined objectives and boundary conditions. MPC is a receding-horizon optimization. It depends on the preview and estimation of upcoming disturbances and calculates the optimal control input trajectory over the preview horizon. It is a form of feedback control because only the first control input is used. Subsequently, the optimization starts again based on the current system states. These are either measured, or estimated from output signals.

Figure 2.17 shows the schematics of a MPC. From large to small, the MPC uses the known or predicted disturbances over the preview horizon $\tilde{v}(t)$ to calculate the sequence of optimal control inputs $\tilde{u}(t)$, based on a MPC-plant model and a cost function J . The first input for the next time-step is used to manipulate the system dynamics of the plant, which is subject to the disturbance v . As for a state-feedback controller, the system states $x(t)$ have to be measured or estimated from outputs $y(t)$. In case of a linear output MPC, the difference of the predicted outputs $\tilde{y}(t)$ to their reference trajectories $\tilde{y}_{set}(t)$ over the prediction horizon is used to formulate a convex cost function J . Multiple outputs can be weighted with factors inside the weighting matrix W . The optimization can be subject to constraints on the outputs y_{lim} and inputs u_{lim} .

It has been shown that MPC can be used for vertical vehicle dynamics control [179, 180, 181, 182, 183]. For the application in real vehicles, the real-time capability of MPC is crucial, which leads to fast MPC techniques [184, 185, 186]. Other options for real time capable MPC are explicit MPC with neural networks or region-less explicit MPC [187, 188]. Another option is stochastic MPC in combination with a cloud-based road disturbance estimation [189].

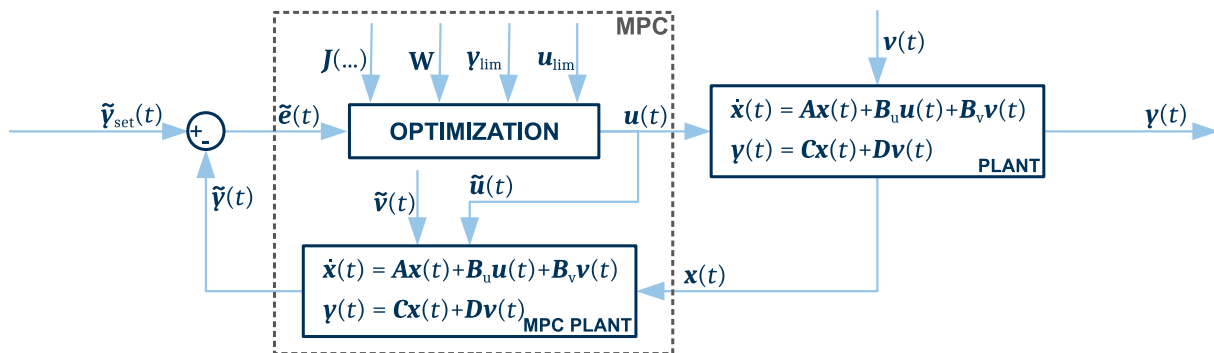


Figure 2.17: Model-predictive controller

Non-Linear and Adaptive Control

Apart from the previously described controllers, which were primarily linear controllers and only a selection from the vast amount of published approaches, there are non-linear approaches to vertical vehicle dynamics control. Velocity-based linearization can be applied to derive a non-linear control law and maintain linear analysis and design methods [190]. Actuator dynamics can be incorporated, as well as actuator and state constraints [191, 192, 193].

Preview information can be incorporated into non-linear control algorithms [194, 195, 196, 197, 198]. Different methods for the road profile estimation have been investigated as well [199, 200, 201]. An analysis of the performance potential of road preview for vertical dynamics control has shown that sensor technology is the challenge for the successful implementation in real vehicles [202].

Linear parameter varying control can be used for fault-tolerant damper control and the use of H_∞ controller design for semi-active suspensions [203, 204]. Adaptive control can be used to consider

the current driving style, compensate suspension system uncertainties, and adjust for different road profiles [205, 206, 207]. Other controllers are based on fuzzy logic or neural networks [208, 209]. The interested reader can find further information on vertical vehicle dynamics controllers in various literature reviews [210, 211, 167, 212].

2.3.4 Road Models and Classification

An integral part of vertical vehicle dynamics is the description of road surface profiles. Single obstacles like bumps and potholes can be detected using modern road vehicles' camera systems [213]. Their frequency of occurrence is one way to describe the quality of a road surface. Likewise, it is necessary to know and describe the stochastic road surface profile for vehicle dynamics simulations. These profiles determine the disturbance excitation of the suspension system based on the vehicle speed, the wheelbase, and the track-width.

Road profiles can be classified according to ISO 8608 [214] by using the displacement PSD $G_d(n)$ in the spatial-frequency n domain, defined as:

$$G_d(n) = G_d(n_0) \cdot (n/n_0)^w, \quad (2.17)$$

with

$$n_0 = 0.1 \text{ m}^{-1}$$

$$w = 2$$

$G_d(n_0)$ is the reference displacement PSD value, which is defined as mean value for the road classes A to H according to Table 2.1.

Table 2.1: Reference PSD values for different road classes according to ISO 8608 [214]

	A	B	C	D	E	F	G	H
$G_d(n_0) / 10^6 \text{ m}^{-3}$	16	64	256	1024	4094	16384	65536	262144

This classification is utilizable to generate artificial road profiles [215]. It can be performed based on an inverse FFT method [216, 217], or based on white noise filtering [218]. A comparison of the two methods has shown that white noise filtering with low-frequency cut-off, and the inverse FFT method (superposition of harmonics) are both suitable to generate artificial road profiles [219].

A stationary Gaussian process can be combined with distinct superimposed irregularities to account for manually set, deterministic obstacles like potholes [220]. The coherence between two tracks, which describes their linear dependency, is a function of the track-width and depends on the road(-section) [221, p. 148]. A pure isotropic assumption for the coherence is incorrect, and better results can be obtained with a parametric model [222].

Artificial profiles are useful for a first sensitivity analysis but should be later accompanied by simulations on real profiles to assess the ride comfort [223]. Another option to classify roads is to use the International Roughness Index (IRI), as described by Sayers [224, pp. 45–52].

ISO 8608 [214] is used to classify road profiles within this research. Artificially generated profiles were applied during the development of the simulation method presented in Chapter 7, but laser-scanned real road profiles were used for the final investigation.

3 Research Gap

The previous chapter has shown the state-of-the-art regarding ride comfort and vertical vehicle dynamics. It has indirectly shown the main criticism leading to the research gap. There is no bridge between works related to comfort (discomfort) using customer centric methods and vertical dynamic suspension development.

Investigations regarding ride comfort are mostly related to development-centric methods, not considering possible changes due to automated driving. In automated driving all drivers become passengers, having their own virtual chauffeur, possibly changing objectives when purchasing a vehicle. Previous research in semi-active and active suspension systems is not linked to passenger (customer) ride comfort requirements, because these have not been defined yet.

Biomechanically, motion interferes with fine motor skills and the perception of small visual details, which should be taken into account when considering human performance in moving environments [225]. Self-driving cars cannot be just seen as living rooms, offices, or entertainment venues on wheels [226]. It is unknown how this will influence ride comfort requirements, and in consequence vertical vehicle dynamics control systems.

This work builds upon the current state of research. It has been shown that soft factors like attention, context, and activities can influence comfort perception [22]. Naddeo [227] defines three elements determining the comfort perception inside a car: the person, the task, and the environment.

To date, ongoing research regarding discomfort and comfort has not been adapted to ride comfort development. It is unclear how current suspension systems will perform in automated driving conditions. No objective target value exists for automated driving ride comfort. There is no method to derive requirements on vertical vehicle dynamics control system actuators based on vehicle ride comfort targets. The following section will give an overview of the latest research in ride comfort concerning automated driving, and vertical vehicle dynamics control systems. It will underline the stated gap in research.

3.1 Latest Research in the Field

The longitudinal and lateral dynamics for automated driving have been subject to extensive research in the last couple of years. An automated driving maneuver should be as comfortable as possible while being as dynamic as needed [228]. Several investigations analyze and recommend characteristics for a comfortable driving style of the automated vehicle [229, 230, 231, 232, 233, 234]. The driving style in terms of longitudinal and lateral trajectories can be combined with vertical dynamics roll and pitch motion to announce these maneuvers [235, 236, 237, 238].

Another main research topic is the occurrence and avoidance of motion sickness [239, 226, 240]. The public acceptance of automated and autonomous vehicles was reviewed by Eimler [241]. It has been found that the vehicle attributes „*comfort*“ and „*vehicle dynamics*“ have low pre-purchase but high post-purchase importance to the customer [242].

In vertical vehicle dynamics, the current research is focused on virtual testing methods, connected vehicles, and the generalized formulation of requirements. Berberich [243] developed a method to assess ride comfort in a ride comfort simulator. Comfort-based route planning, with the aim of a comfort-optimal route instead of time-optimal or distance-optimal, has been proposed by Li [244].

Cloud-based vehicle ride height control, road damage detection, and road network coverage models are considered for future application [245, 246, 247, 248, 249]. The energy harvesting potential for suspension systems is negligible except for extreme scenarios with high speeds and uneven roads [250].

Development-based ride comfort requirements, and integrated vehicle dynamics development, defined as a unified approach towards planar and vertical vehicle dynamics, is possible [251, 252]. An initial suspension layout in terms of ride comfort, as a base setup for real vehicle testing, is derivable from simulation [253]. Driving dynamics requirements based on solution spaces have been investigated [254, 255]. A control system design procedure for active ARBs is described in [256]. A development-based approach for the quantification of active suspension system performance has been introduced [257].

Suspension system can be characterized using equivalent suspension parameters [258]. The interaction between dampers and top-mounts was extensively studied by Stretz [259]. The potential of active suspension systems to mitigate motion sickness was investigated by Ekchian [127] and Dizio [260]. Wenzelis [261] defined a sensation-based objectification method for vehicle roll control under lateral acceleration. Vertical dynamics controllers considering occupant dynamics were compared by Sigl [262].

To the best knowledge of the Author, no publications exist regarding the influence of actuator properties on the achievable ride comfort, except some investigations of selected properties regarding the control system performance. In the year 1988, Miller [263] investigated damper hardware limitations for an on/off semi-active suspension system. Qin [264] examined the influence of control system time delay on semi-active suspension control strategies. Schickram [265] explored the impact of sensor faults on ride comfort performance. The lack of investigations regarding ride comfort targets and the role of actuator limitations leads to the criticism of the current state of research.

3.2 Criticism

It is expected that analog to the general importance of comfort, the share of ride comfort (from vertical dynamics) will increase for automated driving vehicles. This expectation needs further investigation and proof. The performance of current suspension systems in automated driving conditions is unknown and needs investigation. Side tasks may influence the perception of road disturbances, but have not been investigated yet.

An objective target value for ride comfort in automated driving has to be derived to enable objective development methods, obtaining reliable and repeatable results. Current development-

based objectification methods are not suitable to develop automated vehicles, because of no previous experience to set relative targets, and because of a missing link to the subjective assessment of passengers. Target values might differ depending on the vehicle class, which should be investigated.

The influence of suspension system actuator limitations on achievable ride comfort needs investigation. A method is required that allows development based on target values for ride comfort during an automated drive. Current active suspension systems have not been tested regarding their ride comfort performance in relation to their actuator properties, nor to passive or semi-active suspensions.

3.3 Aim and Limitations

This thesis work should contribute to research regarding vertical vehicle dynamics ride comfort, particularly in hindsight of automated driving. It interrogates the assumption of an increasing ride comfort importance. The performance of current suspension systems is analyzed for automated driving conditions. An objective target value for ride comfort during automated driving is determined as Key Performance Indicator (KPI). Additionally, a method is developed for deriving and investigating suspension system requirements based on an objective target value for ride comfort.

A cornerstone for this PhD thesis are pre-investigations regarding the difference between conventional and automated driving ride comfort, performed in close collaboration with Georg Burkhard [45, 46] (University of Duisburg-Essen). A second foundation is an investigation regarding suitable objectification methods for ride comfort based on vehicle measurements, conducted within the scope of Felix Fent's Bachelor's Thesis at Technical University of Munich (TUM) [39].

This research is subject to some limitations. The effect of longitudinal and lateral vehicle dynamics on ride comfort is excluded. Steady-state driving under low longitudinal and lateral accelerations is the focus. It is expected to be one of the first use-cases for automated driving on highways. The inter-dependency and order regarding ride comfort from longitudinal, lateral, and vertical dynamics are not investigated. Long-term effects are excluded from this research. All content is related to a duration of up to half an hour, due to the driving duration for test-persons in the driving-simulator studies. Long-distance driving comfort or long-term motion sickness need separate investigations.

3.4 Research Questions

How does a shift towards automated driving vehicles affect vertical vehicle dynamics ride comfort requirements, and what does it imply for suspension control systems. To answer this, sub-questions are formulated and grouped in pairs of two. The first pair of questions is investigated with an online survey in Chapter 4, related to the general importance of ride comfort. The following two are answered in Chapter 5, and are related to current suspension systems and passenger state of attention. Questions five and six are studied in Chapter 6, linked to an objective target value for automated driving. The final two questions explored with the help of a new simulation method presented in Chapter 7. This is the complete list of research questions:

RQ 1.1: How decisive is ride comfort to the customer?

RQ 1.2: Will the importance of ride comfort increase considering automated driving?

RQ 2.1: How do current state-of-the-art suspension systems perform in automated driving?

RQ 2.2: Do side tasks effect the sensitivity for road disturbances?

RQ 3.1: What is the objective target value for automated driving ride comfort?

RQ 3.2: Do ride comfort expectations differ for compact and luxury class vehicles?

RQ 4.1: Can suspension actuator requirements be derived from ride comfort targets?

RQ 4.2: What are typical actuator requirements for an ideally comfortable vehicle?

4 Survey on Ride Comfort in Passenger Cars

The literature review showed that there is currently no survey specific to ride comfort in passenger cars. The following survey was conducted to understand the importance of ride comfort for the customer and investigate if it changes from traditional driving to automated driving. This chapter is related to research questions RQ 1.1 and RQ 1.2. The questionnaire design and the applied analysis methods are described in Section 4.1, before the results are shown in Section 4.2. Finally, these results are interpreted and discussed in Section 4.3.

4.1 Method

The survey was intended for the general public and people older than 18 years. It was conducted in the German language and distributed via e-mail and social media. It took seven to ten minutes to fill in the answers, and the survey was created with the tool „LimeSurvey“.

4.1.1 Questionnaire Design

The questionnaire starts with a short introduction to explain the terms „automated driving“ and „ride comfort“, to assure the same understanding of these terms for all survey takers. Personal information, such as gender, age, and attitude towards automated driving, was gathered next, followed by questions regarding the current vehicle and, if applicable, its vehicle class and the rating of its ride comfort. It was asked which types of suspension systems are known, ranging from passive suspensions to full-active suspensions, and if the suspension system or the ride comfort is something the survey taker explicitly recognizes. Questions regarding the importance of ride comfort in conventional and automated vehicles formed the main body of the survey.

The interviewees were asked to assess the importance of ride comfort while driving and being driven in a conventional car. Later, they were asked to assess the importance when being driven automated. For the assessment, five-point semantic differential scales were used, with the anchor points „unimportant“ and „important“. These scales were used for 21 different buying criteria ratings, once for a conventional vehicle and once for an automated vehicle. This procedure allowed investigating the change in the importance of ride comfort and its relevance compared to other factors. The different criteria have been based on a pre-survey, where people were asked what the essential buying criteria are. The collected answers were grouped into main criteria to be rated in this survey.

After creating the initial survey, it was tested with a small group of 5 people to validate the questionnaire and eliminate errors or misunderstandings. The accessibility was checked for different devices like smartphones and personal computers. The survey was active for two months, from the beginning of July to the end of August 2020.

4.1.2 Analysis

Descriptive statistics, like median, mode, minimum, and maximum, are used for the data analysis. The different ratings are visualized with box plots to give a compact overview of the results. Supplementary bar plots are shown to facilitate the identification of the mode, and give a qualitative representation of skewness or kurtosis in the data.

For inferential statistics, the Wilcoxon signed-rank test is used to test for significant pairwise differences between conventional and automated driving. To avoid the "Look-elsewhere Effect", the Bonferroni correction is applied to the 5% significance threshold. Cohen's *d* is used as a measure of effect strength, which is calculated from the *z*-statistics of the Wilcoxon test. Further information about these methods can be found in Subsection 2.1.4.

4.2 Results

The presentation of the results is split into two parts. The evaluation of the questions on general information of the survey takers is presented in Subsection 4.2.1, the analysis of differences between conventional and automated driving is shown in Subsection 4.2.2.

The sample composition of the survey is shown in Table 4.1. In total, 125 people completed the survey, with an average age of 33.5 years and a standard deviation of 11.9 years. The minimum age was 19 years, the maximum age 68 years. 35.2% of the participants were female, 64.8% were male.

Table 4.1: Sample composition of the online survey

N	avg. age	std. age	min. age	max. age	male / female
125	33.5 yrs	11.9 yrs	19 yrs	68 yrs	64.8% / 35.2%

4.2.1 General Information

Figure 4.1 gives an overview of the survey results regarding the background information. It was asked if the survey taker has regular access to a car. It was further asked if this car is a Sports Utility Vehicle (SUV). It was further asked if ride comfort is a factor with regard to their current vehicle. Additionally, it was asked if they pay attention to the suspension system and the resulting ride comfort or sportiness of a car. Each question could only be answered with yes or no.

The results show that 92.8% possess or have access to a car, 18.1% drive a SUV, 34.4% pay attention to the suspension system, and 27.2% care about ride comfort in their current vehicle. Most of them rate the comfort supplied by their current vehicle as „neutral“ or „rather good“ (see Appendix A.2).

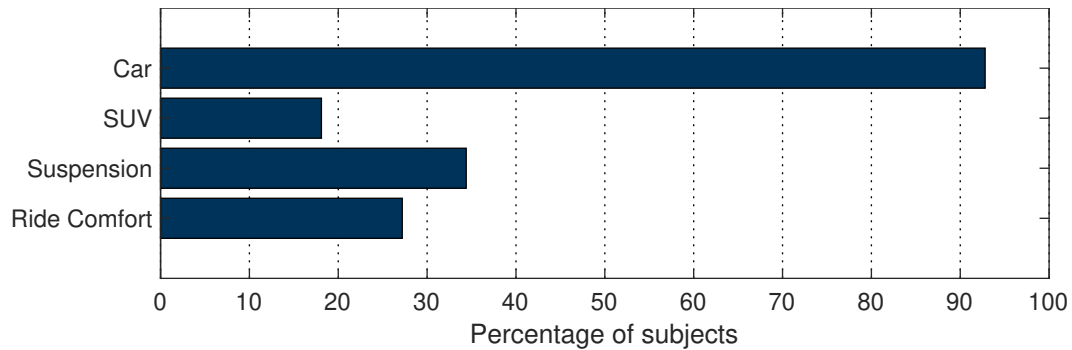


Figure 4.1: Background information on car ownership and attitude towards suspension systems and ride comfort

Another question asked was which types of suspension systems the survey participants were familiar with. There was a short explanation for each type of system with some examples of production car applications. Figure 4.2 shows that 22.4% do not know any type of vehicle suspension system. 76.0% know about passive suspensions, 58.4% know about adaptive systems (e.g. self-leveling), and 37.6% know semi-active dampers. 41.6% have heard of slow-active systems like Mercedes Benz ABC/MBC or the Citroen Hydractive Suspension. Fully active systems like the Bose Active Suspension, Mercedes Benz eABC or the Audi AI Suspension are known to 32.0%.

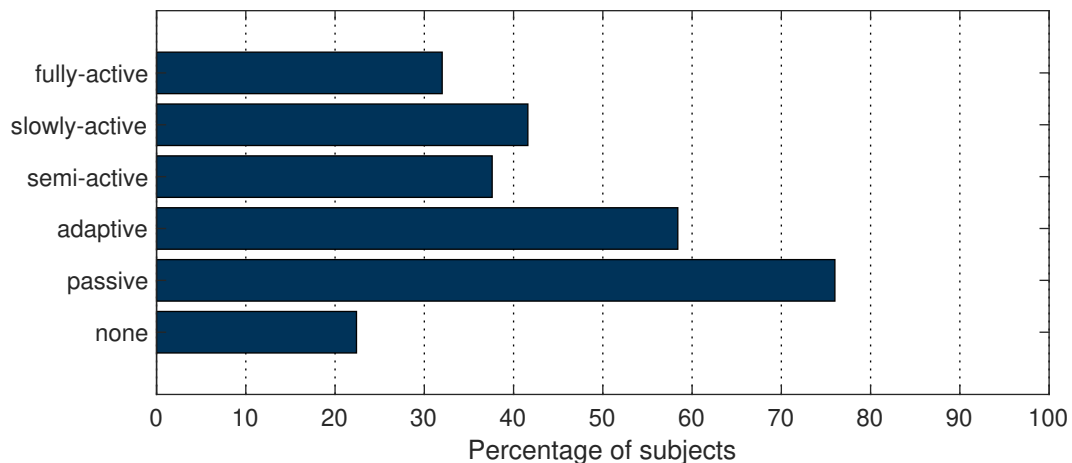


Figure 4.2: The subjects' knowledge of suspension systems

4.2.2 Conventional versus Automated Driving

The survey's main purpose was to investigate changes in the importance of ride comfort from conventional to automated driving. Figure 4.3 displays the ratings of importance for ride comfort. It was asked separately for being a driver and passenger in a conventional vehicle, and being a passenger in an automated vehicle. For conventional driving, both, as a driver and as a passenger, the median is „rather important“, with an interquartile range from „neutral“ to „rather important“ and whiskers at „rather unimportant“ and „important“. For automated driving, the median is „important“, the interquartile range from „rather important“ to „important“ and only a lower whisker at „neutral“. The mode is equal to the median for all three categories. It is „rather important“ for conventional driving and driving as a passenger, and „important“ for autonomous driving. The results hint towards ambivalence for conventional driving and an increase in comfort demand for automated driving. This will be verified with hypothesis tests.

4 Survey on Ride Comfort in Passenger Cars

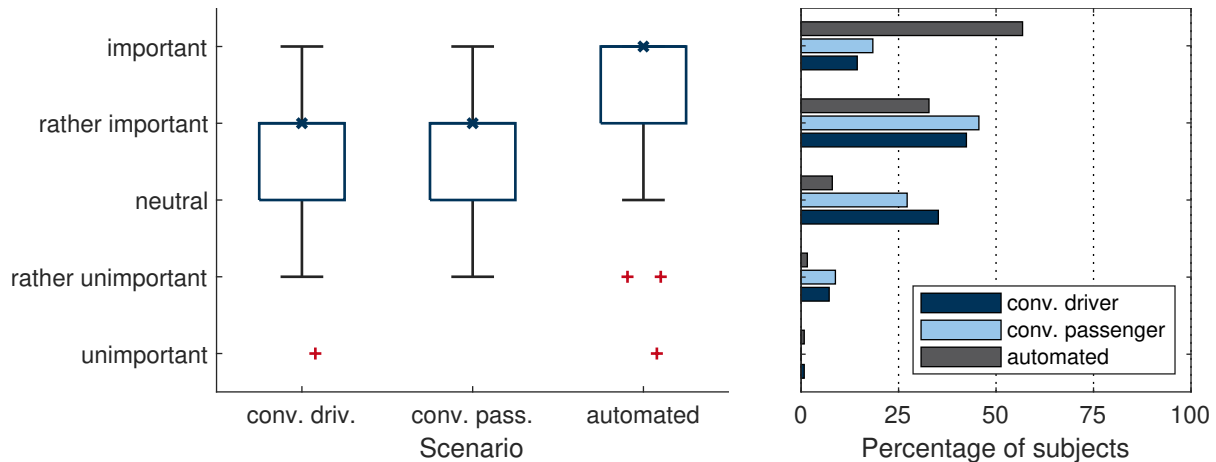


Figure 4.3: How do you rate the importance of ride comfort, as a driver, as a passenger and in automated driving? Red crosses show rating-outliers

The null hypothesis was formulated that ride comfort importance ratings are the same for each of the three scenarios to test for significant differences. A Wilcoxon signed-rank test indicates that the ratings of the automated scenario are significantly higher compared to the ones of the conventional passenger scenario ($Z = 6.6$, $p < 0.001$, $\alpha_{B,5\%} = 0.017$) and the conventional driver scenario ($Z = 6.5$, $p < 0.001$, $\alpha_{B,5\%} = 0.017$).¹ No significant difference is observed for the two conventional scenarios ($Z = 1.2$, $p = 0.245$, $\alpha_{B,5\%} = 0.017$). The effect size, measured in Cohen’s d , corresponds to a medium-size effect ($d = 0.6$) for both significant differences.

Table 4.2: Results of the Wilcoxon significance test for the differences in importance of ride comfort between driving, being a passenger and being driven autonomously

rating difference	median 1st	median 2nd	p-value	rej. of H0	Cohen’s d
dri. - pas.	rather important	rather important	0.245	false	(0.10)
dri - aut.	rather important	important	< 0.001	true	0.6
pas. - aut.	rather important	important	< 0.001	true	0.6

The survey takers were questioned about twenty-one purchase criteria. They should rate these on a five-point semantic scale, ranging from „unimportant“ to „important“. The aim was to assess the importance of ride comfort compared to others. For brevity, the results are summarized in Table 4.3. The individual box- and bar-plots for each category can be found in Appendix A.3.

The Wilcoxon signed-rank test indicates the largest significant effects for the criteria *ease of use* ($Z = 7.1$, $p < 0.001$, $\alpha_{B,5\%} = 0.002$), *ride comfort* ($Z = 7.1$, $p < 0.001$, $\alpha_{B,5\%} = 0.002$), *sportiness* ($Z = -6.7$, $p < 0.001$, $\alpha_{B,5\%} = 0.002$) and *infotainment* ($Z = 6.5$, $p < 0.001$, $\alpha_{B,5\%} = 0.002$). The importance of *ease of use* increases in median from „neutral“ to „important“, of *ride comfort* from „rather important“ to „important“, and of *infotainment* from „neutral“ to „rather important“. A medium size effect was observed for all of them ($d = 0.6$). The importance of *sportiness* decreases in median from „rather important“ to „neutral“, with an effect size of $d = -0.6$.

The criteria *innovation* ($Z = 5.8$, $p < 0.001$, $\alpha_{B,5\%} = 0.002$), *family friendliness* ($Z = 5.4$, $p < 0.001$, $\alpha_{B,5\%} = 0.002$) and *safety* ($Z = 5.1$, $p < 0.001$, $\alpha_{B,5\%} = 0.002$) show the next highest increase in importance, again with an medium effect size ($d = 0.5$). The median of *innovation* increases from „rather important“ to „important“, and the median of *family friendliness* from „neutral“ to „rather

¹Results reported in APA format (https://psych.uw.edu/storage/writing_center/stats.pdf)

important“. The median of *safety* did not change and stayed at „important“, but the 25 % quartile raised to „important“ for the automated case, with only a few outliers below (see Figure A.8 in Appendix A.3).

Table 4.3: Results of the Wilcoxon signed rank sum significance test for different buying criteria of conventional and automated vehicles, at a confidence level of 95 % and effect strength Cohen d derived from z-score

critereon	median conv. pass.	median auto.	p-value	rej. of H0	Cohen's d
<i>ease of use</i>	neutral	important	< 0.001	true	0.6
<i>ride comfort</i>	rather important	important	< 0.001	true	0.6
<i>sportiness</i>	rather important	neutral	< 0.001	true	-0.6
<i>infotainment</i>	neutral	rather important	< 0.001	true	0.6
<i>innovation</i>	rather important	important	< 0.001	true	0.5
<i>fam. friend.</i>	neutral	rather important	< 0.001	true	0.5
<i>safety</i>	important	important	< 0.001	true	0.5
<i>interior</i>	rather important	rather important	< 0.001	true	0.4
<i>CO₂ emissions</i>	neutral	rather important	< 0.001	true	0.4
<i>seat comfort</i>	rather important	important	< 0.001	true	0.4
<i>env. friend.</i>	neutral	rather important	< 0.001	true	0.4
<i>materials</i>	neutral	rather important	< 0.001	true	0.4
<i>easy entry</i>	neutral	neutral	< 0.001	true	0.3
<i>size</i>	neutral	neutral	< 0.001	true	0.3
<i>high seat pos.</i>	ra. unimportant	ra. unimportant	< 0.001	true	0.3
<i>headlight sys.</i>	neutral	neutral	0.006	false	-0.2
<i>design / look</i>	rather important	rather important	0.018	false	-0.2
<i>price / performance</i>	rather important	rather important	0.035	false	-0.2
<i>reliability</i>	important	important	0.161	false	(0.1)
<i>consumption</i>	rather important	rather important	0.205	false	(0.1)
<i>brand image</i>	neutral	neutral	0.512	false	(0.1)

For the features *interior* ($Z = 5.0$, $p < 0.001$, $\alpha_{B,5\%} = 0.002$), *CO₂ emissions* ($Z = 4.3$, $p < 0.001$, $\alpha_{B,5\%} = 0.002$), *seat comfort* ($Z = 4.3$, $p < 0.001$, $\alpha_{B,5\%} = 0.002$), *environmental friendliness* ($Z = 4.1$, $p < 0.001$, $\alpha_{B,5\%} = 0.002$), *high quality materials* ($Z = 4.0$, $p < 0.001$, $\alpha_{B,5\%} = 0.002$), *easy entry* ($Z = 3.8$, $p < 0.001$, $\alpha_{B,5\%} = 0.002$), *size* ($Z = 3.6$, $p < 0.001$, $\alpha_{B,5\%} = 0.002$), and *high seating position* ($Z = 3.6$, $p < 0.001$, $\alpha_{B,5\%} = 0.002$), a small increase in importance is observed ($0.2 < d < 0.5$). The median increases in one step for *seat comfort* to „important“, and for *CO₂ emissions*, *environmental friendliness* and *high quality materials* to „rather important“. The median importance of *interior* („rather important“), *easy entry* and *size* („neutral“), and of *high seating position* („rather unimportant“) does not change.

The other criteria, such as *headlight system*, *design / look*, *price / performance ratio*, *reliability*, *fuel / energy consumption* and *brand image* remain unchanged and do not show significant differences. *Reliability* remains „important“, *design / look*, *price / performance ratio* and *consumption* remain „rather important“. The *brand image* and *headlight system* are seen „neutral“ in both cases.

4.3 Discussion

It could be observed that a majority of the survey takers rate ride comfort as a „rather important“ buying criteria. Most of them rate the supplied ride quality of their current vehicle as „neutral“ or „rather good“. It seems that they are content and do not demand more ride comfort for conventional driving. Their assessment of ride comfort importance was independent of being the driver or the passenger in a conventional vehicle.

A significant increase in importance was found considering automated driving. The median rating of ride comfort significantly changed from „rather important“ to „important“. This result was confirmed when the participants were asked to rate the importance of different buying criteria for a conventional and an automated vehicle. Again, for the conventional case, ride comfort was assessed as „rather important“, and for the automated case as „important“.

The participants rated *safety* as the only „important“ buying criteria for conventional cars. All other criteria are rated as „rather important“ or „neutral“. Solely a *high seating position* was rated as „rather unimportant“. For an automated vehicle, other criteria such as *ease of use*, *ride comfort*, *innovation* and *seat-comfort* were rated „important“ as well. The importance of *safety* increased further for the automated driving scenario. The strongest adverse effect was seen for the feature *sportiness*, which decreased in importance from „rather important“ to „neutral“.

One could observe that the respondents labeled more criteria as important and only a few with decreasing importance for automated driving. The criteria *headlight system*, *design/look* and *price/performance ratio* would show a small significant decrease in importance ($d = -0.2$). It should be further investigated in future studies. The Bonferroni correction is conservative and prone to a type II error, which means it fails to nullify the null hypothesis, even if it might be untrue. The average effect of all significant differences is $d = 0.4$ ($d = 0.3$ without Bonferroni correction). One observes increases in importance with a small effect size for *ease of use*, *ride comfort* and *infotainment*, and a decrease in importance with a strong effect for *sportiness*. Small increases in importance are seen for *innovation*, *family friendliness* and *safety*, and small decreases in importance for the *headlight-system*, *design/look* and the *price/performance ratio*.

As a point of criticism, the small sample size of 125 completed surveys with a young average age of 33.5 years needs to be mentioned. The average age in Germany is about ten years older (44 years) [266]. It would be preferable to have an even gender distribution, and the results of this survey would likely change for less developed regions or countries with other customer preferences. However, the results can be classified as plausible and reliable within this survey's scope for young people in Germany.

After this section, research questions 1.1 and 1.2 can be answered. The importance of ride comfort increases concerning automated driving, and ride comfort is one of the most important buying criteria to the customer. In a next step, it is necessary to investigate the performance of current suspension systems in automated driving scenarios. This analysis will be performed in the next Chapter 5 Driving-Simulator Study I – Suspension Systems.

5 Driving-Simulator Study I – Suspension Systems

In the previous chapter, it was shown that the importance of ride comfort increases considering automated driving. The next step is to investigate current state-of-the-art suspension systems for automated driving. The goal is to find out how passive, semi-active, and active suspensions compare against each other. Therefore a driving simulator study was conducted where the test subjects rated the different systems. Another question that should be investigated was whether passengers are more susceptible to disturbances when not focused on their surroundings, for example, when performing a side task.

This study was conducted in collaboration with Georg Burkhard [267, 268], who used the body based measurements (seat, breast, and head sensor) to develop a new objectification method that extends the method of ISO 2631 [29]. The research regarding the state of attention influencing perceived (dis-)comfort is shared between the author and Georg Burkhard. The main focus of this thesis is on the vehicle and its suspension system. The accelerations of the vehicle fixed sensor are used to calculate an objective measure according to ISO 2631 [29].

The method of this driving simulator investigation is described in Section 5.1, including a subsection on the driving simulator system (Subsection 5.1.1) and its vertical vehicle dynamics validation (Subsection 5.1.6). After the design (Subsection 5.1.2), implementation (Subsection 5.1.3) and execution (Subsection 5.1.4) of this study have been described, the results are displayed in Section 5.2 and discussed in Section 5.3.

5.1 Method

A dynamic platform driving simulator was used to investigate current state-of-the-art suspension systems in automated driving. No SAE Level 3 vehicles were available to perform such a study in an actual scenario on public roads. As an advantage, a simulator allows fast switching between different suspension systems without physically changing a car. In comparison to other investigations which use a driving simulator to rate vehicle performance, for example, rating the lateral dynamics [269], it was decided to use actual vehicle measurements and offline motion-cueing, which will be described in Subsection 5.1.1.

The offline motion-cueing has two main advantages for investigating vertical vehicle dynamics in automated driving. The simulation is not dependent on the quality and accuracy of a simulation model, which needs to be real-time capable. Especially using vertical vehicle dynamics control systems and a detailed vehicle model can become computationally expensive. The other advantage is the fact that the playback of the measurements represents a repeatable automated drive for each test person, within the repetition accuracy of the dynamic driving simulator.

5.1.1 Driving Simulator

The driving simulator used for this study was used again for the second study, which will be explained in Chapter 6 Driving-Simulator Study II – A Target Value for Ride Comfort. It is a driving simulator with a hexapod system mounted on a tripod sled, moving freely on a base plate. The front section of a BMW F80, with digital mirrors (side and rearview), primary dashboard, Central Information Display (CID), air conditioning, and a fully functional center console is used as a mock-up. The mock-up with the hexapod-tripod system is shown in Figure 5.1 on the left.

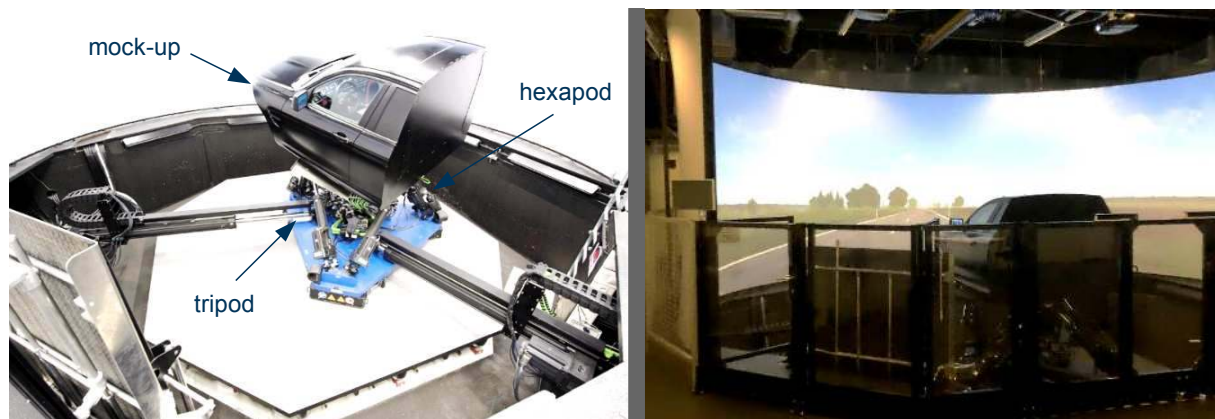


Figure 5.1: VI-Grade Driver in Motion (DiM) driving simulator at the BMW research center in Garching

On the right side of Figure 5.1 the 180° screen can be seen, which is lit up by four projectors hanging from the ceiling. The hexapod-tripod system is recessed into the ground. The mock-up can be accessed via a retractable bridge. Technical information for the driving simulator regarding position, velocity and acceleration limits is summarized in Table 5.1. The low-frequency tripod system is mainly used for the longitudinal and lateral dynamics. The high bandwidth hexapod system is mainly used for the vertical dynamics, including roll, pitch and vertical body movement due to road irregularities. The dynamics of the driving simulator are validated in Subsection 5.1.6.

Table 5.1: Maximum values for the articulation (position, speed, acceleration) of the simulator platform, split for the two different systems

	Hexapod (0–30 Hz)						Tripod (0–5 Hz)		
	x	y	z	φ	θ	ψ	x	y	ψ
position	± 0.28 m	± 0.25 m	± 0.22 m	$\pm 20^\circ$	$\pm 20^\circ$	$\pm 20^\circ$	± 0.80 m	± 0.75 m	$\pm 25^\circ$
velocity	2.0 ms ⁻¹	1.7 ms ⁻¹	1.6 ms ⁻¹	135° s ⁻¹	130° s ⁻¹	135° s ⁻¹	1.7 ms ⁻¹	1.5 ms ⁻¹	165° s ⁻¹
acceleration	25 ms ⁻²	25 ms ⁻²	35 ms ⁻²	2500° s ⁻²	2000° s ⁻²	3000° s ⁻²	12 ms ⁻²	10 ms ⁻²	900° s ⁻²

An additional measurement system was installed inside the mock-up (Figure 5.2). In total, it had four sensors wired to an IPEtronic analog-digital converter, which in turn was connected via Controller Area Network (CAN) to a Vector-Box for recording the signals. The measurement signal was recorded with a sampling rate of 1000 Hz. The Vector box was linked to an Universal Serial Bus (USB) interface of the driving simulator, which allowed to position the laptop to control the measurements inside the operator room. The operator room is located backward from the photo position of Figure 5.1 right. Supplementary to the measurement system were audio and video connections from the operator room to the mock-up.



Figure 5.2: Measurement system installed in the simulator mock-up, with and without a seated test person

As stated before, only the vehicle sensor located inside the center console tray was used for both studies within this thesis work. In this study, it was used to validate the simulation (Subsection 5.1.6) and to check that there was no significant deviation from the intended excitation during the study. In the second study (Chapter 6), this sensor was used to calculate an objective value to a corresponding trigger signal of the test person. The datasheet of this six DoF sensor can be found in Figure B.1, the technical information regarding the IPEtronic in Figures B.2 to B.4, and regarding the Vector-Box in Figures B.5 and B.6, all in Appendix B. Further information on the measurement system, including validation of its accuracy, can be found in [45]. The body measurement system's application methods have been filed as a patent by Burkhard and the author [270].

Three different components are needed to create a driving simulation with offline motion-cueing: the visual, the acoustic, and the motion component. Figure 5.3 gives an overview of the different development steps for each component. For the visual component, different track sections were modeled using OpenDrive Road Designer from VIRES Simulationstechnologie GmbH. A track for the simulation consists of several subsections, the tiles. The visual road surface, the weather, and the surroundings are modeled on each tile. For both simulator studies, there were tiles for the start of the drive, a demonstration phase, test sections, intermediate sections, and for the end of the drive.

The audio files were recorded for different sections, such as accelerating from and decelerating to a standstill, and for different road irregularities such as good, medium, and bad roads. The recordings were performed with a stereo microphone in real cars. The parts were merged into one audio file by arranging them according to the test plan and crossfading. The Matlab audio toolbox was used to perform these tasks.

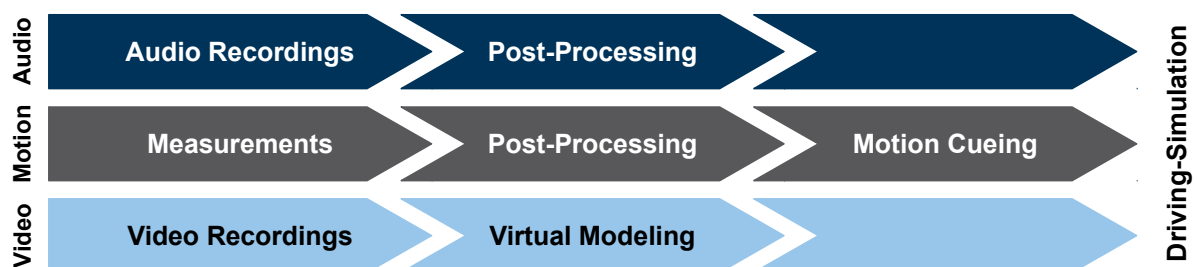


Figure 5.3: Workflow to build a driving simulation with offline motion-cueing

Three steps are needed to generate the motion of the driving simulation. The input data must be taken from vehicle measurements or offline driving simulations. The data must be post-processed, and the vehicle motion must be converted to a suitable driving simulator motion.

For both studies, actual measurements were used to eliminate inaccuracies and shortcomings of simulation models. The data has to define the state and motion of the vehicle body. This requires at least three translational accelerations and three rotational velocities. When only these signals are used, translational velocities and positions and the rotational position need to be obtained by numerical integration with zero-phase filtering to avoid signal drift. The angular accelerations need to be obtained by differentiation, which requires zero-phase low-pass filtering to prevent signal noise. Additional signals, like the vehicle speed and the planar and angular positions, were used to refine these calculations. Signals such as engine speed and current gear are used for the driving simulator dashboard.

During post-processing, the vehicle's position is high-pass filtered in the vertical direction to avoid low-frequency vertical motion due to a waviness with an amplitude more extensive than the vertical position limitations of the system. All signals are plausibility checked and band-pass filtered. For the band-pass filtering, third to fifth-order filters were used with a passband from 0.5 – 25 Hz.

After the post-processing, the signals are processed by a (proprietary) motion-cueing algorithm supplied by BMW and VI-Grade. Motion-cueing is the conversion of simulated vehicle dynamics to required driving simulator actuator movements. Simulator measurements are compared to the original signals in Subsection 5.1.6 Validation of the Driving Simulator, to validate the end result of the motion-cueing after signal processing and playback in the simulator.

The three different components (audio, video, motion) are put together in a BMW self-developed user interface and tested in the driving simulator. The study design is explained in the next section.

5.1.2 Study Design

This study was intended to clarify two further research questions. How do the current state-of-the-art suspension systems perform in automated driving? Does the execution of side tasks affect the sensitivity for road disturbances? The two null-hypotheses are consequently that all suspension systems are rated the same and that there is no difference in the ratings for ancillary tasks. Three different tracks (road excitation) were investigated as well, to obtain a more general result for this investigation. This defines the factors for this experiment, the state of attention, the suspension system, and the track. The effect is the subjective rating of the test person.

Figure 5.4 gives an overview of the applied test procedure. The start of the drive was followed by a short demonstration phase, where the test person was familiarized with the simulation and occurring road disturbances. Thereafter, different test sections formed the main part of the virtual test drive. At the end, the vehicle decelerated to a standstill. Each track was driven in an attentive and an inattentive state. For each state, three different suspension systems were tested. Short sections with a low excitation (neutral sections) were placed between the test sections for track, state, and suspension combinations. A test section had a duration of 40 s, a neutral section of 20 s.

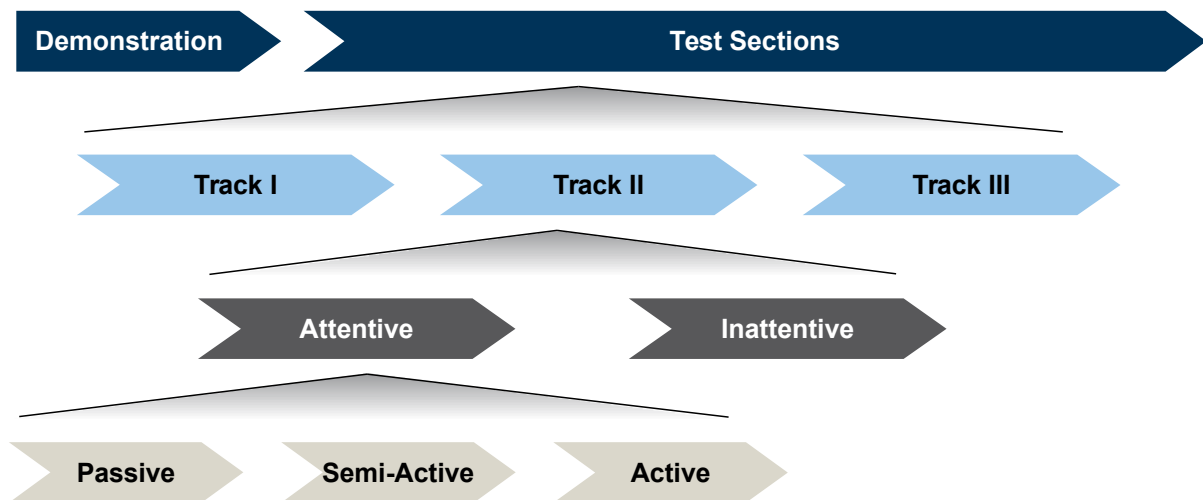


Figure 5.4: Test procedure of driving simulator study I, showing the sub-division into different tracks, states of attention and suspension systems

The rating of the test section was performed during the neutral section where the investigator asked the subject via radio and noted the discomfort rating. To shift the focus of the test person towards the rating, the neutral section was driven in fog, so the test person could not see any surroundings. The six-point Likert Scale that was used for the discomfort ratings was explained to the subjects before the drive, and it was additionally written down in the mock-up. The test person could look at the scale and decide for a rating. The scale is shown in Figure B.8 in the appendix. Since the term discomfort is not properly defined in the German language, the anchor points were chosen as „no disturbance“ (0) and „strong disturbance“ (6). The entire test procedure for one person is described in Subsection 5.1.4 Execution.

Other parameters could influence the discomfort rating of the test person, such as the test order of the different states, tracks, and suspensions. It is likely that the ratings will change with ongoing test duration, because at the beginning the subject has no reference except for the demonstration phase, and later the test subject has experienced all different intensities of disturbances. The test plan was therefore randomized and repetition was introduced as well. The subjects were told that they will experience three different suspension systems on three different tracks in two different states of attention, but they did not know which suspension was currently experienced within a test section.

Table 5.2: Permutation of the three suspension configurations, passive (pas.), semi-active (sem.) and fast-active (act.)

s1	s2	s3	s4	s5	s6
pas./sem./act.	pas./act./sem.	sem./pas./act.	sem./act./pas.	act./pas./sem.	act./sem./pas.

The participants were divided into six groups according to Table 5.2. For each, group there was a certain order of the tracks and states including one repetition. The suspension systems were fully permuted for one subject group (within-subject permutation). The order of the tracks and states of attention were fully permuted between the subject groups (between-subject permutation).

Group	Test Sections						Repetition
	Track 3		Track 2		Track 1		Track 3
1	<i>att.</i>	<i>ina.</i>	<i>att.</i>	<i>ina.</i>	<i>att.</i>	<i>ina.</i>	<i>att.</i>
	s1	s2	s3	s4	s5	s6	s1
	Track 3		Track 1		Track 2		Track 3
2	<i>ina.</i>	<i>att.</i>	<i>ina.</i>	<i>att.</i>	<i>att.</i>	<i>ina.</i>	<i>ina.</i>
	s1	s6	s5	s4	s3	s2	s1
	Track 1		Track 2		Track 3		Track 1
3	<i>att.</i>	<i>ina.</i>	<i>ina.</i>	<i>att.</i>	<i>att.</i>	<i>ina.</i>	<i>att.</i>
	s3	s4	s1	s2	s5	s6	s3
	Track 1		Track 3		Track 2		Track 1
4	<i>ina.</i>	<i>att.</i>	<i>ina.</i>	<i>att.</i>	<i>att.</i>	<i>ina.</i>	<i>ina.</i>
	s3	s2	s5	s4	s1	s6	s3
	Track 2		Track 3		Track 1		Track 2
5	<i>ina.</i>	<i>att.</i>	<i>att.</i>	<i>ina.</i>	<i>att.</i>	<i>ina.</i>	<i>ina.</i>
	s5	s6	s3	s4	s1	s2	s5
	Track 2		Track 1		Track 3		Track 2
6	<i>att.</i>	<i>ina.</i>	<i>ina.</i>	<i>att.</i>	<i>ina.</i>	<i>att.</i>	<i>att.</i>
	s5	s4	s1	s6	s3	s2	s5
	Track 2		Track 1		Track 3		Track 2

Figure 5.5: Study I test plan for 6 subject groups, using 3 tracks in attentive (*att.*) and inattentive (*ina.*) state, with suspension system permutation s1 – s6 according to Table 5.2

Figure 5.5 shows the test plan for this simulator study. This test plan allows a within-subject evaluation of the suspension system, the state of attention, and the track type effects, whereas a between-subject evaluation of the effects of track order, states, and repetition. The test plan is symmetric, meaning that each factor combination is tested equally. The test plan and the measurements are described in the next section.

5.1.3 Implementation

Three suspension systems were measured on three road sections (Track I – III). The same vehicle was used for all the systems. It was done to facilitate the measurements, and avoid side effects from using multiple cars. A BMW 7-series (G12), equipped with semi-active dampers, air springs, and a passive ARB was chosen. This vehicle type is alternatively available with a slow-active ARB, but for this study, the passive ARB was removed to imitate the decoupling effect of a fast-active ARB. This study was focused on straight-line driving with low later-acceleration, allowing to remove the ARB without detrimental effects.

The passive suspension was emulated by disabling the semi-active control logic of the dampers. The electronic valves were set to achieve damping similar to passive dampers, resulting in 25 % critical damping. It resembles a passive suspension tuned for comfort. The vehicle was operated according to its standard specification in the semi-active case.

The different tracks for this study are shown in Figure 5.6. Each track has a different characteristic. Track I has mostly low-frequency excitation in heave and pitch, mainly inducing disturbances in the range of the vehicle body eigenfrequency. Track II has predominantly low- and high-frequency roll motion, combined with stronger wheel-eigenfrequency excitement due to a coarser road surface. Track III was the least comfortable road with low- and high-frequency excitation in heave, pitch, and roll.

All three tracks are rather bad roads for German standards, ranging between class C and E according to ISO 8608 [214]. During measurements, the road ahead was video recorded, which served as a template for the virtual modeling of the test sections. The study subjects could visually differentiate the tracks but were not explicitly informed about their different characteristics.

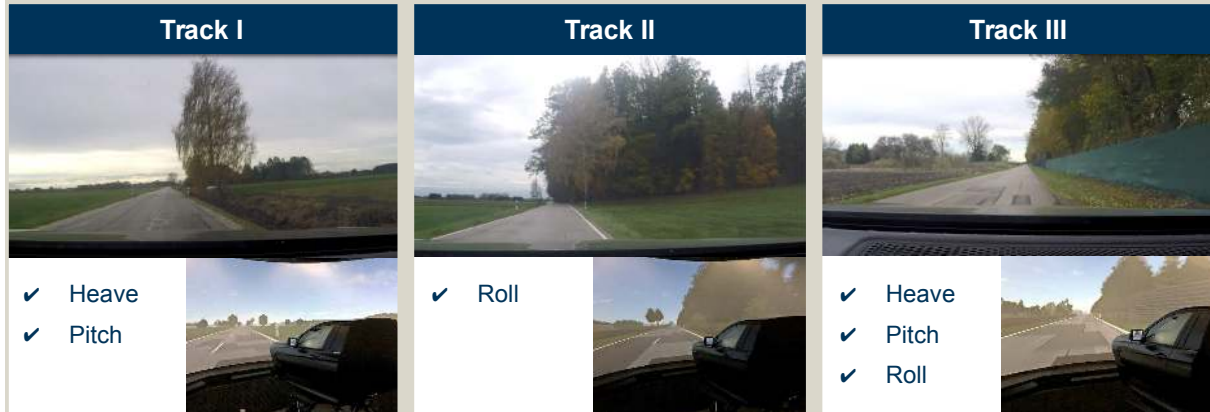


Figure 5.6: The three tracks used in Study I, indicating their predominating road excitation types, and a comparison of the real and virtual view

The vehicle was equipped with sensors to measure and log all relevant signals of the vehicle during a drive. Measurements were performed for the different suspension and track combinations. Figure 5.7 shows the schematics of the installed measurement system in the vehicle.

The laptop was directly connected to the On-Board Diagnostics (OBD) interface of the vehicle to check for errors of the control units. The Automotive Dynamic Motion Analyzer (ADMA), which is a Inertial Measurement Unit (IMU) with Global Positioning System (GPS) specifically designed for automotive measurements, was connected via CAN to a Vector data logging box. The internal signals of the vehicle were logged with this device via a FlexRay connection.

The FlexRay interface was used to manipulate the vertical vehicle dynamics control system of the vehicle to imitate passive dampers. Additionally, a six DoF sensor was installed in the center console and connected to the data logger by using an IPEtronic analog-digital converter. Power was supplied by the 12 V battery of the vehicle. The data-sheets of the measurement system can be found in Appendix B.1.

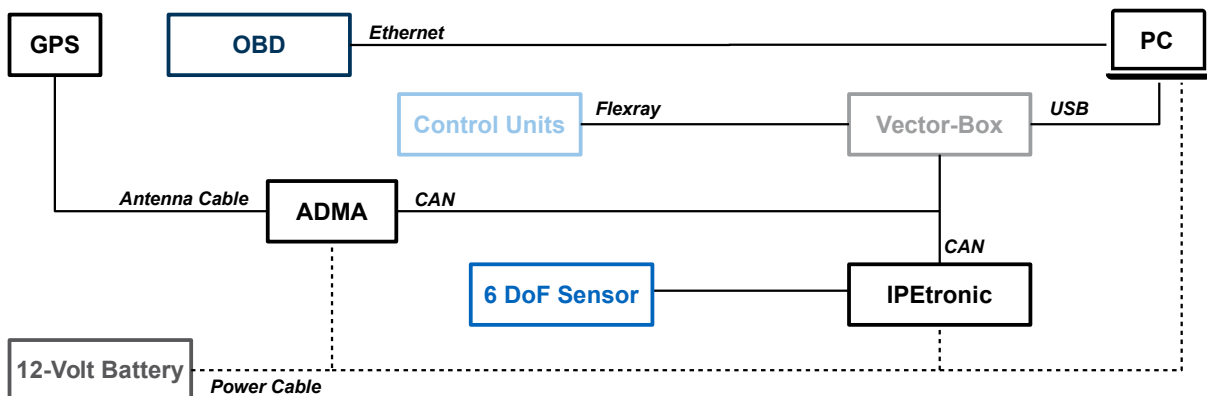


Figure 5.7: Schematics of measurement equipment installation in the test vehicle

The measurement system had redundancy regarding measured accelerations, velocities, and angular rates, allowing for plausibilization of the measurements and better estimation of derived quantities, such as angles and positions. The vehicle installation of the ADMA (a) with its GPS antenna (b), the analog-digital converter (c) and the data logging box (d) is shown in Figure 5.8.

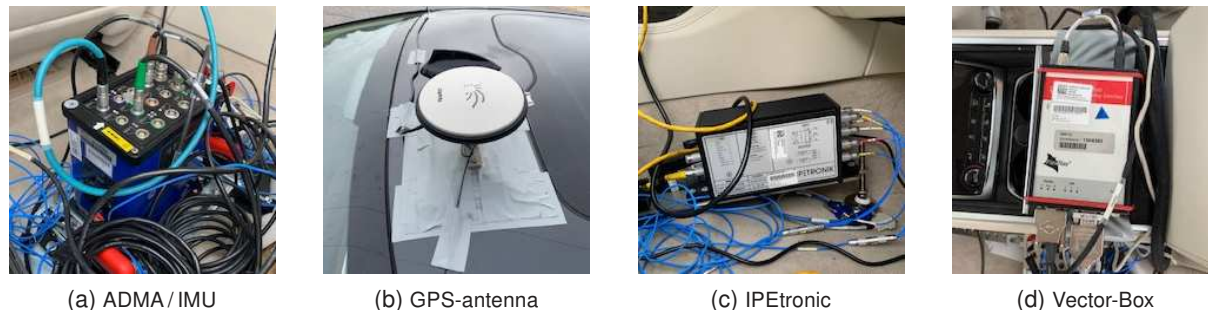


Figure 5.8: Pictures of the measurement equipment installation in the test vehicle

Multiple measurements were performed for each suspension and track combination to check for variance between measurements. It was rather small with $0.01 - 0.05 \text{ m s}^{-2}$ (weighted according to ISO 2631 [29]). The best measurement in terms of constant velocity and low longitudinal and lateral accelerations was chosen for each case. These measurements were used to generate and validate the driving simulation as described in Subsection 5.1.1 and 5.1.6. The experimental procedure for a test subject in the driving simulator study is described in the next section.

5.1.4 Execution

The sequence of the test drive in the driving simulator itself was described in Subsection 5.1.2, which forms the main part of the trial for one test subject. Additionally to the simulator drive, the test person was interviewed before and after it. Figure 5.9 illustrates the timeline for one test person.

In the beginning, the test person was collected at the entrance of the building and given background information regarding the study; for example, it was explained that the objective is on vertical dynamics ride comfort and not on acoustics or the longitudinal and lateral automation of the simulated vehicle. The test person was instructed regarding safety in the driving simulator and concerning his or her data privacy. This procedure took about fifteen minutes. Before starting the simulator drive, the test person was asked to rate his or her current state regarding motion-sickness on the Motion Sickness Indicator (MSI) scale. This scale is displayed in Figure B.10 in the Appendix. Test subjects could further ask questions if anything was left unclear.

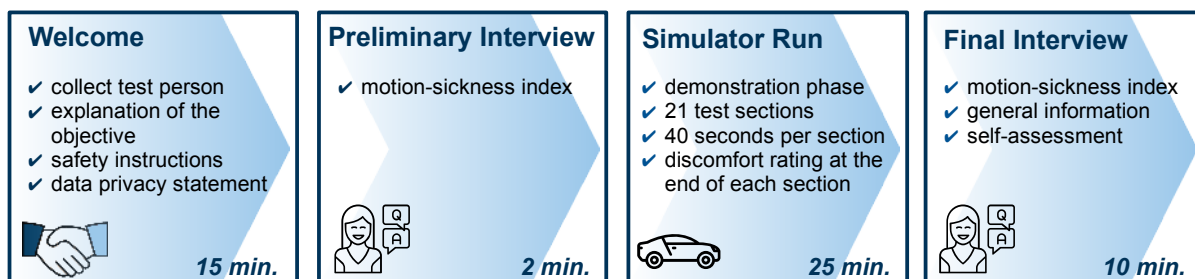


Figure 5.9: Timeline for one test subject in driving simulator study I

As described in Subsection 5.1.2, the simulator runs started with a short demonstration phase, followed by 21 test sections of 40s each. Interim sections of 20s were placed between the

test sections. During these, the subjects had to rate the previously experienced section on the discomfort scale. During the inattentive test sections, the subjects had to perform a quiz on a tablet computer, displayed in Figure B.9 in the Appendix.

The complete simulator run took 25 min. In the end, the test person was asked to rate his current constitution regarding motion-sickness on the MSI scale again. Finally, the subjects filled in a short questionnaire regarding personal information and their self-assessment. In total, one trial lasted about 45 to 60 min per subject. The post-interview results will be shown together with results of the discomfort ratings in Section 5.2. The analysis process applied to visualize the results is described next.

5.1.5 Analysis

Two types of data have been evaluated and analyzed. The subjective data of discomfort ratings and post-interviews, as well as the objective data in terms of the discomfort value according to ISO 2631 [29], combined with PSDs of the accelerations or angular rates. Figure 5.10 gives an overview of the data post-processing.

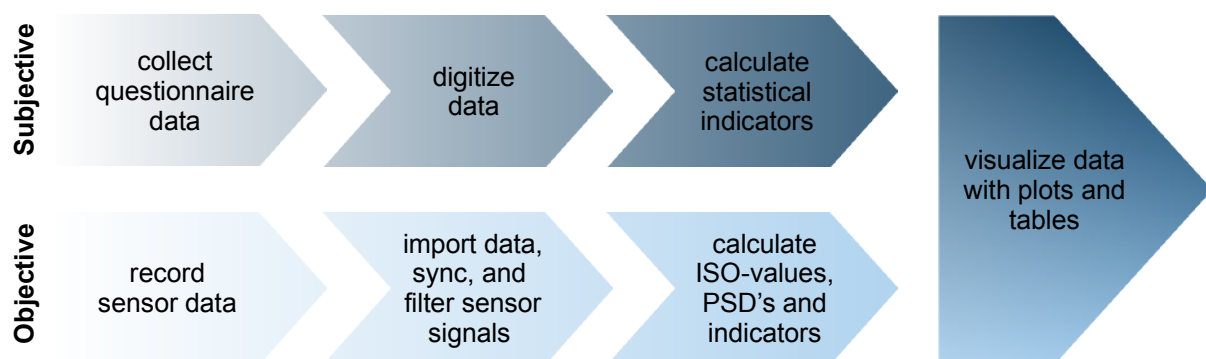


Figure 5.10: Work-flow for the post-processing in study I

The data from the post-interview questionnaires, and the subjective ratings of the different test sections are digitized. Statistical indicators are calculated according to Subsection 2.1.4 to check for significant differences and complementary effect strengths. The objective data is used for driving simulator validation and to rate the intensity for each suspension and track combination. The sensor measurement data is synchronized and low-pass filtered (50 Hz cut-off) before the objective value is calculated. Subjective and objective results are displayed as bar- and box-plots, pie-charts, and PSD-plots. Before the main results of the investigation are shown in Section 5.2, the validation of the driving simulator system is presented next.

5.1.6 Validation of the Driving Simulator

In offline motion-cueing, there are two major steps where the simulation is altered from the actual measurement or any other input signals. The first one is the translation of the input signals into control inputs for the simulator, the so-called motion-cueing algorithm. Signals will be adjusted to stay within the system limits regarding maximum displacement, velocities, and accelerations, see Table 5.1. Additional noise suppression through low-pass filtering is further altering the input signals. The second step is the dynamic simulation itself, where the actuators of the driving simulator cannot follow the reference signal in amplitude or phase.

This research work focuses on ride comfort instead of driving simulator development, hence no differentiation is made between the two sources of inaccuracy. The original measurement signals are directly compared to the measurements obtained in the mock-up, which corresponds to the excitation a test person experiences in the simulator.

Figure 5.11 shows the difference in objective values between vehicle and simulator measurements for three suspensions on three tracks. The vehicle body acceleration, weighted according to ISO 2631 [29] is used for the comparison. For all nine combinations, the simulator's objective value is lower compared to vehicle measurements.

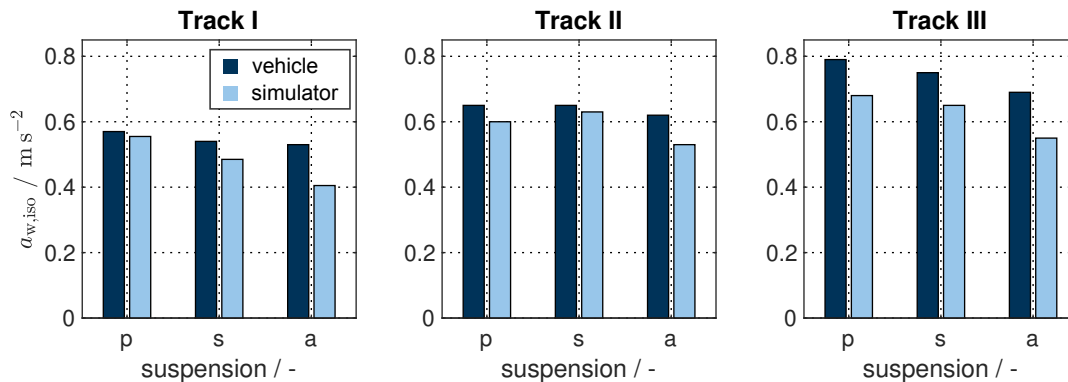


Figure 5.11: Comparison of the objective values for three different tracks, dark blue is from vehicle measurement, light blue is measured in the simulator

The smallest difference is observed for the passive suspension on track I, where the reference is $0.57 m s^{-2}$ and the output $0.56 m s^{-2}$. For the semi-active suspension the reference is $0.54 m s^{-2}$ and the output $0.49 m s^{-2}$, and for the active suspension it is $0.53 m s^{-2}$ and $0.41 m s^{-2}$ respectively. For track I, the improvement from passive to active suspension is exaggerated compared to the actual vehicle.

For track II, the difference between input and output is less pronounced. The passive and the semi-active suspension show similar performance in the actual vehicle, both with an objective value of $0.65 m s^{-2}$. A slightly adverse effect is observed in the simulator. The passive suspension shows a value of $0.60 m s^{-2}$ and the semi-active suspension a value of $0.63 m s^{-2}$. The active suspension has an input value of $0.62 m s^{-2}$ and a output value of $0.53 m s^{-2}$, possibly caused again because the simulator cannot reproduce all low and high-frequency dynamics.

On track III the simulator could not reproduce the intensity of vibration, but showed good performance in keeping the relative relation between the suspension variants. Input values are $0.79 m s^{-2}$, $0.75 m s^{-2}$ and $0.69 m s^{-2}$ from passive to active. The corresponding output values are $0.68 m s^{-2}$, $0.65 m s^{-2}$ and $0.55 m s^{-2}$. To investigate the differences between in- and output in detail over the frequency range from 0–20 Hz, the PSDs of the vertical acceleration, roll rate and pitch rates are plotted for each track in Appendix B.3. The simulator cannot reproduce vibration below 1 Hz, especially in the vertical direction, and above 10 Hz in all directions.

The driving simulator is limited in replicating „low-frequency high amplitude“ motion and „high-frequency low-amplitude“ motion due to the system's limits (Table 5.1). Despite the shortcomings in absolute values compared to the real measurements, the driving simulator has acceptable performance reproducing vertical vehicle dynamics from a subjective point of view. Experienced development engineers and test drivers were used to test and confirm this assessment. Nonetheless, the deviation absolute terms needs consideration when interpreting the study's results.

5.2 Results

The sample composition is summarized in Table 5.3. 64 subjects have participated, with an average age of 31 years. The youngest test person was nineteen years, and the oldest one was sixty-four years old. The standard deviation in age is 12 years, and 91 percent of the subjects were male, 9 percent female. In the following, the objective results are presented based on the in-simulator measurements, followed by the subjective results based on the discomfort ratings and the post-interview.

Table 5.3: Sample composition in driving simulator study I

N	avg. age	std. age	min. age	max. age	male / female
64	36.1 yrs	11.9 yrs	19 yrs	64 yrs	90.6% / 9.4%

5.2.1 Objective Assessment

To quantify the objective difference between the suspension systems and the tracks, and to verify there is significant difference between the attentive and inattentive runs of the subjects, objective values are grouped and displayed as box plots in Figure 5.12. Additionally to the median, quartiles, and whiskers, the mean value is shown as a circle. These three box plots directly refer to the three null hypotheses, which state no difference in subjective and objective ratings between the tracks, the suspension systems, or the states.

Attention has to be paid to the y-axis range in all three plots starting at 0.35 m s^{-2} to facilitate the visual perception of differences. The wide spread in data for each category is mainly caused by the grouping of tracks and systems. For example, category track one (T1) contains the objective values for all three suspension systems. The variability caused by the driving simulator can be seen Figure B.14 in the Appendix. The variability due to the driving simulator is small with a maximum interquartile range of 0.05 m s^{-2} .

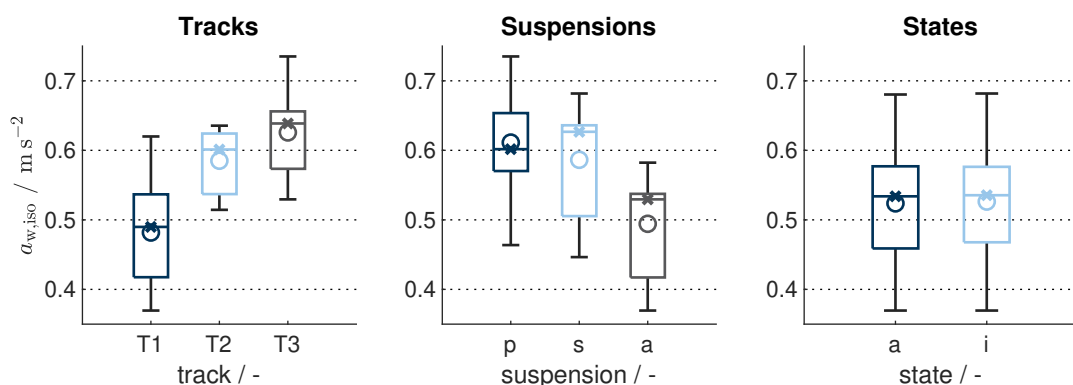


Figure 5.12: Comparison of the ISO values, summarized for the 3 hypothesis. Note the y-axis offset of 0.35 m s^{-2}

The evaluation of objective values (Figure 5.12 left plot) shows that track I is the most comfortable with a mean discomfort value of 0.48 m s^{-2} , followed by track II with a mean value of 0.59 m s^{-2} and track III with a mean value of 0.63 m s^{-2} . The largest variability is observed for track I, the smallest for track II.

The middle plot of Figure 5.12 shows the objective values grouped by suspension systems. The active suspension is most comfortable, resulting in a mean discomfort value of 0.49 m s^{-2} .

It is followed by the semi-active and the passive suspensions with 0.59 m s^{-2} and 0.61 m s^{-2} respectively. The right plot of Figure 5.12 displays the objective values grouped for the two states of attention. The mean values for the attentive and inattentive sections are 0.524 m s^{-2} and 0.526 m s^{-2} .

A independent two-sample t-test with Bonferroni correction is conducted in order to check for significant differences, which were found between track I and II ($t[880] = 28.8$, $p < 0.001$, $\alpha_{B,5\%} = 0.007$), track I and III ($t[880] = 34.4$, $p < 0.001$, $\alpha_{B,5\%} = 0.007$) and track II and III ($t[880] = 11.69$, $p < 0.001$, $\alpha_{B,5\%} = 0.007$). All three differences are categorized as large effects ($d \geq 0.8$).

The three suspension systems can be significantly distinguished in the objective value. The passive suspension is the least comfortable compared to the semi-active ($t[880] = -5.58$, $p < 0.001$, $\alpha_{B,5\%} = 0.007$) and the active suspension ($t[880] = -28.02$, $p < 0.001$, $\alpha_{B,5\%} = 0.007$). The performance of the semi-active suspension is significantly worse compared to the active suspension ($t[880] = -19.56$, $p < 0.001$, $\alpha_{B,5\%} = 0.007$). The differences between the passive and the semi-active suspensions to the active suspension are considered large. The difference in-between the passive and the semi-active suspension is a medium effect.

As expected and necessary, there is no significant difference in objective value between attentive and inattentive test sections ($t[1321] = -19.56$, $p = 0.564$, $\alpha_{B,5\%} = 0.007$). The results of the significance test of the objective values are summarized in Table 5.4.

Table 5.4: Results of the two sample t-test for the differences in tracks, states and suspensions

critereon	mean 1st	mean 2nd	p-value	rej. of H0	Cohen's d
T1 - T2	0.48	0.59	< 0.001	true	1.9
T1 - T3	0.48	0.63	< 0.001	true	2.3
T2 - T3	0.59	0.63	< 0.001	true	0.8
P - S	0.61	0.59	< 0.001	true	-0.4
P - A	0.61	0.49	< 0.001	true	-1.9
S - A	0.59	0.49	< 0.001	true	-0.6
Att. - Ina.	0.52	0.53	0.564	false	(0.0)

5.2.2 Subjective Assessment

The subjective results are presented in Figure 5.13 analog to the objective results and again according to this study's two main research questions. The first question was if there is a significant difference between the discomfort ratings of the three suspension systems. The second question if there is a difference in the discomfort rating depending on the state of attention. The three different tracks were used to assure that the results apply to a specific type of road excitation and checked if the subjects were able to distinguish between the different tracks in their ratings.

In comparison to the objective values, the subjective ratings are less distinct but still resemble the general trend seen in the objective values. Track I was rated best with a median discomfort rating of 2, followed by tracks II and III with median ratings of 4. The interquartile span is ± 1 from the median for all three tracks, with whiskers ranging over the complete span of the rating scale, which indicates a large variability in the subjective ratings.

Regarding suspension systems, the passive and semi-active systems are rated with a median 4 and an interquartile range of ± 1 . The active system is rated with a median of 3 and an interquartile range of ± 2 from the median. Whiskers are again at the endpoints of the scale for all three suspension systems. Attentive and inattentive sections have been rated with a median of 3. The interquartile range for the attentive state is $+1.5/-1$ and for the inattentive state $+2/-1$. Whiskers are once again at the top and the bottom of the scale.

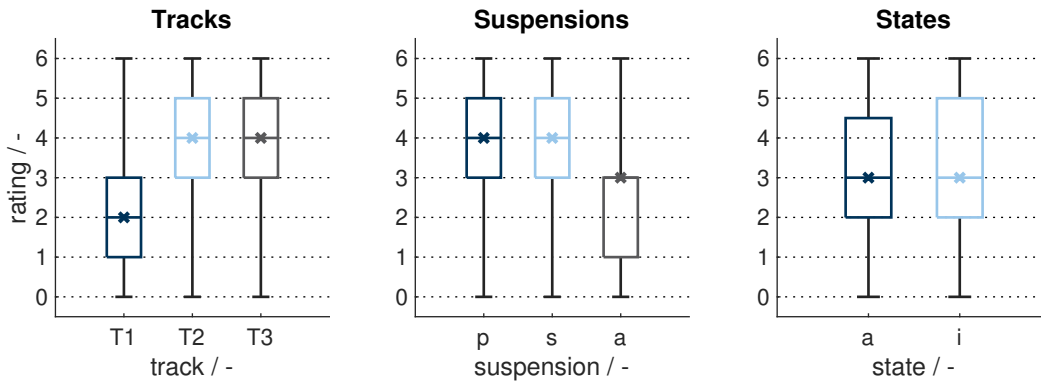


Figure 5.13: Comparison of the discomfort ratings, summarized for the 3 hypothesis

A Wilcoxon signed rank-sum test is applied to check for significant differences in the subjective ratings. This test is designed for dependent test samples, which is the case for this trial as every subject has rated all track, suspension, and state of attention combinations. The difference to a test for independent samples, such as the Mann-Whitney U test, is that it checks for significance in the relative difference of the ratings, which makes it independent of inter-subject variability. An overview of the relative differences is given in Figure B.15 in the Appendix.

The significance test results are summarized in Table 5.5. Significant differences are found between all tracks. A small difference ($d = 0.3$) between track II and III ($Z = 5.4$, $p < 0.001$, $\alpha_{B,5\%} = 0.007$), and medium differences between I and II ($Z = 13.7$, $p < 0.001$, $\alpha_{B,5\%} = 0.007$) and I and III ($Z = 15.3$, $p < 0.001$, $\alpha_{B,5\%} = 0.007$), with effect sizes of 0.7 and 0.8.

Table 5.5: Results of the Wilcoxon significance test for the differences in tracks, states and suspensions

critereon	median 1st	median 2nd	p-value	rej. of H0	Cohen's d
T1 - T2	2	4	< 0.001	true	-0.7
T1 - T3	2	4	< 0.001	true	-0.8
T2 - T3	4	4	< 0.001	true	-0.3
P - S	4	4	0.010	false	(0.1)
P - A	4	3	< 0.001	true	1.9
S - A	4	3	< 0.001	true	1.3
Att. - Ina.	3	3	0.005	true	-0.1

Regarding the suspension systems, significant differences are seen between the passive and the active suspension ($Z = -12.8$, $p < 0.001$, $\alpha_{B,5\%} = 0.007$), and the semi-active and the active system ($Z = -12.6$, $p < 0.001$, $\alpha_{B,5\%} = 0.007$), both considered as medium effects ($d > 0.5$). The difference between the passive and the semi-active system is just not significant due to the Bonferroni correction ($Z = 2.6$, $p = 0.010$, $\alpha_{B,5\%} = 0.007$), but even if significant, the effect would be negligible ($d = 0.1$). The difference between attentive and inattentive discomfort ratings is just significant ($Z = 2.6$, $p = 0.005$, $\alpha_{B,5\%} = 0.007$) but with a arguably small effect size of 0.1.

To investigate the difference between attentive and inattentive sections in more detail, these combinations were tested individually for significant differences, summarized in Table 5.6. A significant difference can be found on two of the nine suspension-track combinations, namely on track I and track II with the active suspension system. In both cases, the ratings were worse for the inattentive states than the attentive state, with an effect size of -0.4 .

Table 5.6: Results of the Wilcoxon signed-rank sum test and effect strength for the differences in comfort-rating, depending on the state of attention, individually for tracks and suspensions

critterion	median att.	median ina.	p-value	rej. of H0	Cohen's d
T1, pas.	2	2	0.0621	false	(-0.2)
T1, sem.	2	2	0.8151	false	(0.0)
T1, act.	1	2	0.0007	true	-0.4
T2, pas.	4	4	0.1654	false	(-0.2)
T2, sem.	4	4	0.6788	false	(0.1)
T2, act.	3	3	0.0047	true	-0.4
T3, pas.	5	4.5	0.2033	false	(0.2)
T3, sem.	5	5	0.5400	false	(0.1)
T3, act.	3	3	0.1158	false	(-0.2)

It was further investigated if there is an effect regarding the repetition of a certain track, suspension, and state combination. For each subject, the first occurrences of combinations were repeated at the end of the simulator drive. They are compared to each other and relative differences are displayed in Figure B.17 in the Appendix. Their significance test results are shown here in Table 5.7.

Significant differences due to the repetition are only found for track I ($Z = -4.6$, $p < 0.001$, $\alpha_{B,5\%} = 0.007$) and track III ($Z = 2.0$, $p < 0.001$, $\alpha_{B,5\%} = 0.007$). Track I was rated better in the repetition with a medium effect strength ($d = 0.6$), track III slightly worse with a little effect strength ($d = 0.2$). For completeness, the individual ratings for each suspension and track combination are shown Figure B.16 in the Appendix.

Table 5.7: Results of the Wilcoxon signed-rank sum test and effect strength between the comfort-rating at the beginning, and the repetition at the end, for the different tracks, states and suspensions

critterion	median att.	median ina.	p-value	rej. of H0	Cohen's d
T1	2	1	3.7562×10^{-6}	true	0.6
T2	4	4	0.2846	false	(-0.1)
T3	4	4	0.0436	true	-0.2
Att.	3	3	0.1338	false	(0.2)
Ina.	3	3.5	0.9353	false	(0.0)
Pas.	4	4	0.0970	false	(0.2)
Sem.	4	4	0.3632	false	(-0.1)
Act.	2	2	0.2870	false	(0.1)

5.2.3 Motion-Sickness and Follow-up Interview

Apart from the discomfort ratings, the subjects were asked to assess their condition regarding motion sickness before and after the simulator drive. The MSI scale ranges from 0 (no problem) to 10 (vomiting). Figure 5.14 shows the ratings before and after the drive as stacked bar plots. In advance of the simulator drive, forty-six subjects rated their current state as „no problem“ (0) and ten subjects said they feel „slightly uneasy“ (1) with no specific symptoms. Eight subjects rated their state at the beginning as „unwell without nausea“ (2-3). Six of the eight subjects rated their un-wellness as „very little“ (2), two of them as „minor“ (3).

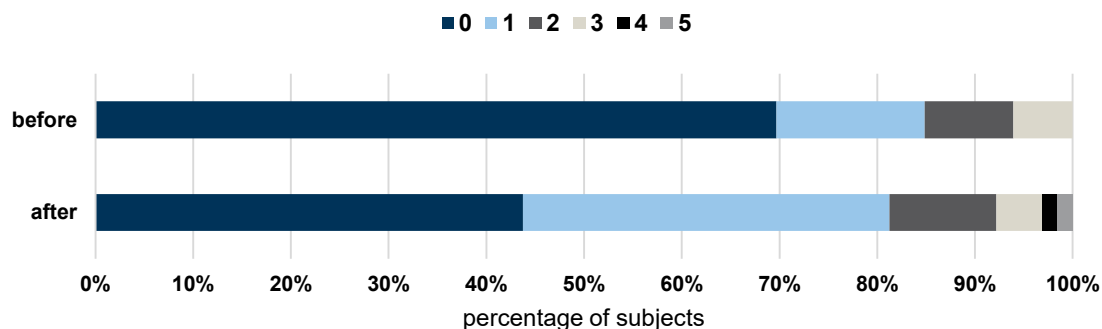


Figure 5.14: Self-determined motion sickness of the subjects before and after study I

After the test session, twenty-eight subjects remained unchanged with „no problem“ (0). Twenty-four persons felt „slightly uneasy“ (1) and twelve persons felt „unwell without nausea“ (2-5). From the twelve persons feeling unwell, seven rated the un-wellness as „very little“ (2), three as „minor“ (3) one as „medium“ (4) and one person as „severe“ (5). There was no nausea for any of the test persons.

The results of the post-interview are summarized as pie-charts in Figure 5.15a. The subjects were asked about their self-perception regarding the effect of the side-task on their discomfort perception. 83% said they think that the side-task did affect their discomfort ratings. 8% think that it did not, 9% could not tell or did not answer the question.

Looking at the 83% thinking that it has had an influence, 41% thought they have a higher susceptibility, and 34% are convinced that they were less sensitive to disturbances. 17% did not know if it was more or less, 8% did not answer.

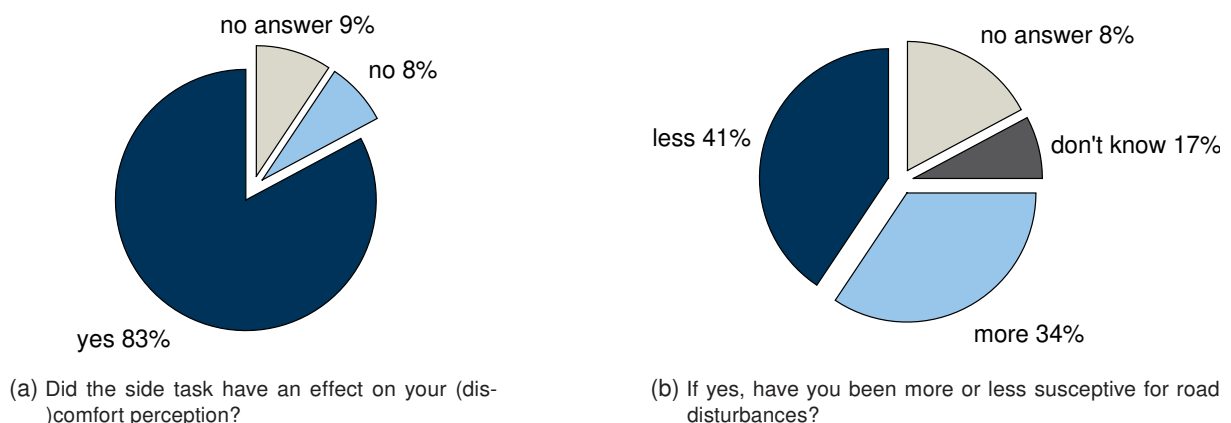


Figure 5.15: Results of post-session interview in study I

5.3 Discussion

The ISO 2631 [29] discomfort value can resemble the subjective ratings of test persons and reflect differences due to road quality or suspension systems. A passive suspension tuned for comfort has comparable ride comfort to a semi-active system with an objective to balance dynamic-wheel load variation and ride comfort. Both systems can potentially be used in automated vehicles; considering speeds below 130 km h^{-1} , and the possibility to preview longitudinal and lateral inputs of the vehicle trajectory controller, should allow lower damping ratios for passive suspension. The semi-active suspension controller could be focused more towards pure ride comfort. Best performance was supplied by the active suspension system, resulting in significantly better subjective and objective scores.

No case of severe motion sickness occurred throughout the whole simulator study. The ratings on the MSI scale indicate a slight worsening in the constitution for some of the test subjects. It might be possible that an increased driving time in the simulator would have led to nausea for some of the subjects. Compared to driving simulator studies focused on longitudinal and lateral dynamics, this study was better in terms of motion sickness. The effect of vertical dynamics on motion sickness might be lower compared to longitudinal and lateral dynamics.

Subjective ratings showed significant differences for the tracks and suspension systems. The advantage of an active system compared to passive and semi-active systems was clearly visible in the subjective assessments. The slight advantage of the semi-active system compared to the passive system was undetected by the test persons. They rated both the same. Only the active system was predominantly rated in the better half of the discomfort scale (rating 0–3). These results are in line with the findings of Cvok [271], who similarly discovered the superior performance of active suspensions for automated driving conditions. These findings point towards the need for active suspension systems if cars should provide substantially better ride comfort noticeable by an everyday customer.

The ratings regarding different states of attention did not show a significant difference. Although 83% of the subjects stated that the state of attention does influence their ratings, this was only confirmed on two of the test tracks (I and II). The effects sizes was minor. It can be argued that it makes sense that discomfort ratings do not depend on the state of attention, because they should solely resemble the perception of vibration discomfort. The discomfort perception is unlikely to change due to aside tasks. However, the comfort perception might be different. For a sensation of comfort, it is relevant what people expect in a particular situation. The quiz might have introduced unwanted side effects. Likely, a difficult question results in greater distraction compared to an easy question.

Summarizing this investigation, the perceived discomfort due to road irregularities is predominantly defined by the suspension system and the severeness of road excitation. Only the active system showed a significant improvement in subjective and objective ride comfort. The influence of a side-task during driving seems to have a minor to no effect on the discomfort perception. Desired or bearable amounts of (dis-)comfort during an automated drive cannot be deduced from this study. The subsequent investigation aims to clarify the influence of the state of attention regarding comfort instead of discomfort, and derive objective target values applicable to suspension development.

6 Driving-Simulator Study II – A Target Value for Ride Comfort

The previous results indicate that a passive suspension tuned for ride comfort performs comparably to a current semi-active system tuned in balance of comfort and road-holding. On good (smooth) roads, these systems are likely to supply the desired amount of ride comfort during an automated drive. On bad roads, as used in the previous simulator study, or on normal roads and high velocities, it seems that only active systems can deliver the desired ride comfort. No objective ride comfort target value, or target value range is available. Study II was executed in an attempt to determine it. ISO 2631 [29] is used once again as an objective measure. This time, the subjects do not rate subjective discomfort. Instead, they should apply a trigger button when their comfort threshold is reached. It is an attempt to define a comfort threshold within a certain environment and situation, using an objective value for discomfort.

The method of the second driving simulator study is described in Section 6.1, using the driving simulator system described in Subsection 5.1.1. The study design is explained in Subsection 6.1.1, the implementation in Subsection 6.1.2, the execution in Subsection 6.1.3 and the analysis methods in Subsection 6.1.4. Finally, the results are shown in Section 6.2 and discussed in Section 6.3.

6.1 Method

The same driving simulator and measurement system is used as in Study I, see Subsection 5.1.1. The vertical dynamics are based on the measurements of the first study but modified to obtain four different intensity ramps within the simulator mock-up. A ramp is defined as a test section of increasing or decreasing intensity for thirty seconds. Two different types of excitation are used, each one as increasing and decreasing ramp. A trigger button is installed in the mock-up, connected to the measurement system. The complete study design is described in the following.

6.1.1 Study Design

This study aims to answer research questions 3.1 and 3.2, which entail target values for automated driving. Since the influence of a secondary activity on expected comfort is unclear, the study will test different states of attention again. Therefore, the first null hypothesis is that the vehicle type does not affect the comfort expectation, and the second is that the state of attention does not affect it either. Additionally, it is tested for differences between the ramp type and directions.

The varied parameters in this study are the type of car, the ramp, the ramp direction, and the state of attention. The effect is the discomfort value at trigger time. The side task was the

smartphone game "Candy Crush", which is displayed in Figure C.1a in the Appendix. This game was chosen because it was anticipated to supply a more continuous distraction level than the quiz used in the previous study.

Figure 6.1 shows that the simulator drive starts again with a short demonstration phase, divided into three subsections followed by the principal testing phase. One subsection per type of car and one repetition. Each subsection is divided into attentive and inattentive parts. For each state of attention, all ramps are tested. The participants were split into four groups, where each group started with a different vehicle or different state of attention.

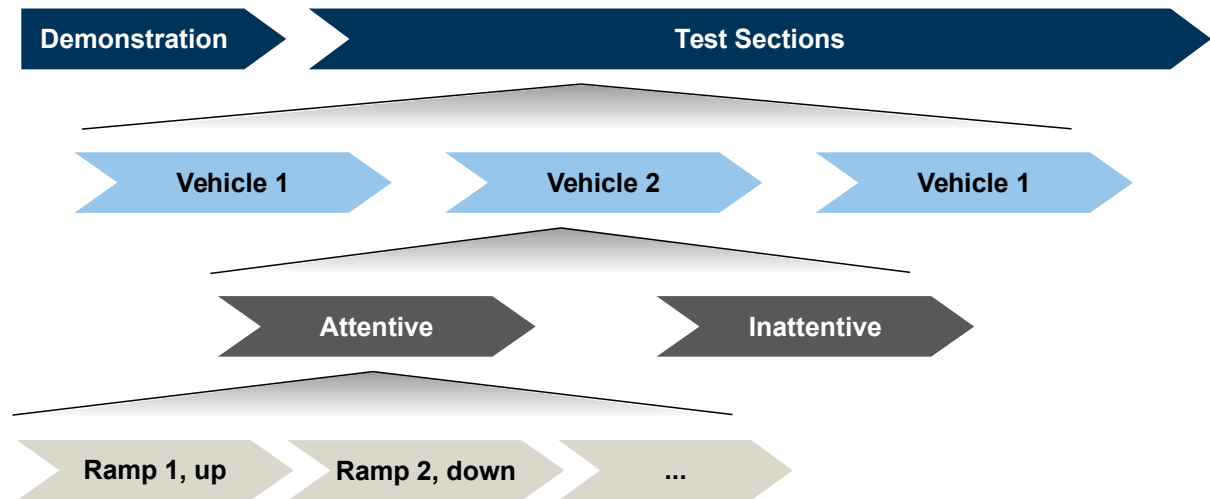


Figure 6.1: Test procedure Study II

Figure 6.2 shows the test plan for one of the three groups. This group started the test section with vehicle one in the attentive state without performing a side task. All ramps are tested for each vehicle-state combination, and the ramp order is permuted over all six combinations. The test plan is symmetric and allows for within-subject evaluation of the vehicles and the state of attention and between-subject evaluation regarding the influence of the order and the repetitions.

Vehicle 1		Vehicle 2		Vehicle 1	
<i>attentive</i>	<i>inattentive</i>	<i>attentive</i>	<i>inattentive</i>	<i>attentive</i>	<i>inattentive</i>
R1-up	R1-up	R2-up	R2-up	R2-up	R1-up
R2-down	R2-down	R1-down	R1-down	R2-down	R1-down
R2-up	R2-up	R1-up	R1-up	R1-up	R2-up
R1-down	R1-down	R2-down	R2-down	R1-down	R2-down
R1-up	R1-up	R2-up	R2-up	R2-up	R1-up
R1-down	R1-down	R2-down	R2-down	R1-down	R2-down
R2-up	R2-up	R1-up	R1-up	R1-up	R2-up
R-down	R-down	R1-down	R1-down	R2-down	R1-down

Figure 6.2: Test plan Study II

The different ramp directions were implemented to balance the calculation of the objective value at a trigger time (Subsection 6.1.4). The calculation uses the acceleration data over the last two seconds. Therefore, it has higher values for down-ramps compared to up-ramps when evaluated at the same intensity point on the ramp. The second ramp type was included to study the objective value's capability in weighting different excitation modes. The characteristic of ramp one was predominantly roll movement; ramp two had predominantly heave and pitch movement.

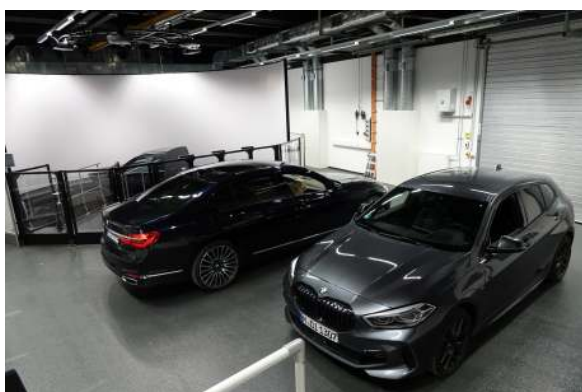
6.1.2 Implementation

The same simulator motion was used for both cars to see the effect of expectations on the desired level of ride comfort. The visual modeling of the test sections and the road sound were identical. Only the engine sound was changed to a deeper sound for the 7-series. The intention was to directly correlate changes in the trigger thresholds to the expected comfort because both vehicles' objective discomfort was the same in the simulator. This reasoning also applies to differences depending on the degree of attention. Figure 6.3 shows the two cars the subjects were virtually driven with, a BMW 1-series as a compact class car, and a BMW 7-series as a luxury-class vehicle.



Figure 6.3: Vehicles of simulator study II

It was expected that only a few, if any, subjects know both of these cars well enough, so they were shown to them before the simulator drive. The subjects could sit in both cars to get a feeling for them. The setup in the driving simulator facility can be seen in Figure 6.4a. In the driving simulator, the CID was used to play a short image movie of the vehicle that is driven next, and always displayed a picture of the car that was currently driven. The test subjects were supplied with material probes of both cars, shown in Figure C.1b in the Appendix. The intention was to supply a haptic impression. A trigger button was installed in the mock-up which had to be pushed by the test person when his comfort threshold was reached. The CID and the trigger can be seen in Figure 6.4b.



(a) Setup in the simulator hall



(b) Trigger and Central Information Display (CID)

Figure 6.4: Study set-up in- and outside of the driving simulator

The different ramps were generated based on the measurements made for Study I. Appropriate sections of twenty seconds with a constant vibration intensity have been taken from track I and track II. These sections were scaled with linearly increasing or decreasing intensity. A ramp was in the intensity range between 1%–100%, to achieve a discomfort value range of $0.01 - 0.5 \text{ m s}^{-2}$, which was determined in pre-tests. The data processing of the trigger points is described in Subsection 6.1.4.

6.1.3 Execution

The experimental procedure is structured by a welcoming, followed by a short pre-interview regarding motion-sickness, the main test in the simulator, and a final interview. The full procedure is summarized in Figure 6.5. Collecting the test person, giving background information on the study objective, the safety instructions, and signing a data privacy statement took 15 minutes. The explanation of the MSI scale and the first rating took 2 minutes. The explanation of the MSI scale and the first rating took 2 minutes.

Before the test person entered the simulator, he or she got the chance to sit in both vehicles and ask questions. The simulator run started after that and was executed as described in Subsection 6.1.1 and 6.1.2. The vehicle demonstration and the simulator run took 30 minutes. At the end of a test run, the MSI rating was repeated, and the subjects had to fill in a short questionnaire on their general information and their self-assessment in this study. In total, this study took one hour per test person.

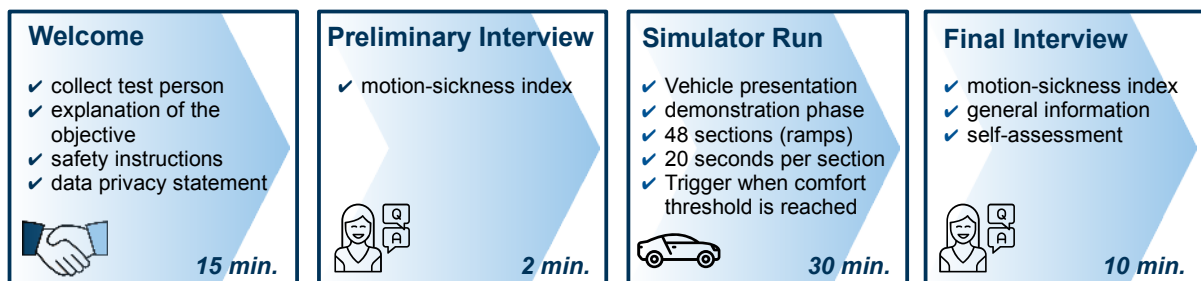


Figure 6.5: Overview of the test procedure in study II

6.1.4 Analysis

The analysis methods applied to this study's data are the ones applied in simulator study I. In study II, most of the data is objective because there are no subjective ratings for test sections during the simulator drive. The only subjective data is from the pre- and post-interview. A ramp's objective rating is obtained through a trigger button that the test subjects could press.

Figure 6.6 shows the basic principle of the trigger. As already stated in Subsection 6.1.2, the measurement system recorded the chassis (mock-up) fixed accelerations and angular rates, which can be used to calculate the objective value. When the trigger button is pressed, the binary signal will switch from zero to one and mark the comfort threshold. The discomfort value according to ISO 2631 [29] is calculated from the sensor signals over the previous two seconds before the trigger was pressed.

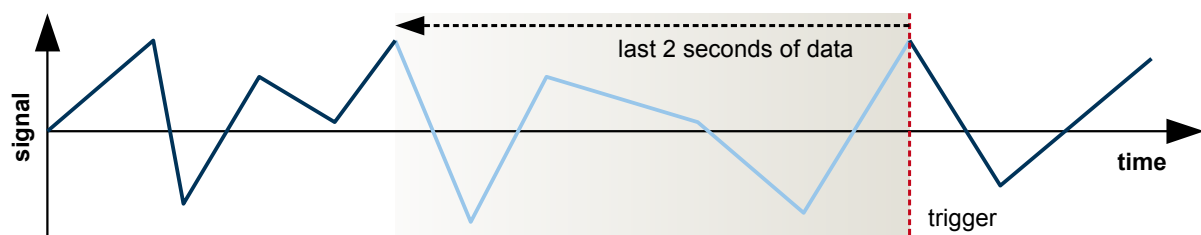


Figure 6.6: Processing the trigger signal

6.2 Results

In total, 49 subjects participated in the second driving simulator study. The average age was 37 years, with a standard deviation of 11 years. The youngest participant was 23, the oldest one 63. 84 percent of the participants were male, and 16 percent were female. The sample composition is summarized in Table 6.1. The objective results of this study will be presented next, followed by the evaluation of the pre- and post-interview.

Table 6.1: Sample composition in study II

N	avg. age	std. age	min. age	max. age	male / female
49	36.9 yrs	11.0 yrs	23 yrs	63 yrs	83.7% / 16.3%

6.2.1 Objective Assessment

Inter- and intra-subject variability is apparent in the results. Using mean and median, quartiles as indicators, a generalized discomfort target value, related to the comfort threshold, can be defined as $0.20 \pm 0.05 \text{ m s}^{-2}$ for an automated drive. Figure 6.7 summarizes the results for the two main hypotheses in box-plots. The left side shows the results for the state of attention. In attentive state, the mean trigger value is 0.20 m s^{-2} with a median value of 0.19 m s^{-2} . The quartile borders are at 0.15 m s^{-2} and 0.25 m s^{-2} , the whiskers at 0.03 m s^{-2} and 0.41 m s^{-2} .

The mean and median values for the inattentive state are likewise 0.20 m s^{-2} and 0.19 m s^{-2} respectively. The quartile borders and the whiskers are the same. A two sample t-test with Bonferroni correction did not show a significant difference between the states of attention ($t(2300) = 1.6$, $p = 0.115$, $\alpha_{B,5\%} = 0.006$).

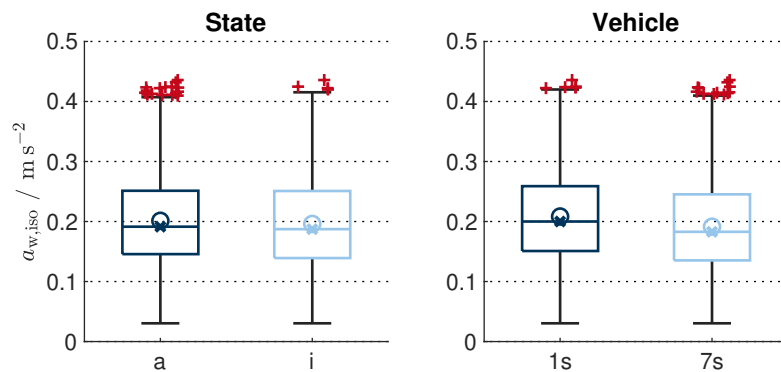


Figure 6.7: Difference in ISO threshold values by state of attention (a: attentive, i: inattentive) and car (1s: 1-series, 7s: 7-series)

The right side of Figure 6.7 shows the results for the vehicle type. For the 1-series, the mean trigger value is 0.21 m s^{-2} with a median value of 0.20 m s^{-2} . The quartile borders are at 0.15 m s^{-2} and 0.26 m s^{-2} , the whiskers are at 0.03 m s^{-2} and 0.42 m s^{-2} .

For the 7-series, the mean is at 0.19 m s^{-2} and the median at 0.18 m s^{-2} . The interquartile range is $0.14\text{--}0.25 \text{ m s}^{-2}$ and the whiskers are at 0.03 m s^{-2} and 0.41 m s^{-2} . The two sample t-test with Bonferroni correction shows a significant difference between the two vehicles ($t(2300) = 5.2$, $p < 0.001$, $\alpha_{B,5\%} = 0.006$) with a small effect size ($d = 0.2$).

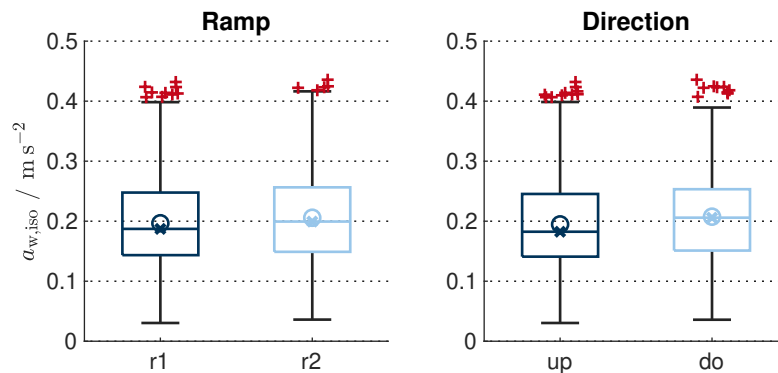


Figure 6.8: Difference in ISO threshold values by ramp type (r1: ramp 1, r2: ramp 2) and direction of the ramp(up: ascending, do: descending)

The other two parameters varied were the ramp type and the ramp direction. Figure 6.8 shows the box-plots for these two parameters. No significant difference was found for the type of ramp ($t(1150) = -2.0$, $p = 0.047$, $\alpha_{B,5\%} = 0.006$), with both ramps having a mean trigger value of 0.18 m s^{-2} .

The impact of the ramp direction is significant ($t(1150) = -2.8$, $p = 0.047$, $\alpha_{B,5\%} = 0.006$), where the ascending ramps have a mean value of 0.19 m s^{-2} and a median value of 0.18 m s^{-2} , with an interquartile range from 0.14 m s^{-2} – 0.25 m s^{-2} and whiskers at 0.03 m s^{-2} and 0.40 m s^{-2} . The descending ramps show a mean value of 0.21 m s^{-2} and a median value of 0.21 m s^{-2} . The interquartile range is 0.15 m s^{-2} – 0.25 m s^{-2} and the whiskers are at 0.04 m s^{-2} and 0.39 m s^{-2} .

The main target of this study was to investigate the influence of the state of attention and the vehicle class on the expected ride comfort. The results are further analyzed in their interdependencies. The data sets are split into states and vehicle types. For each of the splits, the influence of the other factor is evaluated. Figure 6.9 shows the influence of the vehicle type split into the two different states of attention.

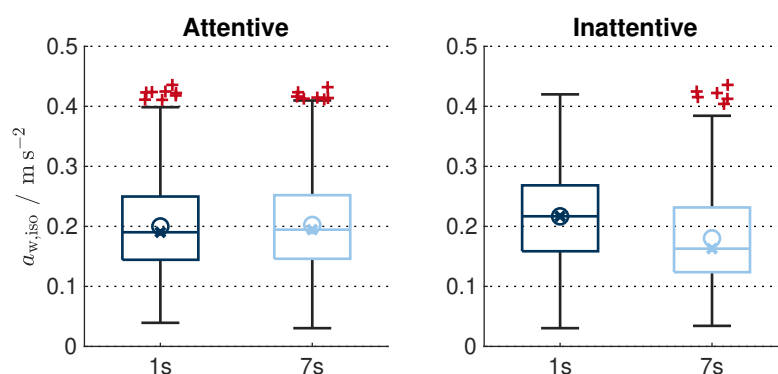


Figure 6.9: Comparison of the ISO threshold values for the two different cars (1s: 1-series, 7s: 7-series) in attentive and inattentive state

One can observe that in attentive state, there is no significant difference for the two vehicles ($t(1150) = -0.5$, $p = 0.584$, $\alpha_{B,5\%} = 0.006$). In the inattentive state there is a significant difference ($t(1150) = 8.0$, $p < 0.001$, $\alpha_{B,5\%} = 0.006$). In the attentive state, the mean value is 0.20 m s^{-2} for both cars. In the inattentive state, the 1-series has a mean value of 0.22 m s^{-2} and the 7-series a mean value of 0.18 m s^{-2} . The difference in median is even greater, with a value of 0.22 m s^{-2} for the 1-series and 0.16 m s^{-2} for the 7-series.

Opposite to the results averaged for both vehicles, the vehicle specific difference between the attentive and the inattentive state is significant in both cases. As shown in Figure 6.10, the subjects have a higher comfort threshold in the inattentive state for the 1-series ($t(1150) = -3.7$, $p < 0.001$, $\alpha_{B,5\%} = 0.006$), and a lower one in the 7-series ($t(1150) = 4.9$, $p < 0.001$, $\alpha_{B,5\%} = 0.006$). The mean discomfort value is 0.20 m s^{-2} in attentive state for both vehicles. In the inattentive state, the mean discomfort value is 0.02 m s^{-2} higher for the 1-series and -0.02 m s^{-2} lower for the 7-series.

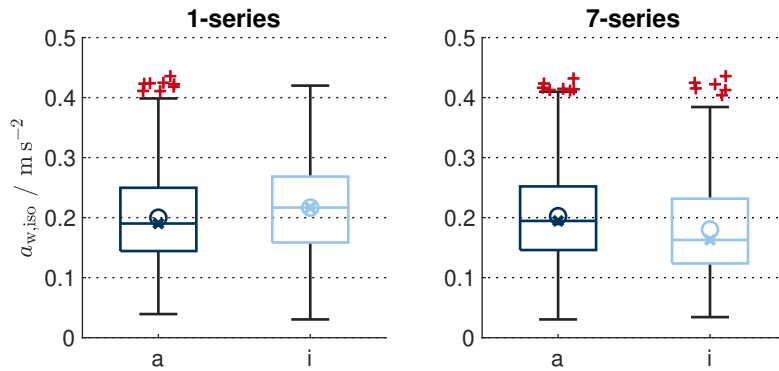


Figure 6.10: Comparison of the ISO threshold values for the two different cars in attentive (a) and inattentive (i) state

Table 6.2 summarizes the results of the eight two-sample t-tests that were performed to check for significant differences in the comfort threshold values. The effect strength value „Cohen’s d“ is listed as well. The largest significant effect is seen for the 1-series and 7-series in inattentive state. The difference has an effect size of $d = 0.5$ corresponding to a medium effect. The other effects are classified as small ($0.2 \leq d < 0.5$), namely the difference in attention for each vehicle, in ramp direction, and between both vehicles overall. No significant differences are observed for the vehicles in inattentive state, the different ramps, and the different states of attention considering both vehicles.

Table 6.2: Results of the two sample t-test and Cohen’s d effect strength for the differences ISO-value, depending on the state of attention, different vehicles, ramps and ramp directions.

critereon	mean 1st	mean 2nd	p-value	rej. of H0	Cohen’s d
Att. - Ina.	0.20	0.20	0.115	false	(0.1)
1-ser. - 7-ser.	0.21	0.19	< 0.001	true	0.2
Ramp 1 - Ramp 2	0.20	0.20	0.047	false	(-0.1)
Up - Down	0.20	0.21	0.005	true	-0.2
1-ser.: Att. - Ina	0.20	0.22	< 0.001	true	-0.2
7-ser.: Att. - Ina	0.20	0.18	< 0.001	true	0.3
Att.: 1-ser. - 7-ser.	0.20	0.20	0.584	false	(0.0)
Ina.: 1-ser. - 7-ser.	0.22	0.18	< 0.001	true	0.5

6.2.2 Motion Sickness and Follow-up Interview

As explained in Subsection 6.1.3, the subjects were asked to rate their current constitution on the MSI scale before and after the simulator drive. The MSI scale ranges from 0 (no problem) to 10 (vomiting). The results of this self-assessment are shown in Figure 6.11. At the start, forty-four

subjects rated their current status as acceptable. Three said they feel slightly unwell, and two subjects stated they feel unwell with minor intensity and no specific symptoms.

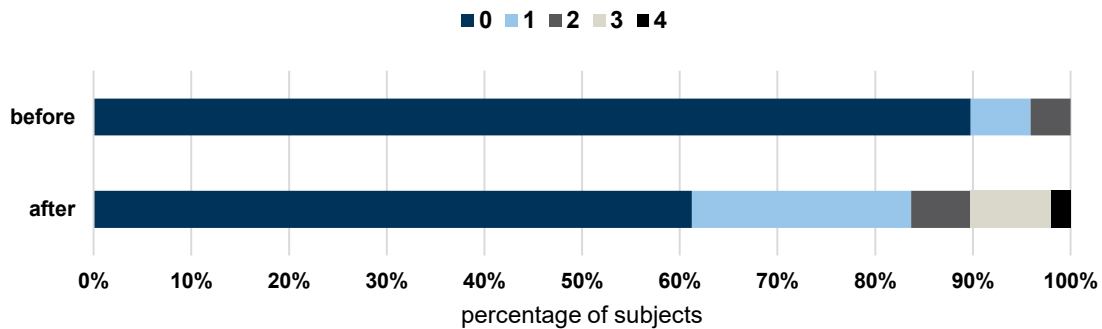


Figure 6.11: Self-determined motion sickness of the subjects before and after study II

After the simulator drive, thirty subjects still did not feel any issues. Eleven subjects felt slightly uneasy, and eight felt unwell without specific symptoms. Of the eight subjects, three felt unwell with negligible intensity, four with minor intensity, and one with medium intensity. None of the subjects felt nausea.

In the post-interview, the subjects were asked if they expect a higher level of comfort in a luxury class vehicle and if they desire more comfort while performing a side task such as working, or playing a game on their cellphone. Both questions are directly related to the research questions investigated in the study and can be compared to the comfort threshold values determined with the trigger.

The results of the self-assessment are shown in Figure 6.12. All subjects state that they expect a higher level of comfort in a premium-class vehicle. In the objective discomfort value, this can only be seen for the inattentive state; there is no significant difference in the attentive state. More than two-thirds of the test persons expect increased comfort when performing a side task. This expectation is only evident for the 7-series in the objective data. An inverse effect is observed for the 1-series, where the subjects had a higher comfort threshold when performing a side-task.

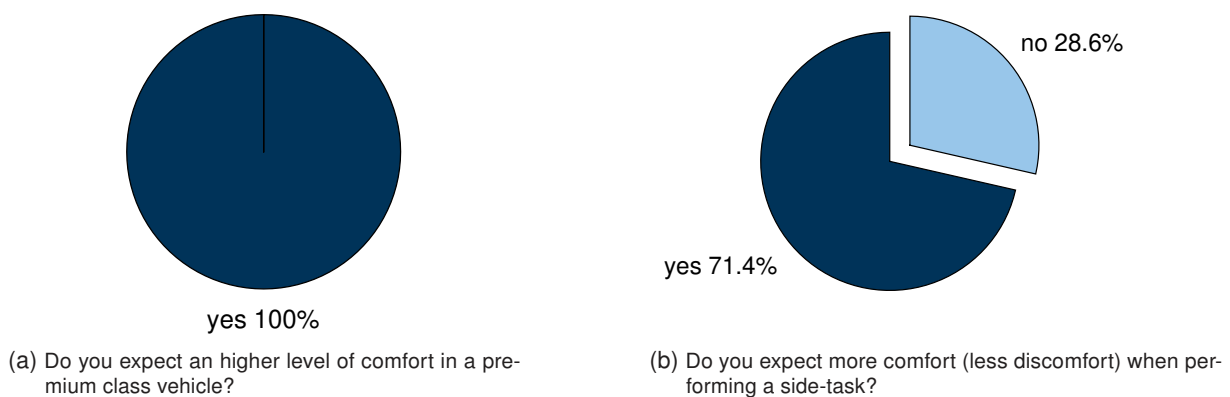


Figure 6.12: Results of the post-session interview in study II

6.3 Discussion

Overall, the results of this simulator study show that $0.20 \pm 0.05 \text{ m s}^{-2}$ according to ISO 2631 [29] can be defined as the ride comfort threshold for an automated drive. Below this threshold, the occupant does not feel disturbed or negatively influenced by the vibration discomfort due to road irregularities. One can expect cars delivering a ride comfort resulting in a discomfort value around this threshold under normal driving conditions to be considered as comfortable. Future investigations should study the threshold value for the barely accepted ride comfort, to define an upper boundary that should not be exceeded.

The discomfort value according to ISO 2631 [29] itself has proven reliable. Two different types of road excitation were used for the ramps, one with predominantly heave and pitch, one primarily with roll motion. No significant difference can be seen in the comfort threshold value for both ramps, which indicates that the directional weighting factors of the ISO 2631 [29] are correct.

It was investigated how the comfort threshold changes for different vehicle types and due to a secondary activity, resulting in an inattentive state of attention. No significant difference was found for the influence of the state of attention averaged over both vehicles. When looking at both vehicle types individually, minor effects are observed, with opposite directions for both vehicles.

In the luxury vehicle (7-series), the test subject demanded increased comfort in an inattentive state. The subjects accepted slightly less comfort in the compact class vehicle (1-series). Comparing this to the results of the post-interview, it could be a subconscious effect in the compact class vehicle. In the luxury class vehicle, the subjects demanded significantly higher comfort by triggering at lower discomfort thresholds. This is analogue to the statement of more than two-thirds in the post-interview. A small significant effect was detected for the influence of the vehicle type when averaged over both states of attention. This effect has a medium size between the vehicles in the inattentive state, whereas no significant difference was found between the two vehicles in the attentive state.

In the post-interview, all of the participants stated that they demand a higher ride comfort in the luxury class vehicle, which is seen for the inattentive state. However, the results for the attentive state show that in a perfect scenario, vehicle passengers would prefer the same ride comfort in a compact-class vehicle as in a luxury vehicle.

In criticism of this investigation, one could ask why defining a comfort threshold value specific to vertical dynamics ride comfort is necessary. A natural target value for ride comfort could be the human perception threshold. However, these perception thresholds and how to define them are still subject to research, as can be seen in various publications [272, 273, 274, 275, 276, 277]. The same is true for difference-perception thresholds for vibration in a vehicle [278, 279]. It is further debatable whether zero vibration would result in the highest comfort perception and if it would be technically and economically feasible to achieve.

The comfort threshold value of $0.20 \pm 0.05 \text{ m s}^{-2}$ can be compared to discomfort values obtained in other modes of (public) transportation. In passenger cars, typical discomfort values are 0.3 m s^{-2} for highway traveling and driving on normal country roads, $0.3 - 0.4 \text{ m s}^{-2}$ for inner city roads and $0.5 - 0.6 \text{ m s}^{-2}$ for bad country roads [280]. In airplanes under normal conditions, discomfort values of $0.2 - 0.3 \text{ m s}^{-2}$ are measured during takeoff and landing, and around $0.1 - 0.2 \text{ m s}^{-2}$ during high altitude cruise flight [280]. In inner-city and suburban public transport, discomfort values are in the range of $0.2 - 0.3 \text{ m s}^{-2}$ for buses, and $0.1 - 0.2 \text{ m s}^{-2}$ for suburban trains [280].

It becomes clear that the target ride comfort value for automated driving falls within the range of discomfort values experienced in air- and rail-transport, but is a fair amount below typical values achieved in current road vehicles.

Something neglected in this investigation is the influence of the seat, which should be investigated in the future. A comparison of three truck seats is made by Wang [281], which shows that the influence of the seat depends on the type of road excitation. The suspension and the seat performance should be tuned in conjunction.

Next investigations should analyze the period used to calculate the discomfort value corresponding to a trigger point. The two seconds have been defined by pre-tests and consistency analysis of calculated discomfort values at different intensity points of a ramp. Future research should validate the results obtained in this simulator study by using longer ramps with an increased trigger time length. A repetition of the study should be performed with compact class and luxury class vehicles from another car brand, aiming to generalize the results for the vehicle classes. Strictly, analyzing the results of this investigation allows solely for conclusions about the BMW 1-series and 7-series.

In conclusion, it can be stated that the target of $0.20 \pm 0.05 \text{ m s}^{-2}$ is not achieved by current series-production suspension systems on medium to low-quality roads. The results from the second study emphasize the result of the first simulator study, where only the active system achieved a desirable level of comfort on low-quality roads. The consequences of a target discomfort threshold of $0.20 \pm 0.05 \text{ m s}^{-2}$ for future suspension systems remain unclear, in general, and particularly for actuators of semi-active and active suspension systems. There are methods for passive suspension systems to derive ride comfort requirements on the springs, dampers, and bushings in simulation. No such methods exist for semi-active and active suspension actuators. The following section presents a new method for deriving these requirements based on a target discomfort value in predefined scenarios.

7 Derivation of Actuator Requirements

Ride comfort in passenger cars depends on the suspension system, the traveling velocity and the condition of the road. While going straight on a smooth road, almost no vertical suspension compliance would be necessary, allowing to travel comfortably with a reference speed of 130 km h^{-1} on a German autobahn. At decreased road quality, either the traveling speed has to be reduced, or the suspension's performance has to be increased, to maintain an equal level of ride comfort.

Chapter 5 gave valuable insight to performance of current suspension systems in automated driving. The results of Chapter 6 show that an ISO 2631 [29] discomfort value of 0.2 m s^{-2} can be used as ride comfort target value. These results are crucial, but do not allow deducting requirements for future suspension systems. Required specifications for active-suspension actuators are unknown. It depends on the scenario, being defined by the road surface quality and the vehicle traveling speed.

The vertical vehicle dynamics controller, which calculates the desired forces for semi-active and active suspensions' actuators, influences suspension actuator requirements. A standard proportional feedback controller will rely on the actuator's slew rate, because it has an effect on the controller's stability. A high slew rate allows an increased controller gain, while maintaining stability and improving performance. This controller requires tuning specific to the actuator's properties. Such a controller cannot be used to investigate general suspension actuator limitation influence on ride comfort. The controller changes depending on actuator characteristics, affecting the actuator's effect. Results would not hold if the controller is changed for a proportional-integral controller, or a state-feedback controller.

The following sections describe the first method to investigate the pure influence of suspension actuator characteristics on ride comfort in different driving scenarios. This section is related to research questions 4.1 and 4.2, asking how suspension actuator requirements can be derived and how they are defined for a reference scenario.

7.1 Method

The method presented next was subject to several student thesis works supervised by the author. After a pre-study, the first student thesis work of Bohlen [282] was conducted, developing the initial method using a quarter vehicle model. This approach was refined and extended, and utilized in a first investigation using artificial road profiles [283]. The student thesis of Reister [284] focused on an extension of the method to a full vehicle model, especially considering roll dynamics. The work of Hartmann [285] used a quarter-vehicle model and focused on implementing semi-active actuator constraints. Kühne [286] extended the method considering actuator accuracy, and investigated the factors sampling rate, and actuator time delay. The

final simulation model presented here is based on the results and effort of all previous works. Background information on the basic principles of MPC, such as the prediction and the control horizon, as well as information on advanced forms of MPC are given in [287, 288]. An overview of MPC history is supplied by Qin [289].

The general model structure can be seen in Figure 7.1. The simulation model includes the vehicle model (Subsection 7.1.1) and the MPC controller (Subsection 7.1.2). The controller contains the solver and the MPC plant model. The MPC controller considers input (\mathbf{u}_{lim}) and output constraints (\mathbf{y}_{lim}), and can be tuned using solver parameters and cost-function weighting matrix \mathbf{W} . Constraints, weighting factors and parameters are explained in Subsection 7.1.3. The simulation scenario (Subsection 7.1.4) contains the road disturbance based on a laser-scanned road profile. The disturbance \mathbf{v}_k influences the plant dynamics and is previewed by the MPC ($\tilde{\mathbf{v}}_k$). The preview is used to calculate the optimal control inputs $\tilde{\mathbf{u}}_k$ over the prediction horizon, based on the outputs $\tilde{\mathbf{y}}_k$ used for the cost function. The optimal control input \mathbf{u}_k , delayed by one time step (\mathbf{u}_{k-1}) is supplied to the plant, resulting in new system states \mathbf{x}_k and outputs \mathbf{y}_k . This simulation model can be considered as an ideal MPC model, because there are no unknown plant dynamics (MPC plant model is exactly the same as the plant model), and there are no unknown external disturbances.

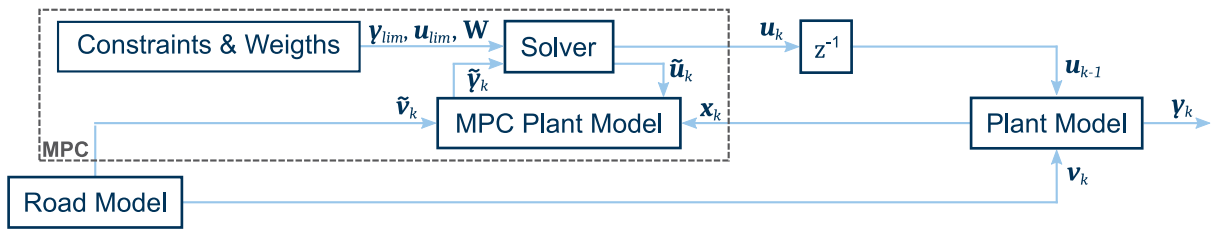


Figure 7.1: Structure of the simulation model

7.1.1 Vehicle Model

The vehicle model is based on the model shown and described in Figure 2.14, Subsection 2.3.2, but with additional ARBs at the front and rear axle. These ARBs (stabilizers) generate a torque around the roll axis, according to the following equation:

$$M_{St} = -c_{St,f} \left(\varphi_{Bo} - \frac{z_{Wh,fl} - z_{Wh,fr}}{b_f} \right) - c_{St,r} \left(\varphi_{Bo} - \frac{z_{Wh,rl} - z_{Wh,rr}}{b_r} \right). \quad (7.1)$$

With these two additional springs, which are only active in body roll or under counter-acting wheel inputs at one axle, the equations of motion of the vehicle model can be derived through the Lagrange formalism:

$$\frac{d}{dt} \left(\frac{\partial T}{\partial \dot{q}_i} \right) - \frac{\partial T}{\partial q_i} + \frac{\partial R}{\partial \dot{q}_i} + \frac{\partial U}{\partial q_i} = Q_i, \quad \text{with } i = 1, \dots, 7. \quad (7.2)$$

The generalized coordinates used for the Lagrange formalism are

$$q = \{ z_{Bo}, \varphi_{Bo}, \theta_{Bo}, z_{Wh,fl}, z_{Wh,fr}, z_{Wh,rl}, z_{Wh,rr} \}, \quad (7.3)$$

the kinetic energy equation is defined as

$$T = \frac{1}{2}m_{Bo}\dot{z}_{Bo}^2 + \frac{1}{2}J_{Bo,x}\dot{\varphi}_{Bo}^2 + \frac{1}{2}J_{Bo,y}\dot{\theta}_{Bo}^2 + \frac{1}{2}m_{Wh,f}(\dot{z}_{Wh,fl}^2 + \dot{z}_{Wh,fr}^2) + \frac{1}{2}m_{Wh,r}(\dot{z}_{Wh,rl}^2 + \dot{z}_{Wh,rr}^2), \quad (7.4)$$

the potential energy equation can be written as

$$\begin{aligned} U = & \frac{1}{2}c_{Bo,f}\left(z_{Bo} - z_{Wh,fl} + \frac{b_f}{2}\varphi_{Bo} - l_f\theta_{Bo}\right)^2 + \frac{1}{2}c_{Bo,f}\left(z_{Bo} - z_{Wh,fr} - \frac{b_f}{2}\varphi_{Bo} - l_f\theta_{Bo}\right)^2 + \dots \\ & + \frac{1}{2}c_{Bo,r}\left(z_{Bo} - z_{Wh,rl} + \frac{b_r}{2}\varphi_{Bo} + l_r\theta_{Bo}\right)^2 + \frac{1}{2}c_{Bo,r}\left(z_{Bo} - z_{Wh,rr} - \frac{b_r}{2}\varphi_{Bo} + l_r\theta_{Bo}\right)^2 + \dots \\ & + \frac{1}{2}c_{St,f}\left(\varphi - \frac{z_{Wh,fl} - z_{Wh,fr}}{b_f}\right)^2 + \frac{1}{2}c_{St,r}\left(\varphi - \frac{z_{Wh,rl} - z_{Wh,rr}}{b_r}\right)^2 + \frac{1}{2}c_{Wh}(z_{Wh,fl} - z_{Ro,fl})^2 + \dots \\ & + \frac{1}{2}c_{Wh}(z_{Wh,fr} - z_{Ro,fr})^2 + \frac{1}{2}c_{Wh}(z_{Wh,rl} - z_{Ro,rl})^2 + \frac{1}{2}c_{Wh}(z_{Wh,rr} - z_{Ro,rr})^2, \end{aligned} \quad (7.5)$$

and the dissipation equation reads

$$\begin{aligned} R = & \frac{1}{2}d_{Bo,f}\left(\dot{z}_{Bo} - \dot{z}_{Wh,fl} + \frac{b_f}{2}\dot{\varphi}_{Bo} - l_f\dot{\theta}_{Bo}\right)^2 + \frac{1}{2}d_{Bo,f}\left(\dot{z}_{Bo} - \dot{z}_{Wh,fr} - \frac{b_f}{2}\dot{\varphi}_{Bo} - l_f\dot{\theta}_{Bo}\right)^2 + \dots \\ & + \frac{1}{2}d_{Bo,r}\left(\dot{z}_{Bo} - \dot{z}_{Wh,rl} + \frac{b_r}{2}\dot{\varphi}_{Bo} + l_r\dot{\theta}_{Bo}\right)^2 + \frac{1}{2}d_{Bo,r}\left(\dot{z}_{Bo} - \dot{z}_{Wh,rr} - \frac{b_r}{2}\dot{\varphi}_{Bo} + l_r\dot{\theta}_{Bo}\right)^2 + \dots \\ & + \frac{1}{2}d_{Wh}(\dot{z}_{Wh,fl} - \dot{z}_{Ro,fl})^2 + \frac{1}{2}d_{Wh}(\dot{z}_{Wh,fr} - \dot{z}_{Ro,fr})^2 + \frac{1}{2}d_{Wh}(\dot{z}_{Wh,rl} - \dot{z}_{Ro,rl})^2 + \dots \\ & + \frac{1}{2}d_{Wh}(\dot{z}_{Wh,rr} - \dot{z}_{Ro,rr})^2. \end{aligned} \quad (7.6)$$

Together with the following external forces

$$\begin{aligned} Q = & \{F_{Ac,fl} + F_{Ac,fr} + F_{Ac,rl} + F_{Ac,rr}, \frac{b_f}{2}(F_{Ac,fl} - F_{Ac,fr}) + \frac{b_r}{2}(F_{Ac,rl} - F_{Ac,rr}), \dots \\ & \dots l_r(F_{Ac,rl} + F_{Ac,rr}) - l_f(F_{Ac,fl} + F_{Ac,fr}), -F_{Ac,fl}, -F_{Ac,fr}, -F_{Ac,rl}, -F_{Ac,rr}\}, \end{aligned} \quad (7.7)$$

the EoM can be obtained by using the Lagrange formalism (Equation (7.2)) and then be written in matrix form

$$\mathbf{M}\ddot{\mathbf{x}} + \mathbf{D}\dot{\mathbf{x}} + \mathbf{K}\mathbf{x} = \tilde{\mathbf{D}}\dot{\mathbf{s}} + \tilde{\mathbf{K}}\mathbf{s} + \mathbf{F}\mathbf{u}, \quad (7.8)$$

where \mathbf{x} , \mathbf{s} and \mathbf{u} are defined as

$$\begin{aligned} \mathbf{x} &= [z_{Bo} \quad \varphi_{Bo} \quad \theta_{Bo} \quad z_{Wh,fl} \quad z_{Wh,fr} \quad z_{Wh,rl} \quad z_{Wh,rr}]^T \\ \mathbf{s} &= [z_{Ro,fl} \quad z_{Ro,fr} \quad z_{Ro,rl} \quad z_{Ro,rr}]^T \\ \mathbf{u} &= [F_{Ac,fl} \quad F_{Ac,fr} \quad F_{Ac,rl} \quad F_{Ac,rr}]^T. \end{aligned}$$

The EoM can be reformulated as continuous-time state-space model

$$\dot{\mathbf{x}}(t) = \mathbf{A}_c\mathbf{x}(t) + \mathbf{B}_c\mathbf{u}(t) \quad (7.9a)$$

$$\mathbf{y}(t) = \mathbf{C}_c\mathbf{x}(t) + \mathbf{D}_c\mathbf{u}(t), \quad (7.9b)$$

with the state-vector

$$\mathbf{x} = [z_{Bo} \quad \varphi_{Bo} \quad \theta_{Bo} \quad z_{Wh,fl} \quad z_{Wh,fr} \quad z_{Wh,rl} \quad z_{Wh,rr} \quad \dot{z}_{Bo} \quad \dot{\varphi}_{Bo} \quad \dot{\theta}_{Bo} \dots \\ \dots \dot{z}_{Wh,fl} \quad \dot{z}_{Wh,fr} \quad \dot{z}_{Wh,rl} \quad \dot{z}_{Wh,rr}]^T,$$

and the input-vector

$$\mathbf{u} = [F_{Ac,fl} \quad F_{Ac,fr} \quad F_{Ac,rl} \quad F_{Ac,rr} \quad z_{Ro,fl} \quad z_{Ro,fr} \quad z_{Ro,rl} \quad z_{Ro,rr} \quad \dot{z}_{Ro,fl} \quad \dot{z}_{Ro,fr} \quad \dot{z}_{Ro,rl} \quad \dot{z}_{Ro,rr}]^T.$$

The system matrix and the input matrix can be obtained from the EoM by performing:

$$A_c = \begin{bmatrix} \mathbf{0}_{7 \times 7} & \mathbf{I}_{7 \times 7} \\ -\mathbf{M}^{-1}\mathbf{K} & -\mathbf{M}^{-1}\mathbf{D} \end{bmatrix} \quad B_c = \begin{bmatrix} \mathbf{0}_{7 \times 4} & \mathbf{0}_{7 \times 4} & \mathbf{0}_{7 \times 4} \\ \mathbf{M}^{-1}\mathbf{F} & \mathbf{M}^{-1}\tilde{\mathbf{K}} & \mathbf{M}^{-1}\tilde{\mathbf{D}} \end{bmatrix}. \quad (7.10)$$

The matrices C_c and D_c are chosen in order to obtain the following output-vector

$$\mathbf{y} = [\ddot{z}_{Bo} \quad \ddot{\varphi}_{Bo} \quad \ddot{\theta}_{Bo} \quad F_{Wh,fl} \quad F_{Wh,fr} \quad F_{Wh,rl} \quad F_{Wh,rr} \quad s_{sus,fl} \quad s_{sus,fr} \quad s_{sus,rl} \dots \\ \dots s_{sus,rr} \quad \dot{s}_{sus,fl} \quad \dot{s}_{sus,fr} \quad \dot{s}_{sus,rl} \quad \dot{s}_{sus,rr}]^T,$$

where the first three rows of the output equation are the same as rows eight to ten of the state equations. The equations for the dynamics wheel loads F_{Wh} , the four suspension deflections s_{sus} and the four suspension velocities \dot{s}_{sus} are shown exemplary for the front left wheel:

$$F_{Wh,fl} = c_{Wh} (z_{Ro,fl} - z_{Wh,fl}) + d_{Wh} (\dot{z}_{Ro,fl} - \dot{z}_{Wh,fl}) \quad (7.11)$$

$$s_{sus,fl} = z_{Bo} - z_{Wh,fl} + \frac{b_f}{2} \varphi - l_f \theta \quad (7.12)$$

$$\dot{s}_{sus,fl} = \dot{z}_{Bo} - \dot{z}_{Wh,fl} + \frac{b_f}{2} \dot{\varphi} - l_f \dot{\theta}. \quad (7.13)$$

For the other wheels, the signs of the coordinates have to be adjusted accordingly. The state-space model has to be discretized to be used as a plant and MPC plant model. A simple way is a forward Euler discretization. For higher accuracy, it is advisable to use the matrix-exponential method, which is implemented in the Matlab transformation function („c2d“).

$$\mathbf{A} = \exp(\mathbf{A}_c t_s) \quad (7.14a)$$

$$\mathbf{B} = [\mathbf{A} - \mathbf{I}_4] \mathbf{A}_c^{-1} \mathbf{B}_c \quad (7.14b)$$

$$\mathbf{C} = \mathbf{C}_c \quad (7.14c)$$

$$\mathbf{D} = \mathbf{D}_c, \quad (7.14d)$$

Using these matrices, the discretized model can be written as:

$$\mathbf{x}_{k+1} = \mathbf{A} \mathbf{x}_k + \mathbf{B} \mathbf{u}_k \quad (7.15a)$$

$$\mathbf{y}_k = \mathbf{C} \mathbf{x}_k + \mathbf{D} \mathbf{u}_k. \quad (7.15b)$$

The input is further split into control input and disturbance input

$$\mathbf{x}_{k+1} = \mathbf{A}\mathbf{x}_k + \mathbf{B}^{(u)}\mathbf{u}_k + \mathbf{B}^{(v)}\mathbf{v}_k \quad (7.16a)$$

$$\mathbf{y}_k = \mathbf{C}\mathbf{x}_k + \mathbf{D}^{(u)}\mathbf{u}_k + \mathbf{D}^{(v)}\mathbf{v}_k, \quad (7.16b)$$

where

$$\mathbf{B} = \begin{bmatrix} \mathbf{B}_{14 \times 4}^{(u)} & \mathbf{B}_{14 \times 8}^{(v)} \end{bmatrix}$$

$$\mathbf{D} = \begin{bmatrix} \mathbf{D}_{14 \times 4}^{(u)} & \mathbf{D}_{14 \times 8}^{(v)} \end{bmatrix}$$

$$\mathbf{u}_k = \begin{bmatrix} \mathbf{u}_{1 \times 4}^{(new)} & \mathbf{v}_{1 \times 8} \end{bmatrix}^T.$$

In the following, the vector $\mathbf{u}_{1 \times 4, k}^{(new)}$ will be denoted as \mathbf{u}_k again. The actuator delay is absorbed into the model by defining four new states, which are the force inputs from the previous time-step, and results in a state-vector \mathbf{x} with eighteen states:

$$\mathbf{x} = [z_{Bo} \quad \varphi_{Bo} \quad \theta_{Bo} \quad z_{Wh,fl} \quad z_{Wh,fr} \quad z_{Wh,rl} \quad z_{Wh,rr} \quad \dot{z}_{Bo} \quad \dot{\varphi}_{Bo} \quad \dot{\theta}_{Bo} \dots \\ \dots \quad \dot{z}_{Wh,fl} \quad \dot{z}_{Wh,fr} \quad \dot{z}_{Wh,rl} \quad \dot{z}_{Wh,rr} \quad F_{Ac,fl}^{(k-1)} \quad F_{Ac,fr}^{(k-1)} \quad F_{Ac,rl}^{(k-1)} \quad F_{Ac,rr}^{(k-1)}]^T.$$

The state-space matrices for the model with input delay are constructed from the old matrices as:

$$\mathbf{A} = \begin{bmatrix} \mathbf{A}_{14 \times 14}^{(old)} & \mathbf{B}_{14 \times 4}^{(u,old)} \\ \mathbf{0}_{4 \times 14} & \mathbf{0}_{4 \times 4} \end{bmatrix}; \quad \mathbf{B}^{(u)} = \begin{bmatrix} \mathbf{0}_{14 \times 4} \\ \mathbf{I}_{4 \times 4} \end{bmatrix}; \quad \mathbf{B}^{(v)} = \begin{bmatrix} \mathbf{B}_{14 \times 8}^{(v,old)} \\ \mathbf{0}_{4 \times 4} \end{bmatrix}; \quad \mathbf{C} = [\mathbf{C}_{15 \times 14}^{(v,old)} \quad \mathbf{D}_{15 \times 4}^{(u,old)}]; \quad \mathbf{D} = \mathbf{D}_{15 \times 8}^{(v,old)}.$$

The feed-through of the actuator force to the output is eliminated and the state-space model becomes:

$$\mathbf{x}_{k+1} = \mathbf{A}\mathbf{x}_k + \mathbf{B}^{(u)}\mathbf{u}_k + \mathbf{B}^{(v)}\mathbf{v}_k \quad (7.17a)$$

$$\mathbf{y}_k = \mathbf{C}\mathbf{x}_k + \mathbf{D}\mathbf{v}_k, \quad (7.17b)$$

with the state solution

$$\mathbf{x}_k = \mathbf{A}^k \mathbf{x}_0 + \sum_{i=0}^{k-1} \mathbf{A}^{k-i-1} (\mathbf{B}^{(u)}\mathbf{u}_k + \mathbf{B}^{(v)}\mathbf{v}_k), \quad (7.18)$$

and the output solution

$$\mathbf{y}_k = \mathbf{C} \left[\mathbf{A}^k \mathbf{x}_0 + \sum_{i=0}^{k-1} \mathbf{A}^{k-i-1} (\mathbf{B}^{(u)}\mathbf{u}_k + \mathbf{B}^{(v)}\mathbf{v}_k) \right] + \mathbf{D}\mathbf{v}_k. \quad (7.19)$$

7.1.2 Controller Synthesis

The core of a model-predictive controller is the cost function, which has to be based on the internal model, combined with a solver. In a real-world application, the exact plant dynamics are unknown, and the MPC plant model is an approximation. States or outputs are measured or estimated and used as initialization of the MPC model in each time step, causing MPC to be a form of feedback control.

The controller uses exact preview information. The optimal inputs are calculated for the control horizon, depending on the cost function over the prediction horizon. The prediction horizon is defined as the time steps used for future prediction, and the control horizon as the number of future time steps the optimal input is calculated for.

In linear MPC, as applied here, the output solution of the linear model is formulated as matrix equations over the prediction horizon. The resulting convex optimization problem is solved iteratively. The optimal solution for the next step is used as control input. Thereafter, the procedure is repeated.

In real-world application, the optimization problem has to be solved within one sampling time-step, or a sub-optimal solution must be used. MPC is considered state of the art in industrial process control with relatively long time-scales of seconds to minutes. It is rarely seen in a real-world application of vertical vehicle dynamics, where the sampling times are in a range of 100–1000 Hz.

In the simulation method here, MPC is used to obtain the theoretical optimal solution for a given scenario. It allows to eliminate the controller's influence when comparing different actuator constraints, such as maximum force or maximum slew-rate. A resulting difference in performance can be traced back to the actuator limitations.

All plant system states and outputs, as well as the future disturbance inputs, are known precisely in the simulation. Compared to a classical optimal control problem, which could be formulated as well, the MPC divides the problem for one scenario into multiple smaller sub-problems, following the principle of dynamic programming. In this way, computation time is reduced, and explicit input and output constraints can be considered.

It follows the cost function derivation. The output solution of the vehicle model in Equation (7.19) can be used to formulate the solutions over the next p steps of the prediction horizon as a vector of vectors:

$$\begin{aligned} \begin{bmatrix} \mathbf{y}_{k+1} \\ \mathbf{y}_{k+2} \\ \dots \\ \mathbf{y}_{k+p} \end{bmatrix} &= \begin{bmatrix} \mathbf{CA} \\ \mathbf{CA}^2 \\ \dots \\ \mathbf{CA}^p \end{bmatrix} \mathbf{x}_k + \begin{bmatrix} \mathbf{CB}^{(u)} & 0 & \dots & 0 \\ \mathbf{CAB}^{(u)} & \mathbf{CB}^{(u)} & \dots & 0 \\ \dots & \dots & \dots & \dots \\ \mathbf{CA}^{p-1}\mathbf{B}^{(u)} & \mathbf{CA}^{p-2}\mathbf{B}^{(u)} & \dots & \mathbf{CB}^{(u)} \end{bmatrix} \begin{bmatrix} \mathbf{u}_k \\ \mathbf{u}_{k+1} \\ \dots \\ \mathbf{u}_{k+p-1} \end{bmatrix} + \dots \\ &\dots + \begin{bmatrix} \mathbf{CB}^{(v)} & \mathbf{D} & 0 & \dots & 0 \\ \mathbf{CAB}^{(v)} & \mathbf{CB}^{(v)} & \mathbf{D} & \dots & 0 \\ \dots & \dots & \dots & \dots & \dots \\ \mathbf{CA}^{p-1}\mathbf{B}^{(v)} & \mathbf{CA}^{p-2}\mathbf{B}^{(v)} & \mathbf{CA}^{p-3}\mathbf{B}^{(v)} & \dots & \mathbf{D} \end{bmatrix} \begin{bmatrix} \mathbf{v}_k \\ \mathbf{v}_{k+1} \\ \dots \\ \mathbf{v}_{k+p} \end{bmatrix}. \quad (7.20) \end{aligned}$$

By defining

$$\tilde{\mathbf{y}} = \begin{bmatrix} \mathbf{y}_{k+1} \\ \mathbf{y}_{k+2} \\ \dots \\ \mathbf{y}_{k+p} \end{bmatrix}; \quad \tilde{\mathbf{u}} = \begin{bmatrix} \mathbf{u}_k \\ \mathbf{u}_{k+1} \\ \dots \\ \mathbf{u}_{k+p-1} \end{bmatrix}; \quad \tilde{\mathbf{v}} = \begin{bmatrix} \mathbf{v}_k \\ \mathbf{v}_{k+1} \\ \dots \\ \mathbf{v}_{k+p} \end{bmatrix}; \quad \Omega = \begin{bmatrix} \mathbf{CA} \\ \mathbf{CA}^2 \\ \dots \\ \mathbf{CA}^p \end{bmatrix},$$

and

$$\Gamma_u = \begin{bmatrix} \mathbf{CB}^{(u)} & 0 & \dots & 0 \\ \mathbf{CAB}^{(u)} & \mathbf{CB}^{(u)} & \dots & 0 \\ \dots & \dots & \dots & \dots \\ \mathbf{CA}^{p-1}\mathbf{B}^{(u)} & \mathbf{CA}^{p-2}\mathbf{B}^{(u)} & \dots & \mathbf{CB}^{(u)} \end{bmatrix}; \quad \Gamma_v = \begin{bmatrix} \mathbf{CB}^{(v)} & \mathbf{D} & 0 & \dots & 0 \\ \mathbf{CAB}^{(v)} & \mathbf{CB}^{(v)} & \mathbf{D} & \dots & 0 \\ \dots & \dots & \dots & \dots & \dots \\ \mathbf{CA}^{p-1}\mathbf{B}^{(v)} & \mathbf{CA}^{p-2}\mathbf{B}^{(v)} & \mathbf{CA}^{p-3}\mathbf{B}^{(v)} & \dots & \mathbf{D} \end{bmatrix},$$

equation (7.20) can be written as

$$\tilde{\mathbf{y}}_k = \mathbf{\Omega}\mathbf{x}_k + \Gamma_u\tilde{\mathbf{u}}_k + \Gamma_v\tilde{\mathbf{v}}_k. \quad (7.21)$$

Inserting Equation (7.21) into a general convex cost function with a weighting matrix $\tilde{\mathbf{W}}$ yields:

$$J_k(\tilde{\mathbf{u}}_k) = (\mathbf{\Omega}\mathbf{x}_k + \Gamma_u\tilde{\mathbf{u}}_k + \Gamma_v\tilde{\mathbf{v}}_k)^T \tilde{\mathbf{W}} (\mathbf{\Omega}\mathbf{x}_k + \Gamma_u\tilde{\mathbf{u}}_k + \Gamma_v\tilde{\mathbf{v}}_k). \quad (7.22)$$

By using matrix calculation and omitting all constant terms which do not depend on the control inputs $\tilde{\mathbf{u}}_k$, the final cost function can be written as:

$$J_k(\tilde{\mathbf{u}}_k) = \frac{1}{2}\tilde{\mathbf{u}}_k^T \Gamma_u^T \tilde{\mathbf{W}} \Gamma_u \tilde{\mathbf{u}}_k + (\mathbf{x}_k^T \mathbf{\Omega}^T + \tilde{\mathbf{v}}_k^T \Gamma_v^T) \tilde{\mathbf{W}} \Gamma_u \tilde{\mathbf{u}}_k. \quad (7.23)$$

7.1.3 Boundary Conditions and Actuator Constraints

As already mentioned in Section 2.3 vertical vehicle dynamics are characterized by the objective conflict between ride comfort and road-holding. Semi-active and active systems can push the performance envelope by partly resolving this conflict, but the objective conflict remains overall. Consequently, a suspension control system optimized for comfort still inherits a trade-off concerning road-holding, which is characterized by the dynamic wheel load variation.

A second aspect that limits the ride comfort performance of vertical vehicle dynamics control systems is the available suspension travel. The suspension travel is finite, and it is essential to keep the suspension close to its center position because otherwise, the suspension is more prone to hit the bump stops, which results in massive discomfort due to a sudden jerk and the resulting acoustics.

Without considering the dynamic wheel load variation and the suspension deflection, an optimal controller, as described above, provided with an optimal actuator, can eliminate the vehicle body acceleration at the cost of substantial dynamic wheel load and suspension deflection variations. The optimal actuator is impossible in reality, and the available power of the system limits the control system's performance. Still, the dynamic wheel loads and the suspension travel are limiting factors to the achievable ride comfort and need to be considered for the investigation. The dynamic wheel load and the suspension travel can be restricted in minimum and maximum value as boundary conditions (output constraints) according to equations (7.24a–h), so at each time step k , the actual dynamic wheel loads and suspension positions are explicitly kept within these limits. Minimum dynamic wheel loads for front and rear axle are $F_{\text{dyn},f,\text{min}}$ and $F_{\text{dyn},r,\text{min}}$ respectively. The maximum dynamic wheel load for all wheels is $F_{\text{dyn},\text{max}}$. Minimum and maximum

suspension travel for all wheels are $s_{\text{sus,min}}$ and $s_{\text{sus,max}}$.

$$F_{\text{dyn},f,\text{min}} \leq F_{\text{dyn},fl,k} \leq F_{\text{dyn},\text{max}} \quad (7.24a)$$

$$F_{\text{dyn},f,\text{min}} \leq F_{\text{dyn},fr,k} \leq F_{\text{dyn},\text{max}} \quad (7.24b)$$

$$F_{\text{dyn},r,\text{min}} \leq F_{\text{dyn},rl,k} \leq F_{\text{dyn},\text{max}} \quad (7.24c)$$

$$F_{\text{dyn},r,\text{min}} \leq F_{\text{dyn},rr,k} \leq F_{\text{dyn},\text{max}} \quad (7.24d)$$

$$s_{\text{sus,min}} \leq s_{\text{sus},fl,k} \leq s_{\text{sus,max}} \quad (7.24e)$$

$$s_{\text{sus,min}} \leq s_{\text{sus},fr,k} \leq s_{\text{sus,max}} \quad (7.24f)$$

$$s_{\text{sus,min}} \leq s_{\text{sus},rl,k} \leq s_{\text{sus,max}} \quad (7.24g)$$

$$s_{\text{sus,min}} \leq s_{\text{sus},rr,k} \leq s_{\text{sus,max}} \quad (7.24h)$$

The core functionality of this method is to investigate the ride comfort performance concerning actuator limitations. A suspension actuator's two most characteristic limitations are its maximum force and its maximum slew rate. In the chosen installation of the actuator in the vehicle model, the actuator works in parallel to a passive spring which carries the static vehicle body weight, and a passive damper which supplies the same amount of damping as a comfortable passive suspension. An installation like this has the advantage of being fail-safe regarding the active system, so the car can still be operated when the active system has a malfunction and is switched off. The vehicle model could be altered to investigate other installation settings. Equations (7.25a–b) show the implementation of the actuator limitations as input constraints. The actuator control force at each time step $F_{\text{Ac},k}$ and its time derivative $\dot{F}_{\text{Ac},k}$ are explicitly kept within these limits $F_{\text{Ac,min}}$, $F_{\text{Ac,max}}$, $\dot{F}_{\text{Ac,min}}$ and $\dot{F}_{\text{Ac,max}}$ are defined symmetrically as $\pm F_{\text{Ac,lim}}$ and $\pm \dot{F}_{\text{Ac,lim}}$.

$$F_{\text{Ac,min}} \leq F_{\text{Ac},k} \leq F_{\text{Ac,max}} \quad (7.25a)$$

$$\dot{F}_{\text{Ac,min}} \leq \dot{F}_{\text{Ac},k} \leq \dot{F}_{\text{Ac,max}} \quad (7.25b)$$

Additionally to the restricted active-suspension vehicle, a passive vehicle, a vehicle with a semi-active suspension, and an unrestricted active suspension are simulated. The passive vehicle is the baseline reference, the unrestricted active vehicle shows the performance limit for the given boundary conditions. Like a passive damper, a continuously variable damper inherits a velocity dependency for the maximum and minimum force that can be supplied.

Figure 7.2 shows the force-velocity map of a semi-active damper. The relative velocity of the damper (x-axis) defines the minimum damping curve (light-blue) and the maximum damping curve (dark blue). These curves are non-linear and cannot be implemented in the linear time invariant MPC. A possibility would be a linearization at zero velocity, but this would lead to a substantial deviation at higher damper velocities above the knee in the maximum damping curve. Here, the semi-active damper map is implemented indirectly by using the predicted damper velocities from the MPC solution of the previous time step. The limits are adjusted for each time step by using the predicted velocities. They are obtained from a lookup-table of the minimum and maximum damping curves.

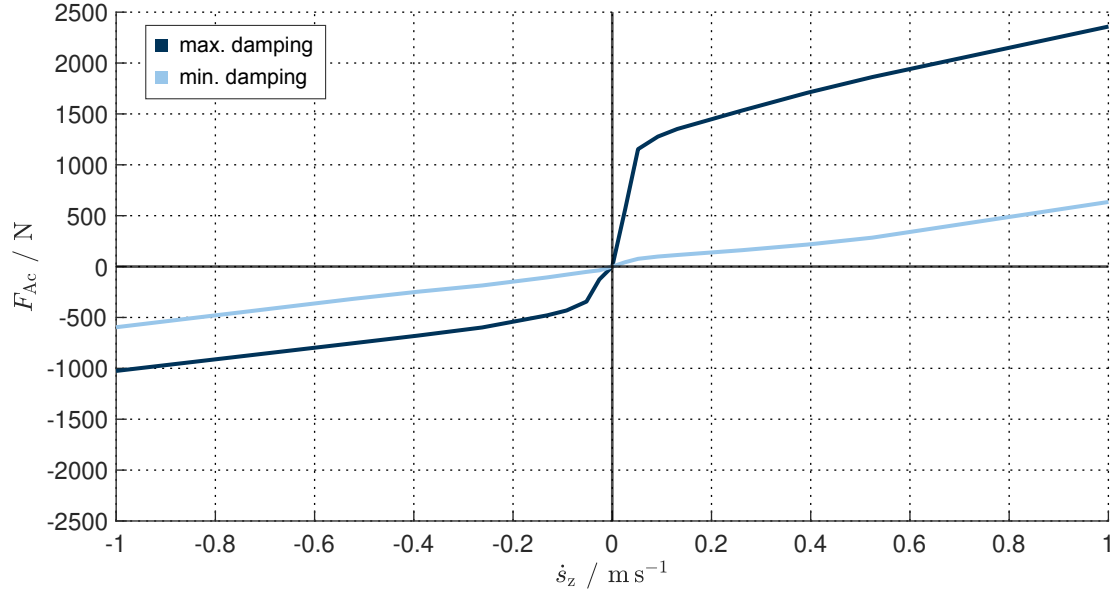


Figure 7.2: Semi-active damper map – dark blue line is maximum damping, light blue line is minimum damping

It is a recursive problem because the relative velocities depend on the relative speed and vice-versa. A sufficiently good approximation is achieved because the estimated velocities are updated in each sampling interval. The relative velocity at a certain point in the future moves through the entire prediction horizon. In each time step, the optimization is handed over a vector with variable minimum and maximum values for the actuator force at each point of the prediction horizon. The passive damping (in parallel to the actuator) is deactivated for the semi-active simulation.

The principle of using the estimated relative velocities from the previous time step is used to implement a power limitation. Additionally to the previous limitations, it can be checked that the desired actuator force does not exceed the maximum force due to the maximum system power, which is defined in Equation (7.26). The power limit was varied from 0–5 kW per actuator.

$$F_{Ac,lim,pow} = \frac{P_{Ac,max}}{\dot{s}_{sus}} . \quad (7.26)$$

Something not considered for the reference scenario is the dynamic behavior of an actuator to a step-input of the desired force. An investigation has shown that the dynamics of an electro-mechanical actuator can be modeled as a PT2 system [133] and implemented in a simulation model [134]. Semi-active dampers show switching dynamics, which can be described as PT1 system [102]. Both could be implemented in the MPC for the future. In this investigation, the inner loop has been excluded and is considered a part of the actuator system.

It is investigated how an unknown disturbance of the desired actuator force deteriorates the performance, achieved by adding a normally distributed error force $F_{Ac,err}$ with zero mean (μ) and a standard deviation $F_{Ac,\sigma}$ to the desired actuator force F_{Ac} . The disturbed actuator force $F_{Ac,dis}$ is defined in Equation (7.27). The standard deviation for the error force of each actuator is varied between 0 – 500 N.

$$F_{Ac,dis} = F_{Ac} + F_{Ac,err} , \text{ with } \mathcal{N}(F_{Ac,err} | \mu = 0, \sigma^2 = F_{Ac,\sigma}^2) . \quad (7.27)$$

7.1.4 Test Scenario Definition

This section presents all relevant simulation settings and parameters. First, the boundary conditions are defined. For the exemplary scenario in this research, the front $F_{dyn,f,min}$ and rear wheels $F_{dyn,r,min}$ are limited to non-negative vertical loads at each time step k , to ensure that the simulations stay within the model's validity range. The dynamic wheel load amplitude may not become smaller than the negative static wheel load, which results in a lower limit of -5648 N for the front wheels and -5339 N for the rear wheels. Maximum wheel load $F_{dyn,max}$ is unrestricted in this scenario. Bump and rebound travel are restricted to 0.10 m and -0.08 m respectively. In general, individual limits can be set for each wheel, but for the reference scenario, this was not necessary. The boundary conditions are summarized in Table 7.1.

Table 7.1: Boundary Conditions (Output Constraints)

Parameter	Value	Unit
$F_{dyn,f,min}$	-5648	N
$F_{dyn,r,min}$	-5339	N
$F_{dyn,max}$	inf	N
$s_{sus,min}$	-0.08	m
$s_{sus,max}$	0.10	m

Table 7.2 shows the different force and slew rate constraints that are tested in the reference scenario. All of the combinations are simulated which results in 64 simulations in total.

Table 7.2: Actuator limitations (input constraints)

$F_{Ac,lim} / \text{kN}$	0.25	0.50	0.75	1.00	1.25	1.50	1.75	2.00
$\dot{F}_{Ac,lim} / \text{kNs}^{-1}$	1.00	2.50	5.00	10.00	20.00	30.00	40.00	50.00

The vehicle parameters are summarized in Table 7.3. These parameters are representative for a BMW 7-series (G12). The total vehicle mass is 2240 kg with unsprung masses of 63 kg and 61 kg per wheel at the front and rear axle, a sprung mass of 1992 kg, a roll inertia of 828 kg m² and a pitch inertia of 4525 kg m². The vehicle weight distribution is 51.4% to the front, resulting in an eigenfrequency of 1.10 Hz for the front axle and 1.21 Hz for the rear axle.

Table 7.3: Model parameters.

Name	Parameter	Value	Unit
Sprung mass	m_{Bo}	1992	kg
Roll inertia	$J_{Bo,x}$	828	kg m ²
Pitch inertia	$J_{Bo,y}$	4525	kg m ²
Unsprung mass front	$m_{Wh,f}$	63	kg
Unsprung mass rear	$m_{Wh,r}$	61	kg
Suspension stiffness front	$c_{Bo,f}$	24400	N m ⁻¹
Suspension stiffness rear	$c_{Bo,r}$	28000	N m ⁻¹
ARB stiffness front	$c_{St,f}$	24400	N m ⁻¹
ARB stiffness rear	$c_{St,r}$	28000	N m ⁻¹
Tire stiffness	c_{Wh}	360000	N m ⁻¹
Suspension damping front	$d_{Bo,f}$	2123	N s m ⁻¹
Suspension damping rear	$d_{Bo,r}$	2209	N s m ⁻¹
Tire damping	d_{Wh}	80	N s m ⁻¹
Center of Gravity (CoG) to front axle	l_f	1.56	m
CoG to rear axle	l_r	1.65	m
Track-width front	b_f	1.62	m
Track-width rear	b_r	1.65	m
Contact patch length	l_{Cp}	0.1	m
Actuator delay	t_{Ac}	0.01	s

The roll eigenfrequency is 1.25 Hz and the pitch eigenfrequency is 1.37 Hz. The vertical tire stiffness is set to 360 000 N m⁻¹ resulting in an unsprung mass frequency of 12.43 Hz at the front axle and 12.79 Hz at the rear axle. Tire damping is set to 80 N s m⁻¹ but does almost not influence the system dynamics and might therefore be neglected as well. The time delay between the control unit and the actuator is assumed to be 0.01 s. The contact patch length is parameterized to 0.1 m.

The simulation settings are shown in Table 7.4. The sampling frequency of the simulation is chosen as 100 Hz, about eight times higher than the highest eigenfrequency in the vehicle model, and five times higher than the maximum frequency analyzed in the frequency domain (20 Hz). Total simulation time is 48 s, resulting from the vehicle speed of 80 km h⁻¹ and the road profile length of 1066 m.

The preview horizon is specified to ten samples or 0.1 s, and the resulting control horizon is nine samples or 0.09 s. Two important settings are the „*presolve*“ and the „*numeric focus*“ for the Gurobi solver [290], which will be explained in Subsection 7.1.5. The „*presolve*“ option is set to aggressive, the „*numeric focus*“ is set conservative, forcing the solver to use smaller step-sizes avoiding numeric errors.

The MPC was tuned with the weighting factors displayed in Table 7.5. The main objective was to minimize the vehicle body accelerations, shown in Section 7.2 Results. The weighting factors for the vertical acceleration $w_{\ddot{z}_{Bo}}$, the roll acceleration $w_{\ddot{\varphi}_{Bo}}$ and the pitch acceleration $w_{\ddot{\theta}_{Bo}}$ are set to one. The weighting factor for the dynamic wheel load variation $w_{F_{dyn}}$ and the suspension deflection $w_{z_{sus}}$ are set to 0.

Table 7.4: Simulation settings.

Name	Parameter	Value	Unit
Sampling time	t_s	0.01	s
Simulation time	t_{end}	48	s
Vehicle speed	v_x	80	km h ⁻¹
Profile length	l_p	1066	m
Preview horizon	t_p	0.1	s
Control horizon	t_c	0.09	s
Gurobi „ <i>presolve</i> “	-	2	-
Gurobi „ <i>numeric focus</i> “	-	3	-

It is possible to investigate other weighting factor combinations. The dynamic wheel load variation and suspension deflection weights should not be zero when implemented in an actual vehicle. For the theoretical experiment, the main interest is to see the pure influence of actuator limitations on achievable ride comfort. In contrast, the actuator limitations influence on minimization of the dynamic wheel load is shown in Appendix D.2.

Table 7.5: Weighting factors for the two optimization objectives.

	$w_{\ddot{z}_{Bo}}$	$w_{\ddot{\varphi}_{Bo}}$	$w_{\ddot{\theta}_{Bo}}$	$w_{F_{dyn}}$	$w_{z_{sus}}$
$\min(\ddot{z}_{Bo})$	1	1	1	0	0
$\min(F_{dyn})$	0	0	0	1	0

The road profile used for the reference scenario is shown in Figure 7.3, displayed in the spatial domain (wavelength n) on macro-scale and with a small cut-out on micro-scale in Figure 7.3a. A comparison to the ISO 8608 [214] classes in the spacial-frequency domain is given in Figure 7.3b. In general, the profile can be classified as class D. In the range of long wavelengths above 30 m ($n < 3 \cdot 10^{-2}$) it can be classified as class D-E.

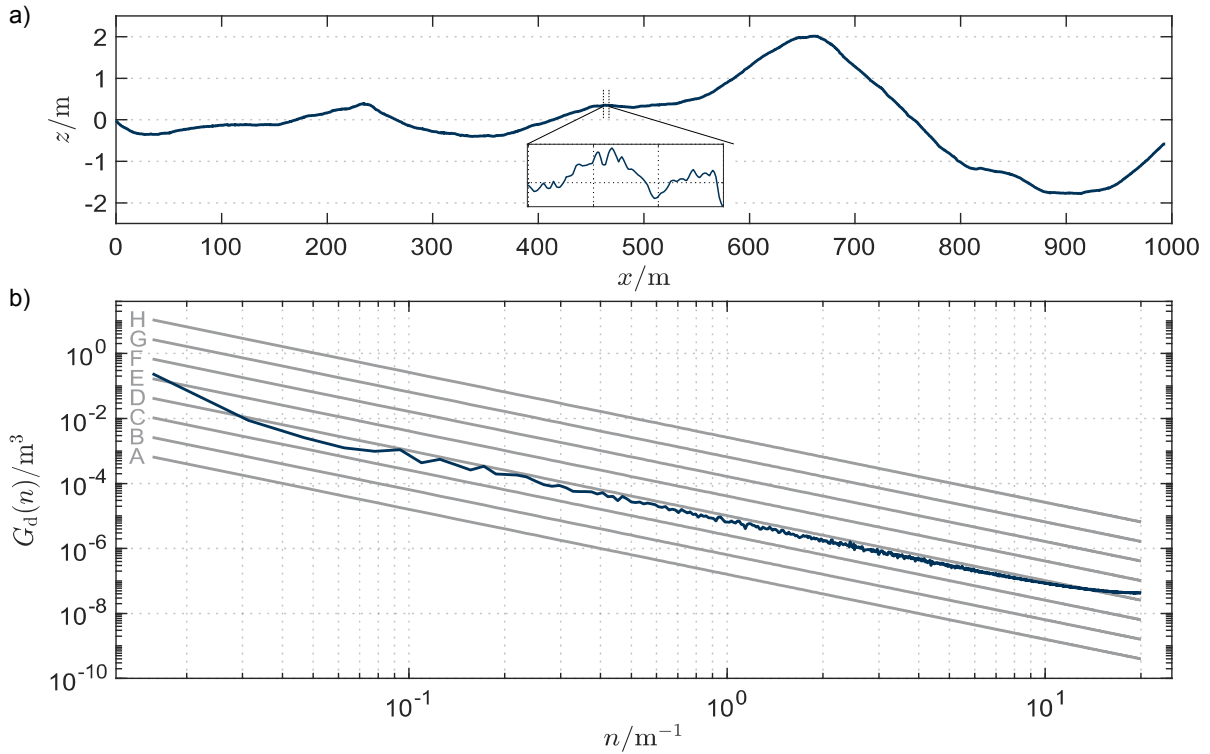


Figure 7.3: Road Profile

7.1.5 Implementation and Analysis Methods

The simulation model was implemented in Matlab using the YALMIP toolbox [291] combined with the Gurobi solver [290]. The Gurobi solver [290] uses an interior-point method to solve linear and non-linear convex optimization problems. An interior-point method is faster than an active-set method for large numbers of optimization variables and constraints [292].

A comparison of the Gurobi solver [290] to the active-set Matlab solver, based on the KWIK-algorithm [293, 294], has been performed by Kühne [286]. It shows that the YALMIP toolbox [291] in combination with the Gurobi solver [290] is 95% faster concerning the presented simulation method [286].

Simulations were performed on a small form factor workstation with an ASRock Z77 Pro4-M motherboard and Windows 10 as operating system. The installed processor is an Intel i7-3770k, a quad-core processor with two threads per core, resulting in eight logical cores. The processor is clocked at 4 GHz, and the computer is equipped with 32 GB DDR3 RAM, clocked at 1600 MHz. A 256 GB Samsung SSD is used as a disk drive. The machine has a 4 GB Nvidia GTX 1050Ti graphics card.

The 64 required simulations for the reference scenario, including pre- and post-processing, took 12 to 16 hours, depending on the optimization objective. It changes for other road profile lengths and is sensitive to the sampling frequency. Duration of an individual simulation depends on actuator constraints and boundary conditions. Unconstrained simulations take 15 to 20 minutes, whereas simulations with strict boundary conditions and low actuator performance limits can take up to 8 hours.

The pre-processing for the simulation contained generation and parametrization of the state space model, preparing the road input from the scanned profile, and the generation of the MPC object. The simulations were paralleled by using the Matlab „*Parallel Computing Toolbox*“ on the local machine. In post-processing, RMS values, PSDs and discomfort values according to ISO 2631 [29] were computed for the individual simulations of the scenario. The RMS and discomfort values were further processed to be presented in surface and contour plots. The following sections analyze the results in time and frequency domain.

7.2 Results

Subsection 7.2.1 will show the vehicle model validation. The results of a sensitivity analysis regarding the preview length will be presented in Subsection 7.2.2, followed by the analysis of the influence of the maximum actuator force and slew rate to ride comfort in Subsection 7.2.3. The investigation of the power limitation and actuator accuracy is carried out in Subsection 7.2.4. The section is closed with the optimal results for a semi-active actuator, which is compared to the results of a passive suspension and an active suspension in Subsection 7.2.5.

7.2.1 Model Validation

The road profile, which is shown in Figure 7.3 and used for the simulation scenario, corresponds to track II in driving simulator study I, which can be seen in Figure 5.6. The vehicle measurements that were made for the study could therefore be used to validate the vehicle model, which is used in the MPC simulation method. Two passive suspension measurements are compared to the passive simulation on the laser-scanned road profile. Figure 7.4 displays the RMS values for for heave, pitch, and roll.



Figure 7.4: RMS values of the z-acceleration, roll-rate and pitch-rate from the simulation (dark blue) and two measurements (light blue) for track II

It can be observed that both measurements are within 0.05 m s^{-2} and 0.05 s^{-2} respectively, which indicates a good repeatability. For all three directions, the RMS value of the simulation is lower compared to the measured ones. The largest difference occurs in heave, where the simulated RMS value of 0.58 s^{-2} is around 23% lower compared to the measured values. In roll, the measured value of 3.56 s^{-2} deviates around 7% from the simulated values. The pitch acceleration RMS value of 1.37 s^{-2} shows a deviation of 7% from the measurements. For a more detailed comparison, the direct measurements of the heave acceleration and the pitch and roll rates are compared in the frequency domain in Figure 7.5.

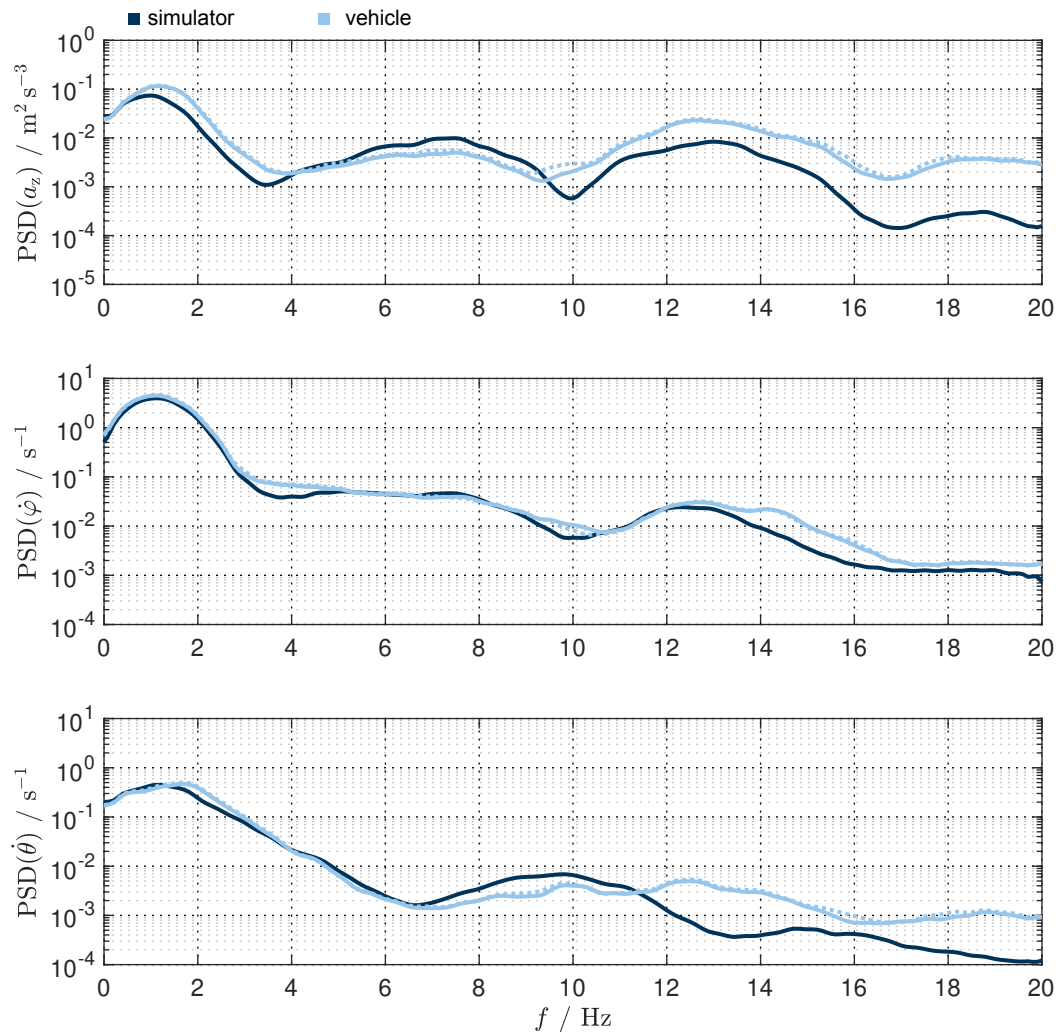


Figure 7.5: PSD plots of the z-acceleration, roll-rate and pitch-rate from the simulation (dark blue) and two measurements (light blue) for track II

The vertical acceleration in the simulation is lower compared to the measurements within 0–5 Hz. From 5–9 Hz, the simulated vertical acceleration is slightly higher than the measured one. Above 9 Hz and up to 20 Hz, the simulated vertical acceleration is significantly lower compared to the measured accelerations. The body eigenfrequency peak at 1.1–1.2 Hz and the wheel eigenfrequency peak at 12–13 Hz are lower and are shifted to slightly higher frequencies in the actual vehicle.

The simulated roll rate matches the measured ones up to 8 Hz, except for a dip at 4 Hz. The body eigenfrequency peak is almost identical to the measurements. The wheel eigenfrequency peak is lower in amplitude and frequency (~12.5 Hz) compared to the measured ones (~13 Hz). At 10 Hz and above 13 Hz, the simulated roll rate is lower than the measurements.

The pitch rate shows good conformity to the measurements in the low-frequency range from 0–7 Hz. The body eigenfrequency peak in the simulation lies at a slightly lower frequency than in the measurements. The same holds for the wheel eigenfrequency peak. It is shifted to the left at 10 Hz for the simulation and at 12.5 Hz for the measurement. Above 12 Hz the simulated pitch rate falls off compared to the measured ones.

The used profile was laser-scanned in the past. The exact age of the recording is unknown. It is unclear how much deviation from simulation to measurements stems from a change in the road surface¹, and how much from the simplifications in the vehicle model. For this reason, a second road profile is used, which corresponds to track I in simulator study I (Figure 5.6).

This second profile's age is unknown as well, but it has similar correlation between simulation and measurements. The deviation is largest in the vertical direction compared to roll and pitch but is less than for track II. The divergence in roll dynamics on track I is the same as for track II. The pitch dynamics on track I match better compared to track I. Some deviations in heave and pitch on track II may originate in an altered road surface. Two traces are cut out from the laser-scanned surface for the simulation. The cut-outs are defined by the track-width of the vehicle and a fixed distance to the side of the road. During real measurements, the vehicle deviates in the lateral direction and will not precisely follow the target path.

The main criteria for the simulation method to investigate actuator limitations is the discomfort value according to ISO 2631 [29]. The discomfort value, which is calculated from the simulations results, is compared to the discomfort value calculated from the measurements, as can be seen in Figure 7.6.

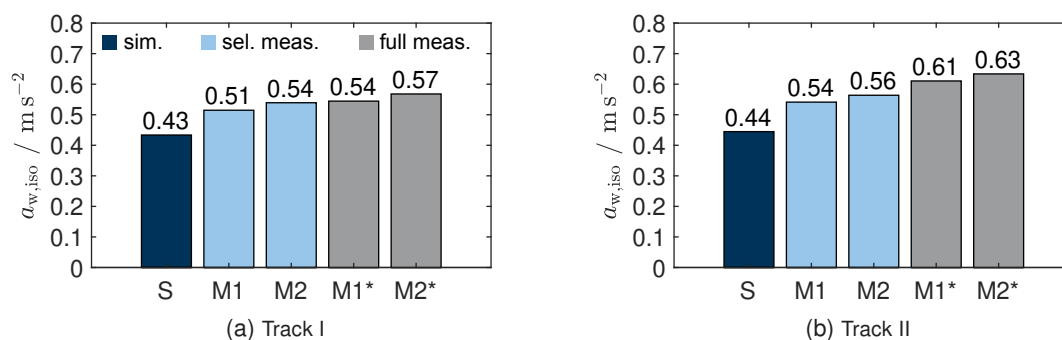


Figure 7.6: Comparison of weighted acceleration values according to ISO-2631 for the full measurements (gray (M1*, M2*)); the selective measurements without lateral, longitudinal and yaw acceleration (light blue (M1, M2)); simulation (dark blue (S))

¹Parts of the road could be darned or repaved, due to damages from weather (frost) and traffic

The discomfort value considers longitudinal and lateral acceleration, and the yaw acceleration. These are measured in the actual vehicle but not implemented in the simulation model. Consequently, it is necessary to compute two discomfort values per measurement, one with all required signals (grey) and one without these (light blue). According to ISO 2631 [29] it is permissible only to use a selection of the signal to compute the discomfort value, with a minimum of one signal, being the vertical acceleration.

Figure 7.6a shows the discomfort value for track I. The average discomfort value from two measurements is 0.56 m s^{-2} when computed with all signals, and 0.53 m s^{-2} when computed from the vertical, heave and pitch acceleration. The simulated discomfort value is 0.43 m s^{-2} , so 0.10 m s^{-2} lower.

The discomfort value for track II can be seen in Figure 7.6b. The full discomfort value average is 0.62 m s^{-2} , the selective discomfort value average is 0.55 m s^{-2} . The simulated discomfort value is 0.11 m s^{-2} lower at 0.44 m s^{-2} . On track II the missing longitudinal, lateral and yaw acceleration leads in average to a 0.07 m s^{-2} lower discomfort value compared to the full discomfort value. On track I this difference considerably lower with 0.03 m s^{-2} .

The passive simulation for the validation was carried out at 1000 Hz. Due to computational constraints on the machine described in Subsection 7.1.5, the MPC simulations were performed at 100 Hz. Additionally, the full profile (not synced to the measurements) was longer and contained a first part of 120 m (5.4 seconds) with no road excitation to initialize the model. In consequence, the discomfort value for the passive 1000 Hz synced simulation is 0.44 m s^{-2} , whereas the discomfort value for the passive 100 Hz un-synced simulation is 0.36 m s^{-2} , which was used as a reference for the active simulations.

7.2.2 Preview Sensitivity

The prediction horizon in MPC has to be sufficiently long to maintain optimality of the global solution. The required length depends on the system dynamics and disturbances. The size of the optimization problem rises with an increasing length of the prediction horizon. The chosen length should just be long enough to obtain a valid solution within feasible computation time.

Figure 7.7 displays the achieved discomfort value in relation to the prediction horizon length for non-restricted actuators. Only the first 10 s of the road profile were used for the sensitivity analysis. The discomfort value for the passive simulation ($t_{\text{pre}} = 0$) is 0.31 m s^{-2} and in consequence lower than the value presented in Subsection 7.2.1.

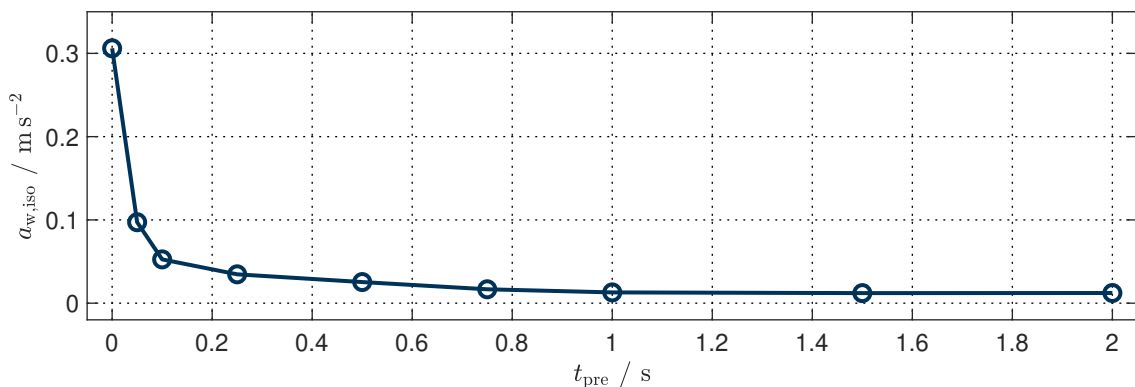


Figure 7.7: Sensitivity of the ISO-Value with regards to the preview time

The Pareto Principle is apparent for the preview horizon length. With a preview length of 1 s or more, the discomfort value converges towards 0.01 m s^{-2} . A 84% reduction in discomfort value is achievable with a preview time of 0.1 s, which corresponds to ten samples at a sampling frequency of 100 Hz. 0.1 s is chosen as preview time in compromise between computation time and accuracy.

7.2.3 Influence of the Maximum Force and Slew-Rate

The maximum force and the maximum slew rate are two criteria defining an actuator for vertical vehicle dynamics control systems. The maximum force determines the ability to work against passive elements like the springs or the damping. The slew rate is significant for vertical dynamics because a high slew rate allows influencing vertical dynamics at higher frequencies. In best-case, up and above the wheel eigenfrequency, which is about 10–12 Hz depending on the vehicle.

Figure 7.8 shows the results for the reference scenario described in Subsection 7.1.4 as surface plots for the discomfort value, the RMS dynamic wheel load variation, the RMS suspension deflection and the RMS actuator force. These plots give a first qualitative overview of how the performance indicators vary with maximum force and slew rate values.

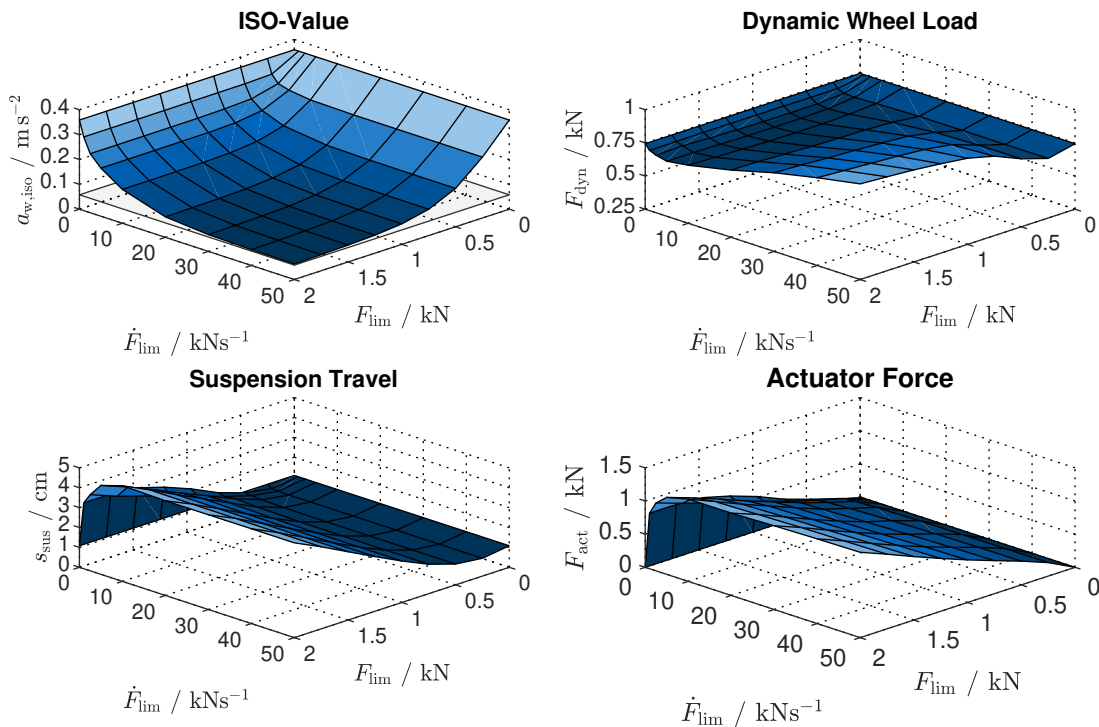


Figure 7.8: Surface plots for the discomfort value, the dynamic wheel load variation and the RMS actuator force, depending on the maximum force and slew-rate limitations

The passive discomfort value for this scenario with initialization and 100 Hz sampling frequency is 0.36 m s^{-2} , as already described at the end of Subsection 7.2.1. The surface plot of the discomfort value shows that it is decreasing with increasing maximum force and slew rate. For this scenario, the discomfort value decreases fast with increasing maximum slew-rates up to 40 kNs^{-1} and only small maximum forces up to 1.5 kN are required. From the surface plot for the dynamic wheel load RMS value, one can see the objective conflict between ride comfort and road-holding, as a reduction in the discomfort value entails an increase in dynamic wheel

load variation. Both the suspension travel RMS and the actuator force RMS show a strong dependency on the maximum force limitation.

Figure 7.9 shows an isoclinical plot for the discomfort value. It corresponds to the discomfort surface plot of Figure 7.8 from top-view with isoclines for fixed discomfort value. The dashed black line shows the gradient descent path (steepest descent) out of the origin, representing a passive suspension. In the range of $0-2\text{ kN}$ and $0-50\text{ kNs}^{-1}$ for each actuator, one can see the biggest improvement for an increased maximum slew rate.

From Chapter 6 it is clear that $0.20 \pm 0.05\text{ m s}^{-2}$ is a reasonable target range for an automated drive. One can see in Subsection 7.2.1 that the simulated discomfort values are around 20% lower than the measured ones. Additionally, the sampling frequency of 100 Hz in combination with the initialization phase further lowers the simulated discomfort value by 15%.

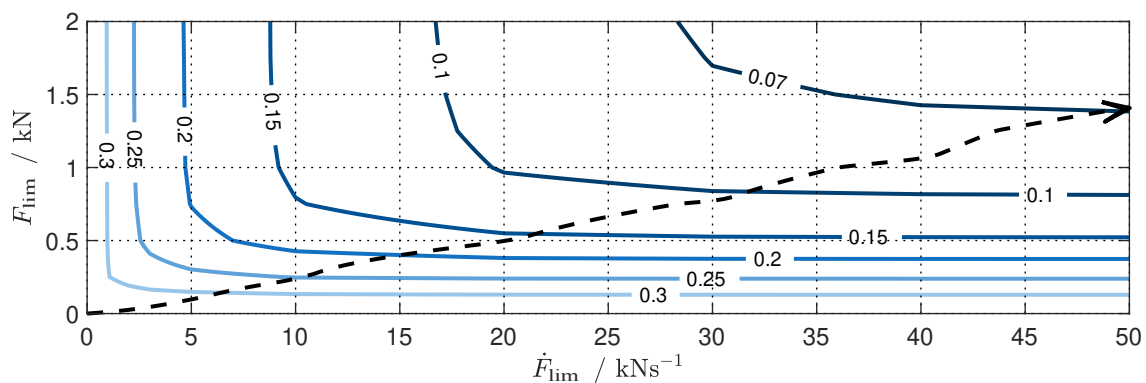


Figure 7.9: Isoclinical plot of the discomfort value (in m s^{-2}) in relation to the maximum force and slew-rate limitation

The optimal discomfort value, which is achievable with a non-restricted actuator for the given scenario is 0.06 m s^{-2} . The deviation from simulation to reality will change with different maximum force and slew rate limitations. It might be a reasonable engineering estimate to set a target value of 0.1 m s^{-2} for the simulation, to achieve a value of 0.2 m s^{-2} in the real vehicle.

For the reference scenario, an actuator with a maximum force of 1 kN and 40 kNs^{-1} at each wheel can achieve a simulation target value of 0.1 m s^{-2} (see Figure 7.9). An actuator with 0.5 kN maximum force and 30 kNs^{-1} would be theoretically sufficient to achieve a target value of 0.2 m s^{-2} , which was determined in Chapter 6, but real controllers will benefit from higher slew-rates. An actuator with 1 kN maximum force and 40 kNs^{-1} slew-rate also follows the 80/20 Pareto-Principle², and will be compared to a passive suspension and a semi-active suspension in detail in Subsection 7.2.5. Before this, the influence of a power limitation and the actuator accuracy will be analyzed.

7.2.4 Power Limitation and Actuator Accuracy

In this research, the system power is assumed to be the sum of the required power for each actuator, which is equally distributed and calculated according to Equation (7.26). A power limitation of 1 kW means a power limit of 0.25 kW per actuator. Figure 7.10 shows the discomfort value in relation to different power limitations. The limitation to 0 kW corresponds to a passive suspension. Most of the reduction in discomfort value is achieved within a power limit of 1 kW .

²80% of a complete result can be achieved with 20% of the total effort, whereas the last 20% of the complete result will require 80% of the total effort.

With a system power larger than 1.6kW the discomfort value can be decreased slightly further. No improvement is seen for power limits above 5kW.

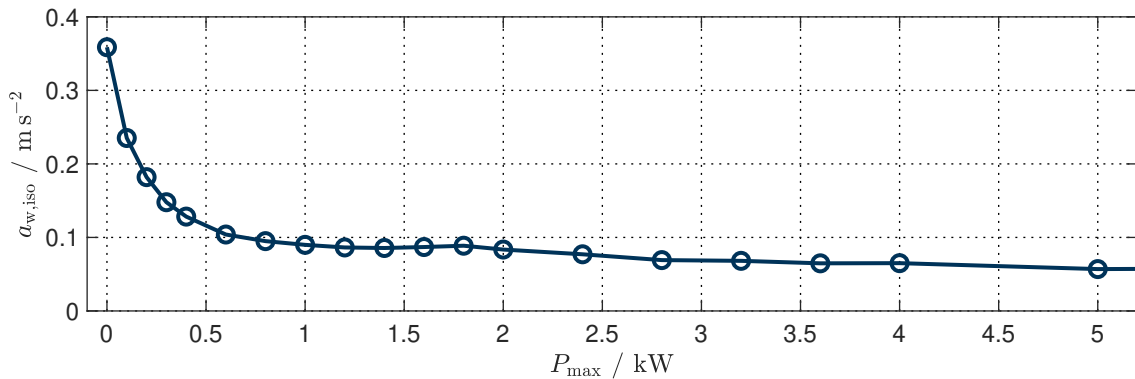


Figure 7.10: Power Sensitivity of the discomfort value

The plateau and following small dip between 1kW and 2kW in Figure 7.10 could originate from the optimal trajectory of the MPC. There was a distinct, more significant undulation of the road, where the optimal trajectory changed depending on the maximum available power. For a maximum power below 1.6kW, the system is not able to fully suppress the resulting body movement. Above 1.6kW it is.

Based on the reference scenario, it would be sufficient to aim for a system power of 1kW, as it allows to reduce the discomfort value to 0.09 m s^{-2} . Even a maximum power of 0.5kW might be sufficient. On the other hand, there should be a safety margin, and it has to be considered that the control units draw power. Nevertheless, from a vertical dynamics perspective, it is unlikely that a system would need to deliver more than 2kW.

To investigate the actuator accuracy, a normally distributed error force with a standard-deviation F_{err} is superimposed to the optimal control force computed by the MPC, as defined in Equation (7.27). Figure 7.11 shows the relationship between the standard error and the discomfort value.

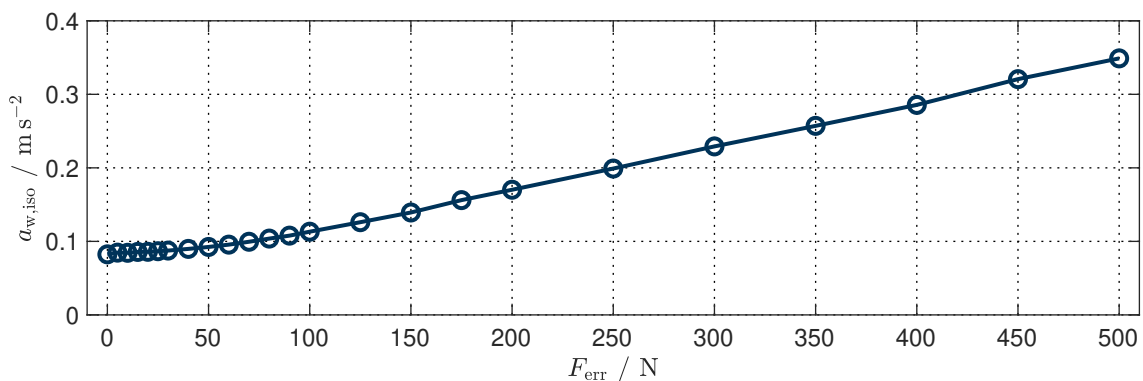


Figure 7.11: Influence of the actuator accuracy on the discomfort value

A standard error force of 0N corresponds to the undisturbed optimal control force. The discomfort value progressively increases up to a standard error of 100N, but is still acceptable with 0.11 m s^{-2} . Above a standard error of 100N, the discomfort value increases nearly linearly up to a standard error of 500N, where the performance is almost fully degraded with a discomfort value of 0.35 m s^{-2} , which is almost equal to the passive discomfort value of 0.36 m s^{-2} . Based on this scenario, an upper limit for the standard error per actuator could be defined as 100N.

7.2.5 Semi-Active Actuator performance

The main restriction of a semi-active actuator is its inherited limitation to dissipative forces in the first and third quadrant of the force-velocity diagram. A damper lookup table defines the minimum and maximum damping curves, representing the force-velocity diagram in Figure 7.2.

It would be possible to investigate different damper maps with this method, analog to the maximum force and slew rate limitations for the active actuator. This research is limited to a representative damper-map, compared to a passive suspension and an active actuator with a maximum force of 1 kN and a slew rate of 40 kN s^{-1} .

Figure 7.12 shows the limitations of the semi-active and the active actuator for comparison as scatter plots in the force-velocity diagram. Each dot represents a delivered control force of an actuator in each time step. The forces of an active actuator are shown in dark blue.

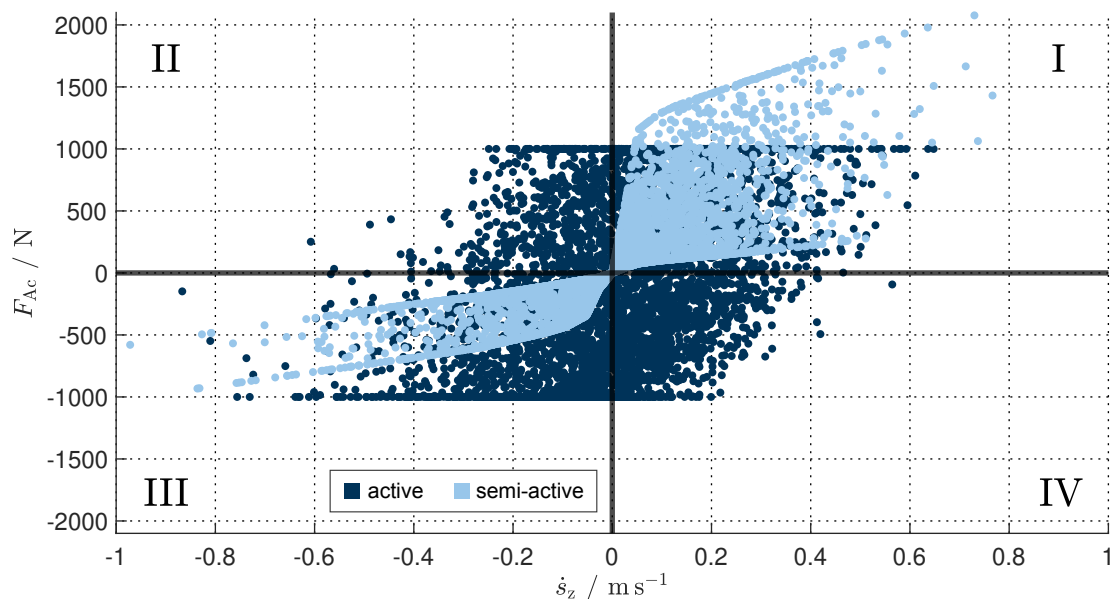


Figure 7.12: Semi-active (light blue) and active (dark blue) actuator force limitations

The limitation to $\pm 1 \text{ kN}$ is easy to recognize. The forces of the semi-active damper are displayed in light blue. In rebound, which is defined by a positive relative velocity s_z , the semi-active damper can supply higher forces than the active actuator due to the characteristic of the maximum damping curve. It is visible that the active actuator delivers a significant amount of non-damping forces, defined by a relative velocity and an opposing force. Furthermore, the active system can supply larger forces at slow relative velocities, especially in compression.

Figure 7.13 shows a comparison of the vertical acceleration in the time domain. Overall, the vibration level of the semi-active suspension (light blue) and the active suspension (dark blue) is reduced compared to the passive suspension (grey). The active suspension can level out characteristic agitations, for example, after the initialization after 5 s or after 15 s. At the start of the road disturbance, it is visible that the active suspension can precondition the suspension even before the excitation starts. The semi-active suspension can suppress higher frequency vibrations but often follows the passive suspension in low-frequency characteristics.

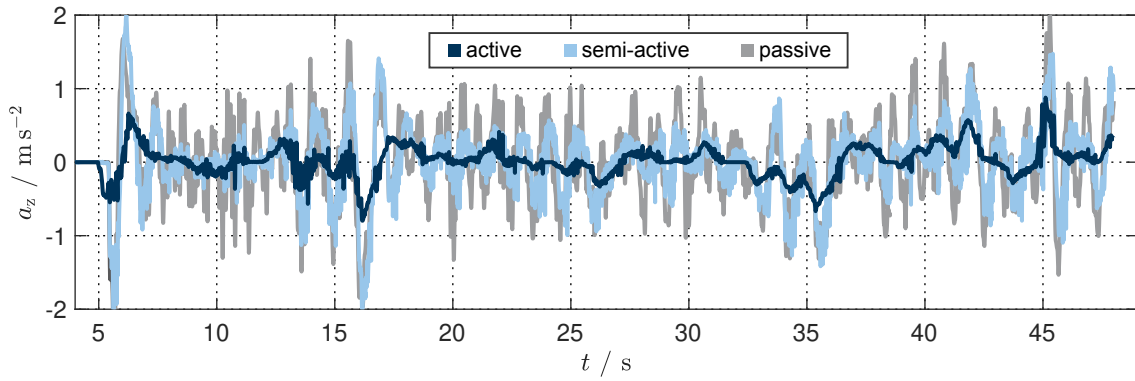


Figure 7.13: Time-series of the vertical acceleration of the passive (gray) semi-active (light blue) and active (dark blue) suspension systems

The discomfort value and the RMS values for the dynamic wheel load variation, the suspension deflection, and the actuator force are displayed as bar graphs in Figure 7.14. The semi-active suspension is able to reduce the discomfort value from 0.36 m s^{-2} (passive suspension) to 0.26 m s^{-2} . This is a good improvement, considering the passive suspension was already set-up comfortably with 30% critical damping. The active suspension, with a maximum force of 1 kN and a maximum slew rate of 40 kN s^{-1} , achieves an almost three times higher reduction of the discomfort value to 0.08 m s^{-2} compared to the semi-active system.

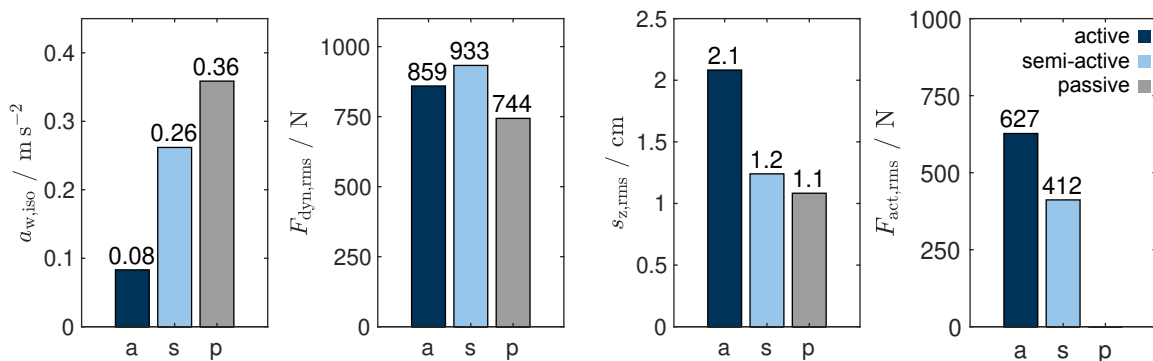


Figure 7.14: Bar-plots of the discomfort value, the dynamic wheel load variation, the suspension deflection and the actuator force for the passive (gray), semi-active (light blue) and active (dark blue) suspension system

The passive suspension has the lowest RMS dynamic wheel load variation. The variation of the semi-active suspension is larger compared to the active suspension. The semi-active suspension has a considerably lower minimum damping than the active suspension. The active suspension actuator is in parallel to the passive damper, whereas the semi-active actuator is the only damper. The minimum damping is defined by the minimum damping curve of the semi-active damper, which is lower than the passive damping in the active suspension.

The suspension deflection for the semi-active and the passive system are similar with RMS values of 1.2 cm and 1.1 cm respectively. The active system has an increased operating range with a RMS value of 2.1 cm. This increased movement is still within the normal operating range of the suspension. The active actuator can work against the passive spring and makes better use of the available travel at each wheel. The RMS actuator force for the active suspension is 627 N, and 412 N for the semi-active suspension.

The PSDs for the vertical acceleration a_z , the roll rate $\dot{\varphi}$, pitch rate $\dot{\theta}$ and the dynamic wheel load of a single wheel F_{dyn} are shown in Figure 7.15. Gray lines representing the passive suspension, dark blue and light blue lines the active and semi-active suspensions. For all three vehicle body-related measures, the active suspension reduces the road disturbance's transmissibility. The body eigenfrequency peaks and the frequency range between 4 Hz and 8 Hz is attenuated compared to the passive and semi-active suspension.

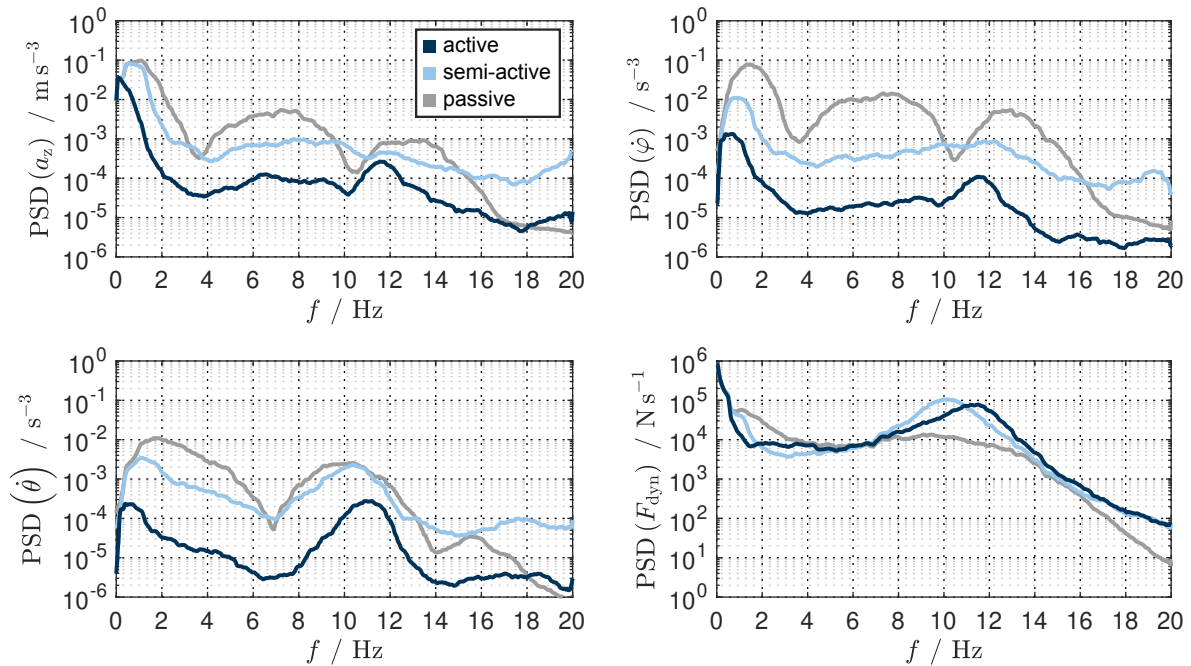


Figure 7.15: PSD curves of the vertical acceleration, pitch and roll rate, and the dynamic wheel load variation, depicted for the passive (gray), semi-active (light blue) and active (dark blue) suspension system

The semi-active system shows improvements in the attenuation of roll vibration. Pitch-dynamics are improved in the low-frequency range from 1 Hz and 6 Hz. The vertical acceleration is lower in-between 4–9 Hz. In the high-frequency range, the semi-active suspension can improve heave and roll dynamics from 11–16 Hz, but shows higher transmissibility than the passive suspension for frequencies above 16 Hz. As expected, the semi-active and active suspension both show a significant increase in dynamic wheel load variation above 7 Hz.

The passive suspension system has the lowest dynamic wheel load variation. Only at low frequencies between 1 Hz and 6 Hz, the dynamic wheel load variation is improved with the active and semi-active system. Dynamic wheel load variations are automatically reduced in this frequency range if body accelerations are minimized. This effect is small compared to the increase in dynamic wheel load variation around the wheel eigenfrequency. At the wheel eigenfrequency, one can see the increased peak of the semi-active system, slightly shifted towards a lower frequency. As already stated, this is caused by the reduced minimum damping of the semi-active suspension compared to the active one, still having a passive damper with a damping ratio of 25% in parallel to the actuator.

Results for an optimization of the dynamic wheel load are shown in Appendix D, Figure D.3–D.4. An actuator with a maximum force of 1 kN, and a maximum slew rate of 40 kN s^{-1} , would be appropriate to minimize dynamic wheel load as well.

7.3 Discussion

The goal to develop a simulation method allowing to investigate the influence of actuator limitations was achieved by using an ideal MPC-controller. It eliminates the influence of the control logic by calculating theoretical optimal control inputs over the prediction horizon. Boundary conditions on the dynamic wheel loads and the suspension deflection are incorporated as explicit output constraints. The method was applied for a reference scenario with a laser-scanned country road, also used to validate the simulation vehicle model.

It has to be emphasized that the results for the reference scenario do not give a complete picture regarding the requirements of a vertical dynamics control system actuator. Changing the vehicle or traveling speed will alter the results. A change of road or altering the constraints on suspension travel and dynamic wheel load variation will also lead to different results. The targeted discomfort value is critical for the choice of actuator requirements. All of these examples are arguments for the developed method. It allows users to vary parameters, define different scenarios, and obtain results which aid to determine suitable actuator specifications.

Current state of the art active suspension systems, like the eABC of Daimler [124], with maximum forces of 6–7 kN, maximum slew rates of 24–20 kNs⁻¹ and a maximum system power of 13 kW, seem to be designed with a focus on longitudinal and lateral dynamics. From the reference scenario, an actuator should supply a twice as high slew rate of 40 kNs⁻¹, but only requires a maximum force of 1 kN, and a system power of 2 kW. Of course requirements from longitudinal and lateral dynamics need consideration, and the eABC system contains semi-active dampers, which allow controlling the system dynamics at higher frequencies, compensating for the lower slew rate of the active actuators.

Suppose a small active-actuator supplying 1 kN maximum force and 40 kNs⁻¹ maximum slew-rate, combined with a passive damper. This system is likely to be lighter, have better cost-efficiency, and be lower in complexity compared to the eABC of Daimler [124]. It might deliver a comparable or even better ride comfort for automated driving. It is recommended to aim for high slew-rate low maximum force system considering future active suspension systems.

The presented method has some limitations. The vehicle model should be validated further by using an newly scanned road, or the older road profiles as an input to a shaker-rig. The obtained actuator requirements should be validated using a real vehicle with a fast-active suspension. Such a system was not available to the author, but should be used to investigate achievable ride comfort depending on maximum force and slew-rate within the performance envelope of the system. These results should be compared to the simulation. Another limitation and, at the same time, a point for future improvements is the correlation between the achieved discomfort from simulation to reality. There will be a difference originating from the performance deficit of a real-world controller. This should be investigated and further validated in future research works.

A field for further technical improvement of the method would be the dynamic behavior of the actuators. These could be refined with the help of linear transfer functions derived from prototype testing [133, 134, 102]. The MPC will compensate for the known system dynamics within the operating range of the actuator, but it might influence the actuator slew rate dependency. Approximated ISO 2631 [29] weighting transfer functions of Zou [295] could be incorporated into the simulation. An initial try lead to an unstable controller [286]. Yet, with some modification, a stable and even better MPC controller might be realized. A method to analyze the stability is presented in [296].

8 Conclusion

This section will summarize the main conclusions of this research work, structured in paragraphs according to the research questions introduced in Section 3.4. The main conclusion is drawn at the end of this section.

RQ 1.1: How decisive is ride comfort to the customer?

The results of the online survey regarding ride comfort of Chapter 4 indicate that costumers are content with the ride comfort supplied by their current conventional vehicles. They rate it as „neutral“ or „rather good“. Concerning the purchase of a new conventional vehicle, customers see ride comfort as a „rather important“ buying criteria. Only the safety and reliability of a conventional vehicle were rated more important. Ride comfort is seen on the same level of importance as fuel consumption, the interior, or the design. It is rated as more important than the infotainment system, the family friendliness, the environmental friendliness, or the brand image. For automated driving vehicles, it is rated as an „important“ buying criteria, putting it at the same level as the ease of use, innovation, safety, seat comfort, and reliability. Based on the findings of this survey, ride comfort belongs to the top five buying criteria for the customer with regard to automated driving.

RQ 1.2: Will the importance of ride comfort increase considering automated driving?

The survey results support the hypothesis of an increasing importance of ride comfort concerning automated driving, compared to conventional driving. Ride comfort may be seen as a luxury asset of a vehicle, but is rated among the top five buying criteria in this survey. It was rated significantly more important for an automated vehicle. These results hold for individual transport using private vehicles. The mobility systems in metropolitan areas might change, and the ride comfort requirements for autonomous shuttles are likely to differ. The focus was on personal (private) vehicles. A higher demand in comfort is expected for these, when automated driving becomes available.

RQ 2.1: How do current state-of-the-art suspension systems perform in automated driving?

The comparison of a passive, semi-active and active suspension system in Chapter 5 has shown that the test subjects were able to distinguish between a passive or semi-active and an active suspension system during automated driving. The active system was identified as the best system of the three. The semi-active system did not show better subjective ratings than the passive system. On the seven-point discomfort rating scale, with anchor values from „no

disturbance“ (0) to „very strong disturbance“ (6), the active suspension achieved a median value of three, the semi-active and passive suspension both had a median of four.

The suspension systems were rated on different test sections, corresponding to different road disturbances. Track I was rated best with a median of two, tracks II and III were rated with four. The results yield two crucial insights. First, the perceived discomfort in a vehicle depends mainly on the road quality combined with the vehicle speed, and can be partially compensated by a more advanced suspension system. Second, only the active suspension system delivered a substantial improvement in the subjective ratings.

RQ 2.2: Do side tasks effect the sensitivity for road disturbances?

The second aspect of study I was whether a secondary activity would influence the discomfort perception. The results did not significantly differ between an attentive and an inattentive rating of the same suspension and track combination. In attentive state, the test person could focus on the vehicle and its surroundings. In inattentive state, the test person performed a quiz on a handheld tablet computer.

The indifference between the two states leads to the assumption, that if a person is still focused on the vibration perception besides a side task, and not highly distracted, for example, by an emotional conversation or simply sleeping, the discomfort perception is the same. This assumption is reasonable considering the perception mechanism is the same, regardless of the state of attention. Furthermore, it does not imply that the comfort perception is the same. The expectation could differ for each state of attention.

Interpersonal differences are apparent in this investigation. The average ratings per person vary, resulting in interquartile ranges of two to three for most parameter combinations. No generalized conclusion can be drawn on the impact of a secondary activity, which is also underlined by the post-interview. The subjects showed varying opinions on the effect of a secondary activity concerning their discomfort perception. Nonetheless, if there is an effect of a secondary activity on the pure discomfort perception (not comfort), it is expected to be minor.

RQ 3.1: What is the objective target value for automated driving ride comfort?

Only the vibration discomfort is measurable, and it is not possible to directly define a comfort target value. Driving simulator study II was conducted to determine a discomfort threshold, depending on the test person's comfort thresholds. An ISO 2631 [29] effective vibration value range of $0.20 \pm 0.05 \text{ m s}^{-2}$ was obtained as a target. It is well below discomfort values experienced in road vehicles on European roads, usually in the range of $0.3 - 0.4 \text{ m s}^{-2}$ [280, p. 50].

There is no significant difference between the attentive and the inattentive target values overall. The test subjects already demanded an high level of comfort (low discomfort) for an attentive automated drive, compared to what is experienced in current road vehicles. A discomfort value of $0.20 \pm 0.05 \text{ m s}^{-2}$ is only seen on smooth roads, at low speeds, or in luxury class vehicles. The results underline the finding from the online survey that there will be an increased demand for ride comfort in automated driving vehicles.

RQ 3.2: Do ride comfort expectations differ for compact and luxury class vehicles?

The compact class vehicle (BMW 1-series) and the luxury class vehicle BMW 7-series show a significant difference in the discomfort threshold values for an attentive drive. The study participant demanded a more ride comfort for the 7-series, with a mean target value of 0.19 m s^{-2} . The mean target value for the 1-series was 0.21 m s^{-2} .

The most significant difference is seen when comparing attentive and inattentive drive results. In the compact class vehicle, the test persons accepted a slightly higher discomfort level for an inattentive drive (0.22 m s^{-2}) compared to the attentive one (0.20 m s^{-2}). In the luxury class vehicle, this effect is the opposite, with an attentive target value of 0.20 m s^{-2} and an inattentive target value of 0.18 m s^{-2} .

In conclusion, a high level of comfort is demanded in automated driving, independent of the vehicle class, but especially for luxury class vehicles, even higher comfort requirements are expected when considering secondary activities. The results indicate a side-effect regarding the vehicle class with respect to the ride comfort expectation in relation to the state of attention, because no overall difference was found for the state of attention, but different effects were observed when the two vehicle classes were analyzed individually.

RQ 4.1: Can suspension actuator requirements be derived from ride comfort targets?

A method was developed and applied allowing to investigate the pure influence of actuator limitations on achievable ride comfort, see Chapter 7. The results are independent of a specific type of control logic. In disadvantage, the simulation results cannot be directly compared to reality, because real controllers always have worse performance than an optimal controller. The deviation should be estimated, but generally the method can be used to derive and investigate actuator requirements. It allows this based on an overall vehicle ride comfort target. The method is a tool requiring good engineering practice to be valid, but also is the first of its kind.

RQ 4.2: What are typical actuator requirements for an ideally comfortable vehicle?

This question is answered for a luxury class vehicle, in specifications similar to a BMW 7-series, for a low-quality road, with the aim to achieve the previously derived ride comfort target value. A reference scenario was defined and investigated using the developed method. The scenario is defined by the vehicle, road profile, vehicle speed, and boundary conditions regarding dynamic wheel loads and the suspension deflections. Generally, high bandwidth is more important than maximum force. This contradicts current state-of-the-art active suspension systems.

Fast-active suspensions should supply a maximum force of 1 kN, combined with a maximum slew rate of 40 kN s^{-1} at the wheel. A vertical vehicle dynamics control system for automated driving needs to deliver a maximum power of at least 1 kW. The standard error in terms of actuator force accuracy shall not exceed 100 N. Slow-active, semi-active or passive suspensions might be cost-efficient alternatives to fast-active systems, but they are not able to reach the desired target discomfort value of $0.20 \pm 0.05 \text{ m s}^{-2}$ according to ISO 2631 [29] on low-quality roads.

Main Conclusion and Recommendation to Industry

It is necessary to distinguish between comfort and discomfort. Only vibration discomfort is directly measurable and influenced by the suspension system performance. The target discomfort value of $0.20 \pm 0.05 \text{ m s}^{-2}$ is challenging. It is questionable whether it can be reached within reasonable financial boundaries for given road qualities and desired traveling velocities. Passive and semi-active suspensions might therefore remain the industry standard due to costs, except for high-end luxury class vehicles. Regarding active suspension-systems, developing an efficient high-bandwidth (40 kN s^{-1} maximum slew-rate) low maximum force (1 kN) system is advisable. OEMs should make use of the increasing importance of ride comfort and pro-actively develop a brand image towards highly comfortable automated driving, similar to Volvo and the image of road vehicle safety.

9 Summary and Outlook

This thesis work shows that the importance of ride comfort increases for automated driving. A target value of $0.20 \pm 0.05 \text{ m s}^{-2}$ according to ISO 2631 [29] has been derived for automated driving conditions. Only an active suspension system can reach this target value for a luxury-class vehicle, traveling with 80 km h^{-1} on a low-quality road profile, specified as class D according to ISO 8608 [214]. A maximum force of 1 kN is sufficient if the actuator can supply a maximum slew rate of 40 kN s^{-1} . The system should supply a maximum power of 1 kW, and the standard error per actuator shall not exceed 100 N. These results depend on the vehicle specification, the road profile, the traveling speed and boundary conditions for the dynamic wheel load variation, and the suspension deflection. The developed method allows to investigate different scenarios and should help during the vehicle development process.

Future research can extend from this thesis work. Both simulator studies should be rebuilt and studied with actual automated vehicles when they are available in the future. The same holds for the method to derive actuator requirements. A fast-active suspension system should be used to investigate the influence of maximum force and slew rate within the performance envelope of the system, artificially restricting it to lower values and analyzing the resultant discomfort value. The performance difference between real-world vertical dynamics controllers and the optimal MPC could be estimated like this. Furthermore, the semi-active and power-restriction implementations are time-varying, and need further investigation regarding their optimality. Another open question is, how vertical dynamics ride comfort stacks up against longitudinal and lateral driving comfort, similar to an investigation of Griffin [297]. Long-term investigations for traveling times exceeding half an hour might be purposeful. Potential for synergies between vehicle suspension and seat development should be checked.

Besides the research presented in this thesis, a control logic focused on easy and independent tuning was developed by the author, based on the modal decomposition principle [298, 299, 300, 168]. This control logic follows an approach which is recommended for future vertical vehicle dynamics development: simplify and standardize. The control algorithm has been filed as a patent by the author [301].

This thesis work should help in developing cost-efficient and comfortable automated driving vehicles, which in return should benefit society. A remaining question is, if an ongoing focus on vehicle development for individual mobility is the right path, or if the focus should shift towards sustainable, efficient mobility solutions in metropolitan areas, and low-emission long-distance transport in rural areas.

List of Figures

Figure 1.1:	Overview of the thesis structure	2
Figure 2.1:	Sitting comfort model according to Looze et al. [21].....	9
Figure 2.2:	Different factors contributing to discomfort, modified in colors from Griffin [24, p. 44]. Red boxes are marked by the author to visualize factors related to vertical vehicle dynamics ride comfort within this thesis work	10
Figure 2.3:	Categorization of objectification methods in vertical vehicle dynamics.....	10
Figure 2.4:	Basic principle of standardized vibration assessment methods according to ISO 2631 [29], BS 6841 [30] and VDI 2057 [31].....	11
Figure 2.5:	Classification of suspension systems as force (y-axis) over velocity (x-axis) pictograms, adapted from Kallenbach et al. [64], with added indicators for control bandwidth and actuator energy consumption	12
Figure 2.6:	Front and rear suspension of a BMW 7-series (F01) [65, 66]	14
Figure 2.7:	Passive suspension elements	14
Figure 2.8:	Bose active suspension [97].....	16
Figure 2.9:	Semi-active suspension systems	16
Figure 2.10:	Mercedes Benz Magic Body Control [117]	17
Figure 2.11:	Slow-active suspension systems for roll control.....	17
Figure 2.12:	Fast-active suspension systems	18
Figure 2.13:	Quarter vehicle models, modified from Jazar [136, p. 856].....	19
Figure 2.14:	5-mass model, similar to Jazar [136, p. 856]	19
Figure 2.15:	PID controller	20
Figure 2.16:	State-feedback controller	21
Figure 2.17:	Model-predictive controller.....	22
Figure 4.1:	Background information on car ownership and attitude towards suspension systems and ride comfort.....	31
Figure 4.2:	The subjects knowledge of suspension systems.....	31
Figure 4.3:	How do you rate the importance of ride comfort, as a driver, as a passenger and in automated driving? Red crosses show rating-outliers	32
Figure 5.1:	VI-Grade DiM driving simulator at the BMW research center in Garching..	36
Figure 5.2:	Measurement system installed in the simulator mock-up, with and without a seated test person.....	37
Figure 5.3:	Workflow to build a driving simulation with offline motion-cueing	37
Figure 5.4:	Test procedure of driving simulator study I, showing the sub-division into different tracks, states of attention and suspension systems.....	39
Figure 5.5:	Study I test plan for 6 subject groups, using 3 tracks in attentive (<i>att.</i>) and inattentive (<i>ina.</i>) state, with suspension system permutation s1 – s6 according to Table 5.2	40
Figure 5.6:	The three tracks used in Study I, indicating their predominating road excitation types, and a comparison of the real and virtual view	41
Figure 5.7:	Schematics of measurement equipment installation in the test vehicle	41

Figure 5.8:	Pictures of the measurement equipment installation in the test vehicle.....	42
Figure 5.9:	Timeline for one test subject in driving simulator study I.....	42
Figure 5.10:	Work-flow for the post-processing in study I.....	43
Figure 5.11:	Comparison of the objective values for three different tracks, dark blue is from vehicle measurement, light blue is measured in the simulator.....	44
Figure 5.12:	Comparison of the ISO values, summarized for the 3 hypothesis. Note the y-axis offset of 0.35 m s^{-2}	45
Figure 5.13:	Comparison of the discomfort ratings, summarized for the 3 hypothesis...	47
Figure 5.14:	Self-determined motion sickness of the subjects before and after study I..	49
Figure 5.15:	Results of post-session interview in study I.....	49
Figure 6.1:	Test procedure Study II.....	52
Figure 6.2:	Test plan Study II.....	52
Figure 6.3:	Vehicles of simulator study II.....	53
Figure 6.4:	Study set-up in- and outside of the driving simulator.....	53
Figure 6.5:	Overview of the test procedure in study II.....	54
Figure 6.6:	Processing the trigger signal.....	54
Figure 6.7:	Difference in ISO threshold values by state of attention (a: attentive, i: inattentive) and car (1s: 1-series, 7s: 7-series).....	55
Figure 6.8:	Difference in ISO threshold values by ramp type (r1: ramp 1, r2: ramp 2) and direction of the ramp(up: ascending, do: descending).....	56
Figure 6.9:	Comparison of the ISO threshold values for the two different cars (1s: 1-series, 7s: 7-series) in attentive and inattentive state.....	56
Figure 6.10:	Comparison of the ISO threshold values for the two different cars in attentive (a) and inattentive (i) state.....	57
Figure 6.11:	Self-determined motion sickness of the subjects before and after study II.	58
Figure 6.12:	Results of the post-session interview in study II.....	58
Figure 7.1:	Structure of the simulation model.....	62
Figure 7.2:	Semi-active damper map – dark blue line is maximum damping, light blue line is minimum damping.....	69
Figure 7.3:	Road Profile.....	73
Figure 7.4:	RMS values of the z-acceleration, roll-rate and pitch-rate from the simulation (dark blue) and two measurements (light blue) for track II.....	74
Figure 7.5:	PSD plots of the z-acceleration, roll-rate and pitch-rate from the simulation (dark blue) and two measurements (light blue) for track II.....	75
Figure 7.6:	Comparison of weighted acceleration values according to ISO-2631 for the full measurements (gray ($M1^*$, $M2^*$)); the selective measurements without lateral, longitudinal and yaw acceleration (light blue ($M1$, $M2$)); simulation (dark blue (S)).....	76
Figure 7.7:	Sensitivity of the ISO-Value with regards to the preview time.....	77
Figure 7.8:	Surface plots for the discomfort value, the dynamic wheel load variation and the RMS actuator force, depending on the maximum force and slew-rate limitations.....	78
Figure 7.9:	Isoclinical plot of the discomfort value (in m s^{-2}) in relation to the maximum force and slew-rate limitation.....	79
Figure 7.10:	Power Sensitivity of the discomfort value.....	80
Figure 7.11:	Influence of the actuator accuracy on the discomfort value.....	80
Figure 7.12:	Semi-active (light blue) and active (dark blue) actuator force limitations ...	81

Figure 7.13:	Time-series of the vertical acceleration of the passive (gray) semi-active (light blue) and active (dark blue) suspension systems	82
Figure 7.14:	Bar-plots of the discomfort value, the dynamic wheel load variation, the suspension deflection and the actuator force for the passive (gray), semi-active (light blue) and active (dark blue) suspension system	82
Figure 7.15:	PSD curves of the vertical acceleration, pitch and roll rate, and the dynamic wheel load variation, depicted for the passive (gray), semi-active (light blue) and active (dark blue) suspension system	83
Figure A.1:	Comfort rating of the currently used vehicle	xi
Figure A.2:	How do you rate the importance of "ease of use" when buying a conventional or an automated car	xi
Figure A.3:	How do you rate the importance of ride comfort when buying a conventional or an automated car?	xli
Figure A.4:	How do you rate the importance of the "sportiness" when buying a conventional or an automated car	xli
Figure A.5:	How do you rate the importance of the infotainment system when buying a conventional or an automated car	xli
Figure A.6:	How do you rate the importance of innovation when buying a conventional or an automated car?	xlii
Figure A.7:	How do you rate the importance of the family friendliness when buying a conventional or an automated car?	xlii
Figure A.8:	How do you rate the importance of safety when buying a conventional or an automated car?	xlii
Figure A.9:	How do you rate the importance of the car interior when buying a conventional or an automated car?	xliii
Figure A.10:	How do you rate the importance of the seating comfort when buying a conventional or an automated car?	xliii
Figure A.11:	How do you rate the importance of the quality of materials when buying a conventional or an automated car?	xliii
Figure A.12:	How do you rate the importance of the environmental friendliness when buying a conventional or an automated car?	xliv
Figure A.13:	How do you rate the importance of an easy entry when buying a conventional or an automated car?	xliv
Figure A.14:	How do you rate the importance of CO ₂ emissions when buying a conventional or an automated car?	xliv
Figure A.15:	How do you rate the importance of a high seating position when buying a conventional or an automated car?	xlv
Figure A.16:	How do you rate the importance of the styling when buying a conventional or an automated car?	xlv
Figure A.17:	How do you rate the importance of the headlights when buying a conventional or an automated car?	xlv
Figure A.18:	How do you rate the importance of the vehicle size when buying a conventional or an automated car?	xlvi
Figure A.19:	How do you rate the importance of the reliability when buying a conventional or an automated car?	xlvi
Figure A.20:	How do you rate the importance of the price-performance ratio in conventional and automated driving?	xlvi

Figure A.21: How do you rate the importance of fuel consumption when buying a conventional or an automated carxlvi

Figure A.22: How do you rate the importance of brand image when buying a conventional or an automated carxlvi

Figure B.1: Dytran 7556A sensor xlix

Figure B.2: IPEtronic (1/3) I

Figure B.3: IPEtronic (2/3) li

Figure B.4: IPEtronic (3/3) lii

Figure B.5: Vector VN7640 (1/2) liii

Figure B.6: Vector VN7640 (2/2) liv

Figure B.7: ADMA lv

Figure B.8: Six-point Likert-Scale to rate the perceived discomfort lvi

Figure B.9: Tablet with the quiz app used as side task during the study lvi

Figure B.10: Original BKV Motion Sickness Scale which was used in the Study lvi

Figure B.11: PSD mean (dark blue) and standard-deviation (light blue) compared to the input signal (black) in heave pitch and roll for the three suspensions, recorded in the simulator mock-up for Track I..... lvii

Figure B.12: PSD mean (dark blue) and standard-deviation (light blue) compared to the input signal (black) in heave pitch and roll for the three suspensions, recorded in the simulator mock-up for Track II..... lviii

Figure B.13: PSD mean (dark blue) and standard-deviation (light blue) compared to the input signal (black) in heave pitch and roll for the three suspensions, recorded in the simulator mock-up for Track III lix

Figure B.14: Detailed display of ISO values for the different settings, calculated from mock-up measurement lx

Figure B.15: Comparison of the differences, summarized for the 3 hypothesis lxi

Figure B.16: Detailed display of the ratings for different tracks, suspensions and states lxii

Figure B.17: Influence of the repetition, summarized for the three hypothesis lxiii

Figure C.1: Screenshot of the side task (a) and the test samples for the two cars (b).. lxv

Figure D.1: RMS values of the z-acceleration, roll-rate and pitch-rate from the simulation and two measurements for track I.....lxvii

Figure D.2: PSD plots of the z-acceleration, roll-rate and pitch-rate from the simulation and two measurements for track Ilxviii

Figure D.3: Surface plots..... lxix

Figure D.4: ISO plot..... lxix

List of Tables

Table 2.1:	Reference PSD values for different road classes according to ISO 8608 [214]	23
Table 4.1:	Sample composition of the online survey	30
Table 4.2:	Results of the Wilcoxon significance test for the differences in importance of ride comfort between driving, being a passenger and being driven autonomously	32
Table 4.3:	Results of the Wilcoxon signed rank sum significance test for different buying criteria of conventional and automated vehicles, at a confidence level of 95 % and effect strength Cohen d derived from z-score.....	33
Table 5.1:	Maximum values for the articulation (position, speed, acceleration) of the simulator platform, split for the two different systems	36
Table 5.2:	Permutation of the three suspension configurations, passive (pas.), semi-active (sem.) and fast-active (act.)	39
Table 5.3:	Sample composition in driving simulator study I	45
Table 5.4:	Results of the two sample t-test for the differences in tracks, states and suspensions	46
Table 5.5:	Results of the Wilcoxon significance test for the differences in tracks, states and suspensions	47
Table 5.6:	Results of the Wilcoxon signed-rank sum test and effect strength for the differences in comfort-rating, depending on the state of attention, individually for tracks and suspensions.....	48
Table 5.7:	Results of the Wilcoxon signed-rank sum test and effect strength between the comfort-rating at the beginning, and the repetition at the end, for the different tracks, states and suspensions	48
Table 6.1:	Sample composition in study II.....	55
Table 6.2:	Results of the two sample t-test and Cohen's d effect strength for the differences ISO-value, depending on the state of attention, different vehicles, ramps and ramp directions.	57
Table 7.1:	Boundary Conditions (Output Constraints)	70
Table 7.2:	Actuator limitations (input constraints)	70
Table 7.3:	Model parameters.....	71
Table 7.4:	Simulation settings.....	72
Table 7.5:	Weighting factors for the two optimization objectives.....	72
Table B.1:	Results of the Wilcoxon signed-rank sum test and effect strength between the comfort-rating at the beginning, and the repetition at the end, for the different tracks, states and suspensions	Ixiii

Bibliography

- [1] C. Starmann and J. Knipperts, „Factsheet Automatisiertes Fahren: Aktuelle Einstellungen in Deutschland,“ Bertelsmann Stiftung, Gütersloh, Germany, 2017.
- [2] S. Barthelmes, A. Czeh, Y. Guo, G. Landfester, J. Lönne and T. Schumann, „Autonomes Fahren. Erwartungen an die Mobilität der Zukunft,“ Dornier Consulting International GmbH, Berlin, Germany, 2017.
- [3] T. Hecht, E. Darlagiannis and K. Bengler, „Non-driving Related Activities in Automated Driving – An Online Survey Investigating User Needs,“ in *International Conference on Human Systems Engineering and Design: Future Trends and Applications*, Cham, Switzerland, 2020, pp. 182–188.
- [4] Taxonomy and Definitions for Terms Related to Driving Automation Systems for On-Road Motor Vehicles, SAE J3061, 2021.
- [5] D. Döring, *Eine kurze Einführung in die Systemtheorie*, 1. Edition, Springer, 2011.
- [6] R. Gasch, K. Knothe and R. Liebich, *Strukturdynamik*, 2. Edition, Springer, 2012.
- [7] D. Karnopp, D. Margolis and R. Rosenberg, *System Dynamics*, 5. Edition, Wiley, 2006.
- [8] M. Meyer, *Signalverarbeitung*, 8. Edition, Springer, 2017.
- [9] G. Mastinu, M. Gobbi and C. Miano, *Optimal Design of Complex Mechanical Systems*, 1. Edition, Springer, 2006.
- [10] E. Cramer and U. Kamps, *Grundlagen der Wahrscheinlichkeitsrechnung und Statistik*, 4. Edition, Springer, 2017.
- [11] H. Coolican, *Research Methods and Statistics in Psychology*, 7. Edition, Routledge, 2019.
- [12] T. Lumley, P. Diehr, S. Emerson and L. Chen, „The importance of the normality assumption in large public health data sets.“ *Annual Review of Public Health*, vol. 23, no. 1, pp. 151–169, 2002.
- [13] C. O. Fritz, P. E. Morris and J. J. Richler, „Effect size estimates: Current use, calculations, and interpretation,“ *Journal of Experimental Psychology: General*, vol. 141, no. 1, pp. 2–18, 2012.
- [14] J. Cohen, *Statistical Power Analysis for the Behavioral Sciences*, 2. Edition, Routledge, 1988.
- [15] K. Siebertz, D. van Bebber and T. Hochkrichen, *Statistische Versuchsplanung*, 1. Edition, Springer, 2010.
- [16] T. Schäfer, *Statistik II – Inferenzstatistik*, 1. Edition, VS Verlag, 2011.
- [17] C. Schimmel, „Entwicklung eines fahrerbasierten Werkzeugs zur Objektivierung subjektiver Fahreindrücke,“ Dissertation, Technical University of Munich, Germany, 2010.

- [18] R. S. Pietsch, „Gesamtfahrzeugmodellbasierte Objektivierung von Querdynamik und Lenkgefühl,“ Dissertation, Technical University of Munich, Germany, 2012.
- [19] M. Mitschke and H. Wallentowitz, *Dynamik der Kraftfahrzeuge*, 5. Edition, Springer Fachmedien Wiesbaden, 2014.
- [20] L. Zhang, M. G. Helander and C. G. Drury, „Identifying Factors of Comfort and Discomfort in Sitting,“ *Human Factors*, vol. 38, no. 3, pp. 377–389, 1996.
- [21] M. P. de Looze, L. F. M. Kuijt-Evers and J. van Dieen, „Sitting comfort and discomfort and the relationships with objective measures,“ *Ergonomics*, vol. 46, no. 10, pp. 985–997, 2003.
- [22] P. Vink and S. Hallbeck, „Comfort and discomfort studies demonstrate the need for a new model,“ *Applied Ergonomics*, vol. 43, no. 2, pp. 271–276, 2012.
- [23] A. Naddeo, N. Cappetti, M. Vallone and R. Califano, „New trend line of research about comfort evaluation: proposal of a framework for weighing and evaluating contributes coming from cognitive, postural and physiologic comfort perceptions,“ in *Proceedings of the 5th International Conference on Applied Human Factors and Ergonomics (AHFE)*, Krakow, Poland, 2014, pp. 503–515.
- [24] M. Griffin, *Handbook of Human Vibration*, 1. Edition, Elsevier, 1990.
- [25] N. J. Mansfield, *Human Response to Vibration*, 1. Edition, CRC Press, 2004.
- [26] M. J. Griffin, „Discomfort from feeling vehicle vibration,“ *Vehicle System Dynamics*, vol. 45, no. 7-8, pp. 679–698, 2007.
- [27] D. Simic, „Beitrag zur Optimierung der Schwingungseigenschaften des Fahrzeuges,“ Dissertation, Technical University of Berlin, Germany, 1970.
- [28] C. C. Smith, D. Y. McGehee and A. J. Healey, „The prediction of passenger riding comfort from acceleration data,“ *Journal of Dynamic Systems, Measurement, and Control*, vol. 100, no. 1, pp. 34–41, 1978.
- [29] Mechanical vibration and shock – Evaluation of human exposure to whole-body vibration, ISO 2631, 1997.
- [30] Guide to the measurement and evaluation of human exposure to whole-body mechanical vibration and repeated shock, BS 6841, 1987.
- [31] Human exposure to mechanical vibrations: Whole-body vibration, VDI 2057, 2002.
- [32] H. Bubb, K. Bengler, R. E. Grünen and M. Vollrath, *Automobilergonomie*, 1. Edition, Springer, 2015.
- [33] H. Dupuis, „Fahrzeugschwingungen – Wirkungen auf den Menschen und deren Beurteilung,“ in *Fahrzeug Dynamik*, W. Stühler, ed. Wiesbaden, Germany: Vieweg+Teubner, 1988, pp. 208–230.
- [34] I. Rericha, „Methoden zur objektiven Bewertung des Fahrkomforts,“ *Automobil-Industrie*, vol. 2, no. 86, pp. 175–182, 1986.
- [35] B. Klinger, „Einfluß der Motorlagerung auf Schwingungskomfort und Geräuschanregung im Kraftfahrzeug,“ Dissertation, Technical University of Braunschweig, Germany, 1996.
- [36] M. Mitschke and B. Klingner, „Schwingungskomfort im Kraftfahrzeug,“ *ATZ – Automobil-technische Zeitschrift*, vol. 100, no. 1, pp. 18–24, 1998.
- [37] D. Hennecke, „Zur Bewertung des Schwingungskomforts von Pkw bei instationären Anregungen,“ Dissertation, Fortschrittberichte VDI: Reihe 12, Verkehrstechnik, Fahrzeugtechnik; Nr. 237, Technical University of Braunschweig, Germany, 1995.

- [38] S. Cucuz, „Schwingempfindung von Pkw-Insassen,“ Dissertation, Technical University of Braunschweig, Germany, 1992.
- [39] F. Fent, „Objektivierung von Vertikaldynamikkomfort in Personenkraftwagen,“ Bachelorarbeit, Technische Universität München, Germany, 2018.
- [40] T. Bitter, „Objektivierung des dynamischen Sitzkomforts,“ Dissertation, Technical University of Braunschweig, Germany, 2006.
- [41] K. Stammen, „Bewertung des Schwingungskomforts in PKW mit Hilfe von Regressionsmodellen und künstlichen neuronalen Netzen,“ Dissertation, Helmut-Schmidt-University Hamburg, Germany, 2009.
- [42] P. Knauer, „Objektivierung des Schwingungskomforts bei instationärer Fahrbahnanregung,“ Dissertation, Technical University of Munich, Germany, 2010.
- [43] S. Lennert and H. P. Wölfel, „Approach to objectify vibrational riding comfort and explanation with a practical example,“ in *Human Vibration, Effects on Health – Performance – Comfort, VDI Berichte 2002*, Dresden, Germany, 2007, pp. 215–228.
- [44] S. Lennert, „Zur Objektivierung von Schwingungskomfort in Personenkraftwagen - Untersuchung der Wahrnehmungsdimensionen,“ Dissertation, Technical University of Munich, Germany, 2009.
- [45] G. Burkhard, E. Enders, S. Vos, N. Munzinger and D. Schramm, „Acquiring requirements on drive comfort by quantifying the accelerations affecting vehicle occupants,“ in *AmE 2018-Automotive meets Electronics – 9th GMM-Symposium*, Dortmund, Germany, 2018, pp. 1–6.
- [46] G. Burkhard, S. Vos, N. Munzinger, E. Enders and D. Schramm, „Requirements on driving dynamics in autonomous driving with regard to motion and comfort,“ in *18. Internationales Stuttgarter Symposium*, Germany, 2018, pp. 683–697.
- [47] E. Enders, G. Burkhard, F. Fent, M. Lienkamp and D. Schramm, „Objectification methods for ride comfort: Comparison of conventional methods and proposal of a new method for automated driving conditions,“ *Forschung im Ingenieurwesen / Engineering Research*, vol. 83, no. 4, pp. 885–898, 2019.
- [48] D. K. Kudritzki, „Ridemeter – Calculated Ride Comfort,“ in *SAE Noise and Vibration Conference and Exhibition / SAE Technical Paper 2007-01-2388*, St. Charles, Illinois, USA, 2007, pp. 1–9.
- [49] B. Jörißen, „Objektivierung der menschlichen Schwingungswahrnehmung unter Einfluss realer Fahrbahnanregungen,“ Dissertation, University Duisburg-Essen, Germany, 2012.
- [50] K. Strandemar, „On Objective Measures for Ride Comfort Evaluation,“ PhD Thesis, KTH Royal Institute of Technology, Stockholm, Sweden, 2005.
- [51] K. Strandemar and B. Thorvald, „Ride diagram: A tool for analysis of vehicle suspension settings,“ *Vehicle System Dynamics*, vol. 44, no. Sup. 1, pp. 913–920, 2006.
- [52] N. Fischer-von Rönn and M. Meywerk, „Predicting the ride comfort of passenger cars for single-obstacle crossings through an innovative feature extraction method consisting of non-linear geometric approximations of wavelet-transformed acceleration data and airborne sound,“ *Proceedings of the Institution of Mechanical Engineers, Part D: Journal of Automobile Engineering*, vol. 228, no. 4, pp. 357–369, 2014.
- [53] M. Hazelaar, „Fahrwerkschwingungen und Komfortbeurteilung bei kurzweiliger Anregung (Achsrauhigkeit),“ Dissertation, Technical University of Braunschweig, Germany, 1994.

- [54] W. El Falou, J. Duchêne, M. Grabisch, D. Hewson, Y. Langeron and F. Lino, „Evaluation of driver discomfort during long-duration car driving,“ *Applied Ergonomics*, vol. 34, no. 3, pp. 249–255, 2003.
- [55] C. J. Schickedanz, „Zum Übertragungsverhalten nichtlinearer Mehreingangssysteme,“ Dissertation, Johann Wolfgang Goethe-University Frankfurt, Germany, 2012.
- [56] M. Eisenbarth, G. Boisdequin and F. Gauterin, „Consistent assessment of chassis relevant ride comfort on roads and test rigs,“ in *14. Internationales Stuttgarter Symposium*, Germany, 2014, pp. 41–53.
- [57] M. Kosfelder, „Die Objektivierung des Schwingungskomforts von Kraftfahrzeugen auf der Grundlage globaler Bewegungsformen,“ in *14. Aachener Kolloquium Fahrzeug- und Motorentechnik*, Germany, 2005, pp. 1631–1644.
- [58] W. Schiehlen, „White noise excitation of road vehicle structures,“ *Sadhana*, vol. 31, no. 4, pp. 487–503, 2006.
- [59] R. A. Williams, „Automotive active suspensions Part 1: Basic principles,“ *Proceedings of the Institution of Mechanical Engineers, Part D: Journal of Automobile Engineering*, vol. 211, no. 6, pp. 415–426, 1997.
- [60] R. A. Williams, „Automotive active suspensions Part 2: Practical considerations,“ *Proceedings of the Institution of Mechanical Engineers, Part D: Journal of Automobile Engineering*, vol. 211, no. 6, pp. 427–444, 1997.
- [61] D. Karnopp, „How significant are transfer function relations and invariant points for a quarter car suspension model?,“ *Vehicle System Dynamics*, vol. 47, no. 4, pp. 457–464, 2009.
- [62] Y. Zhuang, S. Nie, F. Chen and J. Xie, „A study on invariant points of semi-active suspension,“ in *Advanced Vehicle Control AVEC'16*, J. Edelmann, M. Plöchel and P. E. Pfeffer, ed. London, United Kingdom: Taylor & Francis, 2016, pp. 645–650.
- [63] S. Nie, Y. Zhuang, F. Chen and J. Xie, „Invariant points of semi-active suspensions,“ *Advances in Mechanical Engineering*, vol. 10, no. 7, pp. 1–14, 2018.
- [64] R. Kallenbach, D. Kunz and W. Schramm, „Optimierung des Fahrzeugverhaltens mit Semiaktiven Fahrwerkregelungen,“ in *Berechnung im Automobilbau (VDI Berichte)*. vol. 699 Düsseldorf, Germany: Verein Deutscher Ingenieure (VDI), 1988, pp. 121–135.
- [65] Bayerische Motorenwerke AG. „Suspension of the BMW F01,“ 2022. [Online]. Available: https://www.7-forum.com/modelle/f01/galerie/fahrwerk%7B%5C_%7Dp0044083-b.jpg [visited on Jan. 2, 2022].
- [66] F. Eichenseer and T. Müller, „Akustik und Schwingungskomfort,“ *ATZextra – BMW 7er*, vol. 13, no. 8, pp. 84–87, 2008.
- [67] E. Boyraz, C. Kandler, M. Gantikow and D. Schramm, „Investigation of methods for the objective assessment of the dynamic system behaviour of air springs,“ in *17. Internationales Stuttgarter Symposium*, 2017, pp. 1431–1447.
- [68] E. Boyraz, C. Kandler, M. Gantikow and D. Schramm, „Objective assessment of the dynamic system behavior of multi-chamber air springs,“ in *8th International Munich Chassis Symposium*, 2017, pp. 255–270.
- [69] C. Stengel, U. Lux, S. Fischer and M. Pauligk, „Achssystem und Luftfederung,“ *ATZextra – Audi A6*, vol. 15, no. 11, pp. 118–125, 2010.

- [70] Thyssenkrupp Bilstein GmbH. „Coilover Spring,“ 2022. [Online]. Available: <https://workshop.bilstein.com/wp-content/uploads/2021/02/bilstein-b3-productimage.png> [visited on Jan. 2, 2022].
- [71] Thyssenkrupp Bilstein GmbH. „Air-Spring,“ 2022. [Online]. Available: https://workshop.bilstein.com/wp-content/uploads/2021/02/bilstein-b3_air-spring_productimage.png [visited on Jan. 2, 2022].
- [72] ZF Friedrichshafen AG. „ZF Damping Modules,“ 2022. [Online]. Available: https://www.zf.com/products/media/en/pim/ct___suspension_technology/chassis_4/FSC_750x500_png_3_2_748px.png [visited on Jan. 2, 2022].
- [73] Thyssenkrupp AG. „Stabilizer,“ 2022. [Online]. Available: [https://ucpcdn.thyssenkrupp.com/_legacy/UCPthyssenkruppBACTSchattenseite/assets.files/media/bact_bilder/produkte/federn-und-stabilisatoren-\(springs-and-stabilizers\)/stabilisatoren/massiver_stabilisator_image_w997_h749.jpg](https://ucpcdn.thyssenkrupp.com/_legacy/UCPthyssenkruppBACTSchattenseite/assets.files/media/bact_bilder/produkte/federn-und-stabilisatoren-(springs-and-stabilizers)/stabilisatoren/massiver_stabilisator_image_w997_h749.jpg) [visited on Jan. 2, 2022].
- [74] J. F. Wallace, „Hydropneumatic Shock Absorber,“ United States of America Patent US1967641, 1934.
- [75] R. L. Gruss, „Shock Absorbing Device,“ United States of America Patent US1918697, 1933.
- [76] J. C. Dixon, *The Shock Absorber Handbook*, 2. Edition, Wiley, 2007.
- [77] M. W. Neal, W. Cwycyshyn and I. Badiru, „Tuning Dampers for Ride and Handling of Production Vehicles,“ *SAE International Journal of Commercial Vehicles*, vol. 8, no. 1, pp. 152–159, 2015.
- [78] J. Bukovics, E. Cabes-Roca, W. Gerschütz and H. Kolm, „Auslegung von Akustik und Schwingungskomfort,“ *ATZextra – Audi Q5*, vol. 13, no. 2, pp. 100–107, 2008.
- [79] A. Buder, W. Gerschütz, H. Kolm and R. Rotter, „Auslegung von Akustik und Schwingungskomfort,“ *ATZextra – Audi A6*, vol. 15, no. 11, pp. 150–157, 2010.
- [80] J. Berghus, A. Ott, M. Ohmenhäuser, A. Wetzel and H. Litzenberger, „Abstimmung der Fahreigenschaften,“ *ATZextra – Mercedes-Benz SL*, vol. 17, no. 1, pp. 206–215, 2012.
- [81] H. Glaser, T. Rossie, R. Niboer, J. Rüger, S. Revelant, A. Hopf, R. Wagner and H.-G. Spengel, „Fahrwerk,“ in *Audi Q3 (ATZ/MTZ-Typenbuch)*, H.-J. Rudolph, ed. Wiesbaden, Germany: Springer, 2013, pp. 35–45.
- [82] R. Alkhatib, G. Nakhaie Jazar and M. Golnaraghi, „Optimal design of passive linear suspension using genetic algorithm,“ *Journal of Sound and vibration*, vol. 275, no. 3-5, pp. 665–691, 2004.
- [83] L. R. C. Drehmer, W. J. Paucar Casas and H. M. Gomes, „Parameters optimisation of a vehicle suspension system using a particle swarm optimisation algorithm,“ *Vehicle System Dynamics*, vol. 53, no. 4, pp. 449–474, 2015.
- [84] F. Havelka and M. Musil, „Multi-Objective Optimization of Vehicle Suspension Parameters Considering Various Road Classes,“ *Scientific Proceedings. Faculty of Mechanical Engineering, Slovak University of Technology in Bratislava*, vol. 22, no. 1, pp. 26–31, 2014.
- [85] M. D. Bedük, K. Çalışkan, R. Henze and F. Küçükay, „Advanced parameter analysis for damper influence on ride dynamics,“ *Journal of Vibration and Control*, vol. 24, no. 8, pp. 1393–1411, 2018.

- [86] L. Dragon, R. Faul, T. Grossmann and J. Coldiz, „Objektive und subjektive Abstimmung der Fahrkultur mittels digitaler Prototypen unter Einbeziehung von Simulatoren,“ in *Human Vibration, Effects on Health – Performance – Comfort, VDI Berichte 2002*, Dresden, Germany, 2007, pp. 181–196.
- [87] A. Citroen, „Improvement in and relating to Suspension Systems for Vehicles,“ United Kingdom Patent GB601731, 1948.
- [88] A. Citroen, „Improvements in or relating to Suspension Systems,“ United Kingdom Patent GB803381, 1958.
- [89] D. Karnopp, M. J. Crosby and R. A. Harwood, „Vibration Control Using Semi-Active Force Generators,“ *Journal of Engineering for Industry*, vol. 96, no. 2, pp. 619–626, 1974.
- [90] Y. Yokoya, K. Asami, T. Hamajima and N. Nakashima, „Toyota Electronic Modulated Suspension (TEMS) System for the 1983 Soarer,“ in *SAE International Congress and Exhibition (SAE Technical Paper 840341)*, Detroit, Michigan, USA, 1984, pp. 1–11.
- [91] K. Howard, „Active Suspension,“ *Motorsport Magazine*, vol. 12/01, pp. 1777–1782, 2001.
- [92] P. G. Wright and D. A. Williams, „Application of Active Suspension To High Performance Road Vehicles,“ in *Proceedings of the IMechE Conference on Microprocessors in Fluid Power Engineering (C239/84)*, Bath, UK, 1984, pp. 23–28.
- [93] D. A. Williams, P. G. Wright and J. P. Davis, „Control System for Controlling the Suspension of a Land Vehicle,“ Unites States of America Patent US005217246, 1993.
- [94] M. B. Packer, „Active Ride Control – A Logical Step from Static Vehicle Attitude Control,“ in *1978 Automotive Engineering Congress and Exposition / SAE Technical Paper 780050*, Detroit, Michigan, USA, 1978, pp. 1–9.
- [95] T. Merker, J. Wirtz, M. Hill and M. Jeglizka, „Das SL Fahrwerk – Dynamik und Komfort vereint,“ *Sonderausgabe von ATZ und MTZ – Mercedes SL*, pp. 84–91, 2001.
- [96] S. N. Brown, „Active Vehicle Suspension,“ USA Patent US007427072, 2008.
- [97] Bose Corporation. „Bose Active Suspension System,“ 2022. [Online]. Available: https://media.techeblog.com/images/bose_1.jpg [visited on Jan. 2, 2022].
- [98] O. Raynauld and S. Fath, „MagneRide-Stoßdämpfer für den Range Rover Evoque,“ *ATZ - Automobiltechnische Zeitschrift*, vol. 114, no. 2, pp. 136–141, 2012.
- [99] P. Causemann, „Modern vibration damping systems,“ *ATZ Worldwide*, vol. 105, no. 11, pp. 10–13, 2003.
- [100] ZF Friedrichshafen AG. „ZF CDC Damper,“ 2022. [Online]. Available: https://www.zf.com/products/media/en/pim/ct___suspension_technology/chassis_4/CDCevo_750x500_png_3_2_748px.png [visited on Jan. 2, 2022].
- [101] Audi AG. „Audi Magnetic-Ride Damper,“ 2022. [Online]. Available: https://www.audi.ca/content/dam/nemo/ca/NoMo/search-term/1300x551-stage-header/1300x551_Audi-magnetic-ride.jpg [visited on Jan. 2, 2022].
- [102] M. Rambach, „Kennfeldbasierte Modellierung eines semi-aktiven Dämpfers,“ Semesterarbeit, Technical University of Munich, Germany, 2020.
- [103] D. C. Batterbee, „Magnetorheological shock absorbers : Modelling, design, and control,“ PhD Thesis, University of Sheffield, United Kingdom, 2006.
- [104] J. Kasprzyk, J. Wyrwal and P. Krauze, „Automotive MR damper modeling for semi-active vibration control,“ in *IEEE/ASME international conference on advanced intelligent mechatronics*, Besancon, France, 2014, pp. 500–505.

- [105] R. Jeyasenthil, D. S. Yoon and S.-B. Choi, „Response time effect of magnetorheological dampers in a semi-active vehicle suspension system: performance assessment with quantitative feedback theory,“ *Smart Materials and Structures*, vol. 28, no. 5, pp. 1–13, 2019.
- [106] G. Hu, Y. Lu, S. Sun and W. Li, „Development of a self-sensing magnetorheological damper with magnets in-line coil mechanism,“ *Sensors and Actuators A: Physical*, vol. 255, pp. 71–78, 2017.
- [107] M. Ahmadian, „Magneto-rheological suspensions for improving ground vehicle’s ride comfort, stability, and handling,“ *Vehicle System Dynamics*, vol. 55, no. 10, pp. 1618–1642, 2017.
- [108] D. Konik, W. Bauer, K. J. Huber, B. Jordan, S. Kolbel, S. Schopp and M. Wimmer, „Electronic Damping Control with Continuously(ly) working damping valves (EDCC) - system description and functional improvements,“ in *AVEC’96 International Symposium Symposium on Advanced Vehicle Control*, Aachen, Germany, 1996, pp. 88–104.
- [109] M. Nyenhuis and M. Fröhlich, „Das Verstelldämpfersystem des BMW X5,“ *ATZ - Automobiltechnische Zeitschrift*, vol. 109, no. 3, pp. 248–255, 2006.
- [110] M. Jautze, A. Bogner, J. Eggendinger, G. Rekowitz and A. Stumm, „Das Verstelldämpfersystem,“ *ATZextra – BMW 7er*, vol. 13, no. 8, pp. 100–103, 2008.
- [111] A. M. Soliman and M. M. Kaldas, „Semi-active suspension systems from research to mass-market – A review,“ *Journal of Low Frequency Noise Vibration and Active Control – Special Collection: Advances in Semi-Active Suspension Systems for Automotive Applications*, vol. 0, no. 0, pp. 1–19, 2019.
- [112] A. Schindler, „Neue Konzeption und erstmalige Realisierung eines aktiven Fahrwerks mit Preview-Strategie,“ Dissertation, Karlsruhe Institute of Technologie, Germany, 2009.
- [113] M. Münster, U. Mair, H. J. Gilsdorf, A. Thomä, C. Müller, M. Hippe and J. Hoffmann, „Electromechanical active body control,“ *ATZ - Automobiltechnische Zeitschrift*, vol. 111, no. 9, pp. 44–48, 2009.
- [114] N. Amati, A. Tonoli, L. Castellazzi and S. Ruzimov, „Design of electromechanical height adjustable suspension,“ *Proceedings of the Institution of Mechanical Engineers, Part D: Journal of Automobile Engineering*, vol. 232, no. 9, pp. 1253–1269, 2018.
- [115] A. Rizzo, X. Moreau, A. Oustaloup and V. Hernette, „A New CRONE Suspension: More Compact and More Efficient: Part 2—Synthesis and Achievement,“ in *Proceedings of the ASME 2009 International Design Engineering Technical Conferences and Computers and Information in Engineering Conference. Volume 4: 7th International Conference on Multibody Systems, Nonlinear Dynamics, and Control, Parts A, B and C*, San Diego, California, USA, 2009, pp. 1103–1111.
- [116] J.-L. Bouvin, X. Moreau, A. Benine-Neto, V. Hernette, P. Serrier and A. Oustaloup, „Modelling and design of a pneumatic CRONE suspension architecture for ride comfort,“ *Vehicle System Dynamics*, vol. 59, no. 6, pp. 890–906, 2020.
- [117] Mercedes-Benz AG. „Magic Body Control Suspension,“ 2022. [Online]. Available: https://www.mercedes-benz.com.sg/passengercars/mercedes-benz-cars/models/s-class/coupe/explore/intelligent-drive-technologies/magic-body-control/_jcr_content/par/prod uctinfotextimage/media/slides/videoimageslide_9afe/image.MQ6.12.20180612102412.jpeg [visited on Jan. 3, 2022].

- [118] S. Sagewka, T. Fiebig, C. Schmid and D. Wostal, „Mechatronic Roll Control for the 48-V Electrical System,“ *ATZ Worldwide*, vol. 119, no. 3, pp. 58–63, 2017.
- [119] D. Konik, „Development of the Dynamic Drive for the new 7 Series of the BMW Group,“ *International Journal of Vehicle Design*, vol. 28, no. 1-3, pp. 131–149, 2002.
- [120] ZF Friedrichshafen AG. „ZF Electromechanic Roll Control System,“ 2022. [Online]. Available: https://www.zf.com/products/media/en/pim/ca___chassis_actuators/chassis_6/eRC_800x600_png_3_2_748px.png [visited on Jan. 3, 2022].
- [121] Schaeffler AG. „Schaeffler Electro-Mechanical Roll Stabilizer,“ 2022. [Online]. Available: https://www.schaeffler.com/remotemedien/media/_shared_media/05_products_services/passenger_cars_1/wheel_bearings___applications_in_chassis/0001A6C1.jpg [visited on Jan. 3, 2022].
- [122] A. Gavine, „Body Control Technology,“ *Vehicle Dynamics International*, vol. May/June, pp. 4–5, 2019.
- [123] Audi AG. „Audi AI-Suspension System,“ 2022. [Online]. Available: https://audimediacent er-a.akamaihd.net/system/production/media/49824/images/1875dc30a2164ed602f80e0d1dbed1f961aae719/A178215_full.jpg?1582357915 [visited on Jan. 3, 2022].
- [124] S. Cytrynski, U. Neerpasch, R. Bellmann and B. Danner, „Das aktive Fahrwerk des neuen GLE von Mercedes-Benz,“ *ATZ - Automobiltechnische Zeitschrift*, vol. 120, no. 12, pp. 42–45, 2018.
- [125] B. Gysen, J. Paulides, J. Janssen and E. Lomonova, „Active Electromagnetic Suspension System for Improved Vehicle Dynamics,“ *IEEE Transactions on Vehicular Technology*, vol. 59, no. 3, pp. 1156–1163, 2010.
- [126] E. Lenz, P. Hedrich and P. F. Pelz, „Aktive Luftfederung – Modellierung, Regelung und Hardware-in-the-Loop-Experimente,“ *Forschung im Ingenieurwesen / Engineering Research*, vol. 82, no. 3, pp. 171–185, 2018.
- [127] J. Ekchian, W. Graves, Z. Anderson, M. Giovanardi, O. Godwin, J. Kaplan, J. Ventura, J. R. Lackner and P. DiZio, „A High-Bandwidth Active Suspension for Motion Sickness Mitigation in Autonomous Vehicles,“ in *SAE 2016 World Congress and Exhibition / SAE Technical Paper 2016-01-1555*, Detroit, Michigan, USA, 2016, pp. 1–10.
- [128] K. Reybrouck, B. Vandersmissen and K. Six, „ACOCAR: ultimate comfort and safety through the energy-efficient active damping system of Tenneco,“ in *21st Aachen Colloquium Automobile and Engine Technology*, Germany, 2012, pp. 1–15.
- [129] P. Schäfer. „ZF präsentiert das vollaktive Fahrwerksystem sMotion,“ 2022. [Online]. Available: <https://www.springerprofessional.de/fahrwerk/automatisiertes-fahren/zf-praesentiert-das-vollaktive-fahrwerksystem-smotion/15847750> [visited on Jan. 3, 2022].
- [130] L. P. Mair, „Analyse und Bewertung heutiger und zukünftiger Aktuatoren aktiver Fahrwerke in Hinblick auf das hochautomatisierte Fahren,“ Semesterarbeit, Technical University of Munich, Germany, 2018.
- [131] B. Heißing, M. Ersoy and S. Gies, *Fahrwerkhandbuch*, (ATZ/MTZ-Fachbuch), 4. Edition, Springer, 2013.
- [132] R. Isermann, *Mechatronische Systeme – Grundlagen*, 2. Edition, Springer, 2008.
- [133] A. Zilkens, „Charakterisierung von Aktoren aktiver Fahrwerke durch Prüfstandsversuche,“ Masterarbeit, Technical University of Munich, Germany, 2019.

- [134] R. Tutzauer, „Kennfeld basierte Modellierung von Aktoren aktiver Fahrwerkssysteme,“ Semesterarbeit, Technical University of Munich, Germany, 2019.
- [135] B. Wegele, „Aufbau eines Fahrzeugmodells zur Durchführung von Vertikaldynamiksimulationen mit OpenCRG Straßenprofilen in Matlab / Simulink,“ Semesterarbeit, Technical University of Munich, Germany, 2019.
- [136] R. N. Jazar, *Vehicle Dynamics: Theory and Application*, 3. Edition, Springer, 2017.
- [137] A. N. Thite, „Development of a refined quarter car model for the analysis of discomfort due to vibration,“ *Advances in Acoustics and Vibration*, vol. 2012, no. 863061, 2012.
- [138] D. Schramm, M. Hiller and R. Bardini, *Modellbildung und Simulation der Dynamik von Kraftfahrzeugen*, 1. Edition, Springer, 2010.
- [139] W. Matschinsky, *Radführungen der Straßenfahrzeuge*, 3. Edition, Springer, 2007.
- [140] E. Kutluay and H. Winner, „Validation of vehicle dynamics simulation models – a review,“ *Vehicle System Dynamics*, vol. 52, no. 2, pp. 186–200, 2014.
- [141] C. Halfmann and H. Holzmann, *Adaptive Modelle für die Kraftfahrzeugdynamik*, 1. Edition, Springer, 2003.
- [142] M. Viehof and H. Winner, „Stand der Technik und der Wissenschaft: Modellvalidierung im Anwendungsbereich der Fahrdynamiksimulation,“ Technical University of Darmstadt, Germany, 2017.
- [143] J. Castillo, A. P. D. L. Blanca, J. A. Cabrera and A. Simón, „An optical tire contact pressure test bench,“ *Vehicle System Dynamics*, vol. 44, no. 3, pp. 207–221, 2006.
- [144] C. Minca, „The Determination and Analysis of Tire Contact Surface Geometric Parameters,“ *Review of the Air Force Academy*, vol. 28, no. 1, pp. 149–154, 2015.
- [145] M. G. Pottinger, „Chapter 7: Contact Patch (Foot Print) Phenomena,“ in *Pneumatic Tire*, A. N. Gent and J. D. Walter, ed. Washington D.C., USA: U.S. Department of Transport – National Highway Traffic Safety Administration (nhtsa), 2006, pp. 231–286.
- [146] R. Matsuyaki and A. Todoroki, „Intelligent Tires Based on Measurement of Tire Deformation,“ *Journal of Solid Mechanics and Materials Engineering*, vol. 2, no. 2, pp. 269–280, 2008.
- [147] V. Ivanov, „Analysis of Tire Contact Parameters Using Visual Processing,“ *Advances in Tribology*, vol. 2010, no. 491723, pp. 1–11, 2010.
- [148] C. Gangkofer, „Modellierung des Reifen-Fahrbahn-Kontakts für bauliche Hindernisse im Straßenverkehr,“ Bachelorarbeit, Technical University of Munich, Germany, 2017.
- [149] P. Můčka and L. Gagnon, „Influence of tyre-road contact model on vehicle vibration response,“ *Vehicle System Dynamics*, vol. 53, no. 9, pp. 1227–1246, 2015.
- [150] F. Besinger, D. Cebon and D. Cole, „Force Control of a Semi-Active Damper,“ *Vehicle System Dynamics*, vol. 24, no. 9, pp. 695–723, 1995.
- [151] M. Fröhlich, „Ein robuster Zustandsbeobachter für ein semiaktives Fahrwerkregelsystem,“ Dissertation, Technical University of Munich, Germany, 2008.
- [152] D. Karnopp, „Active Damping in Road Vehicle Suspension Systems,“ *Vehicle System Dynamics*, vol. 12, no. 6, pp. 291–311, 1983.
- [153] D. Karnopp, „Active and Semi-Active Vibration Isolation,“ *Journal of Vibration and Acoustics*, vol. 117, no. B, pp. 177–185, 1995.

- [154] C. Lauwerys, J. Swevers and P. Sas, „A model free control design approach for a semi-active suspension of a passenger car,“ in *Proceedings of the 2005 American Control Conference*, Portland, Oregon, USA, 2005, pp. 2206–2211.
- [155] M. Valasek and M. Novak, „Ground Hook for Semi-Active Damping of Truck’s Suspension,“ in *TU Brno and CTU Prague Workshop 96* Brno, Poland: Czech Technical University Prague, 1996, pp. 467–468.
- [156] M. Valasek, M. Novak, Z. Sika and O. Vaculin, „Extended ground-hook – New concept of semi-active control of truck’s suspension,“ *Vehicle System Dynamics*, vol. 27, no. 5-6, pp. 289–303, 1997.
- [157] S. M. Savaresi and C. Spelta, „Mixed Sky-Hook and ADD: Approaching the Filtering Limits of a Semi-Active Suspension,“ *Journal of Dynamic Systems Measurement and Control*, vol. 129, no. 4, pp. 382–392, 2007.
- [158] M. Corno, O. Galluppi, G. Panzani, A. Sinigaglia, P. Capuano, J. Cecconi and S. M. Savaresi, „Design and Validation of a Full Body Control Semi-Active Suspension Strategy for a Supercar,“ *IFAC-PapersOnLine*, vol. 52, no. 5, pp. 667–672, 2019.
- [159] E. Katsuyama, „Improvement of ride comfort by triple Skyhook control,“ in *9th International Munich Chassis Symposium 2018*, Germany, 2019, pp. 215–234.
- [160] W. F. Milliken, „Active Suspension,“ in *39th Annual Earthmoving Industry Conference / SAE Technical Paper 880799*, Peoria, Illinois, USA, 1988, pp. 1–6.
- [161] A. G. Thompson and B. R. Davis, „A Technical Note on the Lotus Suspension Patents,“ *Vehicle System Dynamics*, vol. 20, no. 6, pp. 381–383, 1991.
- [162] K. Furihata, K. Toyofuku, A. Takahashi, A. Kitigawa and K. Sanada, „A Study of an Active Suspension System with Modal Control Algorithm,“ *JSAE Review*, vol. 14, no. 4, pp. 42–48, 1993.
- [163] F. Braghin, F. Resta and E. Sabbioni, „A suspension control strategy for improving ride comfort of high-performance vehicles,“ in *10th Mini Conference on Vehicle System Dynamics, Identification and Anomalies (VSDIA 2006)*, Budapest, Hungary, 2006, pp. 521–530.
- [164] F. Braghin, F. Resta and E. Sabbioni, „A modal control for active/semi-active suspension systems,“ in *IEEE/ASME International Conference on Advanced Intelligent Mechatronics*, Zürich, Switzerland, 2007, pp. 1–6.
- [165] C. U. Dogruer, „Improving Ride-Comfort of a Quarter-Car Model using Modal Control,“ in *7th International Conference on Control, Mechatronics and Automomation*, Delft, Netherlands, 2019, pp. 237–242.
- [166] F. Yakub, P. Muhammad, Z. H. C. Daud, A. Y. A. Fatah and Y. Mori, „Ride comfort quality improvement for a quarter car semi-active suspension system via state-feedback controller,“ in *11th Asian Control Conference (ASCC)*, Gold Coast, Australia, 2017, pp. 406–411.
- [167] D. E. Williams, „Active Suspension: Future Lessons from The Past,“ *SAE International Journal of Vehicle Dynamics, Stability, and NVH*, vol. 2, no. 2, pp. 147–165, 2018.
- [168] E. Enders, P. Karle, G. Bonelli, D. Killian and G. Burkhard, „Modal Vertical Vehicle Dynamics Control for Semi-Active and Active Suspension Systems,“ in *Fifteenth International Conference on Ecological Vehicles and Renewable Energies (EVER) / IEEE Xplore Paper 9242985*, Monte-Carlo, Monaco, 2020, pp. 1–9.

- [169] J. G. Chen, J. S. Cheng and Y. H. Nie, „Research on the Decoupling Control Algorithm of Full Vehicle Semi-Active Suspension,“ *Advanced Materials Research*, vol. 479–481, pp. 1355–1360, 2012.
- [170] C. Wang, W. Zhao, Z. Luan, Q. Gao and K. Deng, „Decoupling control of vehicle chassis system based on neural network inverse system,“ *Mechanical Systems and Signal Processing*, vol. 106, pp. 176–197, 2018.
- [171] A. G. Thompson, „Optimal and Suboptimal Linear Active Suspensions for Road Vehicles,“ *Vehicle System Dynamics*, vol. 13, no. 2, pp. 61–72, 1984.
- [172] D. Hrovat, „A class of active LQG optimal actuators,“ *Automatica*, vol. 18, no. 1, pp. 117–119, 1982.
- [173] A. Unger, „Serientaugliche quadratisch optimale Regelung für semiaktive Pkw-Fahrwerke,“ Dissertation, Technical University of Munich, Germany, 2012.
- [174] P. Brezas and M. C. Smith, „Linear Quadratic Optimal and Risk-Sensitive Control for Vehicle Active Suspensions,“ *IEEE Transactions on Control Systems Technology*, vol. 22, no. 2, pp. 543–556, 2014.
- [175] J. Yao, S. Taheri, S. Tian, Z. Zhang and L. Shen, „A novel semi-active suspension design based on decoupling skyhook control,“ *Journal of Vibroengineering*, vol. 16, no. 3, pp. 1318–1325, 2014.
- [176] T. P. Van Der Sande, B. L. Gysen, I. J. Besselink, J. J. Paulides, E. A. Lomonova and H. Nijmeijer, „Robust control of an electromagnetic active suspension system: Simulations and measurements,“ *Mechatronics*, vol. 23, no. 2, pp. 204–212, 2013.
- [177] K. K. Afshar and A. Javadi, „Constrained H-inf control for a half-car model of an active suspension system with actuator time delay by predictor feedback,“ *Journal of Vibration and Control*, vol. 25, no. 10, pp. 1673–1692, 2019.
- [178] J. Kasprzyk, P. Krauze and J. Wyrwal, „The clipped LQ control oriented on driving safety of a half-car model with magnetorheological dampers,“ in *Trends in Advanced Intelligent Control, Optimization and Automation – Proceedings of KKA 2017 – The 19th Polish Control Conference, Krakow, Poland* (Advances in Intelligent Systems and Computing). vol. 577, W. Mitkowski, J. Kacprzyk, K. Oprzedkiewicz and P. Skruch, ed. Wiesbaden, Germany: Springer, 2017, pp. 214–223.
- [179] C. Göhrle, A. Wagner, A. Schindler and O. Sawodny, „Active suspension controller using MPC based on a full-car model with preview information,“ in *American Control Conference (ACC)*, Montreal, Canada, 2012, pp. 497–502.
- [180] C. Göhrle, A. Schindler, A. Wagner and O. Sawodny, „Model Predictive Control of semi-active and active suspension systems with available road preview,“ in *European Control Conference (ECC)*, Zürich, Switzerland, 2013, pp. 1499–1504.
- [181] M. Nguyen, M. Canale, O. Sename and L. Dugard, „A Model Predictive Control approach for semi-active suspension control problem of a full car,“ in *55th Conference on Decision and Control (CDC)*, Las Vegas, Nevada, USA, 2016, pp. 721–726.
- [182] X. Sun, C. Yuan, Y. Cai, S. Wang and L. Chen, „Model predictive control of an air suspension system with damping multi-mode switching damper based on hybrid model,“ *Mechanical Systems and Signal Processing*, vol. 2017, no. 94, pp. 94–110, 2017.
- [183] K. M. M. Rathai, M. Alamir and O. Sename, „Experimental Implementation of Model Predictive Control Scheme for Control of Semi-active Suspension System,“ *IFAC-Papers-OnLine*, vol. 52, no. 5, pp. 261–266, 2019.

- [184] M. Canale and M. Milanese, „FMPC: A Fast Implementation of Model Predictive Control,“ *IFAC Proceedings Volumes*, vol. 38, no. 1, pp. 391–396, 2005.
- [185] M. Canale, M. Milanese and C. Novara, „Semi-Active Suspension Control Using “Fast” Model-Predictive Techniques,“ *IEEE Transactions on Control Systems Technology*, vol. 14, no. 6, pp. 1034–1046, 2006.
- [186] C. U. Dogruer, „Constrained model predictive control of a vehicle suspension using Laguerre polynomials,“ *Proceedings of the Institution of Mechanical Engineers, Part C: Journal of Mechanical Engineering Science*, vol. 234, no. 6, pp. 1253–1268, 2020.
- [187] R. Dessort and C. Chucholowski, „Explicit model predictive control of semi-active suspension systems using Artificial Neural Networks (ANN),“ in *8th International Munich Chassis Symposium*, Germany, 2017, pp. 207–228.
- [188] J. Theunissen, A. Sorniotti, P. Gruber, S. Fallah, M. Ricco, M. Kvasnica and M. Dhaens, „Regionless Explicit Model Predictive Control of Active Suspension Systems with Preview,“ *IEEE Transactions on Industrial Electronics*, vol. 67, no. 6, pp. 4877–4888, 2020.
- [189] J. Guanetti and F. Borrelli, „Stochastic MPC for cloud-aided suspension control,“ in *56th Annual Conference on Decision and Control (CDC)*, Melbourne, Australia, 2017, pp. 238–243.
- [190] M. M. Herrnberger, „Robuste nichtlineare Regelung mittels geschwindigkeitsbasierter Linearisierung für eine aktive Radaufhängung,“ Dissertation, Technical University of Munich, Germany, 2012.
- [191] S. Kilicaslan, „Control of active suspension system considering nonlinear actuator dynamics,“ *Nonlinear Dynamics*, vol. 91, no. 2, pp. 1383–1394, 2018.
- [192] E. Pellegrini, „Model-Based Damper Control for Semi-Active Suspension Systems,“ Dissertation, Technical University of Munich, Germany, 2012.
- [193] E. Pellegrini, S. Spirk, K. J. Diepold, R. Dessort and B. Lohmann, „Nonlinear control of a semi-active suspension system considering actuator and state constraints using methods of optimal control,“ in *American Control Conference (ACC)*, Washington D.C., USA, 2013, pp. 2833–2839.
- [194] A. Malekshahi, M. Mirzaei and S. Aghasizade, „Non-Linear Predictive Control of Multi-Input Multi-Output Vehicle Suspension System,“ *Journal of Low Frequency Noise, Vibration and Active Control*, vol. 34, no. 1, pp. 87–105, 2015.
- [195] G. Prokop and R. Sharp, „Performance enhancement of limited-bandwidth active automotive suspensions by road preview,“ *IEE Proceedings - Control Theory and Applications*, vol. 142, no. 2, pp. 140–148, 1995.
- [196] M. Bär, „Vorausschauende Fahrwerkregelung zur Reduktion der auf die Insassen wirkenden Querbeschleunigung,“ Dissertation, RWTH Aachen, Germany, 2014.
- [197] C. Göhrle, „Methoden und Implementierung einer vorausschauenden Fahrwerksregelung für aktive und semi-aktive Federungssysteme,“ Dissertation, University of Stuttgart, Germany, 2014.
- [198] J. Michael, „Optimale Steuerung in der vertikalen Fahrzeugdynamik – Echtzeitfähige proaktive Vorausschau und impulsive Systemdynamik,“ Dissertation, University of the Armed Forces Munich, 2017.
- [199] M. Doumiati, A. Victorino, A. Charara and D. Lechner, „Estimation of road profile for vehicle dynamics motion: Experimental validation,“ in *American Control Conference (ACC)*, San Francisco, California, USA, 2011, pp. 5237–5242.

- [200] S. Barton-Zeipert, „Fahrbahnprofilerfassung für ein aktives Fahrwerk,“ Dissertation, Helmut-Schmidt-University Hamburg, Germany, 2014.
- [201] C. Göhrle, A. Schindler, A. Wagner and O. Sawodny, „Road Profile Estimation and Preview Control For Low-Bandwidth Active Suspension Systems,“ *IEEE/ASME Transactions on Mechatronics*, vol. 20, no. 5, pp. 2299–2310, 2015.
- [202] K. Caliskan, R. Henze and F. Kucukay, „Potential of Road Preview for Suspension Control under Transient Road Inputs,“ *IFAC-PapersOnLine*, vol. 49, no. 3, pp. 117–122, 2016.
- [203] C. Poussot-Vassal, O. Sename, L. Dugard, P. Gáspár, Z. Szabó and J. Bokor, „A new semi-active suspension control strategy through LPV technique,“ *Control Engineering Practice*, vol. 16, no. 12, pp. 1519–1534, 2008.
- [204] M. Fleps-Dezasse, F. Svaricek and J. Brembeck, „Design and Experimental Assessment of an Active Fault-Tolerant LPV Vertical Dynamics Controller,“ *IEEE Transactions on Control Systems Technology*, vol. 27, no. 3, pp. 1267–1274, 2019.
- [205] G. Koch, „Adaptive Control of Mechatronic Vehicle Suspension Systems,“ Dissertation, Technical University of Munich, Germany, 2011.
- [206] W. Sun, H. Pan and H. Gao, „Filter-Based Adaptive Vibration Control for Active Vehicle Suspensions with Electrohydraulic Actuators,“ *IEEE Transactions on Vehicular Technology*, vol. 65, no. 6, pp. 4619–4626, 2016.
- [207] K. Löhe, „Ein modellgestütztes Konzept zur fahrbahnadaptiven Fahrwerksregelung,“ Dissertation, FAU University Press, Friedrich Alexander University Nürnberg-Erlangen, 2018.
- [208] F. J. D’Amato and D. E. Viassolo, „Fuzzy control for active suspensions,“ *Mechatronics*, vol. 2000, no. 10, pp. 897–920, 2000.
- [209] A. Gustafsson and A. Sjögren, „Neural network controller for semi-active suspension systems with road preview,“ Master’s Thesis, Chalmers University of Technology, Gothenburg, Sweden, 2019.
- [210] W. S. Aboud, S. M. Haris and Y. Yaacob, „Advances in the control of mechatronic suspension systems,“ *Journal of Zhejiang University – SCIENCE C (Computers and Electronics)*, vol. 15, no. 10, pp. 848–860, 2014.
- [211] H. E. Tseng and D. Hrovat, „State of the art survey: Active and semi-active suspension control,“ *Vehicle System Dynamics*, vol. 53, no. 7, pp. 1034–1062, 2015.
- [212] G. B. Khandavalli, M. Kalabis, D. Wegener and L. Eckstein, „Potentials of modern active suspension control strategies – from model predictive control to deep learning approaches,“ in *10th International Munich Chassis Symposium*, Germany, 2019, pp. 179–199.
- [213] M. Bömer, „Detektion und Klassifizierung von Straßenschäden und Hindernissen auf Basis von Kamerabildern,“ Masterarbeit, Technical University of Munich, Germany, 2018.
- [214] Mechanical vibration – Road surface profiles – Reporting of measured data, ISO 8608, 1997.
- [215] M. Agostinacchio, D. Ciampa and S. Olita, „The vibrations induced by surface irregularities in road pavements – a Matlab® approach,“ *European Transport Research Review*, vol. 6, no. 3, pp. 267–275, 2014.
- [216] D. Cebon and D. E. Newland, „Artificial Generation of Road Surface Topography by the Inverse F.F.T. Method,“ *Vehicle System Dynamics*, vol. 12, no. 1-3, pp. 160–165, 1983.

- [217] D. Cebon, *Handbook of Vehicle Road Interaction, Chapter 3 – Road Surface Topology*, (Advances in Engineering), 1. Edition, Taylor & Francis, pp. 21–28, 1999.
- [218] K. Löhe, T. Zehelein and G. Roppenecker, „Modellierung und Parametrierung stochastischer Fahrbahnunebenheiten mit Hub-, Wank-, Nick- und Verspannanteil,“ in *15. Internationale VDI-Tagung Reifen-Fahrwerk-Fahrbahn, VDI-Bericht Nr. 2241*, Hannover, Germany, 2015, pp. 259–274.
- [219] C. S. Dharankar, M. K. Hada and S. Chandel, „Numerical generation of road profile through spectral description for simulation of vehicle suspension,“ *Journal of the Brazilian Society of Mechanical Sciences and Engineering*, vol. 39, no. 6, pp. 1957–1967, 2017.
- [220] K. Bogsjö, „Development of analysis tools and stochastic models of road profiles regarding their influence on heavy vehicle fatigue,“ *Vehicle System Dynamics*, vol. 44, no. sup1, pp. 780–790, 2006.
- [221] D. Ammon, P. Frank, H. Gimmler, J. Götz, J. Rauh, K. D. Hilf, G. Scheible and P. Stiess, „Fahrzeugschwingungen - Von der Fahrbahnregung bis zum Komfortempfinden,“ in *VDI Tagung Humanschwingungen, VDI Berichte Nr. 1821*, Darmstadt, Germany, 2004, pp. 139–158.
- [222] K. Bogsjö, „Coherence of road roughness in left and right wheel-path,“ *Vehicle System Dynamics*, vol. 46, no. sup1, pp. 599–609, 2008.
- [223] G. Loprencipe and P. Zoccali, „Use of generated artificial road profiles in road roughness evaluation,“ *Journal of Modern Transportation*, vol. 25, no. 1, pp. 24–33, 2017.
- [224] M. W. Sayers and S. M. Karamihas, *The little book of profiling*, 1. Edition, University of Michigan, 1998.
- [225] A. H. Wertheim, „Working in a moving environment,“ *Ergonomics*, vol. 41, no. 12, pp. 1845–1858, 1998.
- [226] C. Diels and J. E. Bos, „Self-driving carsickness,“ *Applied Ergonomics*, vol. 2016, no. 53, pp. 374–382, 2016.
- [227] A. Naddeo, R. Califano, N. Cappetti and M. Vallone, „The effect of external and environmental factors on perceived comfort: the car-seat experience,“ in *Proceedings of the Human Factors and Ergonomics Society Europe*, Groningen, Netherlands, 2015, pp. 291–308.
- [228] A. Lange, M. Albert and K. Bengler, „Automatisiertes Fahren - So komfortabel wie möglich, so dynamisch wie nötig,“ in *30. VDI-VW-Gemeinschaftstagung Fahrerassistenz und Integrierte Sicherheit, VDI Berichte Nr. 2223*, Wolfsburg, Germany, 2014, pp. 215–228.
- [229] M. Elbanhawi, M. Simic and R. Jazar, „In the Passenger Seat: Investigating Ride Comfort Measures in Autonomous Cars,“ *IEEE Intelligent Transportation Systems Magazine*, vol. 7, no. 3, pp. 4–17, 2015.
- [230] H. Bellem, T. Schönenberg, J. F. Krems and M. Schrauf, „Objective metrics of comfort: Developing a driving style for highly automated vehicles,“ *Transportation Research Part F: Traffic Psychology and Behaviour*, vol. 2016, no. 41, pp. 45–54, 2016.
- [231] H. Bellem, M. Klüver, M. Schrauf, H.-P. Schöner, H. Hecht and J. F. Krems, „Can We Study Autonomous Driving Comfort in Moving-Base Driving Simulators? A Validation Study,“ *Human Factors: The Journal of the Human Factors and Ergonomics Society*, vol. 59, no. 3, pp. 442–456, 2017.

- [232] I. Bae, J. Moon and J. Seo, „Toward a Comfortable Driving Experience for a Self-Driving Shuttle Bus,“ *Electronics*, vol. 8, no. 9, p. 943, 2019.
- [233] M. Beggiato, F. Hartwich and J. Krems, „Physiological correlates of discomfort in automated driving,“ *Transportation Research Part F: Traffic Psychology and Behaviour*, vol. 2019, no. 66, pp. 445–458, 2019.
- [234] M. Festner, „Objektivierte Bewertung des Fahrstils auf Basis der Komfortwahrnehmung bei hochautomatisiertem Fahren in Abhängigkeit fahrfremder Tätigkeiten,“ Dissertation, University Duisburg-Essen, Germany, 2019.
- [235] S. Cramer, B. Miller, K.-H. Siedersberger and K. Bengler, „Perceive the difference: Vehicle pitch motions as feedback for the driver,“ in *IEEE International Conference on Systems, Man, and Cybernetics (SMC)*, Banff, Canada, 2017, pp. 1699–1704.
- [236] S. Cramer, A. Lange, S. Bültjes and J. Klohr, „Design Possibilities for Vehicle Roll Motions as Feedback for the Driver during Automated Driving,“ in *Proceedings of the 9th International Conference on Automotive User Interfaces and Interactive Vehicular Applications (AutomotiveUI '17)*, Oldenburg, Germany, 2017, pp. 152–157.
- [237] S. Cramer, K.-H. Siedersberger and K. Bengler, „Active Vehicle Pitch Motions as Feedback-Channel for the Driver during Partially Automated Driving,“ in *11. Workshop Fahrerassistenzsysteme und automatisiertes Fahren*, Walting, Germany, 2017, pp. 74–83.
- [238] S. Cramer and J. Klohr, „Announcing Automated Lane Changes: Active Vehicle Roll Motions as Feedback for the Driver,“ *International Journal of Human–Computer Interaction*, vol. 35, no. 11, pp. 980–995, 2019.
- [239] N. Karlsson and H. Tjärnbro, „Motion sickness in cars: Physiological and psychological influences on motion sickness,“ Master’s Thesis, Chalmers University of Technology, Gothenburg, Sweden, 2012.
- [240] T. Wada, „Motion sickness in automated vehicles,“ in *Advanced Vehicle Control AVEC'16*, J. Edelmann, M. Plöchel and P. E. Pfeffer, ed. London, United Kingdom: Taylor & Francis, 2016, pp. 169–176.
- [241] S. C. Eimler and S. Geisler, „Zur Akzeptanz Autonomen Fahrens – Eine A-Priori Studie,“ in *Mensch und Computer 2015 - Workshopband*, A. Weisbecker, M. Burmester and A. Schmidt, ed. Stuttgart: Oldenbourg, 2015, pp. 533–540.
- [242] M. Kukova, C. Diels, P. Jordan, M. Franco-Jorge, J. Anderson and H. Kharouf, „Do we really know which vehicle attributes are important for customers?,“ in *10th International Conference on Design and Emotion – Celebration and Contemplation*, Amsterdam, Netherlands, 2016, pp. 428–436.
- [243] L. Berberich, „Subjektive Schwingungskomfortbewertung in einem Simulator,“ Dissertation, Technical University of Munich, Germany, 2016.
- [244] Z. Li, I. V. Kolmanovsky, E. M. Atkins, J. Lu, D. P. Filev and Y. Bai, „Road Disturbance Estimation and Cloud-Aided Comfort-Based Route Planning,“ *IEEE Transactions on Cybernetics*, vol. 47, no. 11, pp. 3879–3891, 2017.
- [245] K. Riedl, T. Einmüller, A. Noll, A. Allgayer, D. Reitze and M. Lienkamp, „Cloud-Based Vehicle Ride-Height Control,“ in *IEEE International Conference on Connected Vehicles and Expo (ICCVE) / IEEE Xplore paper 8964864*, Graz, Austria, 2019, pp. 1–6.

- [246] K. Riedl, A. Noll and M. Lienkamp, „Ride Comfort Optimization using Predictive Adaptation of Ride Height and Damper Control on Single Obstacles,“ in *28th Aachen Colloquium Automobile and Engine Technology*, Aachen, Germany, 2019.
- [247] K. Riedl, S. Schaer, J. Kreibich, M. Lienkamp, S. Cannon and C. Schimmel, „Ride comfort evaluation of predictive ride height and damper control adaptation on single obstacles,“ in *20. Internationales Stuttgarter Symposium*, Germany, 2020, pp. 223–235.
- [248] K. Riedl, S. Huber, M. Bomer, J. Kreibich, F. Nobis and J. Betz, „Importance of Contextual Information for the Detection of Road Damages,“ in *Fifteenth International Conference on Ecological Vehicles and Renewable Energies (EVER) / IEEE Xplore Paper 9242985*, Monte-Carlo, Monaco, 2020, pp. 1–9.
- [249] K. Riedl, S. Kurscheid, A. Noll, J. Betz and M. Lienkamp, „Road Network Coverage Models for Cloud-Based Automotive Applications: A Case Study in the City of Munich,“ in *IEEE Intelligent Vehicles Symposium (IV)*, Paris, France, 2019, pp. 1855–1860.
- [250] C. Riese, O. Stump and F. Gauterin, „Investigation of the energy recuperation potential of the damper system for a compact class passenger car,“ *International Journal of Vehicle Design*, vol. 74, no. 4, p. 281, 2017.
- [251] C. Angrick, G. Prokop and P. Knauer, „Design of Ride Comfort Characteristics on Subsystem Level in the Product Development Process,“ in *Automotive Systems Engineering II*, H. Winner, G. Prokop and M. Maurer, ed. Wiesbaden, Germany: Springer, 2018, pp. 3–29.
- [252] P. Kvasnicka and P. Dick, „Integrated Development of Vehicle Dynamics Demonstrated on the New BMW 3 Series,“ in *Proceedings of the FISITA 2012 World Automotive Congress*, Beijing, China, 2013, pp. 379–389.
- [253] K. Röske, „Eine Methode zur simulationsbasierten Grundausslegung von PKW-Fahrwerken mit Vertiefung der Betrachtungen zum Fahrkomfort,“ Dissertation, Technical University of Munich, Germany, 2012.
- [254] A. Zare, K. Michels, L. Rath-Maia and M. Zimmermann, „On the design of actuators and control systems in early development stages,“ in *8th International Munich Chassis Symposium*, Germany, 2017, pp. 337–352.
- [255] M. Eichstetter, „Design of Vehicle System Dynamics using Solution Spaces,“ Dissertation, Technical University Berlin, Germany, 2018.
- [256] C. Braunholz, J. Wiedemann, J. Neubeck, I. Scharfenbaum, U. Schaaf and A. Wagner, „Active Roll Stabilization Design Considering Battery-Electric Vehicle Requirements,“ in *26th Aachen Colloquium Automobile and Engine Technology*, Germany, 2017, pp. 1459–1482.
- [257] K. Arvidsson and R. M. Runolfsson, „Development of methods for objectively quantifying performance of active suspension systems,“ Master’s Thesis, Chalmers University of Technology, Gothenburg, Sweden, 2019.
- [258] F. Klinger, J. Edelmann and M. Plöchl, „Characterization and potential analysis of passive and (semi-)active suspension systems by means of equivalent suspension parameters,“ in *10th International Munich Chassis Symposium 2019*, Germany, 2020, pp. 389–403.
- [259] A. Stretz, „Komfortrelevante Wechselwirkung von Fahrzeugschwingungsdämpfern und den elastischen Dämpferlagern,“ Dissertation, Technical University of Darmstadt, Germany, 2012.

- [260] P. Dizio, J. Ekchian, J. Kaplan, J. Ventura, W. Graves, M. Giovanardi, Z. Anderson and J. R. Lackner, „An active suspension system for mitigating motion sickness and enabling reading in a car,“ *Aerospace Medicine and Human Performance*, vol. 89, no. 9, pp. 822–829, 2018.
- [261] A. M. Wenzelis, „Optimiertes Wankverhalten durch aktive Fahrwerksysteme und empfindungsorientierte Objektivierung,“ Dissertation, Technical University of Munich, Germany, 2018.
- [262] M. Sigl, „Potentialanalyse zur Vertikaldynamikregelung mit Insassen,“ Masterarbeit, Technische Universität München, Germany, 2018.
- [263] L. R. Miller, „The effect of hardware limitations on an on/off semi-active suspension,“ in *Proceedings of the International Conference on Advanced Suspensions (C442/88)*, London, United Kingdom, 1988, pp. 199–206.
- [264] Y. Qin, F. Zhao, Z. Wang, L. Gu and M. Dong, „Comprehensive Analysis for Influence of Controllable Damper Time Delay on Semi-Active Suspension Control Strategies,“ *Journal of Vibration and Acoustics*, vol. 139, no. 3, pp. 1–12, 2017.
- [265] S. Schickram, „Auswirkungen von Sensorfehlern auf die semiaktive Verstelldämpferregelung und das subjektive Komfortempfinden des Fahrers,“ Diplomarbeit, Technical University of Munich, Germany, 2009.
- [266] „Durchschnittsalter der Bevölkerung (1871-2019),“ Bundesinstitut für Bevölkerungsforschung (BiB), Wiesbaden, Germany, 2021. Available: <https://www.bib.bund.de/DE/Fakten/Fakt/B19-Durchschnittsalter-Bevoelkerung-ab-1871.html>.
- [267] G. Burkhard, T. Berger, E. Enders and D. Schramm, „Objectifying Ride Comfort in Autonomous Driving: An extended Model of the ISO-2631 Standard to Objectify the Ride Comfort of an Inattentive Occupant,“ in *Proceedings of The Second International Conference on Comfort ICC2019*, Delft, Netherlands, 2019, pp. 1–8.
- [268] G. Burkhard, T. Berger, E. Enders and D. Schramm, „An extended model of the ISO-2631 standard to objectify the ride comfort in autonomous driving,“ *Work*, vol. 68, no. s1, pp. 37–45, 2021.
- [269] M.-T. Nguyen, J. Pitz, W. Krantz, J. Neubeck and J. Wiedemann, „Subjective Perception and Evaluation of Driving Dynamics in the Virtual Test Drive,“ in *17. Internationales Stuttgarter Symposium*, Germany, 2017, pp. 565–578.
- [270] G. Burkhard, N. Munzinger, S. Vos and E. Enders, „Method for determining a comfort state of at least one vehicle occupant of a vehicle,“ Germany Patent DE102018203433, March 07, 2018.
- [271] I. Cvok, M. Hrgetić, M. Hoić, J. Deur, D. Hrovat and H. E. Tseng, „Analytical and Experimental Evaluation of Various Active Suspension Alternatives for Superior Ride Comfort and Utilization of Autonomous Vehicles,“ *Journal of Autonomous Vehicles and Systems*, vol. 1, no. 1, pp. 1–21, 2021.
- [272] K. Parsons and M. Griffin, „Whole-body vibration perception thresholds,“ *Journal of Sound and Vibration*, vol. 121, no. 2, pp. 237–258, 1988.
- [273] M. A. Bellmann, „Perception of Whole-Body Vibrations: From basic experiments to effects of seat and steering-wheel vibrations on the passenger’s comfort inside vehicles,“ Dissertation, University of Oldenburg, Germany, 2002.

- [274] M. A. Bellmann, H. Remmers and V. Mellert, „Grundlegende Experimente zur Wahrnehmung von vertikalen Ganzkörpervibrationen,“ in *VDI Tagung Humanschwingung, VDI Bericht 1821*, Darmstadt, Germany, 2004, pp. 1–20.
- [275] V. A. R. Pais, M. Mulder, M. M. Van Paassen, M. Wentink and E. L. Groen, „Modeling human perceptual thresholds in self-motion perception,“ in *AIAA Modeling and Simulation Technologies Conference and Exhibit*, Keystone, Colorado, USA, 2006, pp. 1–15.
- [276] A. Nesti, M. Barnett-Cowan, H. H. Büthoff and P. Pretto, „Roll rate thresholds in driving simulation,“ in *Driving Simulation Conference (DSC'12)*, Paris, France, 2012, pp. 1–6.
- [277] B. Dupuits, M. Pleshkov, F. Lucieer, N. Guinand, A. Pérez Fornos, J. P. Guyot, H. Kingma and R. van de Berg, „A New and Faster Test to Assess Vestibular Perception,“ *Frontiers in Neurology*, vol. 10, no. 707, pp. 1–8, 2019.
- [278] N. J. Mansfield and M. J. Griffin, „Difference thresholds for automobile seat vibration,“ *Applied Ergonomics*, vol. 31, no. 3, pp. 255–261, 2000.
- [279] R. P. Gräbe, C.-J. Kat, P. Jacobus van Staden and P. S. Els, „Difference thresholds for a vehicle on a 4-poster test rig,“ *Applied Ergonomics*, vol. 87, no. 103115, pp. 1–11, 2020.
- [280] E. Eriksson, „Analysis of the frequency discomfort in various modes of transportation,“ Semesterarbeit, Technical University of Munich, Germany, 2019.
- [281] F. Wang, H. Davies, B. Du and P. W. Johnson, „Comparing the Whole Body Vibration Exposures across Three Truck Seats,“ *Proceedings of the Human Factors and Ergonomics Society Annual Meeting*, vol. 60, no. 1, pp. 933–936, 2016.
- [282] H. Bohlen, „Ermittlung des maximal möglichen Fahrkomforts unter Berücksichtigung von Aktorbeschränkungen,“ Masterarbeit, Technical University of Munich, Germany, 2019.
- [283] E. Enders, G. Burkhard and N. Munzinger, „Analysis of the influence of suspension actuator limitations on ride comfort in passenger cars using model predictive control,“ *Actuators*, vol. 9, no. 3, pp. 1–40, 2020.
- [284] F. Reister, „Untersuchung des Schwingungskomforts in Straßenfahrzeugen unter Berücksichtigung von Aktorbeschränkungen mittels modellprädiktiver Regelung,“ Semesterarbeit, Technical University of Munich, Germany, 2020.
- [285] F. Hartmann, „Entwurf einer Modellprädiktiven Regelung für Fahrzeuge mit Semi-Aktiven Dämpfern,“ Semesterarbeit, Technical University of Munich, Germany, 2020.
- [286] A. Kühne, „Erweiterung und Analyse einer modellprädiktiven Regelung für Fahrzeuge mit aktiven Fahrwerksaktoren,“ Masterarbeit, Technical University of Munich, Germany, 2020.
- [287] E. F. Camacho and C. Bordons, *Model Predictive control*, (Advanced Textbooks in Control and Signal Processing), 2. Edition, Springer, 2007.
- [288] J. B. Rawlings, D. Q. Mayne and M. M. Diehl, *Model Predictive Control*, 2. Edition, Nob Hill Publishing, LLC, 2017, isbn: 9780975937730.
- [289] S. J. Qin and T. A. Badgwell, „A survey of industrial model predictive control technology,“ *Control Engineering Practice*, vol. 11, no. 7, pp. 733–764, 2003.
- [290] L. Gurobi Optimization. „Gurobi Optimizer,“ 2022. [Online]. Available: <https://www.gurobi.com/> [visited on Jan. 6, 2022].
- [291] J. Lofberg, „YALMIP : A Toolbox for Modeling and Optimization in MATLAB,“ in *IEEE International Symposium on Computer Aided Control Systems Design*, Taipei, Taiwan, 2004, pp. 284–289.

-
- [292] M. S. K. Lau, S. P. Yue, K. V. Ling and J. M. Maciejowski, „A comparison of interior point and active set methods for FPGA implementation of model predictive control,“ in *European Control Conference (ECC)*, Budapest, Hungary, 2009, pp. 156–161.
- [293] D. Goldfarb and A. Idrani, „A numerically stable dual method for solving strictly convex quadratic programs,“ *Mathematical Programming*, vol. 27, no. 1, pp. 1–33, 1983.
- [294] C. Schmid and L. Biegler, „Quadratic programming methods for reduced hessian SQP,“ *Computers and Chemical Engineering*, vol. 18, no. 9, pp. 817–832, 1994.
- [295] L. Zuo and S. Nayfeh, „Low order continuous-time filters for approximation of the ISO 2631-1 human vibration sensitivity weightings,“ *Journal of Sound and Vibration*, vol. 265, no. 2, pp. 459–465, 2003.
- [296] J. Pannek and K. Worthmann, „Stability and performance guarantees for model predictive control algorithms without terminal constraints,“ *ZAMM-Journal of Applied Mathematics and Mechanics / Zeitschrift für Angewandte Mathematik und Mechanik*, vol. 94, no. 4, pp. 317–330, 2014.
- [297] M. J. Griffin and M. M. Newman, „An experimental study of low-frequency motion in cars,“ *Proceedings of the Institution of Mechanical Engineers, Part D: Journal of Automobile Engineering*, vol. 218, no. 11, pp. 1231–1238, 2004.
- [298] P. Karle, „Entwurf und Analyse einer modalen Vertikaldynamikregelung für semiaktive und aktive Fahrwerke,“ Masterarbeit, Technical University of Munich, Germany, 2019.
- [299] A. Bach, „Entwicklung einer Logik zur frequenzabhängigen Parametrierung eines Vertikaldynamikreglers,“ Semesterarbeit, Technical University of Munich, Germany, 2020.
- [300] G. Bonelli, „Enhancement and Evaluation of a Vertical Vehicle Dynamics Controller,“ Masterarbeit, Technical University of Munich, Germany, 2020.
- [301] E. Enders, P. Karle, D. Killian and E. Pellegrini, „Signal processing device and means of locomotion for regulating driving dynamics of the means of locomotion,“ Germany Patent DE102020110693, April 20, 2020.

Prior Publications: Journals; Scopus / Web of Science listed (peer-reviewed)

- [47] E. Enders, G. Burkhard, F. Fent, M. Lienkamp and D. Schramm, „Objectification methods for ride comfort: Comparison of conventional methods and proposal of a new method for automated driving conditions,“ *Forschung im Ingenieurwesen / Engineering Research*, vol. 83, no. 4, pp. 885–898, 2019.
- [268] G. Burkhard, T. Berger, E. Enders and D. Schramm, „An extended model of the ISO-2631 standard to objectify the ride comfort in autonomous driving,“ *Work*, vol. 68, no. s1, pp. 37–45, 2021.
- [283] E. Enders, G. Burkhard and N. Munzinger, „Analysis of the influence of suspension actuator limitations on ride comfort in passenger cars using model predictive control,“ *Actuators*, vol. 9, no. 3, pp. 1–40, 2020.

Prior Publications: Conferences; Scopus / Web of Science listed (peer-reviewed)

- [45] G. Burkhard, E. Enders, S. Vos, N. Munzinger and D. Schramm, „Acquiring requirements on drive comfort by quantifying the accelerations affecting vehicle occupants,“ in *AmE 2018-Automotive meets Electronics – 9th GMM-Symposium*, Dortmund, Germany, 2018, pp. 1–6.
- [168] E. Enders, P. Karle, G. Bonelli, D. Killian and G. Burkhard, „Modal Vertical Vehicle Dynamics Control for Semi-Active and Active Suspension Systems,“ in *Fifteenth International Conference on Ecological Vehicles and Renewable Energies (EVER) / IEEE Xplore Paper 9242985*, Monte-Carlo, Monaco, 2020, pp. 1–9.

Prior Publications: Conferences; not Scopus / Web of Science listed (not peer-reviewed)

- [46] G. Burkhard, S. Vos, N. Munzinger, E. Enders and D. Schramm, „Requirements on driving dynamics in autonomous driving with regard to motion and comfort,“ in *18. Internationales Stuttgarter Symposium*, Germany, 2018, pp. 683–697.
- [267] G. Burkhard, T. Berger, E. Enders and D. Schramm, „Objectifying Ride Comfort in Autonomous Driving: An extended Model of the ISO-2631 Standard to Objectify the Ride Comfort of an Inattentive Occupant,“ in *Proceedings of The Second International Conference on Comfort ICC2019*, Delft, Netherlands, 2019, pp. 1–8.

Prior Publications: Patent Applications

- [270] G. Burkhard, N. Munzinger, S. Vos and E. Enders, „Method for determining a comfort state of at least one vehicle occupant of a vehicle,“ Germany Patent DE102018203433, March 07, 2018.
- [301] E. Enders, P. Karle, D. Killian and E. Pellegrini, „Signal processing device and means of locomotion for regulating driving dynamics of the means of locomotion,“ Germany Patent DE102020110693, April 20, 2020.

Supervised Student Thesis Works

- [39] F. Fent, „Objektivierung von Vertikaldynamikkomfort in Personenkraftwagen,“ Bachelorarbeit, Technische Universität München, Germany, 2018.
- [102] M. Rambach, „Kennfeldbasierte Modellierung eines semi-aktiven Dämpfers,“ Semesterarbeit, Technical University of Munich, Germany, 2020.
- [130] L. P. Mair, „Analyse und Bewertung heutiger und zukünftiger Aktuatoren aktiver Fahrwerke in Hinblick auf das hochautomatisierte Fahren,“ Semesterarbeit, Technical University of Munich, Germany, 2018.
- [133] A. Zilkens, „Charakterisierung von Aktoren aktiver Fahrwerke durch Prüfstandsversuche,“ Masterarbeit, Technical University of Munich, Germany, 2019.
- [134] R. Tutzauer, „Kennfeld basierte Modellierung von Aktoren aktiver Fahrwerkssysteme,“ Semesterarbeit, Technical University of Munich, Germany, 2019.
- [262] M. Sigl, „Potentialanalyse zur Vertikaldynamikregelung mit Insassen,“ Masterarbeit, Technische Universität München, Germany, 2018.
- [280] E. Eriksson, „Analysis of the frequency discomfort in various modes of transportation,“ Semesterarbeit, Technical University of Munich, Germany, 2019.
- [282] H. Bohlen, „Ermittlung des maximal möglichen Fahrkomforts unter Berücksichtigung von Aktorbeschränkungen,“ Masterarbeit, Technical University of Munich, Germany, 2019.
- [284] F. Reister, „Untersuchung des Schwingungskomforts in Straßenfahrzeugen unter Berücksichtigung von Aktorbeschränkungen mittels modellprädiktiver Regelung,“ Semesterarbeit, Technical University of Munich, Germany, 2020.
- [285] F. Hartmann, „Entwurf einer Modellprädiktiven Regelung für Fahrzeuge mit Semi-Aktiven Dämpfern,“ Semesterarbeit, Technical University of Munich, Germany, 2020.
- [286] A. Kühne, „Erweiterung und Analyse einer modellprädiktiven Regelung für Fahrzeuge mit aktiven Fahrwerksaktoren,“ Masterarbeit, Technical University of Munich, Germany, 2020.
- [298] P. Karle, „Entwurf und Analyse einer modalen Vertikaldynamikregelung für semiaktive und aktive Fahrwerke,“ Masterarbeit, Technical University of Munich, Germany, 2019.
- [299] A. Bach, „Entwicklung einer Logik zur frequenzabhängigen Parametrierung eines Vertikaldynamikreglers,“ Semesterarbeit, Technical University of Munich, Germany, 2020.
- [300] G. Bonelli, „Enhancement and Evaluation of a Vertical Vehicle Dynamics Controller,“ Masterarbeit, Technical University of Munich, Germany, 2020.

Appendix

- A Survey on Ride Comfortxxxix**
 - A.1 Background Informationxxxix**
 - A.2 General Questions..... xl**
 - A.3 Difference between Conventional and Automated Driving..... xl**
- B Driving Simulator Study Ixlix**
 - B.1 Measurement System Data Sheetsxlix**
 - B.2 Execution of Study I..... lvi**
 - B.3 Simulator Validation lvii**
 - B.4 Objective Assessment lx**
 - B.5 Subjective Assessment..... lxi**
- C Driving Simulator Study II..... lxv**
 - C.1 Implementation Study II lxv**
- D Derivation of Actuator Requirementslxvii**
 - D.1 Model Validationlxvii**
 - D.2 Optimization for the Dynamic Wheel Loadlxix**

A Survey on Ride Comfort

A.1 Background Information

Die folgende Umfrage geht ca. 7 Minuten und behandelt das Thema Fahrkomfort im automatisierten Fahren. Wir bitten Sie, die Fragen wahrheitsgemäß und vollständig zu beantworten, so sichern Sie uns die bestmöglichen Forschungsergebnisse.

Mit dem Begriff "autonomes Fahren" ist das Fahren in einem Fahrzeug ohne aktive Teilnahme am Verkehrsgeschehen gemeint. Der Insasse gibt dem Fahrzeug nur noch an, wo es hinfahren muss und wird ohne weiteres Zutun an diesen Ort gefahren. Aktuell wird von automatisiertem Fahren gesprochen, damit werden gewisse Stufen auf dem Weg zum autonomen Fahren beschrieben, bei denen die Verantwortung zur Fahrzeugführung weiterhin beim Fahrer liegt. Dabei sind speziell Level 2 und 3 nach SAE J3016 relevant. Auf Level 2 wird der Fahrer unterstützt, indem ihm gewisse Assistenzsysteme zur Kontrolle des Fahrverhaltens zur Verfügung stehen. Auf Level 3 wird dem Fahrer zeitweise die Kontrolle über das Auto abgenommen, er muss jedoch in gewissen Situationen diese wieder übernehmen. Beim automatisierten Fahren wird also zeitweise die Fahraufgabe vom Fahrzeug übernommen, was zu einem teilautonomen Fahren führt.

Der Begriff "Fahrkomfort" wird in dieser Umfrage stellvertretend für "Schwingungskomfort" verwendet. "Unter Schwingungskomfort wird [...] der wahrgenommene und quantifizierbare Schwingungseindruck bzw. die subjektive Schwingungsbeanspruchung verstanden, welche von den Reifen über das Fahrwerk, mit all seinen Komponenten und der Karosserie, ins Fahrzeug übertragen und dort von Fahrzeuginsassen wahrgenommen wird.

Einfach ausgedrückt geht es also um wahrnehmbare Schwingungen und Vibrationen des Fahrzeugaufbaus, welche durch den Kontakt zur Straße hervorgerufen werden. Nicht dazu gehören Schwingungen, die durch den Motor/Antriebsstrang verursacht werden, oder die akustische Wahrnehmung.

The following survey requires about 7 minutes of your time and deals with the topic of driving comfort in automated driving. We ask you to answer the questions truthfully and completely, thus you ensure us the best possible research results.

The term "autonomous driving" refers to driving in a vehicle without active participation in traffic. The occupant defines the destination and is autonomously driven to this location without further intervention. Currently, the term "automated driving" is often used in the media. Automated driving defines distinct stages on the way to autonomous driving, where the responsibility for driving the vehicle remains with the driver. In context of this survey, levels 2 and 3 according to SAE J3016 are referred to with the term "automated driving". At level 2, the driver is supported by certain assistance systems, which are available to control/assist the driving behavior. At Level 3, the driver is temporarily relieved of the driving task, but must retake control of the car again in

certain situations. Hence, in automated driving, the driving task is temporarily taken over by the vehicle, which leads to semi-autonomous driving.

The term "driving comfort" is used in this survey as a proxy for "vibration comfort". "Vibration comfort is [...] the perceived and quantifiable vibration dose or subjective vibration stress, which is caused by road irregularities, transmitted via the tires, suspension, chassis, and seat to the vehicle perceiving vehicle occupant.

In simple terms, this means the perceptible oscillations and vibrations of the vehicle, which are caused by contact with the road. It excludes vibration caused by the engine/drivetrain and acoustic perception.

A.2 General Questions

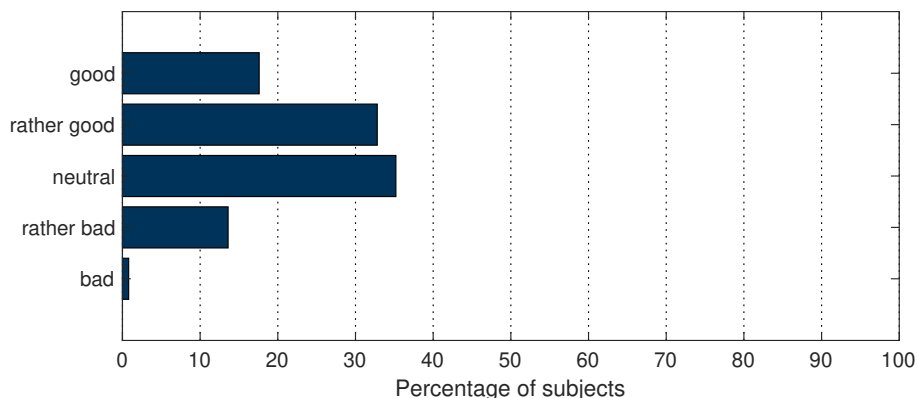


Figure A.1: Comfort rating of the currently used vehicle

A.3 Difference between Conventional and Automated Driving

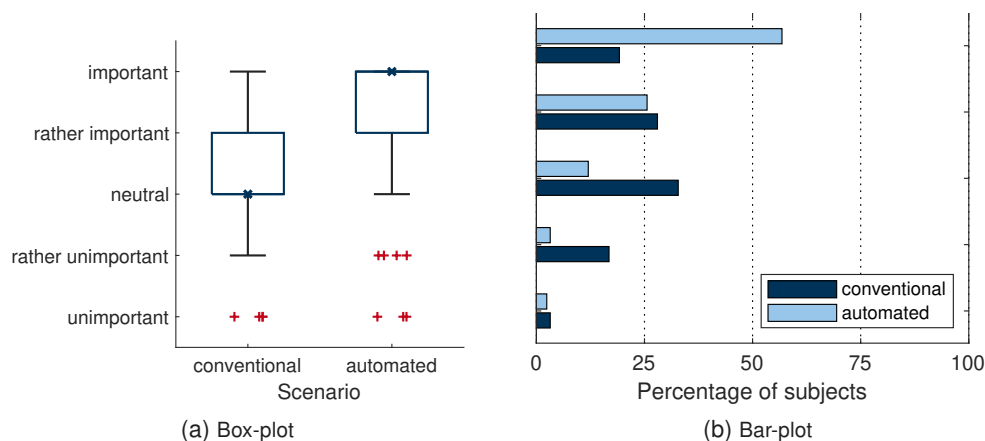


Figure A.2: How do you rate the importance of "ease of use" when buying a conventional or an automated car

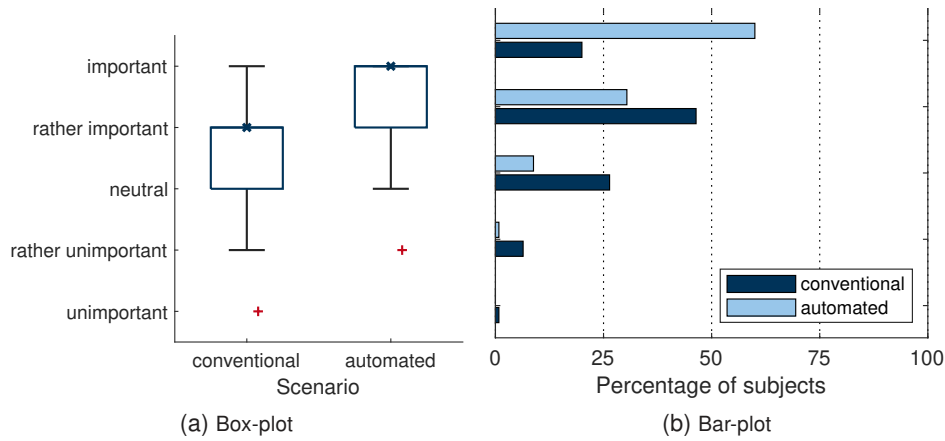


Figure A.3: How do you rate the importance of ride comfort when buying a conventional or an automated car?

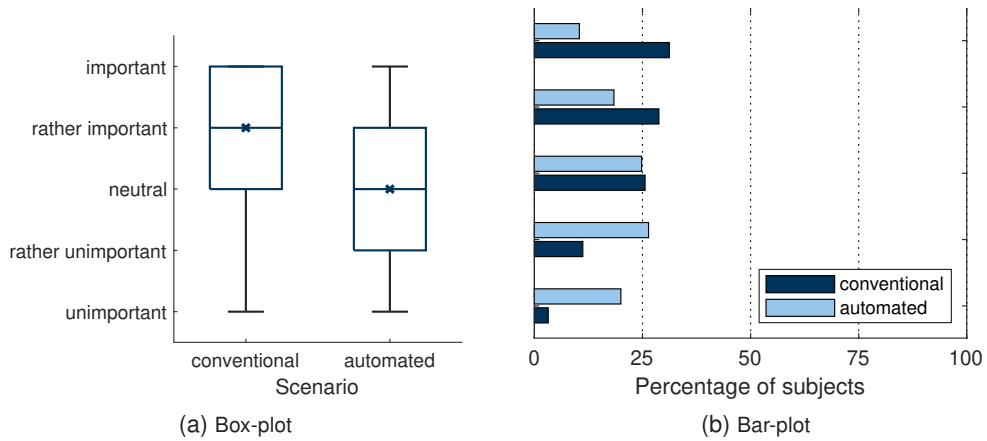


Figure A.4: How do you rate the importance of the "sportiness" when buying a conventional or an automated car

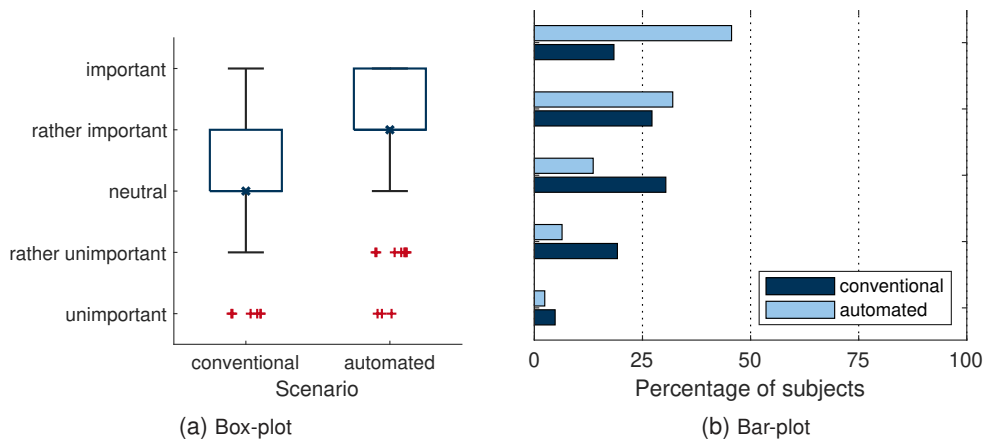


Figure A.5: How do you rate the importance of the infotainment system when buying a conventional or an automated car

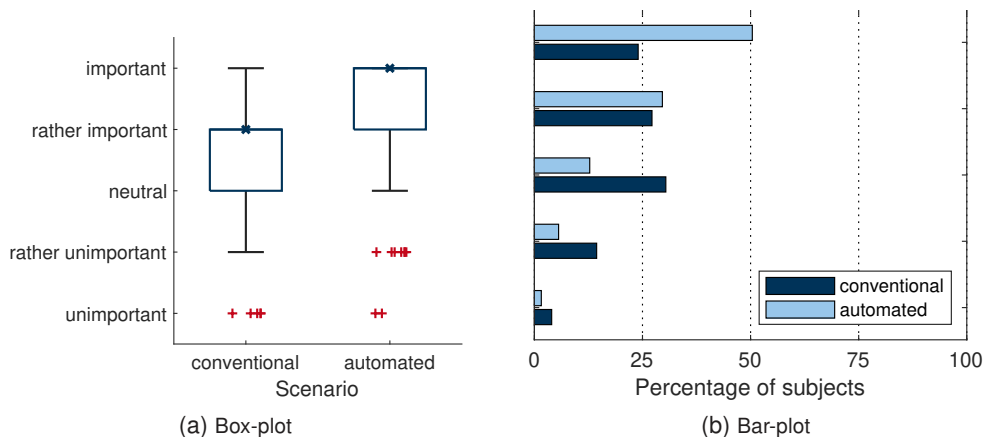


Figure A.6: How do you rate the importance of innovation when buying a conventional or an automated car?

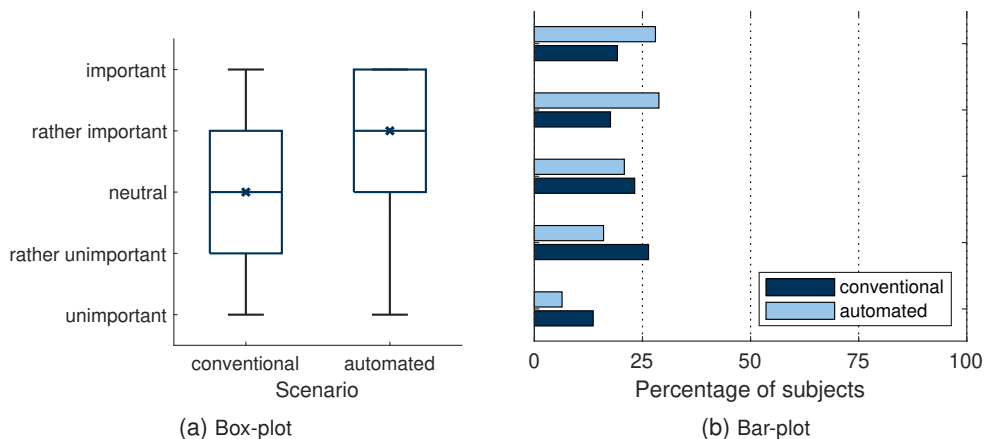


Figure A.7: How do you rate the importance of the family friendliness when buying a conventional or an automated car?

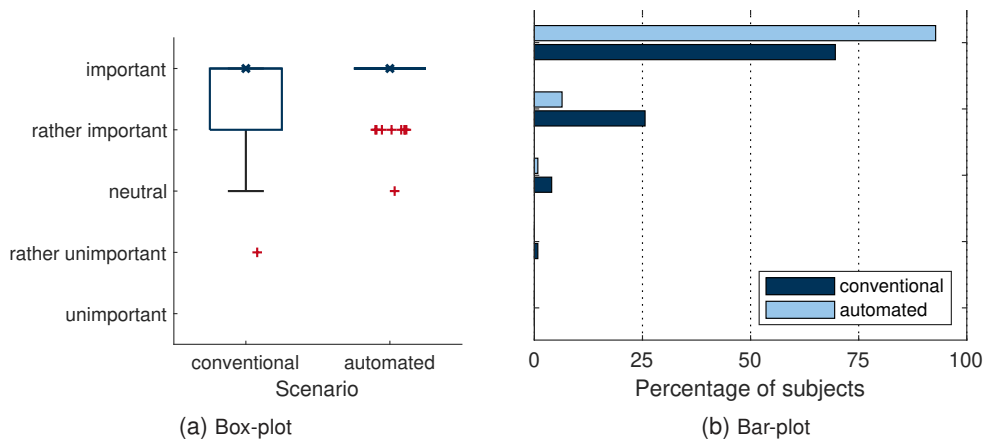


Figure A.8: How do you rate the importance of safety when buying a conventional or an automated car?

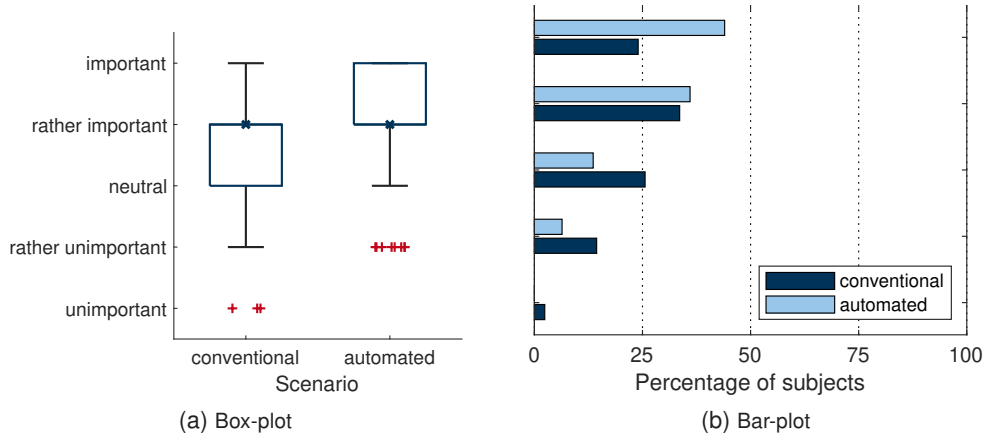


Figure A.9: How do you rate the importance of the car interior when buying a conventional or an automated car?

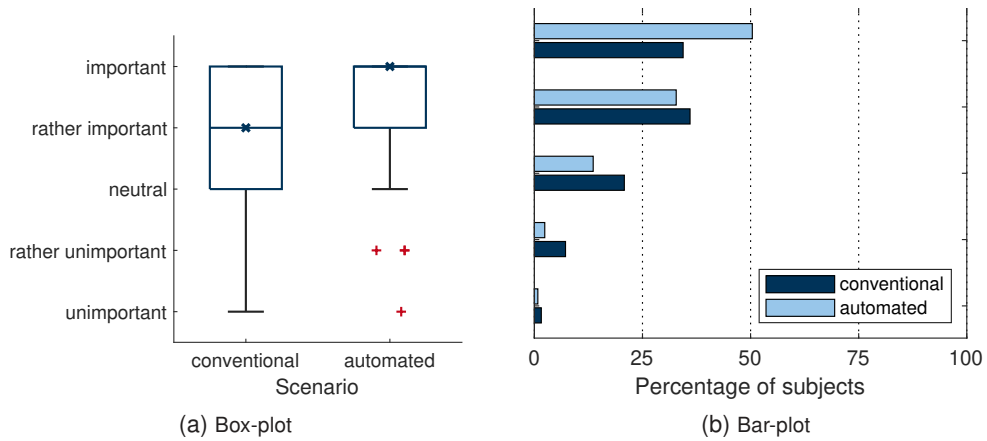


Figure A.10: How do you rate the importance of the seating comfort when buying a conventional or an automated car?

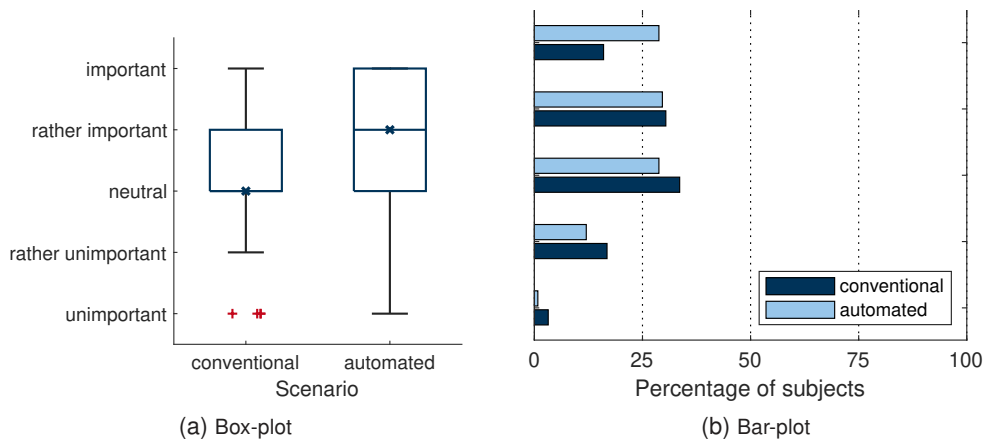


Figure A.11: How do you rate the importance of the quality of materials when buying a conventional or an automated car?

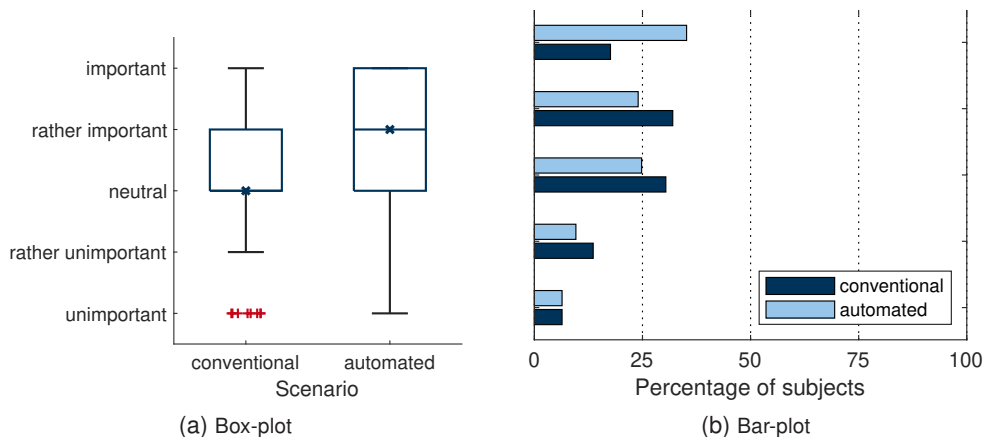


Figure A.12: How do you rate the importance of the environmental friendliness when buying a conventional or an automated car?

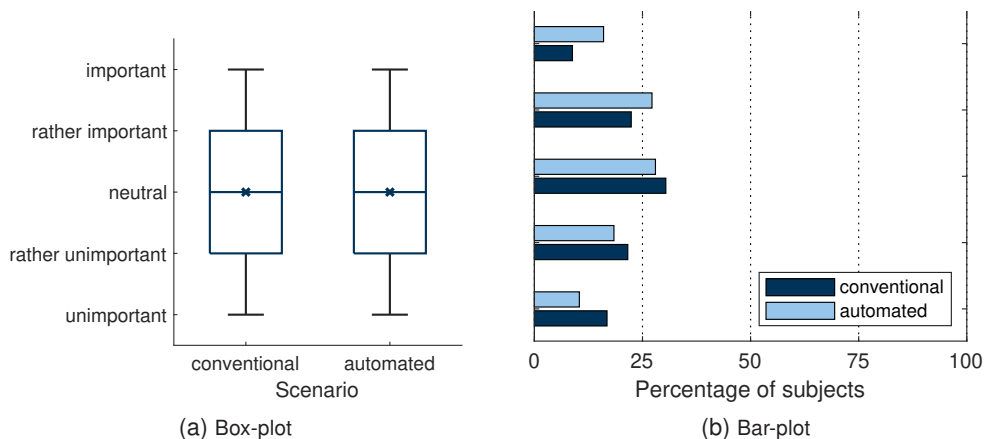


Figure A.13: How do you rate the importance of an easy entry when buying a conventional or an automated car?

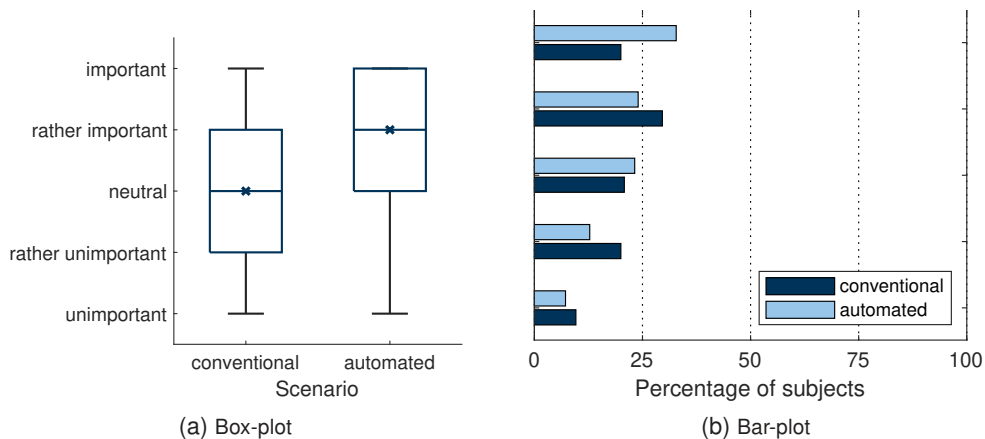


Figure A.14: How do you rate the importance of CO₂ emissions when buying a conventional or an automated car?

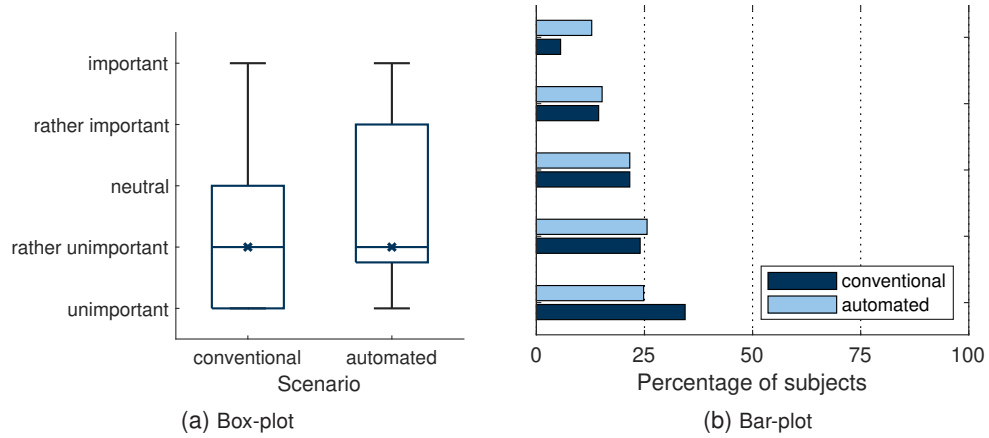


Figure A.15: How do you rate the importance of a high seating position when buying a conventional or an automated car?

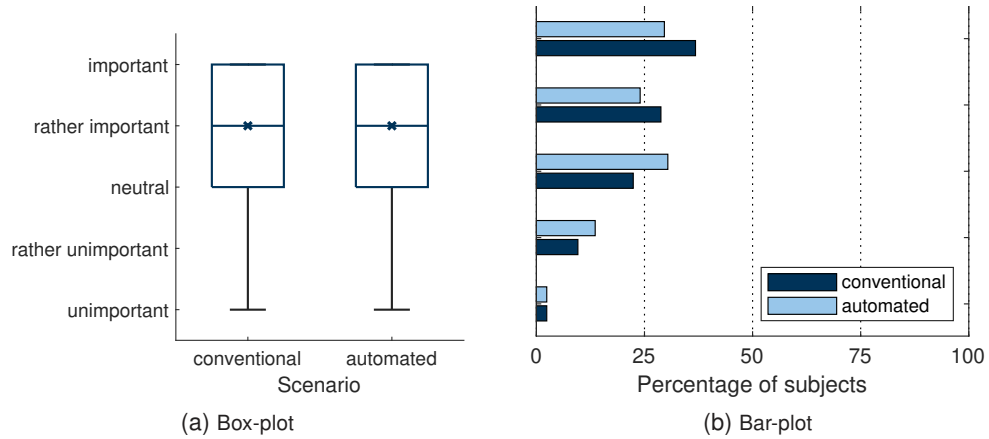


Figure A.16: How do you rate the importance of the styling when buying a conventional or an automated car?

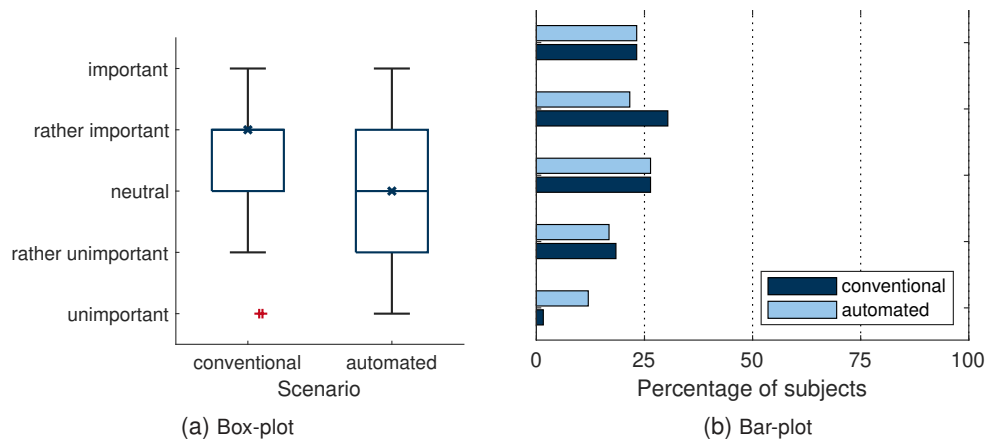


Figure A.17: How do you rate the importance of the headlights when buying a conventional or an automated car?

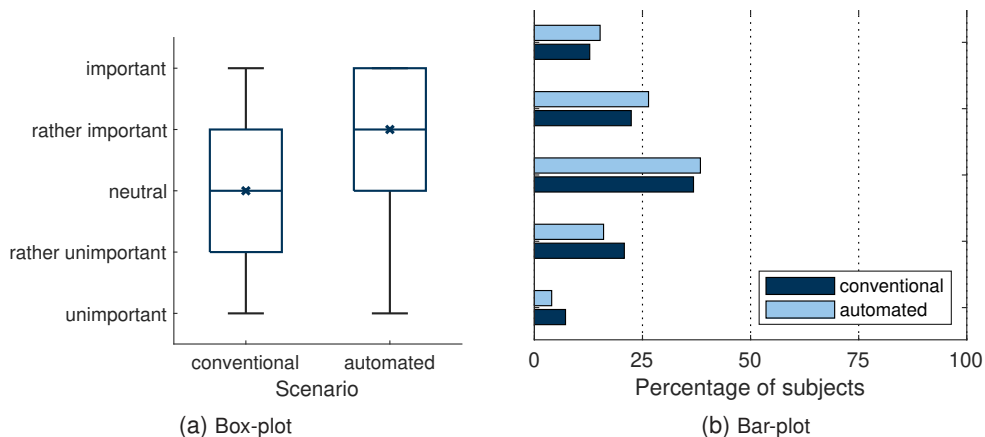


Figure A.18: How do you rate the importance of the vehicle size when buying a conventional or an automated car?

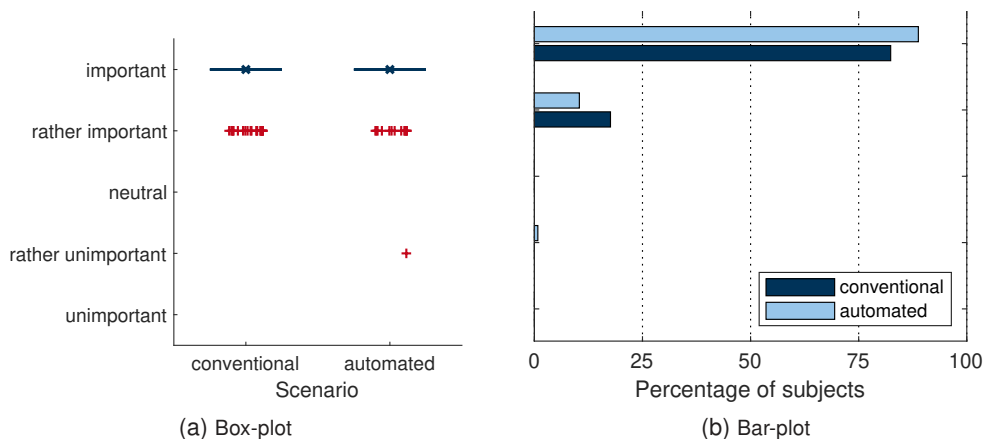


Figure A.19: How do you rate the importance of the reliability when buying a conventional or an automated car?

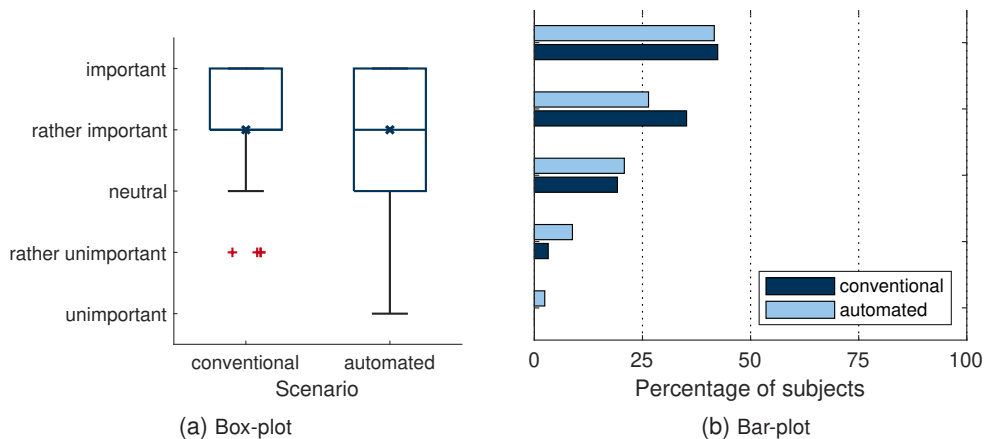


Figure A.20: How do you rate the importance of the price-performance ratio in conventional and automated driving?

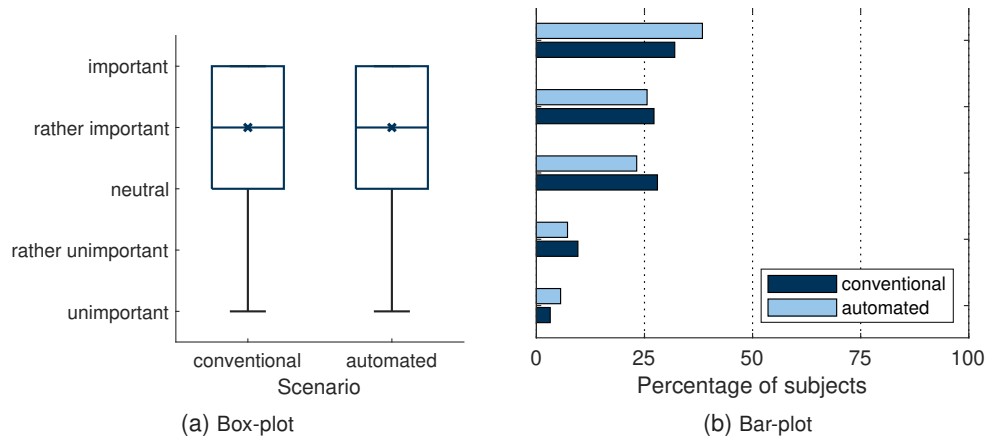


Figure A.21: How do you rate the importance of fuel consumption when buying a conventional or an automated car

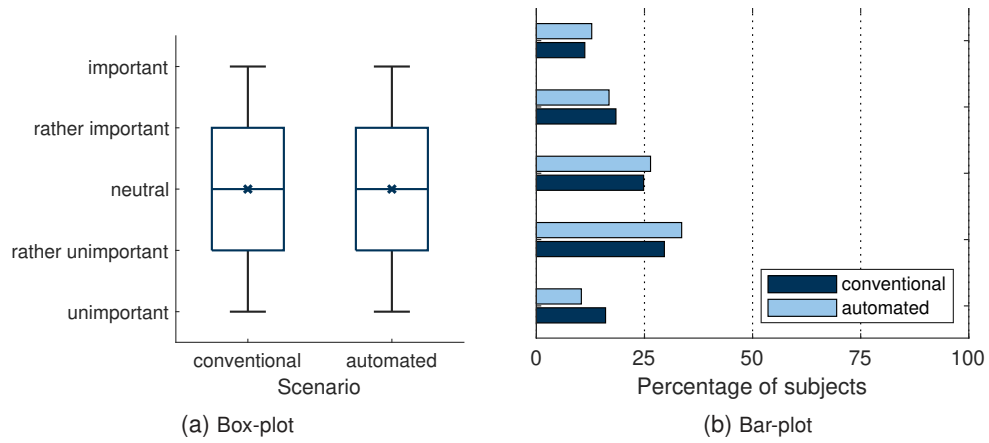



Figure A.22: How do you rate the importance of brand image when buying a conventional or an automated car

B Driving Simulator Study I

B.1 Measurement System Data Sheets

Model Number: 7556A1		PERFORMANCE SPECIFICATION 6DOF VIBRATION SENSOR				DOC NO P5756A1																																																																																																	
		<p>This family also includes:</p> <table border="1"> <tr> <td>Model</td> <td>IEU AccelGyro</td> <td>Accuracy</td> <td>Max Shock (0.1ms)</td> <td>Noise</td> </tr> <tr> <td>7556A2</td> <td>±5% ±100</td> <td>±3000 (±1.5)</td> <td>±200 (0.1)</td> <td>(7) Lines Above 0.5g</td> </tr> </table>						Model	IEU AccelGyro	Accuracy	Max Shock (0.1ms)	Noise	7556A2	±5% ±100	±3000 (±1.5)	±200 (0.1)	(7) Lines Above 0.5g																																																																																						
		Model	IEU AccelGyro	Accuracy	Max Shock (0.1ms)	Noise																																																																																																	
7556A2	±5% ±100	±3000 (±1.5)	±200 (0.1)	(7) Lines Above 0.5g																																																																																																			
<p>Refer to the performance specifications of the products in this family for details not described.</p> <p>Standard Accessories:</p> <ul style="list-style-type: none"> 1) Accelerated calibration certificate (ISO 17025) 2) Mounting screw model 87503 8x32 UNF-2A, Qty 2 3) Mounting washer model 87534, Qty 2 4) Mounting screw model 8887 M4 x 0.7, Qty 2 <p>Notes:</p> <ul style="list-style-type: none"> [1] Measured Jmg Earth Gravity [2] Root Mean Square Line Motion [3] Over file listed as per value in gage. [4] In the interest of constant product improvement, we reserve the right to change specifications without notice. 		<p>Notes:</p> <ul style="list-style-type: none"> [1] Measured Jmg Earth Gravity [2] Root Mean Square Line Motion [3] Over file listed as per value in gage. [4] In the interest of constant product improvement, we reserve the right to change specifications without notice. 		<p>Notes:</p> <ul style="list-style-type: none"> [1] Measured Jmg Earth Gravity [2] Root Mean Square Line Motion [3] Over file listed as per value in gage. [4] In the interest of constant product improvement, we reserve the right to change specifications without notice. 		<p>Notes:</p> <ul style="list-style-type: none"> [1] Measured Jmg Earth Gravity [2] Root Mean Square Line Motion [3] Over file listed as per value in gage. [4] In the interest of constant product improvement, we reserve the right to change specifications without notice. 																																																																																																	
<p>• VARIABLE CAPACITANCE TECHNOLOGY</p> <p>• 6 DEGREES OF FREEDOM MEASUREMENTS</p> <p>• HERMETICALLY SEALED</p> <p>• DC RESPONSE</p> <p>• 0 VOLTS FOR 0 EU NOMINAL OUTPUT</p> <p>• INTERNATIONAL TRAFFIC IN ARMS REGULATION (ITAR) FREE</p>		<p>EVLSH</p> <table border="1"> <tr> <td>0.3"</td> <td>02</td> <td>25</td> <td>g 18/18</td> </tr> <tr> <td>5/16-32 UNF-2A</td> <td></td> <td>5/16-32 UNF-2A</td> <td></td> </tr> <tr> <td>Titanium Alloy</td> <td></td> <td>Titanium Alloy</td> <td></td> </tr> </table>		0.3"	02	25	g 18/18	5/16-32 UNF-2A		5/16-32 UNF-2A		Titanium Alloy		Titanium Alloy		<p>ACCELEROMETER PERFORMANCE</p> <table border="1"> <tr> <td>±3</td> <td>g</td> <td>±0.43</td> <td>m/s²</td> </tr> <tr> <td>0-500</td> <td>Hz</td> <td>0-500</td> <td>Hz</td> </tr> <tr> <td>400</td> <td>m/s²</td> <td><1</td> <td>m/s²</td> </tr> <tr> <td>0.0001</td> <td>g rms/√Hz</td> <td>0.00068</td> <td>m/s²/√Hz</td> </tr> <tr> <td>0.5</td> <td>% F.S.</td> <td>0.5</td> <td>% F.S.</td> </tr> <tr> <td>5</td> <td>%</td> <td>5</td> <td>%</td> </tr> </table>		±3	g	±0.43	m/s ²	0-500	Hz	0-500	Hz	400	m/s ²	<1	m/s ²	0.0001	g rms/√Hz	0.00068	m/s ² /√Hz	0.5	% F.S.	0.5	% F.S.	5	%	5	%	<p>GYRO PERFORMANCE</p> <table border="1"> <tr> <td>±500</td> <td>°/sec</td> <td>±500</td> <td>°/sec</td> </tr> <tr> <td>0-750</td> <td>Hz</td> <td>0-150</td> <td>Hz</td> </tr> <tr> <td>3</td> <td>m/s²/sec</td> <td>3</td> <td>m/s²/sec</td> </tr> <tr> <td>0.004</td> <td>(°/sec)/√Hz</td> <td>0.004</td> <td>(°/sec)/√Hz</td> </tr> <tr> <td>0.5</td> <td>% F.S.</td> <td>0.5</td> <td>% F.S.</td> </tr> <tr> <td>0</td> <td>%</td> <td>0</td> <td>%</td> </tr> </table>		±500	°/sec	±500	°/sec	0-750	Hz	0-150	Hz	3	m/s ² /sec	3	m/s ² /sec	0.004	(°/sec)/√Hz	0.004	(°/sec)/√Hz	0.5	% F.S.	0.5	% F.S.	0	%	0	%	<p>ENVIRONMENTAL</p> <table border="1"> <tr> <td>500</td> <td>gpk</td> <td>4905</td> <td>m/s² peak</td> </tr> <tr> <td>-70 to +185</td> <td>°F</td> <td>-70 to +185</td> <td>°C</td> </tr> <tr> <td>±3</td> <td>%</td> <td>±3</td> <td>%</td> </tr> <tr> <td>Hermetic</td> <td></td> <td>Hermetic</td> <td></td> </tr> </table>		500	gpk	4905	m/s ² peak	-70 to +185	°F	-70 to +185	°C	±3	%	±3	%	Hermetic		Hermetic		<p>ELECTRICAL</p> <table border="1"> <tr> <td>2</td> <td>Ω</td> <td>2</td> <td>Ω</td> </tr> <tr> <td>5 to 30</td> <td>VDC</td> <td>5 to 30</td> <td>VDC</td> </tr> <tr> <td>12</td> <td>mA DC</td> <td>12</td> <td>mA DC</td> </tr> <tr> <td>365</td> <td>dB</td> <td>365</td> <td>dB</td> </tr> </table>		2	Ω	2	Ω	5 to 30	VDC	5 to 30	VDC	12	mA DC	12	mA DC	365	dB	365	dB
0.3"	02	25	g 18/18																																																																																																				
5/16-32 UNF-2A		5/16-32 UNF-2A																																																																																																					
Titanium Alloy		Titanium Alloy																																																																																																					
±3	g	±0.43	m/s ²																																																																																																				
0-500	Hz	0-500	Hz																																																																																																				
400	m/s ²	<1	m/s ²																																																																																																				
0.0001	g rms/√Hz	0.00068	m/s ² /√Hz																																																																																																				
0.5	% F.S.	0.5	% F.S.																																																																																																				
5	%	5	%																																																																																																				
±500	°/sec	±500	°/sec																																																																																																				
0-750	Hz	0-150	Hz																																																																																																				
3	m/s ² /sec	3	m/s ² /sec																																																																																																				
0.004	(°/sec)/√Hz	0.004	(°/sec)/√Hz																																																																																																				
0.5	% F.S.	0.5	% F.S.																																																																																																				
0	%	0	%																																																																																																				
500	gpk	4905	m/s ² peak																																																																																																				
-70 to +185	°F	-70 to +185	°C																																																																																																				
±3	%	±3	%																																																																																																				
Hermetic		Hermetic																																																																																																					
2	Ω	2	Ω																																																																																																				
5 to 30	VDC	5 to 30	VDC																																																																																																				
12	mA DC	12	mA DC																																																																																																				
365	dB	365	dB																																																																																																				
<p>PHYSICAL</p> <p>Weight, Max</p> <p>Connector</p> <p>Material</p>		<p>ENVIRONMENTAL</p> <p>Operating Temperature Range</p> <p>Shock Factor Temperature Shift [1]</p> <p>Seal</p>		<p>ENVIRONMENTAL</p> <p>Maximum Mechanical Shock (2 1 ms)</p> <p>Operating Temperature Range</p> <p>Shock Factor Temperature Shift [1]</p> <p>Seal</p>		<p>ELECTRICAL</p> <p>Output Impedance Nom</p> <p>Operating Voltage</p> <p>Operating Current, Typ</p> <p>Power Supply Rejection Ratio</p>																																																																																																	

21592 Manila Street, Chatsworth, California 91311 Phone: 818.700.7818 Fax: 818.700.7880 www.dytran.com
For permission to reprint this content, please contact: info@dytran.com



Figure B.1: Dytran 7556A sensor

SIM-STG



Fast 8-Channel Multi-Analog Measurement Device with Excitation

- ▶ 8 analog signal inputs for voltage measurements
- ▶ Measurement modes: SENS, STG, ICP, individual for each input
- ▶ Hardware filter and DSP software filter
- ▶ 8 separate dual sensor excitations (up to ± 15 V, up to ± 45 mA)
- ▶ Offset and target adjust functions, shunt check
- ▶ Internal resistors for bridge completion selectable
- ▶ Measurement data output to CAN
- ▶ Complete galvanic isolation (inputs, excitation, CAN, power supply, enclosure)
- ▶ Designed for automotive in-vehicle use

Measurement modes	SENS up to ± 50 V, STG up to ± 2 V, ICP up to ± 5 V
Input voltage (IN+ \leftrightarrow IN-)	max. ± 100 V (nominal voltage), ± 500 V (pulse voltage)
Input resistance dual (differential) single (ground related)	10 M Ω 5 M Ω
Channel sample rates	1/ 2/ 5/ 10/ 20/ 50/ 100/ 200/ 500 Hz 1/ 2/ 5 kHz
Internal sample rate	10 kHz
Voltage supply	12, 24, 42 V _{DC} power supply systems Switch-off for voltage < 6 V
Power consumption, typical	7.0 W (all excitations off)
Working temperature range	-40 °C ... +85 °C (-40 °F ... +185 °F)
Storage temperature range	-55 °C ... +125 °C (-67 °F ... +257 °F)
IP-Code	IP 54 (DIN EN 60529)
Dimensions	W69 mm x H112 mm x D185 mm (W2.72 in x H4.41 in x D7.28 in)
Weight	1400 g (3.09 lb)

Figure B.2: IPETronic (1/3)

SIM-STG

Measurement input general	
Resolution (SAR ADC)	16 Bit
Pre-filter (HF) Cut-off frequency f_c Type Accuracy	4.75 kHz RC 2-pole 25 %
Hardware filter Cut-off frequency f_c Type Accuracy	1200 Hz, can be switched off Butterworth 8-pole 10 %
Software filter (DSP) Cut-off frequency f_c , selectable Type, selectable Accuracy	1.0/ 1.25/ 1.667/ 2.5/ 5.0/ 6.667/ 10/ 12.5/ 16.67/ 25/ 50/ 66.67/ 100/ 125/ 166.7/ 250 Butterworth, Bessel, Elliptic 8-pole 0.1 %
Wire break detection for sensor excitation	Enable/ disable per software
Galvanic isolation input ↔ module power supply excitation ↔ module power supply input ↔ input	nominal voltage pulse voltage ±100 V ±500 V ±100 V ±500 V ±100 V ±500 V
Aggregate sample rate	12 kHz @ 500 kBit/s 16 kHz @ 1 MBit/s 20 kHz @ 1 MBit/s (4 channels each set to 5 kHz)
Input female connectors 7-pin (SIM-DMS compatible) 8-pin (TEDS, Lemo 2B)	EGG 1B 307 EGG 2B 308
SENS Mode	
Measuring ranges unipolar / bipolar Accuracy @ $T_a = 25\text{ °C}$ Drift	Voltages up to ±50 V 0.01 / 0.02 / 0.05 / 0.1 / 0.2 / 0.5 / 1 / 2 / 5 / 10 / 20 / 50 V 0,075 % corresponding to the absolute value of the range selected 30 ppm/K
Sensor excitation Output voltage, selectable Bipolar Unipolar Accuracy @ $T_a = 25\text{ °C}$ Drift Output current	2-wire connection ±0.5/ ±1.25/ ±2.5/ ±5/ ±10/ ±12/ ±15 V 0.5/ 1.25/ 2.5/ 5/ 10/ 12/ 15 V 0.5 % 30 ppm/K 45 mA, short-circuit proof, (software controlled)
Offset adjust (also during measurement)	manual adjust with channel multiple selection

Figure B.3: IPEtronic (2/3)

SIM-STG

STG Mode	Differential voltages up to ± 2 V	
Measuring ranges Range 1 Accuracy @ Ta = 25 °C Drift Range 2 Accuracy @ Ta = 25 °C Drift Range 3 Accuracy @ Ta = 25 °C Drift	$\pm 2 \dots \pm 62$ mV $\pm 0.10 \% + 15 \mu\text{V}$ 30 ppm/K $\pm 64 \dots \pm 998$ mV $\pm 0.075 \% + 7 \mu\text{V}$ 30 ppm/K $\pm 1000 \dots \pm 2000$ mV $\pm 0.05 \% + 7 \mu\text{V}$ 30 ppm/K	adjustable in 2 mV steps corresponding to the absolute value of the range configured adjustable in 2 mV steps corresponding to the absolute value of the range configured adjustable in 2 mV steps corresponding to the absolute value of the range configured
Special functions Bridge adjust Shunt check Shunt resistor simulation Resistors for bridge completion	zero adjust resp. target value adjust by hardware on all 4 arms of the bridge, on command also during the measurement executable 5 ... 390 k Ω , (depending on excitation voltage) 120, 350, 1000 Ω software selectable	
Sensor excitation Output voltage, selectable Accuracy @ Ta = 25 °C Drift Output current	4-wire-/ 6-wire connection $\pm 0.5/ \pm 1.25/ \pm 2.5/ \pm 5$ V 0.1 % 30 ppm/K 45 mA, short-circuit proof, (software controlled)	
ICP Mode	Piezo electric sensors	
Nominal current, regulated Measuring range Lower / upper cut-off frequency Off-load voltage	4,5 mA ± 10 % $\pm 0.1/ \pm 0.2/ \pm 0.5/ \pm 1.0/ \pm 2.0/ \pm 5.0$ V filter switched off / 0.1 Hz / 4750 Hz ± 20 % 24 V	
Interfaces	CAN	
CAN 2.0B (High Speed) Data transfer rate, selectable	max. 1 MBit/s according to ISO11898-2	
Data format resolution / format	8 Bit (Byte) resp. 16 Bit (Word)	
Configuration interface	CAN	

Figure B.4: IPETronic (3/3)

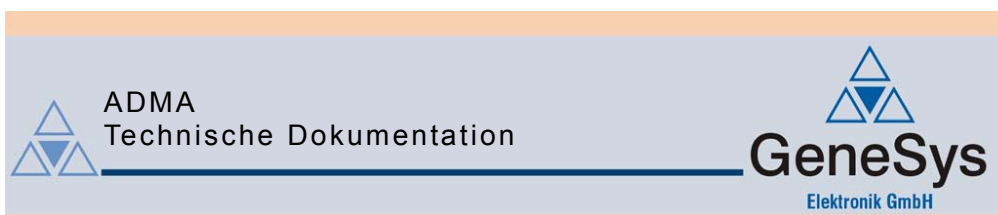
2.10 Technical Data

FlexRay communication-controller	Analysis Bosch E-Ray (FPGA) Startup Bosch E-Ray (FPGA)
FlexRay channel	Max. 1 channel A and B at channel 1 (configurable via Piggyback) 2 MB memory for data transmission
CAN/CAN FD channels	Max. 4 (configurable via Piggybacks) CAN: up to 2 Mbit/s CAN FD: up to 8 Mbit/s
LIN channels	Max. 4 (configurable via Piggybacks), up to 330 kbit/s
K-Line channels	Max. 1 at channel 4 (with LINpiggy 7269mag)
Ethernet Channels/transceiver	1 x BCM54811S
Physical layer	IEEE 802.3 (100BASE-TX/1000BASE-T) and BroadR-Reach (100 MBit; physical layer not fully compliant to Automotive Ethernet / 100BASE-T1)
Channel configurations	Configurable with Piggybacks 1x FlexRay, 3 x CAN 1x FlexRay, 2x CAN, 1x LIN (1x K-Line) 4x CAN 3x CAN, 1x LIN (1x K-Line) 2x CAN, 2x LIN (1x K-Line) 1x CAN, 3x LIN (1x K-Line) 4x LIN (1x K-Line) Additional: Digital/analog IO channel Ethernet port
Analog input	10 bit Input 0 V...18 V ($R_i = 1.1 \text{ M}\Omega$) Voltage tolerance up to 30 V Details on the extended measuring range see on page 17.
Digital input	Range 0 V...32 V Schmitt trigger high 2.8 V, low 2.3 V Input frequencies up to 1 kHz
Digital output	Open Drain External supply up to 32 V Output frequency up to 1 kHz Current max. 500 mA Short circuit / over voltage protected

Figure B.5: Vector VN7640 (1/2)

Digital input/output	Push/Pull mode (e.g. DoIP Activation Line) or Push-Mode only (e.g. Wake-up Triggers) Output high (no load): 13 V Output high (load 346 Ω): 5.5 V Output low: 0 V Input range: 0 V...16 V Input Schmitt trigger high: 3.4 V Input Schmitt trigger low: 2.5 V Rout: approx. 500 Ω
Time stamps	Resolution: 8 ns Accuracy (in device): 1 μs Accuracy software sync: typ. 50 μs Accuracy hardware sync: typ. 1 μs
PC interface	USB 2.0 or Ethernet (100BASE-TX, 1000BASE-T)
External power supply	Power-up: min. 6 V Continuous operation: 5 V ... 36 V
Power consumption	Typical 6...7 W
Temperature range (ambient temp. of the device)	Operation: -40 °C ... +65 °C Storage: -40 °C ... +85 °C
Relative humidity of ambient air	15 %...95 %, non-condensing
Dimensions (LxWxH)	Approx. 124 mm x 111 mm x 45 mm
Weight	Approx. 500 g
Operating system requirements	Windows 7 SP1 (32 bit / 64 bit) Windows 8.1 (32 bit / 64 bit) Windows 10 (64 bit)

Figure B.6: Vector VN7640 (2/2)



6 Technische Daten des Systems

6.1 Version ADMA-G

	ADMA-G
Messbereich	
Lage	$\pm 60^\circ$
Kurs	0° - 360°
Max. Drehrate (Roll / Nick / Kurs)	$\pm 320^\circ/\text{s}$
Beschleunigung	$\pm 5.0 \text{ g}$
Position (relativ)	$\pm 50 \text{ km}$
Position (absolut, (D)GPS)	Weltweit (Längen- und Breitengrad in Dezimalgrad)
Auflösung Systemintern	(Auflösung Datenausgabe siehe Kap. 3.6)
Winkel	0.005°
Drehrate (Roll / Nick) @ $360^\circ/\text{s}$	$0.00004^\circ/\text{s}$
Drehrate (Roll / Nick) @ $98^\circ/\text{s}$	$0.000012^\circ/\text{s}$
Drehrate (Kurs)	$0.00004^\circ/\text{s}$
Beschleunigung	0.0001 g
Position (relativ, (D)GPS)	0.01 m
Genauigkeit	
Roll / Nick Statisch (typisch)	0.05°
Roll / Nick Dynamisch (typisch)	0.1°
Position (Single L1 ... DGPS-RTK2)	$1.8 \dots 0.02 \text{ m} (1\sigma)$
Schnittstellen	
	CAN 2.0b mit bis zu 1 Mbaud
	Ethernet 10Mbit/100Mbit/1Gbit
	RS232 mit 115 kbaud
	8 Bit Daten, 1 Stopbit, No Parity
	USB
Versorgungsspannung	12 VDC nominal (Spannungsbereich 9-32 VDC)
Leistungsaufnahme	max. 25 W
Datenausgabe	
Update rate	50, 100, 200, 250, 400 Hz
Latenz	<1 ms
Abmessungen (B x T x H)	172 x 113 x 197 mm
Gewicht	3.3 kg
Umgebungsbedingungen	
Lagertemperatur	$-30 \dots +70^\circ\text{C}$
Betriebstemperatur	$-20 \dots +60^\circ\text{C}$

GeneSys Elektronik GmbH · In der Spöck 10 · D-77656 Offenburg · Tel. 0781 / 969279-0 · Fax 0781 / 969279-11 · mail@gensys-offenburg.de · www.gensys-offenburg.de

Figure B.7: ADMA

B.2 Execution of Study I

0	1	2	3	4	5	6
Keine Störung						sehr starke Störung
o	o	o	o	o	o	o

Figure B.8: Six-point Likert-Scale to rate the perceived discomfort

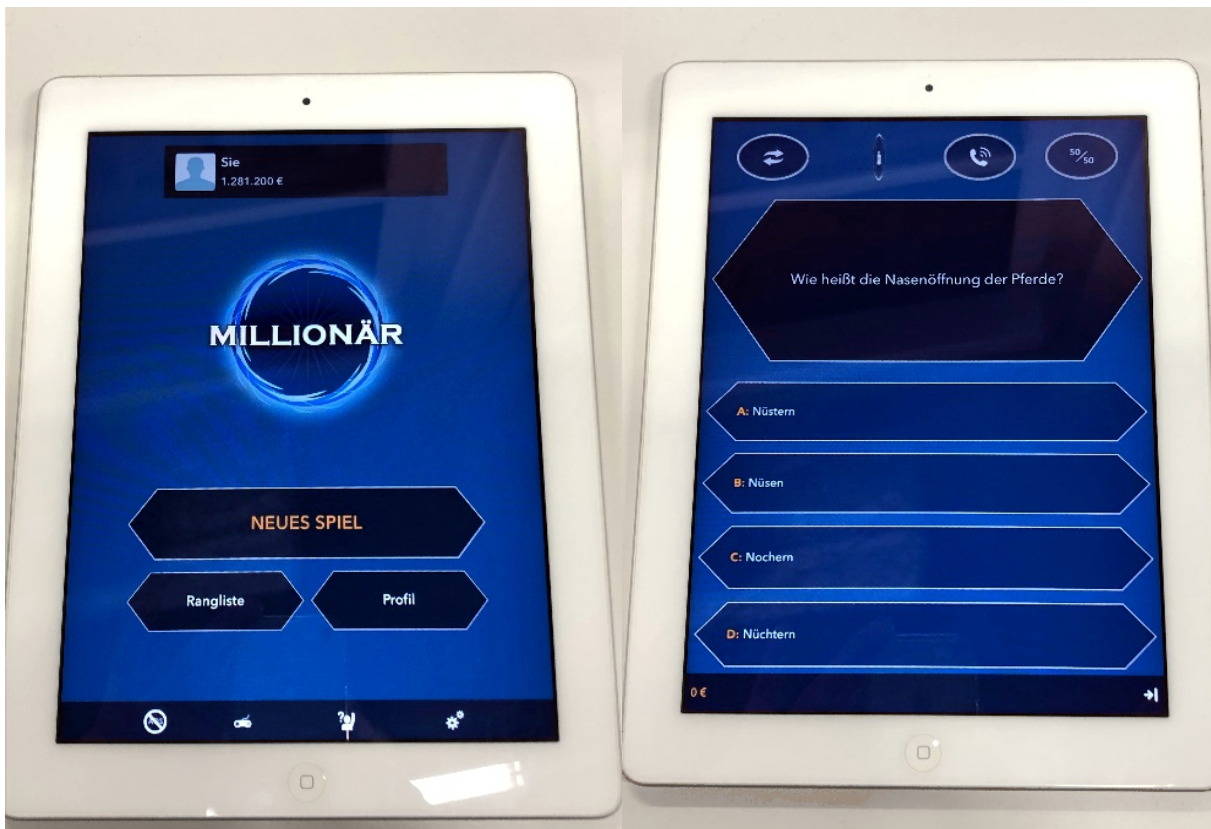


Figure B.9: Tablet with the quiz app used as side task during the study

kein Problem	etwas unwohl (keine eindeutigen Symptome)	Unwohlsein aber keine Übelkeit: gähnen, Müdigkeit, kalt/heiß, schwitzen, Schwindel, verschwommene Sicht, Kopfschmerzen, Speichelfluss, Reizung im Magen/Hals, aufstoßen,				Übelkeit			Würgen	Übergeben
0	1	2	3	4	5	6	7	8	9	10
		sehr gering	gering	mittel	stark	gering	mittel	stark		

Figure B.10: Original BKV Motion Sickness Scale which was used in the Study

B.3 Simulator Validation

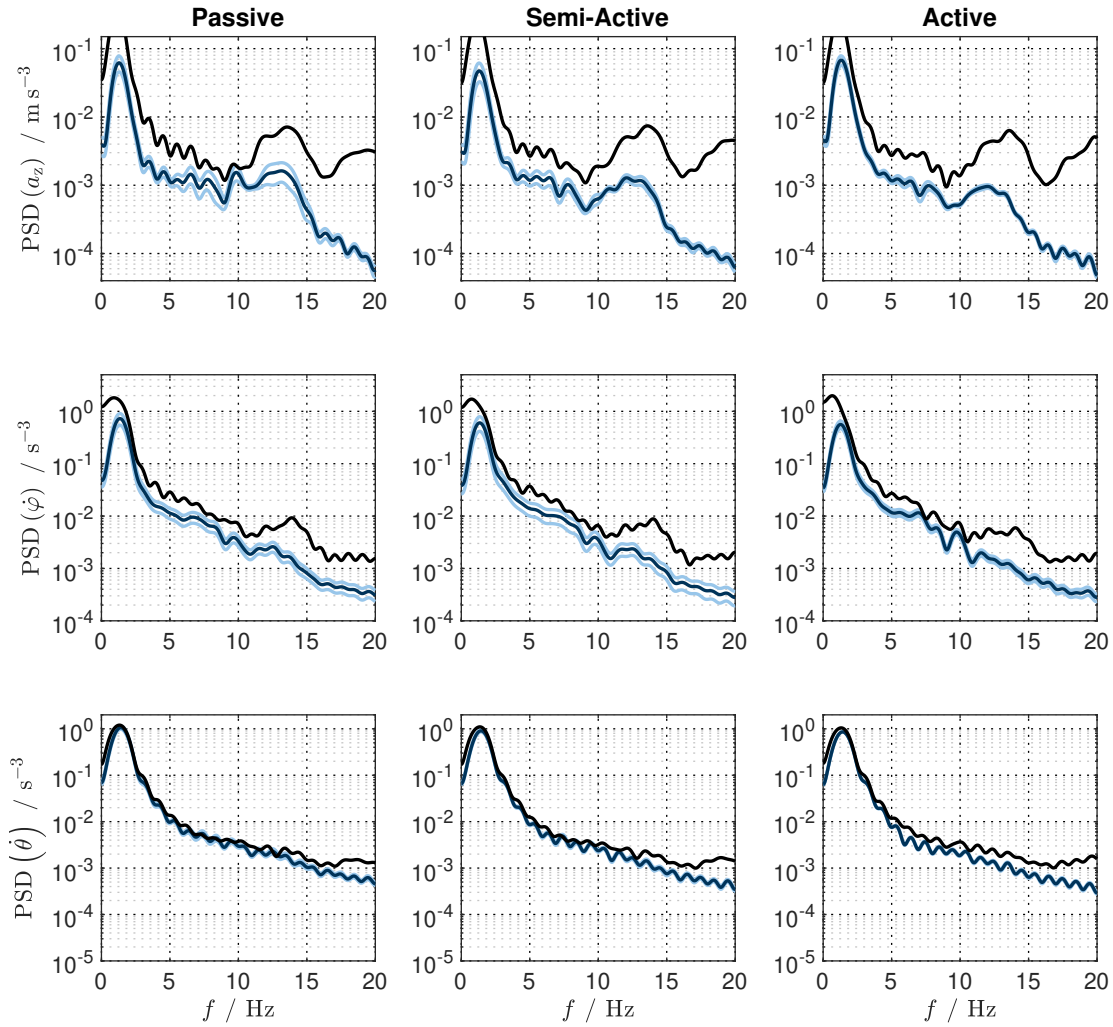


Figure B.11: PSD mean (dark blue) and standard-deviation (light blue) compared to the input signal (black) in heave pitch and roll for the three suspensions, recorded in the simulator mock-up for Track I

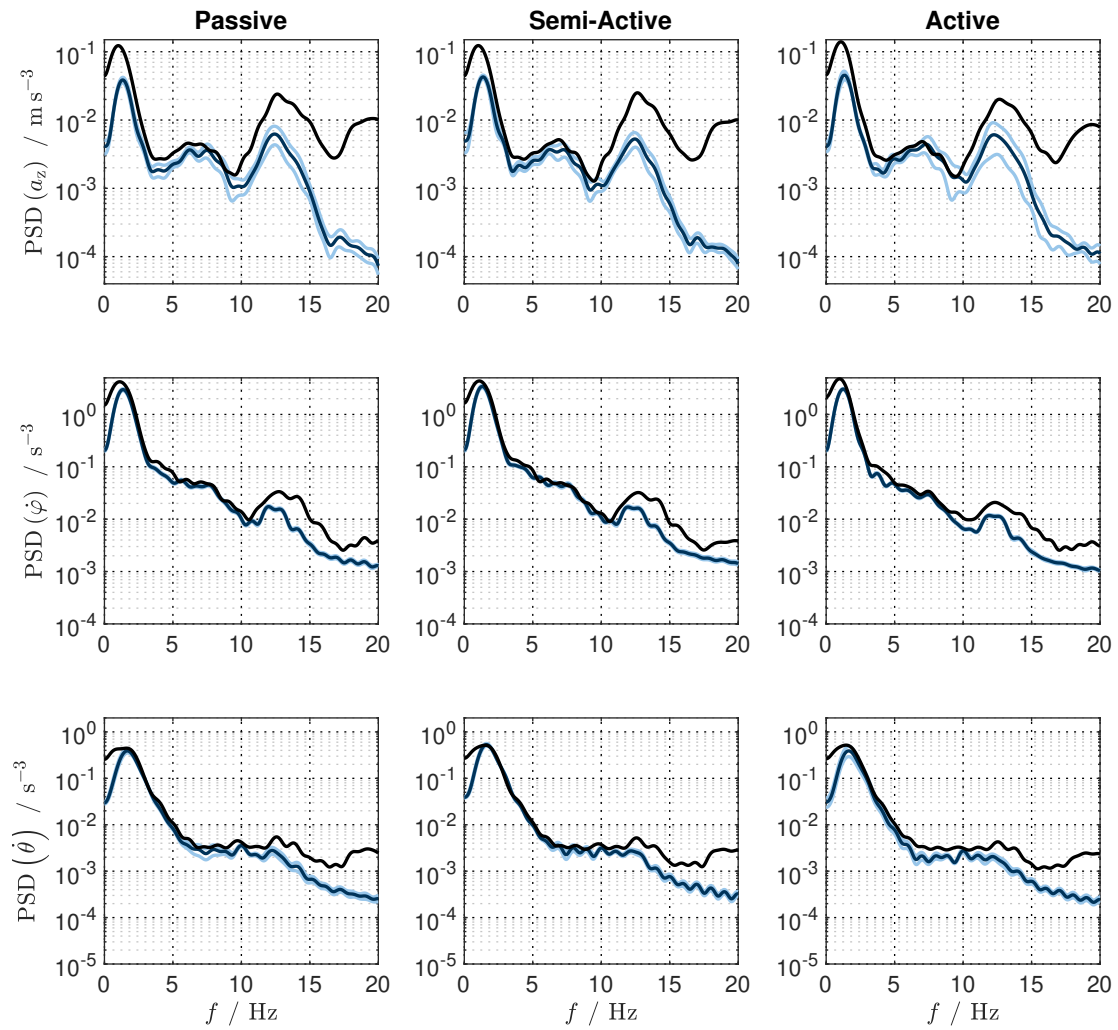


Figure B.12: PSD mean (dark blue) and standard-deviation (light blue) compared to the input signal (black) in heave pitch and roll for the three suspensions, recorded in the simulator mock-up for Track II

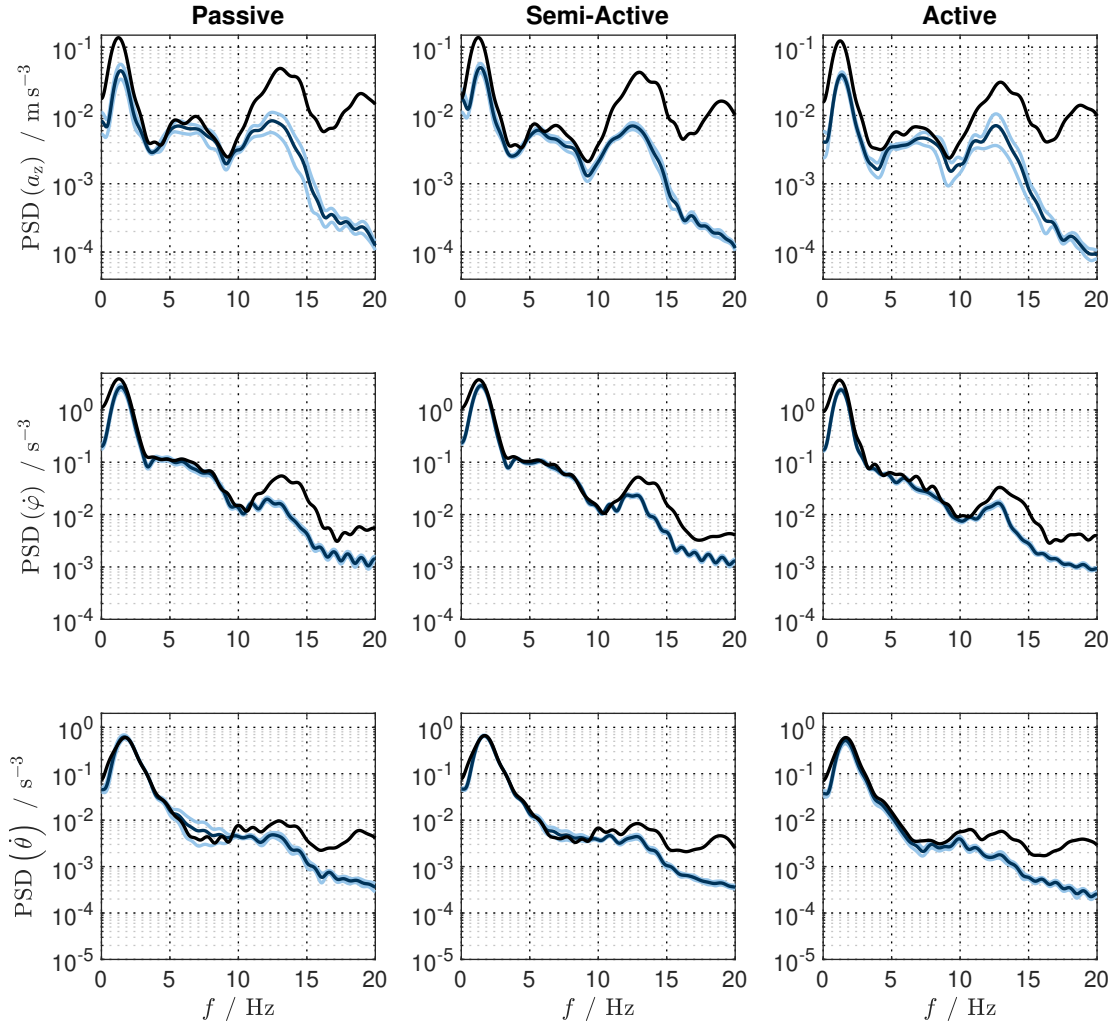


Figure B.13: PSD mean (dark blue) and standard-deviation (light blue) compared to the input signal (black) in heave pitch and roll for the three suspensions, recorded in the simulator mock-up for Track III

B.4 Objective Assessment

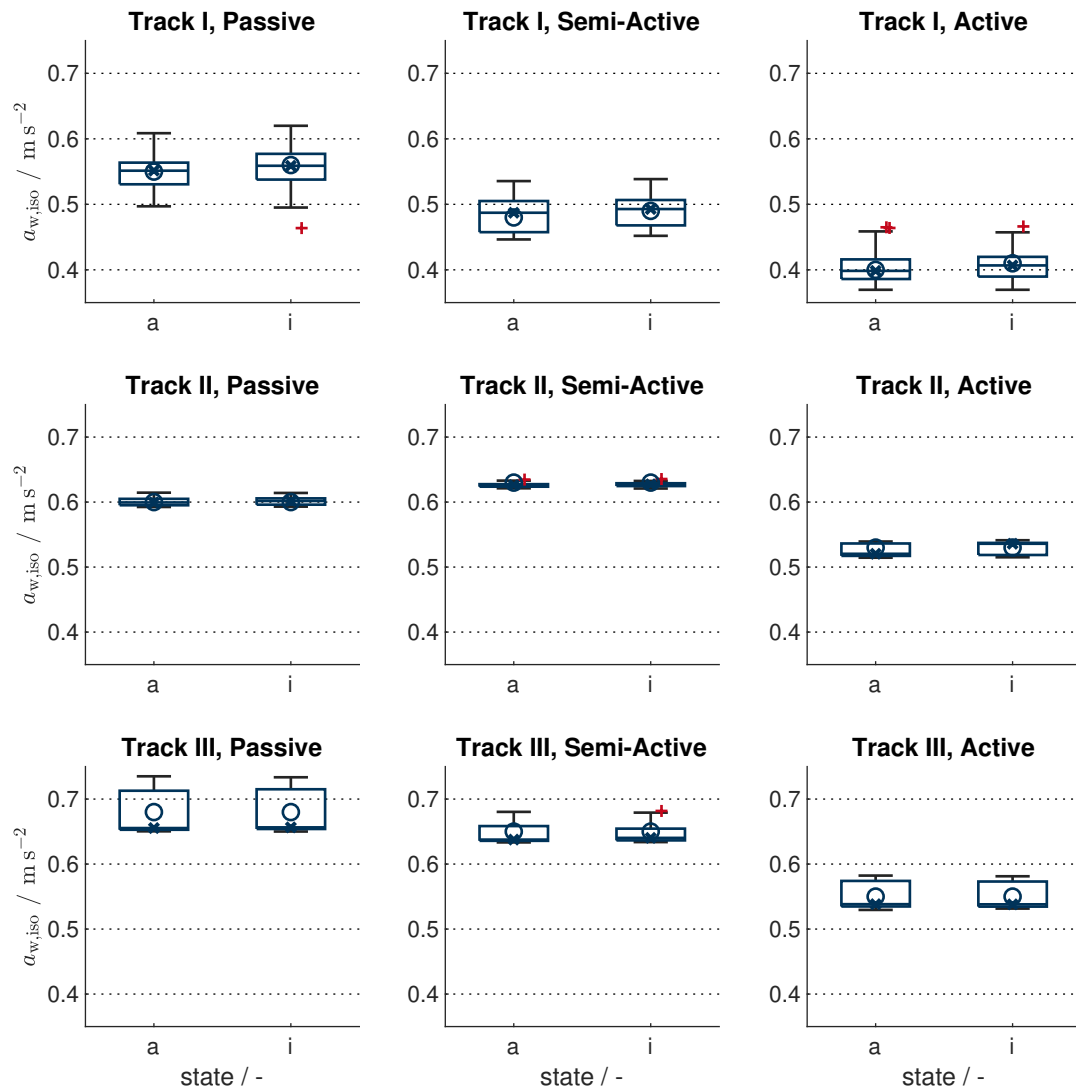


Figure B.14: Detailed display of ISO values for the different settings, calculated from mock-up measurement

B.5 Subjective Assessment

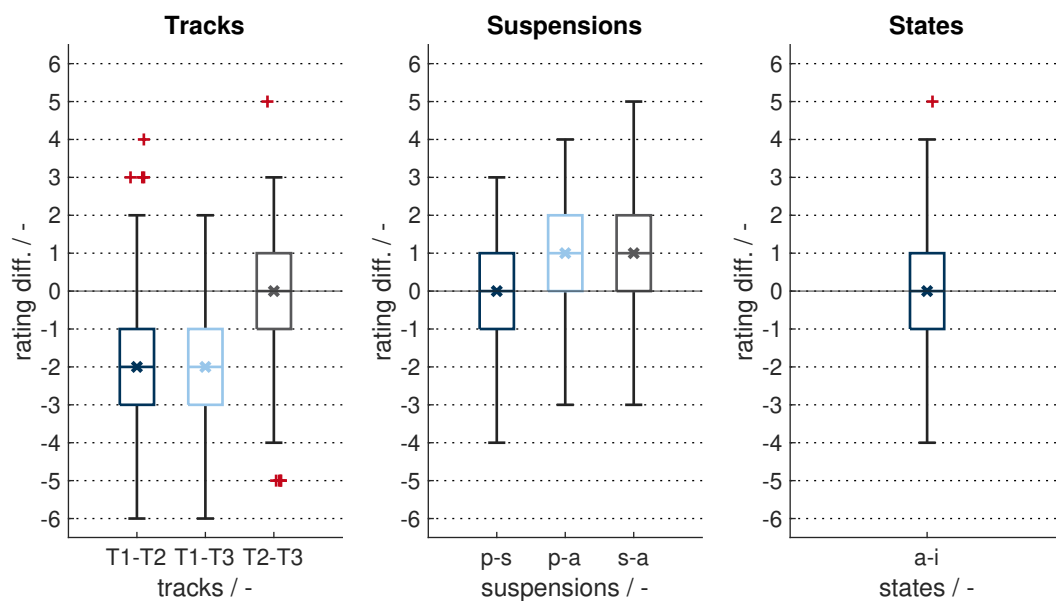


Figure B.15: Comparison of the differences, summarized for the 3 hypothesis

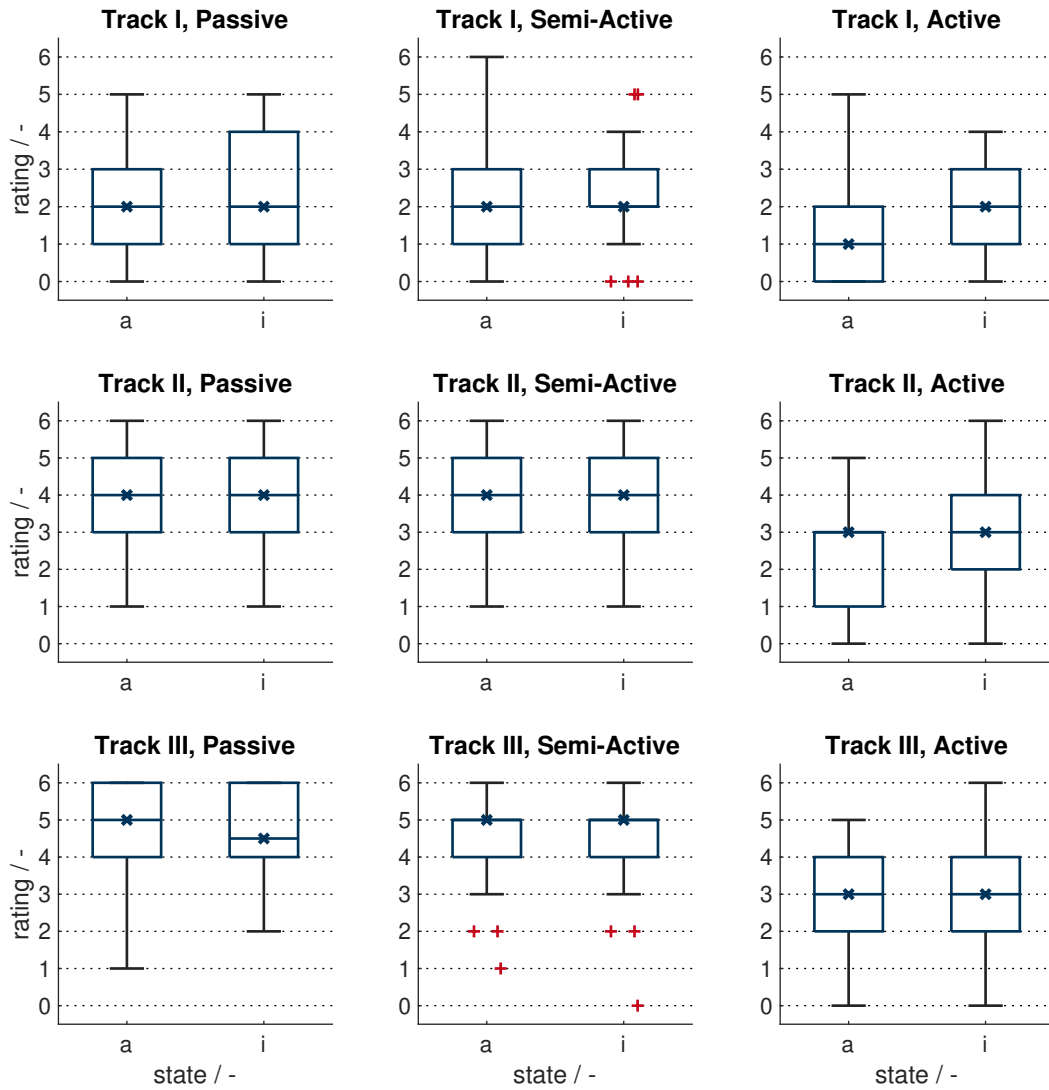


Figure B.16: Detailed display of the ratings for different tracks, suspensions and states

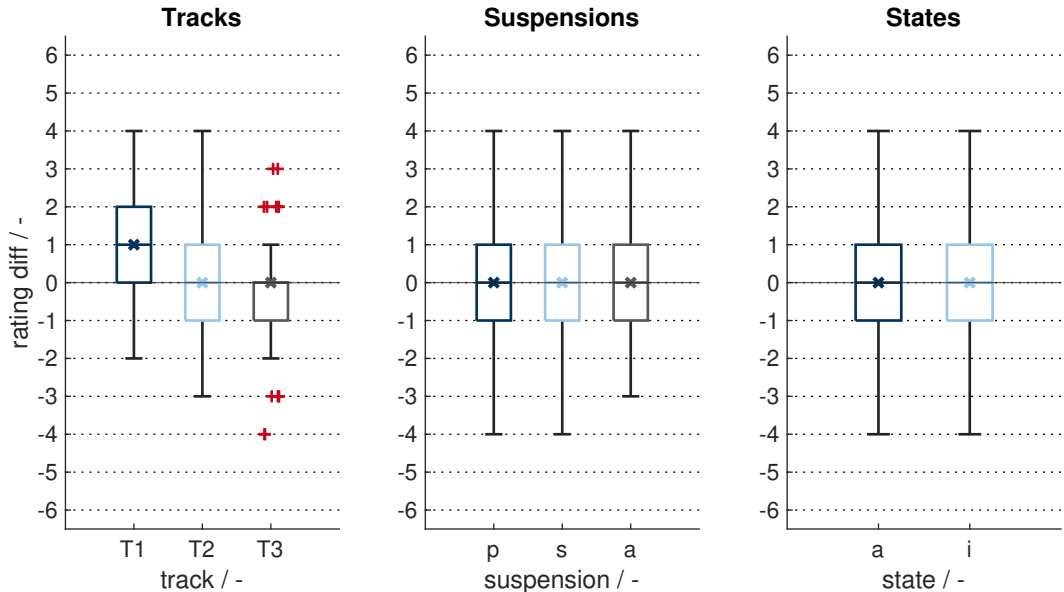


Figure B.17: Influence of the repetition, summarized for the three hypothesis

Table B.1: Results of the Wilcoxon signed-rank sum test and effect strength between the comfort-rating at the beginning, and the repetition at the end, for the different tracks, states and suspensions

critereon	median att.	median ina.	p-value	rej. of H0	Cohen's d
T1	2	1	3.7562×10^{-6}	true	0.6
T2	4	4	0.2846	false	(-0.1)
T3	4	4	0.0436	true	-0.2
Att.	3	3	0.1338	false	(0.2)
Ina.	3	3.5	0.9353	false	(0.0)
Pas.	4	4	0.0970	false	(0.2)
Sem.	4	4	0.3632	false	(-0.1)
Act.	2	2	0.2870	false	(0.1)

C Driving Simulator Study II

C.1 Implementation Study II

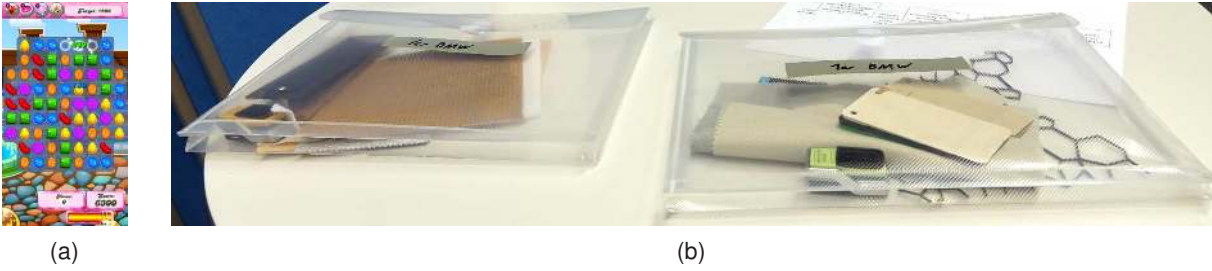


Figure C.1: Screenshot of the side task (a) and the test samples for the two cars (b)

D Derivation of Actuator Requirements

D.1 Model Validation

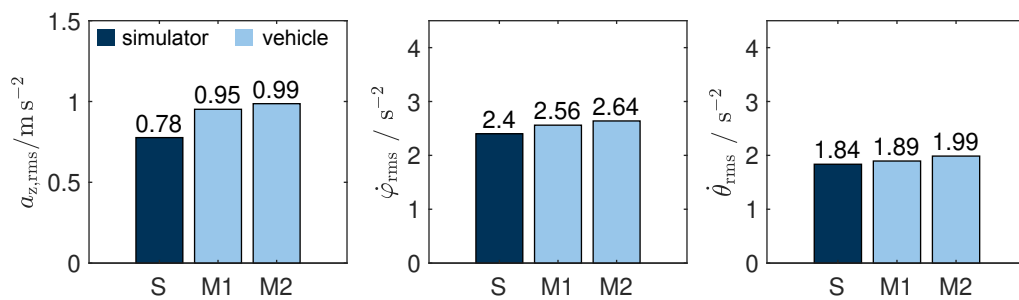


Figure D.1: RMS values of the z-acceleration, roll-rate and pitch-rate from the simulation and two measurements for track I

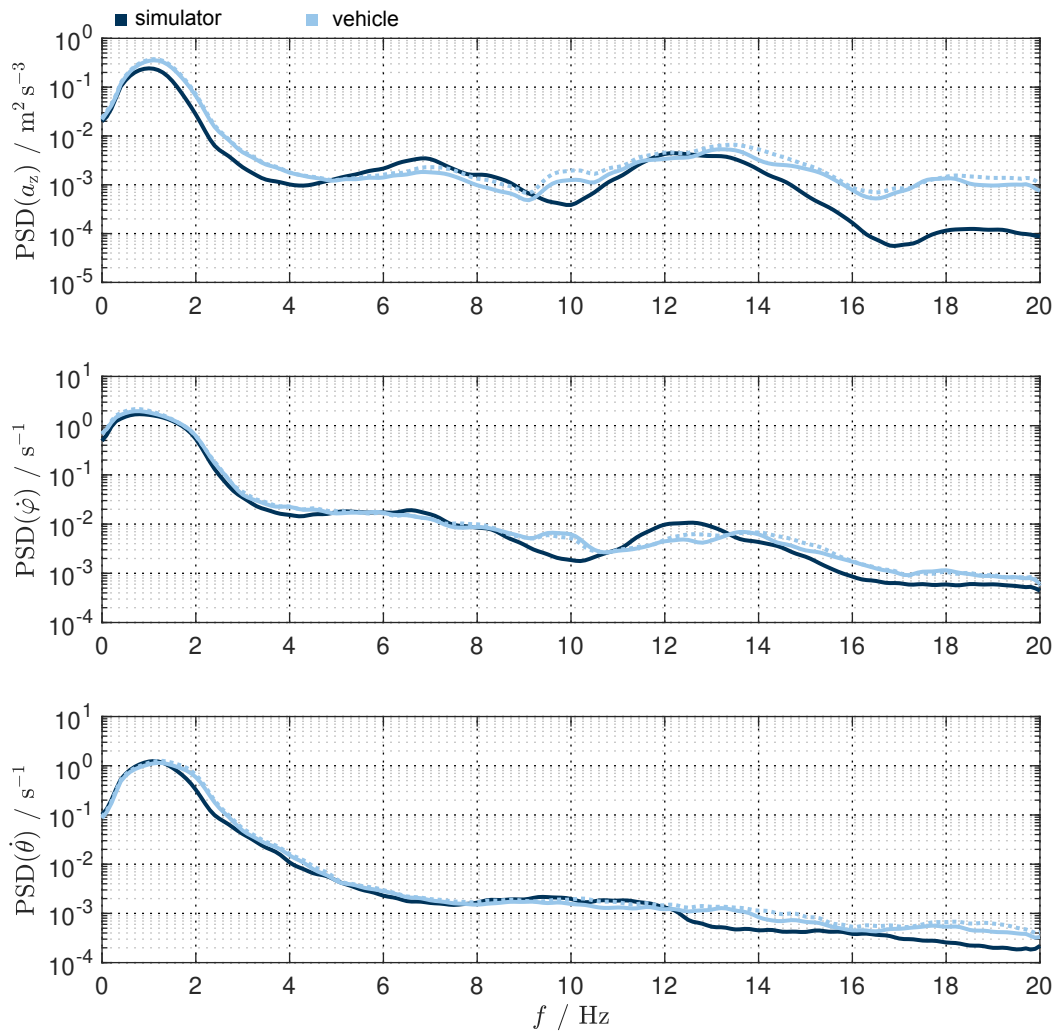


Figure D.2: PSD plots of the z-acceleration, roll-rate and pitch-rate from the simulation and two measurements for track I

D.2 Optimization for the Dynamic Wheel Load

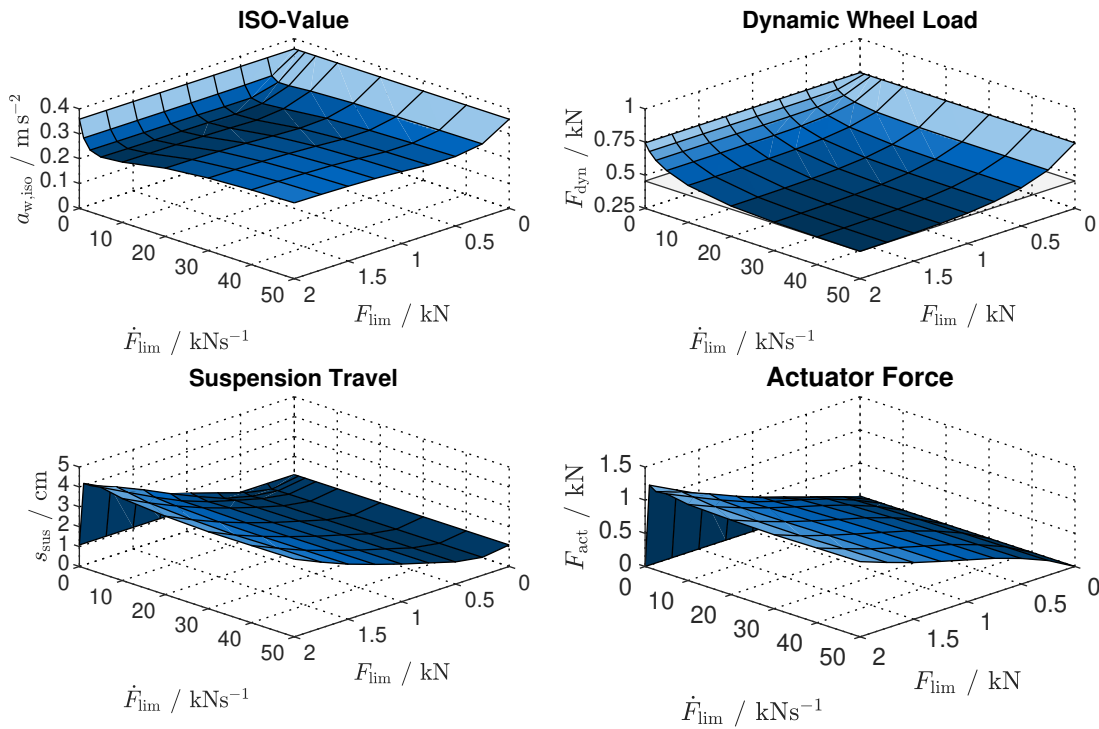


Figure D.3: Surface plots

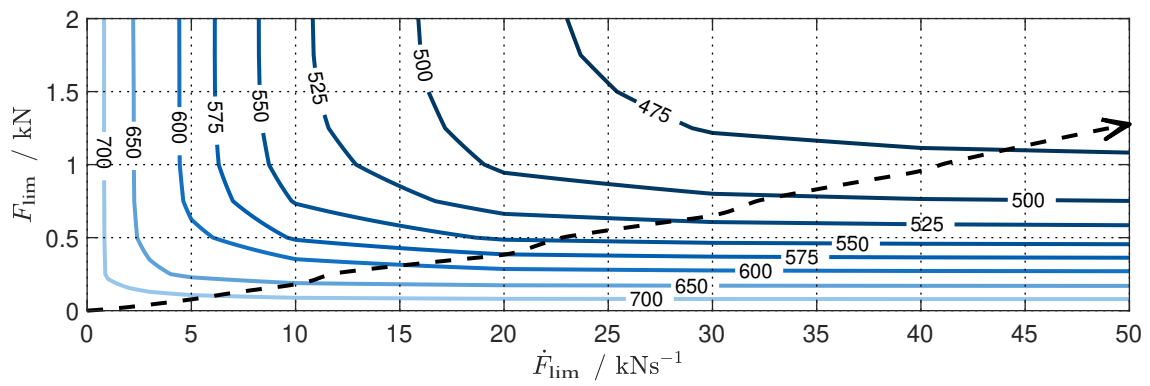


Figure D.4: ISO plot